UNDERSTANDING THE EFFECTS OF STRUCTURE ON THE CHARGE TRANSPORT PROPERTIES AND DOPING OF DIOXYTHIOPHENE POLYMERS

A Dissertation
Presented to
The Academic Faculty

by

Sandra L. Pittelli

In Partial Fulfillment
of the Requirements for the Degree
Doctor of Philosophy in the
School of Chemistry and Biochemistry

Georgia Institute of Technology
December 2019

UNDERSTANDING THE EFFECTS OF STRUCTURE ON THE CHARGE TRANSPORT PROPERTIES AND DOPING OF DIOXYTHIOPHENE POLYMERS

Approved by:

Dr. John R. Reynolds, Advisor
School of Chemistry and Biochemistry
School of Materials Science and Engineering
Georgia Institute of Technology

Dr. Carlos Silva
School of Chemistry and Biochemistry
Georgia Institute of Technology

Dr. Lawrence Bottomley
School of Chemistry and Biochemistry
Georgia Institute of Technology

Dr. Zhiqun Lin
School of Materials Science and Engineering
Georgia Institute of Technology

Dr. David Collard
School of Chemistry and Biochemistry
Georgia Institute of Technology

Date Approved: Sept. 24th, 2019

To my parents, Frank and Linda

ACKNOWLEDGEMENTS

It is strange to feel that my journey towards obtaining a Ph.D. is coming to an end, because while it was happening, honestly, it felt as if it would never end. The path towards a scientific Ph.D. is truly a unique and unpredictable one. When I moved to Atlanta in August of 2014, I had no way of knowing the experience that I would have, but I am truly grateful for the experience that I did have. One cannot simply obtain a Ph.D. without the assistance and support of others, and for that there are a number of people that I would like to thank for making this experience possible.

First and foremost, I would like to thank my family, and especially my mother and father, Linda Pittelli and Dr. Frank Pittelli. Throughout my life, you have always expressed your value for the sciences and emphasized the opportunities that are available throughout life if one is highly educated. I would like to thank you for providing me with the childhood, education, and intelligence that has allowed me the opportunity to pursue a Ph.D. In addition, I would like to thank you for your love, unwavering support, good luck charms, and advice during stressful times, that has guided me towards completing this journey. I hope you will be proud to know that it is because of you that I will get to say to telemarketers, “Excuse me, it’s Dr. Pittelli” when they address me as simply “Ms. Pittelli”.

I would also like to express my gratitude to my research advisor, Dr. John Reynolds. Thank you for accepting me into your research group five years ago and allowing me to study conjugated polymers. You have provided me with the best graduate experience I could have imagined. I am proud to say that whenever anyone asked what it

was like to be in the Reynolds Research Group, I could say in full honesty that it was the best group to work for at Georgia Tech. It is evident that both your dedication to your students and passion for science have made for a positive and thoughtful work environment, for which I am eternally grateful. I especially appreciate that you expect good work, but also understand that we have lives outside of the research lab. I would also like to thank you for challenging me to think about the big impact of my work, and for allowing me to pursue multiple professional development experiences outside of the lab. I could not have been on the executive boards of two student organizations, or gone to two international conferences without your support. Thank you for everything.

I would like to thank my undergraduate research advisors, Dr. Wilfredo Colón and Dr. Michael Gonsior for introducing me to academic scientific research. Your guidance helped me to develop my skills in presenting scientific work and designing experiments. You have also taught me the value in finding conferences and collecting data in exotic and fun places, and showing me that a career in science can also let you see the world. Additionally, I would like to thank the members of my Ph.D. thesis committee: Dr. David Collard, Dr. Zhquin Lin, Dr. Lawrence Bottomley, Dr. Carlos Silva, and Dr. Joseph Perry for their input at my candidacy exam, data review, and thesis defense. Thank you for the time that you have dedicated towards my professional development.

I would like to thank the collaborators that made this work possible. I would have never been able to generate the results or analysis presented in this dissertation without your help. I would like to thank Drs. Anna Österholm and Eric Shen for their assistance in the experimental design and data analysis that resulted in the work presented in Chapter 3. Anna and Eric, beyond your assistance with this project, you have served as

my mentors in the characterization lab and I am grateful for the countless hours that you have dedicated towards my development as a scientist and the countless hours we have spent discussing all things under the sun every day at lunch. I would not be the scientist or the person I am today without these conversations. I would also like to thank Dr. James Ponder, Dr. Michel de Keersmaeker, and Dr. Melony Ochieng for their assistance and input in the work presented in Chapter 4. I would also like to thank Dr. James Ponder (again) and Shawn Gregory for their help with the work presented in Chapter 5. Having thoughtful and enthusiastic scientists as collaborators makes a world of difference and I cannot thank you enough.

I would like to thank the executive board members who served alongside me in the Student Polymer Network (SPN) at Georgia Tech and the Women in Chemistry (WiC) organizations. The planning and participation of events for these two organizations truly enhanced my graduate experience. Not only did I have something to talk about at job interviews, but I also formed friendships and had a lot of fun. In no particular order, thank you to the SPN members: Brian Schmatz, Paul Balding, Alyssa Blake, Zhibo Yuan, Yao Ma, Ronald Smith, Ashley Johns, Luc Le, and Brian Khau. I would also like to thank our academic advisors: Dr. Paul Russo, Dr. Elsa Reichmanis, Dr. Blair Brettmann, and Dr. Will Gutekunst for their guidance and leadership. In no particular order, thank you to the WiC board members: Dr. Allison Geoghan Aioub, Dr. Johanna Smeekens, Dr. Hailey Bureau, Breanne Ellis, Asheley Chapman, Kirstie Thompson, Courtney Moore, and Ariel Parker. I would also like to thank our organization advisors Dr. Kenyetta Johnson and Dr. Christine Conwell. Finally, in regards to WiC, I would also like to thank Dr. Kelly Sepcic Pfeil for her support and creation of the Annual Women in Chemistry

Professional Development Retreat and Sepcic Pfeil Graduate Student Fellowship. Through organizing and participating in this retreat, I gained valuable professional development skills that I am sure I will use throughout the rest of my career.

Finally, I would like to thank my friends. Without your support and friendship I would never have had the positive graduate experience that I did. Thank you for the memories, the laughs, and the overall good times. I would like to thank my "ladies in science" from my childhood and undergraduate university, for consistently reminding me that we will always be there for each other. Thank you to: my cousin Joanna Peth, and my friends Jacqueline Brockhurst, Jenny Harding, Katie Ziegler, and Kelly Buckley. I would also like to thank my friends at Georgia Tech for being there during troubling scientific times, but also just being there to hang out. Thank you for the memories of playing kickball and Aces, shooting the hooch, and watching the demise of Game of Thrones. I have always been grateful for the social atmosphere of the Reynolds Research Group, and the Chemistry department in general. Graduate life would not have been nearly as much fun with out you. From the Reynolds Group, thank you to: Ian Pelse, Gus Lang, Lisa Savagian, Linda Nhon, Brandon DiTullio, Dylan Christansen, Kin Lo, Austin Jones, Zach Seibers, and Graham Collier. From our family of "obnoxious people" in the department, thank you to: Osiris Martinez Guzman, Eric Drew, Abe Jordan, Audrey Scholz, Krista Bullard, and Dom Sirianni. Thanks again and hope to see you soon.

TABLE OF CONTENTS

LIST OF TABLES

LIST OF FIGURES

LIST OF SYMBOLS AND ABBREVIATIONS

a*	Greenness or redness
α_i	Angle of incidence
AA	Atomic abundance
AcDOT	acyclic DOT
AFM	Atomic force microscopy
A_{rel}	Integrated area of fitted XPS spectrum
b*	Blueness or yellowness
CE	Counter electrode
CP	Conjugated polymer
CTC	Charge transfer complex
CV	Cyclic voltammetry
d	Interplane distance
DMP	2,2'-dimethyl-3,4-propylenedioxythiophene
DOP	3,4-dioxypyrrole
DOTT	3,4-dioxythienothiophene
DPV	Differential pulse voltammetry
e	Elementary charge
EA	Electron affinity
$E_{binding}$	Binding energy
ECD	Electrochromic device
EDOT	3,4-ethylenedioxythiophene

E_g	Energy gap
EH	(2-ethyl)hexyl
$E_{kinetic}$	Kinetic energy
E_{photon}	Energy of the photon
F4TCNQ	2,3,5,6-Tetrafluoro-tetracyanoquinodimethane
FWHM	Full width half max
GIWAXS	Grazing-incidence wide-angle x-ray scattering
GPC	Gel permeation chromatography
HOMO	Highest occupied molecular orbital
HTFSI	Bis(trifluoromethanesulfonyl)imide acid
IP	Ion pair
ITO	Indium tin oxide
K	Scherrer constant
λ	Wavelength
L	Coherence length
L*	Lightness
LiTFSI	Bis(trifluoromethane)sulfonamide lithium salt
LUMO	Lowest unoccupied molecular orbital
n	Number of charge carriers
NeoDOT	Neopentyl dioxythiophene
NMR	Nuclear magnetic resonance
Oct	n-octyl
OFET	Organic field effect transistor
OPV	Organic photovoltaic
OTf	Trifluoromethanesulfonate

ϕ	Energy for electron to be liberated
P3EHT	Poly(3-(2'-ethyl)hexylthiophene)
P3HT	Poly(3-hexylthiophene)
PBTTT	Poly[2,5-bis(thiophen-2-yl)thieno[3,2-*b*]thiophene]
PC	Propylene carbonate
PEDOT	Poly(3,4-ethylenedioxythiophene)
ProDOT	3,4-propylenedioxythiophene
q	Scattering vector
RE	Reference electrode
RFS	Radio frequency shielding
RSF	Relative sensitivity factor
σ	Electrical solid-state conductivity
SSRL	Stanford synchrotron radiation lightsource
θ	One half of diffraction angle
θ_d	Dihedral angle
$TBAPF_6$	Tetrabutylammonium hexafluorophosphate
TCE	Transparent conducting electrode
Tos	P-toluenesulfonate
μ	Mobility of charge carriers
WE	Working electrode
XPS	X-ray photoelectron spectroscopy
XRD	X-ray diffraction

SUMMARY

Redox-active conjugated polymers have been investigated for a multitude of applications including electrochromic displays, transistors, and transparent conducting electrodes. As with all fields of polymer science, the material properties observed for these conjugated polymers are determined by their structure. While the groundwork for probing their fundamental structure-property relationships has been established, there is still much to be explored in order to have a holistic understanding of these systems. This dissertation aims to investigate how the structure of dioxythiophene polymers can affect the processes of chemical and electrochemical oxidation, their charge transport properties, and their use in electrochemical and solid-state applications.

Chapter 1 provides an introduction to the fundamental properties and concepts of conjugated polymers, and their use in potential applications. Characterization methods used in this work, including electrochemical experimentation and dry-film characterizations are highlighted in Chapter 2. Chapter 3 describes the work exploring how the use of chemical oxidants and phosphonic acids can be used as pre-treatment steps in the construction of electrochemical devices. A family of polymers including two dixoythiophenes (DOTs) and one dioxypyrrole (DOP) were exposed to a series of chemical oxidant salts with the oxidizing agent either being Ag^{+} or Fe^{3+}. The structure and redox properties of the conjugated polymers were shown to affect the overall extent of oxidation. Specifically, the DOT polymer that had the highest onset of oxidation in the family was oxidized to a lesser extent when using Ag^{+} as the chemical oxidant rather than Fe^{3+}. In contrast, the DOT polymer with the lowest onset of oxidation in the family was

oxidized to the same extent using both dopants. Using Fe^{3+} was shown to disrupt the interface between films of each polymer in the family and the conducting substrate, however this was rectified through modification of the surface energy of the substrate using phosphonic acids. Ultimately, it was shown that devices constructed after chemical pre-oxidation had comparable electrochromic contrasts to those using an electrochemical pre-oxidation step. Chapter 4 explores the effects of side chain alteration on the charge transport properties of a family of either 3,4-propylenedioxythiophene (ProDOT) or acyclic dioxythiophene (AcDOT) homopolymers. It was shown that the incorporation of linear side chains rather than branched side chains for both the ProDOT and AcDOT polymers allowed for a decrease in the onset of electrochemical oxidation by 300 mV and a 2 order of magnitude increase in the solid-state in-plane conductivity (10^{-3} vs 10^{-1} S/cm) after chemical oxidation. This study ultimately showed that there is a delicate balance in the degree of ordering of the polymer film and effective charge transport. Chapter 5 further supported this concept of balance by probing a family of soluble dioxythienothiophene (DOTT) polymers for their structure-property relationships. These polymers also showed that too much intermolecular ordering inhibits the processes of oxidation and charge transport. Specifically, the DOTT homo polymer showed higher degrees of intermolecular ordering according to GIWAXS measurements, and had an electrochemical onset of oxidation that was almost 700 mV higher (0.05 vs -0.62 V) than the less ordered DOTT co-polymerized with two EDOT units (DOTT-BiEDOT). The introduction of two EDOT units also raised the solid-state in-plane conductivity by 4 orders of magnitude (10^{-3} vs 10^{1} S/cm).

CHAPTER 1. INTRODUCTION

Redox-active, π-conjugated polymers have been shown to be useful for applications ranging from organic photovoltaics (OPVs)[1] to electrochromic displays.[2-4] The variety of applications available to conjugated polymers (CPs) is due to their ability to conduct both electronic and ionic charge. In order for these materials to conduct, charge either needs to be injected, or the polymer backbone must undergo redox reactions.[5-7] The focus of the work highlighted in this dissertation has to do with understanding the redox processes of CPs and how these processes relate to polymer structure. In order to properly understand these investigations, a discussion of the structure and theory of charge transport of CPs is required.

1.1 Structure and Fundamental Theory of Conjugated Polymers

Heeger, Shirakawa, and MacDiarmid received the Nobel Prize in Chemistry in 2000 for conducting some of the most notable, and frequently cited, work in the field of conjugated polymers: their discovery of conducting polyacetylene.[8] Polyacetylene is a structurally simple CP in that its repeat unit consists of alternating double and single carbon-carbon bonds (conjugation), and only hydrogen atoms are substituted onto the carbon atoms. This conjugated system leads to the creation of the polymer's electronic system through the overlap of the p-orbitals of the carbon atoms and allows for the conduction of electrons, which will be discussed later on.

1.1.1 Increasing Conjugation and Closing the Gap

It has been established that as the number of conjugated bonds is increased, new and discrete energy levels are formed,[9] as shown in Figure 1.1-1. These bonds are stabilized by delocalization of electrons along the π-system, and upon the addition of more conjugated bonds, the molecule's energy gap (E_g) is decreased.[10]

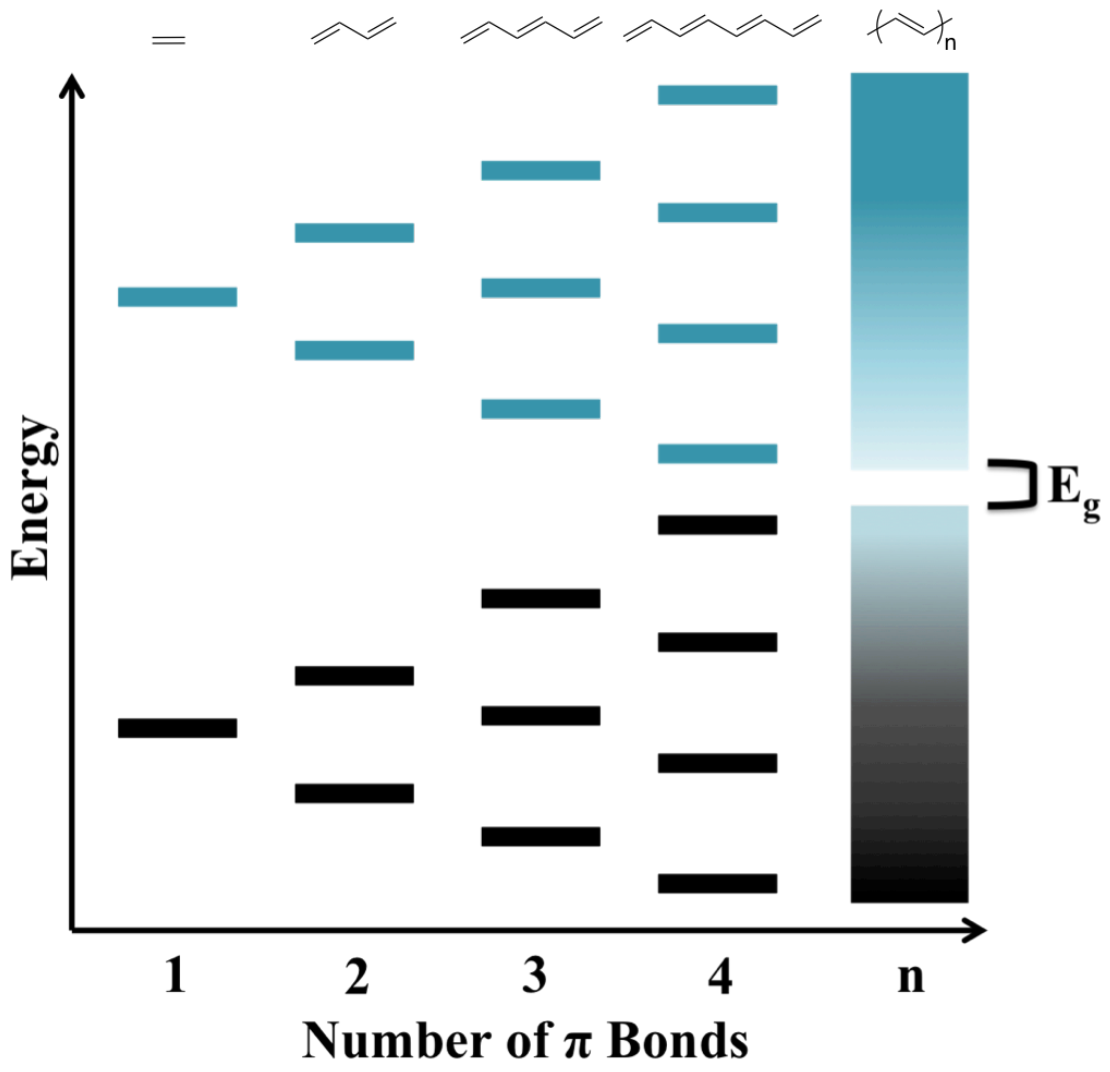

Figure 1.1-1 – Illustration of the shift in energy levels with the extent of conjugation in polyacetylene and evolution of the energy gap (E_g). The "filled" (HOMO) levels are represented in black and the "empty" (LUMO) levels are represented in teal. Adapted from Salzner *et al.*[10]

This phenomenon is due to the molecule's highest occupied molecular orbital (HOMO, in black in Figure 1.1-1) being raised and the lowest unoccupied molecular orbital (LUMO, in teal in figure 1.1-1) being lowered when increasing the number of conjugated carbon-carbon bonds. In theory, if an infinite polyacetylene chain were to exist, the E_g would be negligible and metallic-like conduction could be attained.[11] In reality, this phenomenon is prevented due to what is called the Peierls distortion (which can be related to the inorganic chemistry concept of the Jahn-Teller effect), which is a distortion due to the instability of the quasi one-dimensional structure of the chain and the need for stabilization.[12] This means that long chains of equal bond lengths are unstable. A stabilization of the chain is realized through bond-length alternation between the double and single bonds as illustrated in Figure 1.1-2, and results in lowering the HOMO and raising the LUMO. The distortion of the bond lengths in the conjugated chain and separation of the energy levels is what prevents CPs from achieving the zero-energy gap seen by conducting metals and places them in the category of "semiconductors".

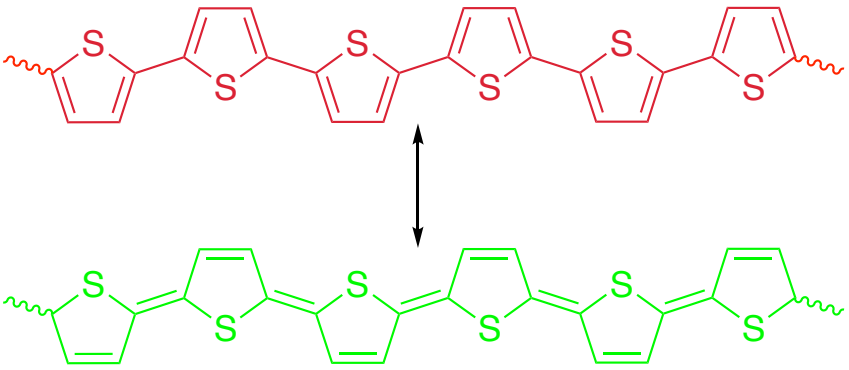

Figure 1.1-2 – An illustration of the bond-length alternation effect caused by the Peierls distortion. Top structure shown in red shows an example a thiophene chain in the aromatic resonance form and the bottom structure shown in green shows the thiophene chain in the quinoidal resonance form. These resonance structures provide energy stabilization and result in bond length alternation of the polymer chain.

1.1.2 Effects of Structure on Electronic Properties

For the work discussed herein, it is important to highlight how alteration of the polymer backbone structure can affect the electronic properties of the polymer. These concepts will be discussed in more detail in the subsequent chapters, however a few points will be briefly highlighted here. First, it is important to understand that the backbone structure is directly related to the ease of removal of an electron from the π-system, or process of oxidation. As will be discussed in the next section, the addition of electron-donating substitutents onto the backbone of the polymer results in a material that is easier to oxidize due to the increased electron richness of the system.[13] Second, the bulkiness of the substituents on the backbone of the polymer will also affect the electronic properties. In their neutral state, CPs favor an "aromatic" structure, which results in the monomer units twisting out of plane,[5] as shown in Figure 1.1-2 for an example polythiophene structure.

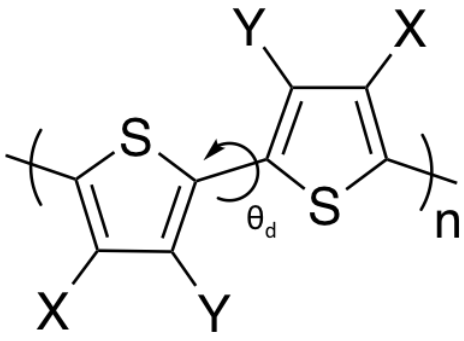

Figure 1.1-3 – Illustration of the backbone twisting as shown by the dihedral angle θ_d , of an example polythiophene structure.

Bulky substituents along the backbone (represented by X and Y in Figure 1.1-3) cause these units to further twist out of plane, which can affect the degree of overlap of

the p-orbitals of the π-system and make the polymer harder to oxidize. This phenomenon not only affects the ease with which an electron can be removed from the π-system, but also affects the polymer's absorption of light, and ultimately the neutral-state color of the material.[14]

1.2 Development of Poly(3,4-alkylenedioxythiophenes) (PXDOTs)

In addition to polyacetylene, polyheterocycles such as such as polypyrrole and polythiophene were also being investigated for their properties as conjugated and conducting polymers.[15] During the 1980's the Bayer Central Research Department was investigating a way to commercialize polyacetylene, however these efforts did not result in an oxidized material that was stable.[15,16] In order to overcome this, they investigated and developed polyheterocycle polymers, where the heteroatom of these materials was able to stabilize the polymer's oxidized form. Of the two previously mentioned polyheterocycles, polypyrrole is more electron rich, though synthetically more challenging to substitute with solubilizing groups than polythiophene. Polythiophene and its derivatives on the other hand, have been heavily investigated in the literature for their properties as conducting and color-changing electrochromic polymers.[17]

1.2.1 PEDOT and ProDOT

Unfortunately, polythiophene, like polypyrrole, suffers from β-position coupling defects during oxidative polymerization, due to the open and exposed 3,4-positions on the thiophene ring.[18] Given this, Heywang and Jonas reported on the synthesis of a 3,4-ethylenedioxythiophene-based polymer (PEDOT), which can be seen in Figure 1.2-1.[13]

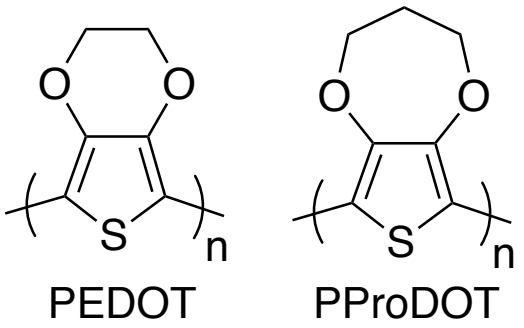

Figure 1.2-1 – The structures of poly(3,4-ethylenedioxythiophene) and poly(3,4-propylenedioxythiophene).

The incorporation of the dioxyethylene bridge allowed for the protection of the open sites available for defect coupling and for electron density donation from the oxygen atoms into the π-system, raising the HOMO of the polymer and making it easier to oxidize. Building from PEDOT, the dioxypropylene-bridged analogue, ProDOT, was also reported in the same study in 1992.[13] During the 1990's, PEDOT and PProDOTs were investigated as electrochromic polymers due to their vibrantly colored neutral states and transmissive oxidized states.[19-22]

1.2.2 Incorporation of Solubilizing Side Chains

The introduction of the dioxypropylene bridge to ProDOT allowed for further substitution of the dioxythiophene to create polymers that were soluble in organic solvent through substitution of the 2' position on the propylene bridge.[23,24] The solution processing of conjugated polymers gives this family of materials many advantages in that; 1) polymers can be synthesized in solution, rather than being electrochemically polymerized, 2) films can be coated on a variety of substrates with relatively low costs, 3) specific colors can be targeted through solution co-processing, and 4) polymers can be

chemically oxidized also through solution co-processing. In the case of ProDOT, it was shown that the substitution of the 2-position of the dioxypropylene bridge caused only minimal alteration of the electrochromic properties of the polymer.[25] Over the years however, significant efforts have been made towards a better understanding of how these solubilizing side chains can affect not only electrochromic properties, but charge transport properties as well.[26] This idea will be expanded upon in Chapter 4, where it is shown that an alteration of the solubilizing side chain does have an effect on both the neutral state color and charge transport properties of dioxythiophene-based polymers.

1.2.2.1 Side Chain Selection and Solubility

Commonly used solubilizing groups for ProDOT-based polymers are long alkyl chains that can either be branched or linear in their structure, although oligoether chains have also been shown to be useful for water-based redox-active applications.[27] The organic-based alkyl side chains allow for excellent solubility (>40 mg/mL) in common solvents such as toluene, which can allow the materials to be processed through methods such as spin, blade, and spray-coating.[24] This solubility is afforded due to the ability of the alkyl groups to break up π-π interactions between the polymer backbones and increase the entropic freedom of the polymer in solution. In general, the solubility of the polymer will increase when increasing the length of the side chain (hexyl, octyl, dodecyl), due to the increased degrees of freedom of the chain. Furthermore, using branched side chains as compared to linear chains will also enhance the solubility, due to the increased surface area and torsional disorder of the branched chains.[26] However, as will be further discussed in Chapter 4, the torsional disorder and increased bulk of a branched side chain can cause steric twisting of the conjugated polymer backbone and

result in altered optical and charge transport properties of dioxythiophene-based materials.

The effects of altered side chains on the optical properties of conjugated polymers was observed in the work presented by Dyer *et al.*,[28] which showed that two acyclic dixoythiophene-based (AcDOT) polymers had different neutral state colors depending on the side chain used. Figure 1.2-2. shows both the structures of the polymers investigated in this study and photographs of polymer films in the colored (neutral) and colorless (oxidized) states.[28]

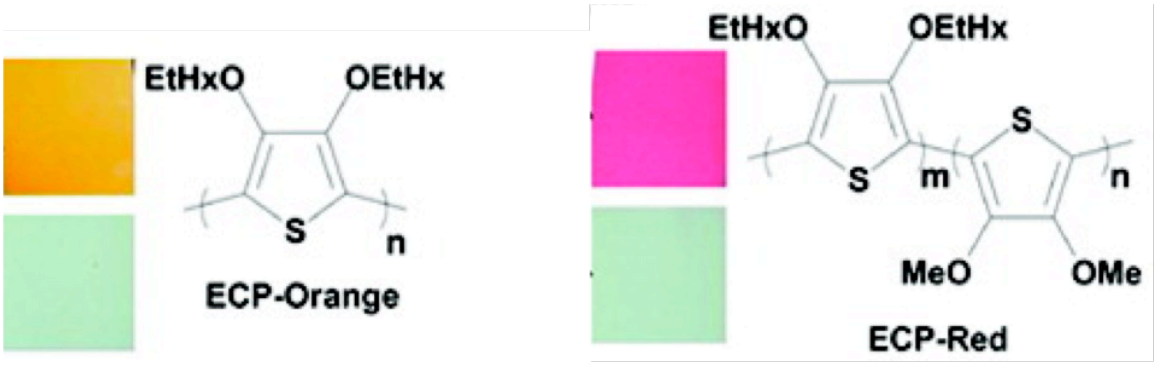

Figure 1.2-2 – Illustration of the effects of steric strain on the optical properties of AcDOT-based polymers. Reprinted with permission from Dyer *et al.*[28] ©2010 American Chemical Society.

The two polymers synthesized consisted of an AcDOT homopolymer with branched ethylhexyl side chains (referred to as ECP-Orange), and an AcDOT co-polymer with alternating branched ethylhexyl side chains and methyl groups (referred to as ECP-Red). It was found that the incorporation of the less bulky methyl groups on the dioxythiophene caused a relaxation in the polymer backbone, which red-shifted the neutral state absorbance by 42 nm and decreased the electrochemical onset of oxidation by 0.16 V as compared to the ECP-Orange polymer.

1.3 Introduction to Optical Properties of Conjugated Polymers

As has been mentioned in the previous sections, the structure of dioxythiophene-based conjugated polymers can affect their optical properties and electrochromic performance. Due to solution-based synthetic methods, we are able to target specific polymer repeat units and control the molecular weight of these conjugated polymers, giving us synthetic control over their optical properties, such as neutral state color. The reader is advised to turn to the dissertations of Dr. Justin Kerszulis,[29] Dr. Rayford Bulloch,[30] and Dr. Melony Ochieng[31] for full discussions of the synthetic color control induced in dioyxthiophene-based polymers, however the general concepts will be discussed here.

1.3.1 How Color is Perceived

The observation of color is due to materials either reflecting (structural color) or absorbing (pigmented color) light. For example, in the case of some butterfly wings, color is observed because of the way that the microstructure of the wing reflects light.[32] In the case of conjugated polymers, we observe a certain color for a given material due to the material absorbing specific wavelengths of light and transmitting others. For example, a ProDOT homo polymer with branched ethyl hexyl side chains absorbs light around 550 nm, and transmits light below 450 nm and above 650 nm (thus transmitting blue and red light) and appears purple to the eye.[24] We see that these materials change color upon oxidation because they absorb light in the IR region of the spectrum and transmit light in the visible region of the spectrum, which causes the material to appear colorless to the eye.

1.3.1.1 Theory of Color in Conjugated Polymers

As discussed previously, a major component affecting the color of conjugated polymers has to do with the structure and degree of twisting in the polymer backbone. Figure 1.3-1 shows the major controls we have over a conjugated heteroatom-based polymer's neutral state color. We can vary: 1) the heteroatom used (purple), 2) the addition of oxygen atoms on the 3 and 4 positions of the ring (navy blue), 3) the absence or presence of an alkylene bridge (cyan), 4) presence of an aryl group that can either contribute to the electron richness of the backbone or serve as an electron-withdrawing group (red), and 5) the side chain of the polymer (green). All of these variables can contribute to the steric interactions of the polymer backbone and cause twisting, which can shift the energy of the π-π^* transition, resulting in altered neutral state colors.

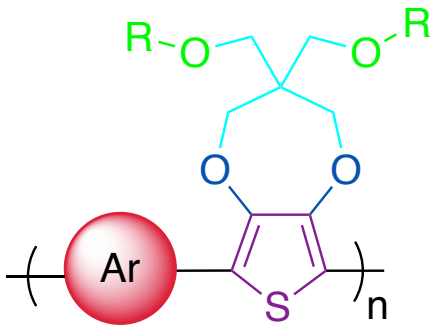

Figure 1.3-1 – Model for structural variables that can be used to tune the optoelectronic properties of conjugated polymers. Adapted from the dissertations of Kerszulis[29] and Bulloch.[30]

Figure 1.3-2 shows the completed color family based on dioxythiophene polymers developed by the Reynolds group. Here, we see that there is less steric strain in the Magenta polymer as compared to Orange due to the addition of the ProDOT unit, which results in a red-shifting of its neutral state color.

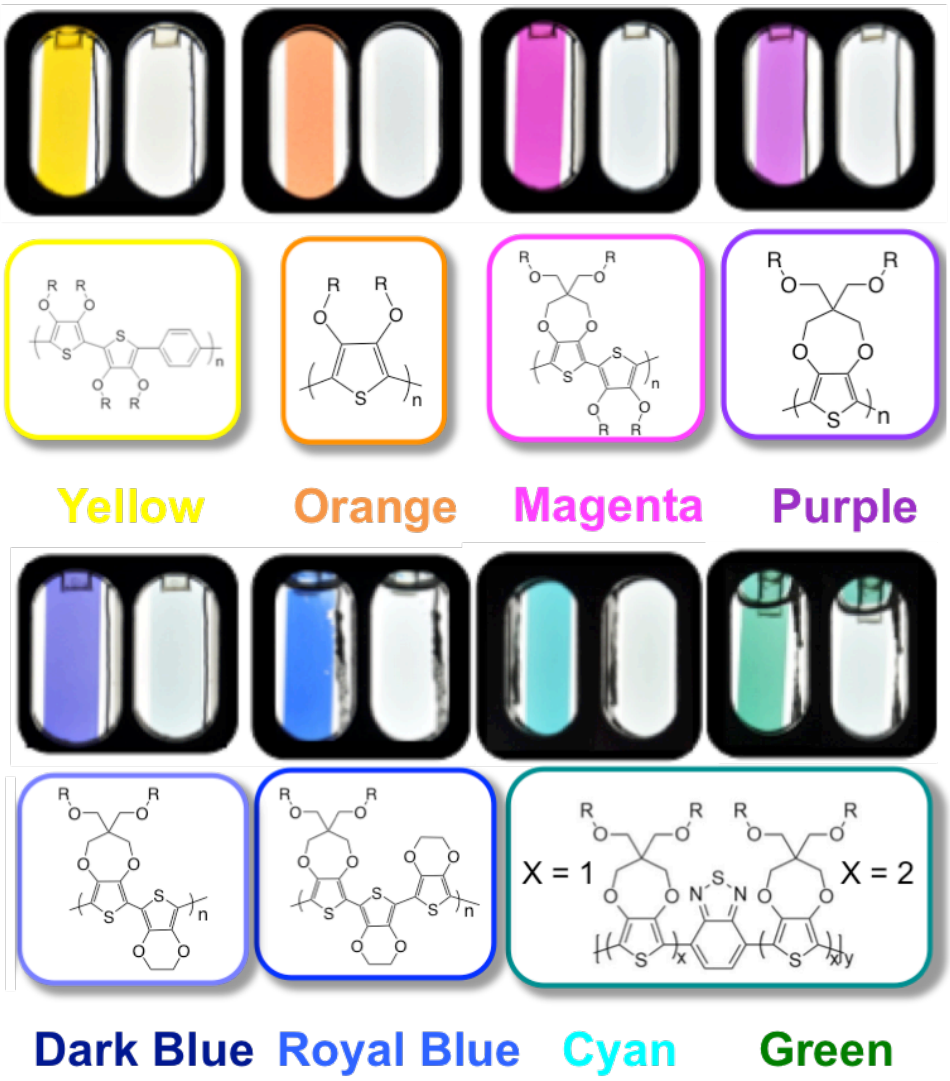

Figure 1.3-2 – Photographs of polymer films in the neutral and oxidized states and polymer repeat units corresponding to the completed color palette of dioxythiophene polymers from the Reynolds group. Adapted from a figure provided by Dr. Anna Österholm.

In the family, Yellow is the most strained polymer, followed by Orange and Magenta. The neutral state colors for Dark Blue and Royal blue are realized through a further relaxation of the polymer backbone from the addition of EDOT units. The neutral state colors for Cyan and Green are due to a dual absorbance of both high and low energy light.[33-35] This dual absorbance was realized through the use of donor-acceptor (D-A)

interactions of electron donating and withdrawing groups. The colors are tuned through the addition of electron-donating groups to provide the absorbance of longer wavelengths of light.

1.3.1.2 Quantifying Color

Color is a rather subjective metric in that it can vary between individuals. A system must be established in order to quantitatively describe the properties possessed by a conjugated polymer so that scientific comparisons can be made. One such system was developed by the International Commission on Illumination (or Commission Internationale De L'Eclairage, or CIE), the CIE L*a*b*.[36] A visual representation of this system can be seen in Figure 1.3-3.

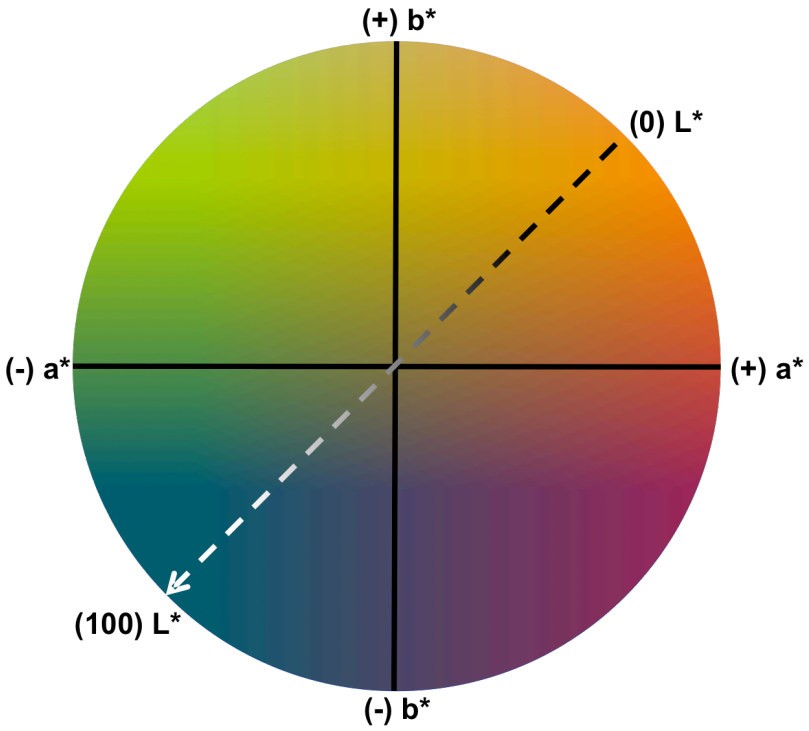

Figure 1.3-3 – A colored illustration of the plotted CIE L*a*b* color coordinate system. The L* component is plotted coming through the page.

The L* component ranges from 0 to 100 and represents the balance between lightness and darkness of the color (white-black balance), with more positive L* values representing lighter colors and more negative L* values representing darker colors. The a* component represents the red-green balance of the color, with more positive values representing red and more negative values representing green. Finally, the b* component represents the yellow-blue balance, with more positive values representing yellow and more negative values representing blue. Materials that have minimal color will appear on the plot close to the origin. With this system we have a quantitative way to plot and compare colors.

1.4 Charge Evolution and Transport

One of the reasons PEDOT has been so heavily investigated over the years is due to its ability to conduct electrons after oxidative doping and demonstrate conductivity values on the order of 10^3 S/cm.[37] In the field of conjugated polymers, doping refers to the process in which electrons are either removed (oxidation) or added (reduction) into the conjugated π-system of the polymer. This dissertation focuses on oxidative doping of conjugated polymers, however the reader should be aware that this is not the only doping route possible for conjugated polymers in general. After the process of doping, conjugated polymers are able to conduct electrons, and exhibit higher solid-state conductivity values, which will be explored in further detail below.

1.4.1 General Oxidation Principles

The oxidative doping of conjugated polymers is a dynamic redox process involving electron transfer, the generation of charge carriers, and alteration of the polymer

backbone geometry. Figure 1.4-1 illustrates the oxidative doping of PEDOT as an example. In its neutral state, conjugated polymers can be thought of as long chains of aromatic units. Aromatic stabilization energies cause the geometry of the backbone to be twisted, in other words monomer units are out of plane relative to each other, as discussed previously. When an electron is removed from the π-system of the polymer through doping, positive charges are incorporated along the backbone and in order to compensate for these introduced charges, the backbone of the polymer shifts to a more planar conformation.[5,38] This new conformation allows for a high degree of π-orbital overlap and also causes the polymer to absorb lower energy photons (longer wavelengths of light), which is why these materials are considered to be electrochromic.[39]

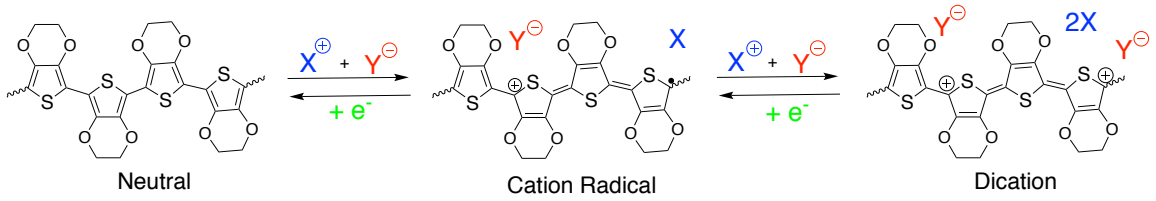

Figure 1.4-1 – Schematic of the stepwise oxidation of PEDOT. Oxidation of the neutral polymer gives a cation radical charged state. X^+ is an electron accepting molecule and Y^- is the charge-balancing anion. Further oxidation with X^+ yields the dicationic charged species, counterbalanced by two Y^- species.

The first electron transfer, as shown as the second species in Figure 1.4-1, leads to the formation of a delocalized cation-radical (sometimes referred to as a polaron). Further oxidation of the polymer, and further relaxation of the backbone leads to the formation of delocalized dications (bipolarons), as the relaxation of the polymer backbone geometry is greater for two coupled charges than for two uncoupled charges. The more planar backbone geometry due to the formation of these new charged states causes the polymer to absorb even longer wavelengths of light.

Because of this altered absorbance, we are able to monitor the extent of oxidation of conjugated polymers through optical absorbance measurements, as shown in Figure 1.4-2 for example polymer Homo DOTT (a material to be further discussed in Chapter 5), due to their optical property dependence on the redox state. As can be seen in Figure 1.4-2, when the polymer is in its neutral state it absorbs around 550 nm. Upon either chemical oxidation (blue curve) with molecular dopant Magic Blue, or electrochemical oxidation (purple and magenta curves), the neutral absorbance is depleted and the material begins to absorb at longer wavelengths beyond 1000 nm.

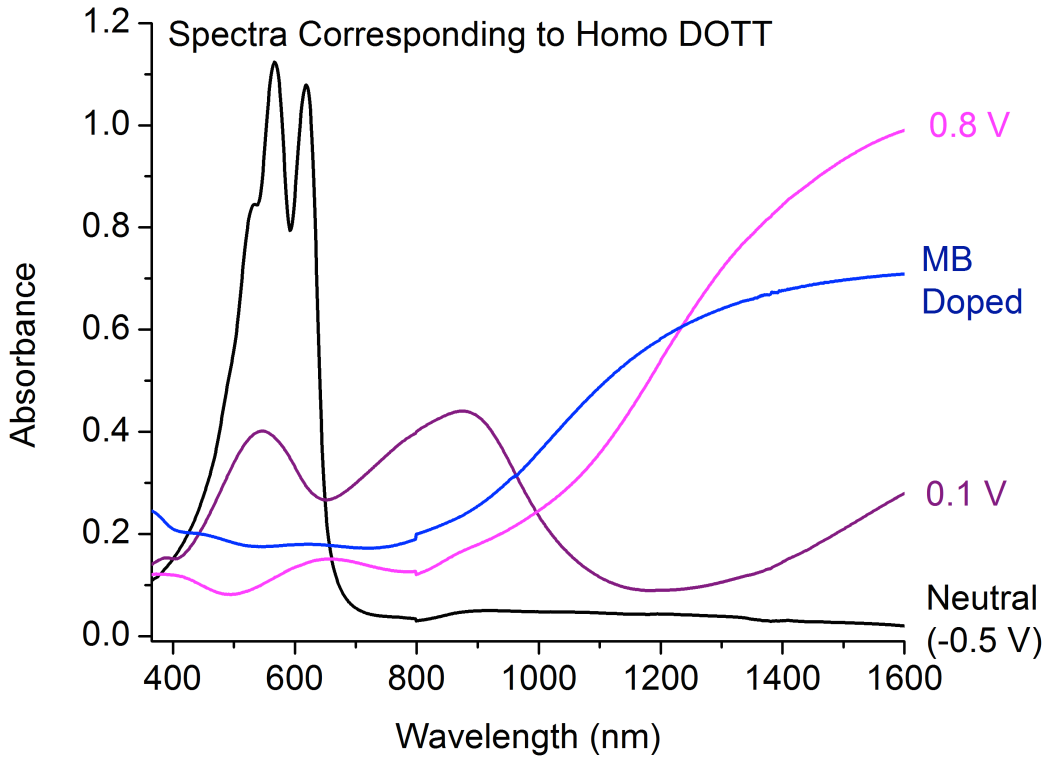

Figure 1.4-2 – Collective UV-vis absorption spectra corresponding to the polymer Homo DOTT (Chapter 5) in the neutral (black), partially electrochemically doped (purple), fully electrochemically doped (magenta), and fully chemically doped state using Magic Blue as the chemical oxidant (blue).

1.4.1.1 Mechanisms of Oxidation

Oxidative doping can occur through two mechanisms, either through chemical oxidation, where an electron-accepting molecule is present either in solution or vapor (shown as X^+ in Figure 1.4-1), or through electrochemical oxidation where a polymer film serves as the working electrode in an electrochemical cell.[40] While these mechanisms are different, the polymer undergoes the same process. In order to compensate for the introduced positive charges along the backbone, charge-balancing anions must penetrate into the polymer matrix (shown as the species Y^- in Figure 1.4-1). In the case of chemical oxidation, these anions come from the chemical oxidant species,[41,42] and in the case of electrochemical oxidation these anions come from the electrolyte of the electrochemical cell.[43,44] This dissertation focuses on the oxidation of polymer films, rather than polymers dissolved in solution, which means that the morphology of the polymer films should also be considered. Furthermore, the reader should be aware that polymer films can also be oxidized through exposure to dopant vapor,[8] but in this dissertation, solution chemical doping will be the focus. During the process of doping polymer films through either chemical or electrochemical oxidation, the film must swell in order to incorporate charge balancing anions as well as solvent molecules,[27] and in the case of chemical oxidation the polymer film must also be able to allow the penetration of the electron-accepting molecule.[45]

1.4.1.2 Charge Transport

After charges have been generated in the polymer film, they must be able to be transported in order for the material to be considered conductive. Charge transport

throughout a conjugated polymer film is a process that is governed by the weak interactions (van der Waal forces) and disorder in organic material. Because of this disorder, there is a range of energetic states in the polymer system and charge transport is realized through hopping-like transport rather than band-like transport as is observed in metals.[6,7,46-51] Charges can be delocalized of along the backbone of the polymer,[7] and also been shown to occur through charge-transfer from one conjugated polymer chain to another.[52]

One of the main focuses of the work presented in this dissertation has to do with the in-plane solid-state charge transport of electrons throughout the polymer film. Though there are multiple metrics, the one focused on here is that of the solid-state electronic conductivity. Equation 1 describes the relationship of solid-state electronic conductivity (σ), on the number of charge carriers (n), their mobility (μ), and elementary charge (e).

$$\sigma = n * \mu * e \tag{1}$$

Since we are discussing electronic charge transport, the elementary charge does not vary, so we will focus our discussion to the variables of the number of charge carriers and their mobility. The number of generated charge carriers depends on the doping level of the conjugated polymer. As the doping level is increased, so is the number of carriers. As mentioned previously, doping conjugated polymers causes the formation of radical-cation (polaron) and di-cation (bipolaron) charge carriers, which must be charge-compensated by negatively charged ions to maintain overall neutrality. Once these charge carriers are introduced, they are trapped by the Coulombic potentials of the negative counterions. At low doping potentials, these Coulomb traps suppress the mobility of the charge carriers,

resulting in low conductivities. Upon further oxidation, which increases both the number of charge carriers and concentration of counterions, these Coulomb traps begin to overlap, and the energy barriers are decreased, which results in a significant increase in the charge carrier mobility and therefore conductivity. Other factors affecting charge transport include the positional and energetic disorder of the system. These factors include variables such as the inter-chain distance, the degree of ordering of the polymer chain (including degree of crystallinity), orientation of the crystalline domains, and the counterion position. It is because of these variables that we should consider collectively: 1) the process and mechanism of doping, 2) the dopant species, and 3) the structural effects of conjugated polymers on their film morphology and degree of ordering.

1.4.2 Effects of Oxidation Conditions on Doping and Charge Transport

There are a number of parameters to consider when understanding the process of the oxidation and charge transport in conjugated polymers. These parameters depend on the mechanism of oxidation, and as such the discussion will be broken down in to discussions pertaining to chemical and electrochemical oxidation.

1.4.2.1 Chemical Oxidation

In terms of the chemical oxidation process, factors that will influence the extent of oxidation and overall electronic conductivity include: 1) the chemical oxidant itself, 2) the polymer structure, and 3) the morphology of the system. The work presented by Jacobs *et al*. provides an excellent review on the processes and understanding of doping of CPs.[53] The chemical oxidation processes discussed in this work involve the exposure of conjugated polymer films to high electron affinity (EA) molecules. In order for

chemical doping to proceed, the energy levels of the chemical oxidant must be properly aligned with those of the conjugated polymer. This concept is illustrated in Figure 1.4-3. It should also be mentioned that conjugated polymers have been shown undergo doping with Lewis acids,[54-60] though this doping process is different than with a high EA molecule, as electrons are not removed from the π-system and is not the focus of the work discussed here.

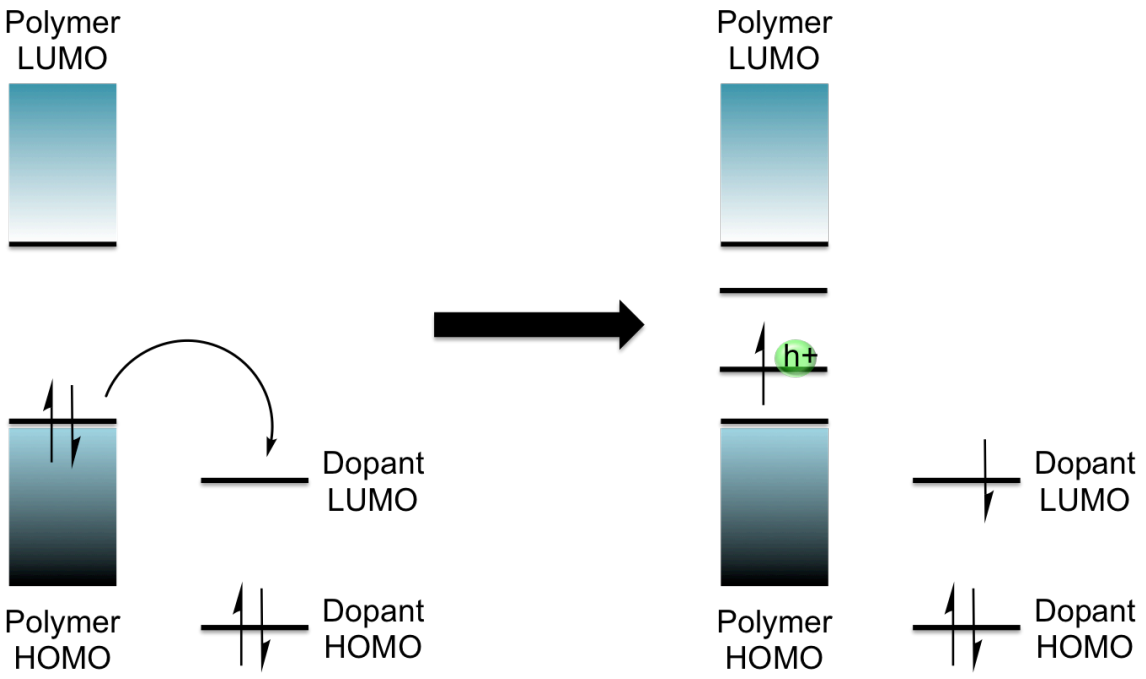

Figure 1.4-3 – An illustration of the simplified doping model for conjugated polymers and molecular electron-accepting dopants. Structures on the left highlight the electron transfer from the polymer to the dopant and structures on the right show the formation of the polymer charge carriers as represented by h^+. Adapted from the thesis of Dr. Teran.[61]

Figure 1.4-3 shows that in order for chemical oxidation to proceed, the LUMO of the oxidative dopant must be deep enough to extract an electron from the HOMO of the conjugated polymer film. These levels can be experimentally estimated through electrochemical experiments, such as cyclic voltammetry or differential pulse

voltammetry. However, as will be discussed throughout this dissertation, one cannot simply predict efficient electron transfer from considering these energy levels alone.

In Figure 1.4-3, it is shown that the electron transfer from the HOMO of the polymer and LUMO of the dopant results in the formation of an ion pair (IP). This is a simplistic view of organic doping and does not consider the fact that it is also possible to form charge transfer complexes (CTC)s. The formation of a CTC occurs if there is only partial charge transfer from the polymer to the electron-accepting molecule, rather than integer charge transfer, which would be the case for IP formation. CTCs were first observed in the 1950s[62] and can be characterized by their spectral signatures.[63] The CTC is formed through the hybridization of the frontier molecular orbitals of the polymer and electron-accepting molecule. Its formation results in the creation of new HOMO and LUMO energy states and the charge is shared between the CP and the acceptor.[64] A difference from the model shown in Figure 1.4-3 is that the newly formed HOMO for the CTC contains the electrons from both the CP and the acceptor, and is inconsistent with the idea that an electron is removed from the donor.

In 2018, Thomas *et al.* published a study showing that one polymer, poly(3-(2'-ethyl)hexylthiophene) (P3EHT) can undergo form both CTCs and IPs depending on the dopant used.[45] It was shown that the creation of an IP resulted in solid-state conductivities that were two orders of magnitude higher as compared to the CTC. Given that no spectral evidence is found for the formation of CTC in Chapters 3, 4, and 5, it is concluded that for the polymers explored in this dissertation only IPs are formed.

There are a large number of chemical oxidants that can be used, such as metal ions like Ag^+ and Fe^{3+}, and electron accepting molecules like NO^+ and F4TCNQ. Connelly and Geiger provide an excellent review on chemical redox agents.[65] These redox agents can vary from their strength (defined by their $E_{1/2}$ value, or EA), geometric size, and physical form after doping (solid metal, gas, organic molecule etc). It has been shown through work in the literature and the work that will be discussed in Chapters 3 and 5, that these dopant properties can have an effect on the overall extent of doping of conjugated polymer films. The counterbalancing anion can also have an effect on the charge transport properties of the system. The bulk of the counterbalancing anion can have an effect on the degree of disruption of the polymer film microstructure and alter the overall conductivity of the system. This idea will be further discussed in the work shown in Chapter 5.

One question that is commonly asked in the work presented in the literature is how the chemical dopant should be introduced to the polymer. As mentioned before, chemical oxidation can be performed through the vapor phase or solution phase doping. In terms of solution phase doping there are two options: 1) solution co-processing and 2) sequential doping. Solution co-processing is a process that involves dissolving the polymer and dopant in the same common solvent and coating films. It has the advantage that polymer films can be doped and processed in one step, however it is limited by the fact that conjugated polymers typically become less soluble or insoluble in organic solvents upon chemical oxidation. These charged materials typically become highly aggregated[66-68] and need to be processed from high-temperature solutions, which has also been shown to reduce doping efficiency and affect film quality.[69] Sequential doping on the other hand,

involves coating neutral polymer films and exposing these films to solutions of chemical oxidants for a period of time. The chemical oxidant solutions must be made in solvents that do not dissolve the polymer film (are orthogonal).

Jacobs *et al*. published a study directly comparing the effects of solution co-processing versus the sequential doping of P3HT with the molecular dopant F4TCNQ.[70] They found that sequential processing resulted in films that were smoother and much more uniform as compared to films that were co-processed. This enhancement in the polymer film morphology resulted in polymer systems that had conductivities that were 3-15 times higher at a given doping level. Scholes *et al.*[41] also highlighted the same concept in their work. Enhancement in the film quality and morphology when using sequential doping versus solution co-processing for films of P3HT doped with F4TCNQ can be seen in their photographs as shown in Figure 1.4-3.

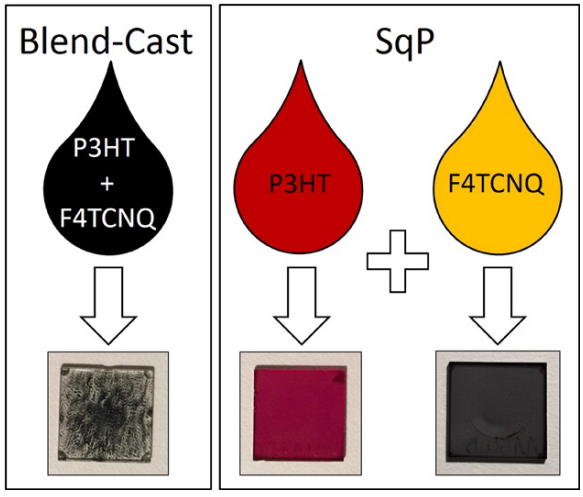

Figure 1.4-4 – Photographs of P3HT polymer films that were solution co-processed (left) versus sequentially doped highlighting that the latter process results in films that are more smooth and continuous. Reprinted with permission from Scholes *et al.*[41] © 2015 American Chemical Society.

1.4.2.2 Electrochemical Oxidation

In terms of electrochemical oxidation, the primary factor that will influence the extent of oxidation is the experimental voltage bias applied to the electrochemical cell. However, it has been shown that tailoring the polymer structure to the electrolyte system used can also affect the electrochemical doping and charge transport processes. The use of oligoether side chains for example has been shown to enhance the redox performance of dioxythiophene polymers in water-based applications.[27,71] These improvements were made because the incorporation of oligoether side chains, rather than alkyl side chains facilitated enhanced hydration and ion penetration of the aqueous electrolyte, resulting in full electrochemical doping. In 2019, Dong *et al*. also showed that by tailoring the side chains of thiophene-based polymers by adding a methylene spacer unit, the ionic conductivity of the polymer could be increased when using a LiTFSI electrolyte.[72] Electrochemical doping processes can also be affected by the degree to which the polymer film is adhered to the working electrode.

1.5 Effects of Structure and Morphology on Conjugated Polymer Charge Transport Properties

Dixoythiophene chemistry is highly versatile and has allowed for the synthesis of many soluble polymers with varying backbone structures. As has been discussed in a number of previous reports, alteration of the structure of conjugated polymers leads to materials with different properties.[2,28,73-82] It has been shown that these structural alterations can result in altered polymer color[76] and redox properties,[74] as well as polymer morphology and the degree of intermolecular ordering.[83-85] This dissertation will focus

primarily on how polymer structure can affect polymer morphology and charge transport properties, especially in Chapters 4 and 5.

1.5.1 Electrochemical Redox Properties

As was discussed in section 1.3, the repeat unit structure of dioxythiophene-based polymers can be altered in order to change the neutral state color of conjugated polymer. Remember, in the neutral state, conjugated polymers can be thought of as long chains of aromatic units that are out of plane, or twisted, relative to each other and the degree of twisting or steric strain can be manipulated in order to target specific properties. During the dynamic process of oxidation these units adopt a more planar geometry in order to compensate for the introduced charges. As such, the polymer backbone geometry plays a role in the ease at which an electron can be removed from the π-system. Increased steric bulk of the π-conjugated backbone can result in polymers that have higher electrochemical onsets of oxidation due to the increased degree of twisting of the polymer backbone.[28,73,76] In addition to steric effects, it has been shown that increasing the electron richness of the polymer backbone can result in lower onsets of oxidation. Work in the literature has also shown that structural alteration of the conjugated polymer backbone can lead to increased redox capacity.[78,79]

Specifically, in 2019 the work by Ponder *et al.* showed that both onset of oxidation, and solid-state conductivity could be tuned through structural manipulation of the conjugated polymer backbone within one family of dixoythiophene polymers.[80] The structures investigated and trends shown in this work can be seen in Figure 1.5-1. The

authors showed that the addition of the EDOT unit could be used to tailor material properties.

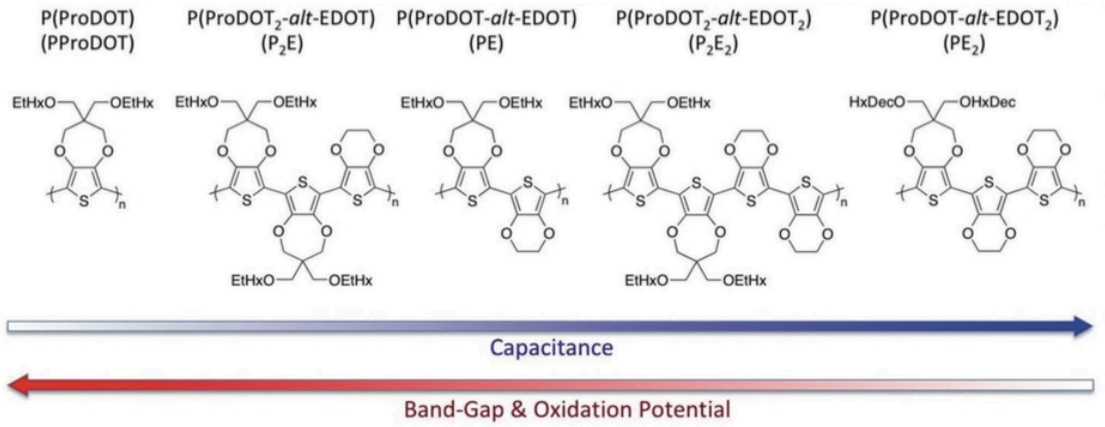

Figure 1.5-1 – Polymer structures developed by Ponder *et al.*[80] showing the increased redox capacitance and decreased electrochemical onset of oxidation upon the addition of EDOT units. Reprinted with permission from Ponder *et al.*[80] © 2019 Advanced Energy Materials.

In comparison to the ProDOT homo polymer, the addition of biEDOT to form the ProDOT-biEDOT polymer lowered the optical gap by 0.16 eV, lowered the electrochemical onset of oxidation by 0.83 V, and raised the electrical conductivity by raised the redox capacity by 3 orders of magnitude. This work formed the basis for the structural design of the polymers investigated in Chapter 5. Furthermore, as will be discussed in Chapter 4, the structural alteration of the backbone and solubilizing side chain of dioxythiophene-based polymers was shown to affect the electrochemical doping kinetics. This idea was also shown in the work presented by Österholm *et al*. in 2019, who showed that alteration of the side chains of copolymers of ProDOT and dimethyl-ProDOT (DMP) units affected their electrochemical doping kinetics.[74] The authors showed that polymers substituted with bulky tetraester side chains had the slowest doping

kinetics of the family in an organic electrolyte. As discussed in the previous section, side chain engineering of thiophene-based polymers has also allowed for the enhancement in redox performance for conjugated polymers in water-based applications, which is especially important for the field of bioelectronics.

In addition to structural engineering, the bioelectronics field has also investigated how the degree of polymer ordering and crystallinity can affect redox properties in water-based applications. Typically, x-ray scattering methods are used in order to understand how polymer chains are aligning in the film. These techniques include x-ray diffraction (XRD) and grazing-incidence wide-angle x-ray scattering (GIWAXS). Details on GIWAXS experimentation will be discussed further in Chapter 2. Furthermore, Rivnay *et al*.[86] provide an excellent review on these x-ray scattering techniques.

In 2018, the work by Kim *et al.*[87] showed how the microstructural crystallinity of PEDOT:PSS films correlated with electrochemical transistor device performance, with devices demonstrating transcondutance values of 20 mS. Efforts are ongoing in this field to fully understand how polymer structure and morphology can affect material charge transport properties. For example, in 2018 Thomas *et al*.[43] probed how the intermolecular spacing distances of P3HT films were altered during the electrochemical switching in a transistor device. During device operation, the authors saw a 12% increase in the lamellar stacking distance and a 4% decrease in the π-π stacking direction, showing that the crystal structure of the polymer film is correlated with charge carrier mobility.

1.5.2 Solid-State Electronic Conductivity and Charge Transport

Both backbone and side chain structure have repeatedly been shown to have an effect on the degree of intermolecular ordering and solid-state conductivity of conjugated polymers. These two properties are intimately related because of the mechanisms of charge transport, as discussed in section 1.4. In order for effective transport, polymer films should be as defect free as possible in order to avoid charge trapping. Many studies have been published on polymers such as PEDOT,[37,88-90] poly(3-hexylthiophene) (P3HT),[41-43,45,66,70,91-93] and poly[2,5-bis(thiophen-2-yl)thieno[3,2-*b*]thiophene] (PBTTT)[67,94-96] in order to understand how polymer microstructure can affect solid-state charge transport and how this relates to polymer structure. In general, it has been shown that conductivity increases with increased intermolecular ordering.

In addition to effects from the polymer repeat unit, CP film morphology relies on the processing method and conditions to coat polymer films. These processing methods and their effects will be discussed further in Chapter 2. The work by Müller *et al*.[97] highlighted this concept by investigating co-processed doped films of P3HT and the molecular dopant F4TCNQ. Films had been dissolved and spin coated from either chloroform or chlorobenzene. This work showed that films that were processed from chloroform had enhanced conjugation lengths of the polymer backbone, which resulted in conductivities that were an order of magnitude higher than those corresponding to films that had been processed with chlorobenzene. Furthermore, through spectroscopic measurements, it was shown that co-processed polymer films from chlorobenzene were more highly aggregated, which is another reason why the overall conductivity was lower for these films.

As mentioned previously, x-ray scattering methods can also be used to understand the degree of intermolecular ordering for chemically doped polymer films. Through x-ray scattering methods, Duong *et al.*[66] was able to show that when doping P3HT with the molecular dopant F4TCNQ, a previously unreported crystalline phase is observed for P3HT films doped above a critical threshold. In this crystalline phase, the F4TCNQ molecules are incorporated into the polymer matrix and cause a higher degree of charge dissociation and therefore higher charge carrier densities. In 2016, Kang *et al*.[98] showed that when doping PBTTT with evaporated F4TCNQ, the dopant resides in the more amorphous regions of the solubilizing side chains and as a result does not disrupt the microstructure of the polymer film, resulting in enhanced charge transport properties.

Studies have also shown that overall conductivity values are affected by the polymer morphology as it relates to the ease at which oxidative dopants can be incorporated into polymer films. Again, turning to the work by Thomas *et al.*,[45] which showed that bulky polymer side chains force the molecular dopant F4TCNQ to reside between the π-stacks of the polymer film. This phenomenon results in only partial charge transfer and therefore lower conductivity values as compared to a polymer-dopant system that had decreased steric effects. Bulky dopants have also been known to cause inefficient doping, as they displace more volume in the CP film and cause a larger disruption of the microstructure as compared to less-bulky dopants. One idea that this dissertation aims to discuss is that of the balance between higher degrees of intermolecular ordering in polymer films that still support sufficient ionic penetration, and the use of molecular dopants that are sufficiently strong enough to oxidize polymer films without unnecessary bulk.

1.6 Conjugated Polymer Devices and Applications

The field of conjugated polymers has developed significantly since the discovery of conducting polyacetylene in the 1970's. Conjugated polymers have been shown to be useful in applications ranging from electrochromic and charge storage devices to transparent conducting electrodes. The following section will discuss these applications and the efforts towards making these devices practically accessible.

1.6.1 Electrochemical Devices

Two commonly studied electrochemical devices that incorporate conjugated polymers as the active electrodes are those for the purposes of electrochromic and charge storage applications. As will be discussed in detail in Chapter 3, these devices can have a sandwich-style architecture, and function by having the polymer electrodes in opposite redox states upon assembly.[99] During switching of the device, simultaneous and opposing redox reactions are occurring at each polymer electrode. Charge-balancing electrolyte is sandwiched in between the electrodes and upon switching ions from the electrolyte must be able to penetrate polymer films. In order for proper function of these devices, the polymer films need to be able to be adhered to the conducting substrate and not delaminate upon repeated cycling and support ion diffusion of the electrolyte. Chapter 3 will investigate a new route towards constructing these devices and considerations of the structure-property relationships that pertain to device performance.

1.6.2 High Electrical Conductivity Applications

Significant effort has been devoted towards understanding how to capitalize on the multiple order of magnitude range of the electrical conductivity of conjugated polymers. As mentioned previously, some of these applications simply rely on the highest conductivity attainable by conjugated polymers and their color-transmissive properties when in the oxidized state for transparent electrode applications.[100,101] Other applications require the tunable conductivity observed in conjugated polymers, for applications such as shielding in electronics.[102,103] Conjugated polymers provide the advantages of being solution processable, with the additional benefit of being highly conductive and having this conductivity be dependent on their redox state. Additionally, conductivity of CPs can be tuned according to their redox state, and therefore a conductivity range that spans multiple orders of magnitude can be observed for these materials in particular. As will be further discussed in Chapters 4 and 5, the ultimate conductive performance of conjugated polymers will be realized when we have a significant grasp on their structure-property relationships.

1.7 Overview of Dissertation

This dissertation aims to discuss the structure-property relationships of soluble dioxythiophene polymers for use in redox and electrically conductive applications. At its core, this work aims to address the question of "How does the structure of a redox-active polymer affect both the morphology and the charge transport properties of the material?" As seen above, Chapter 1 serves as a general introduction to the development of conjugated dixoythiophenes, and describes how the structure of these materials directly

affects their properties. This chapter focuses on the various routes and mechanisms to oxidize these polymers, both through chemical and electrochemical oxidative doping and discusses how polymer structure can affect morphology and charge transport properties.

Chapter 2 will describe the material characterizations that have enabled the work discussed herein. These characterizations include: (1) electrochemical methods such as differential pulse voltammetry (DPV), cyclic voltammetry (CV), and *in situ* conductance, (2) coupled optical and electrochemical methods such as spectroelectrochemistry and chronoabsorptometry, and (3) dry-film solid-state characterizations such as x-ray photoelectron spectroscopy (XPS), in-plane solid-state conductivity, and grazing-incidence wide-angle x-ray scattering (GIWAXS).

Chapter 3 will cover the study conducted on the use of chemical oxidants and phosphonic acids as pre-treatment steps in the construction of electrochemical devices, and will describe what considerations need to be taken for this process and how this process can be used in the manufacture of redox-active devices. Major accomplishments from this work include: (1) the success of chemical oxidation as a pre-treatment step in the scalable construction of electrochemical devices, (2) the relationship between the properties of the polymer and effects of chemical doping, and (3) the concept that chemical doping can cause film delamination, but this effect can be rectified through the use of a surface energy modification step such as the use of phosphonic acid treatments.

Chapter 4 will cover the use of 3,4-propylenedioxythiophene (ProDOT) and acyclic (AcDOT) polymers with branched and linear solubilizing side chains to understand how the structural tuning of the polymer repeat unit can affect the morphology and charge

transport properties of the conducting polymer. This chapter will discuss the various properties of each polymer in the family determined using the characterization methods listed in Chapter 2, and will describe how the structure of each polymer is related to its properties. This will lead to a discussion of the relationship of how solid-state electronic and electrochemical charge transport properties are related. Major accomplishments in this work include: (1) the novel approach of understanding both the electrochemical and solid-state charge transport properties of a dioxythiophene-based polymer family, (2) the delicate balance of intermolecular ordering of polymer chains in the film as it relates to enhancing or inhibiting charge transport, and (3) the idea that polymers can be used and perform well in electrochemical applications even if they do not have high solid-state conductivities.

Chapter 5 will focus on the design of dioxythienothiophene (DOTT) polymers for use in electrochemical and solid-state applications. This work focuses on how DOTT monomers can be co-polymerized with well-known dioxythiophene monomer units to alter the film morphology and how the repeat unit structure of these polymers can affect their charge transport properties. Results from the characterizations listed in Chapter 2 will be discussed. Major accomplishments in this work include: (1) an understanding of the structure-property relationships of the DOTT family, (2) further support for the idea that there is a delicate balance in the degree of ordering in the polymer film and effective charge transport, (3) the comparable post-doping solid-state conductivities of the DOTT materials and state-of-the-art materials currently investigated in the literature, and (4) the advantage of the air-stability of these materials compared to the state-of-the-art.

Chapter 6 will discuss the future steps for each of the sections covered in this dissertation. This chapter is broken into two main themes: that of the future of redox-active devices and high conductivity polymer applications. This will lead into a discussion on making redox-active devices in a practically scalable way and considerations for potential bioelectronic applications. In terms of solid-state applications, design considerations for state-of-the-art polymers will be discussed and how certain properties should be targeted (degree of ordering etc), and the challenges of balancing these opposing properties.

CHAPTER 2. EXPERIMENTAL METHODS AND CHARACTERIZATION TECHNIQUES

The work presented in this dissertation could not have been made possible without the collaboration from a number of individuals from the Georgia Institute of Technology. Dr. James Ponder and Dr. Melony Ochieng in the Reynolds group synthesized and confirmed the structure of the conjugated polymers presented in the work in Additionally, Dr. James Ponder synthesized and confirmed the structure of the conjugated polymers presented in Chapter 5. The sputtering of contacts and measurement of solid-state conductivity for the materials in Chapter 5 were conducted by Shawn Gregory in the Yee Group in the department of Materials Science and Engineering.

This chapter will discuss the experimental methods and characterization techniques conducted to generate the results discussed in this dissertation. Topics will include the general approach to selecting desirable polymer structures and the techniques used to confirm these structures, the procedures for forming polymer films from solution, electrochemical methods, and dry film characterizations.

2.1 Materials, Reagents, and Choice of Polymer Structure

Other than the polymers used in this work, all reagents were purchased from various commercial suppliers and were used without further purification, with the exception of propylene carbonate (PC) which was purified using a solvent purification system from Vac Atmospheres prior to electrochemical characterizations and solution doping experiments. In general, polymers were selected for this work on the basis of their structure. These choices will be motivated in the specific chapters in which each polymer appears. Their common traits include that they are all dioxythiophene polymers with

hydrocarbon solubilizing side chains. All polymers are soluble in chloroform and a selection can also be dissolved in toluene.

2.1.1 General Polymer Synthetic Approach

The polymers presented in this work were polymerized using either direct arylation[104-106] or oxidative[28] polymerization techniques. Both of these synthetic methods involve the linkage of π-conjugated monomers to create a continuous conjugated backbone. The specific synthetic experimental procedures will be described in the appendix of each chapter. For an introduction and description of the synthetic methods used and other synthetic methods to generate conducting polymers, the reader is advised to consult the Ph.D. thesis of Dr. James Ponder.[107]

2.1.2 Structural Characterization

The structure of the polymers used this this work were confirmed by nuclear magnetic resonance spectroscopy (NMR) and gel permeation chromatography (GPC). ^{1}H NMR and ^{13}C NMR spectra were collected on either a Varian Mercury Vx 300 MHz or a Bruker Corporation DRX 700 MHz instrument using $CDCl_3$ as a solvent. The chemical shift was set based on residual $CHCl_3$ (in the $CDCl_3$ solvent) as an internal standard set to 7.26 ppm. The molecular weight and dispersity of the polymers were obtained using either a chloroform GPC at 40°C or a THF GPC at 35°C, both calibrated versus polystyrene standards. For GPC measurements, polymers were dissolved at 1 mg mL^{-1}, and filtered through a 0.45 μm PTFE filter.

2.2 Electrochemical Characterization Techniques and Experimental Procedures

Electrochemical techniques provide information about the redox properties of conjugated polymers.[108,109] These methods can be used to determine properties such as the onset of oxidation, and potential dependent absorbance of these materials. All of the electrochemical data presented in this work has been collected using polymer films, which were coated on a conducting electrode. This section will first describe the process and considerations to be taken when forming these films, as well as the electrochemical techniques used throughout the body of this work.

2.2.1 Film Forming Techniques

As previously discussed, the morphology of conjugated polymer films can affect their redox and charge transport properties. For this reason it is important to take into consideration how the choice of coating method can affect the properties of the polymer film. In this work, three different coating methods are used to form films used in the electrochemical characterization experiments; drop-casting, spray-coating, and blade-coating. Drop-casting and blade-coating are techniques that allow for "slow" evaporation of solvent as compared to spray-casting.[110] Drop-casting is a technique in which polymer solutions are dropped onto a conducting substrate and allowed to dry. This technique is straightforward and can be done without the use of external equipment. Blade-coating on the other hand, is a technique where a doctor blade is dragged across a substrate at a constant speed.[111] This technique produces smooth films and has many variables that can be tuned to target a specific film thickness. For example, the gap-height, blade speed, and loading volume can be altered to give thicker or thinner films. It should be noted that all

polymer films analyzed and discussed in this dissertation that were blade-coated were formed in what is called the Landau-Levich regime. In this regime the doctor blade is dragged at a sufficiently fast speed such that a wet film is formed first and subsequent solvent evaporation deposits the final film. Finally, spray-casting is a technique where a polymer solution is carried by a gas onto the target substrate.[110] This technique allows for polymer films to be coated on substrates that are both non-planar and large in area, but can result in films that are rougher when compared to blade-coating.

2.2.1.1 Procedures for Making Polymer Solutions and Preparing Films

Depending on the electrochemical technique, polymer solutions were prepared at various concentrations in either toluene or chloroform. For techniques such as differential pulse voltammetry (DPV), cyclic voltammetry (CV), and *in situ* conductance, dilute polymer solutions were prepared at a concentration of 1 mg mL^{-1} and drop-cast onto glassy-carbon button electrodes. For techniques such as spectroelectrochemistry, polymer films were formed through either spray or blade-coating, and dissolved at concentrations of either 5 mg mL^{-1} or 30-40 mg mL^{-1}, respectively. Given that the blade-coating solutions were quite viscous, all polymer solutions in this work were used without further filtration. When performing spectroelectrochemical experiments, polymer films were cast onto ITO-glass substrates (24 mm x 75 mm x 0.7 mm, sheet resistance 8-12 Ω sq^{-1}, Delta Technologies, Ltd) that were pre-rinsed and sonicated in solutions of sodium dodecyl sulfate-water, water, acetone, and finally isopropanol, and allowed to air dry. Films were spray-cast using an Iwata-Eclipse HP-BC airbrush with nitrogen as the carrier gas (10-20 psi). Films were blade-coated using a custom blade-coater built in-house, using a gap height of 100 μm and various coating speeds from 10-40 mm/s depending on the solution

viscosity. Details on how the in-house blade coater was constructed can be seen in the Ph.D. thesis of Dr. Jeff Hernandez.[112]

2.2.2 Performing Characterization of Electroactive Polymers

In general, all of the electrochemical characterizations discussed in this dissertation had the same set-up, which is a three-electrode electrochemical cell. The three electrodes in the cell include: the working electrode (WE), counter electrode (CE), and reference electrode (RE). In all measurements, polymer films coated on a conducting electrode (such as a glassy carbon button) served as the WE, a platinum flag served as the CE, and the organic RE consisted of a 10mM $Ag/AgNO_3$ solution in 0.5 M $TBAPF_6$ with acetonitrile as the solvent. In any following figures, the potentials are plotted versus "Ag/Ag^+", which refers to this organic RE. This reference was periodically calibrated versus the Fc/Fc^+ redox couple, and is reported in the appendix after each chapter. The electrolyte used in all measurements consisted of a solution of 0.5 M $TBAPF_6$ dissolved in PC. All electrochemical characterization was performed using either a Princeton Applied Research 273 potentiostat/galvanostat (DPV, CV, spectroelectrochemistry) or a Pine bipotentiostat (model AFCBP1) under control of the Aftermath software (electrochemical conductance, chronoabsorptometry).

2.2.2.1 Voltammetric Measurements

In this work, two primary voltammetry experiments were used: DPV and CV. The difference between these two experimental methods lies in how the potential is applied.[113] In DPV, the potential is applied in a square-wave function, whereas in CV the potential is swept linearly at a constant rate. In DPV, the current is also sampled just

before the application of the next pulse. This is advantageous in that it allows for the decrease of the capacitive current (arising from charging from the electrolytic double-layer), and measures the faradaic current (arising from redox processes at the WE). In this dissertation, DPV is used to determine the onset of oxidation, whereas CV is used to understand both the reproducibility of redox cycling and the amount of charge in a polymer film.

In both DPV and CV, a waveform is used to apply a time-dependent potential between the WE and RE in the electrochemical cell, and the resulting current between the WE and CE is measured as a function of that potential. When applying an oxidizing (positive) potential, electrons are removed from the polymer film and pass through the potentiostat to the CE. On the contrary, when applying a reducing (negative) potential, electrons are removed from the CE, and pass through the potentiostat to the WE. Simultaneous to the movement of electrons during oxidation or reduction, ions and solvent molecules from the electrolyte are either moving in or out of the polymer film. It is for this reason that conjugated polymer films can experience a "break-in" effect.[28,114] This "break-in" effect is what causes subsequent CV or DPV scans to show lower onsets of oxidation than the first scan of the experiment. Unless otherwise noted, all voltammetry data presented in this work is of broken-in polymer films.

2.2.2.2 Electrochemical Conductance

In addition to the voltammetric techniques listed above, electrochemical conductance measurements were also used to understand the charge transport properties of the conjugated polymers in this work. This technique differs from the ones above, in

that polymer films are coated onto interdigitated microelectrodes, to serve as the WE in a four-electrode electrochemical cell.[115,116] The advantage of the use of interdigitated electrodes is that it is possible to hold a potential difference constant on one half of the electrodes (WE1), while at the same time sweeping the potential +/- 5 mV across the other half of the electrodes (WE2) and measuring the resulting current. Following Ohm's law, we can calculate the slope of this current versus potential curve to give the resistance of the material across the insulating portion between each digit of the electrode. The reciprocal of this resistance is the conductance of the polymer. A set of representative electrochemical conductance curves for the DOTT-DMP polymer (Chapter 5) can be seen in Figure 2.2-1.

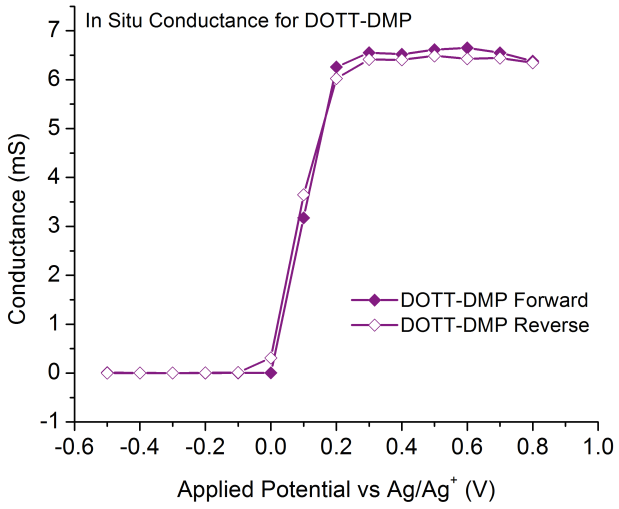

Figure 2.2-1 – Representative electrochemical conductance curve for the polymer DOTT-DMP (Chapter 5). Forward scan is from -0.5 to 0.8 V and reverse scan is from 0.8 to -0.5 V. Measurements made in a 0.5 M $TBAPF_6$ electrolyte in propylene carbonate.

Using this technique we can understand the potential dependent conductance of these polymer films. One thing to note, is that typically the conductance response for a

given polymer will occur at a higher potential than the determined onset of oxidation from DPV. This is due to the fact that in order to conduct charges across the insulating portion of the electrode, the polymer needs to be in a sufficiently conducting state, which may occur at a higher potential than the onset of oxidation determined through DPV. Another general trend for conductance measurements is that typically at high potentials, the conductance of the polymer will drop off slightly, or return to 0 mS. This is because at high potentials many charges are generated and therefore collectively the mobility of all the charges is decreased, thereby decreasing the conductance value. Interestingly, this is not observed for DOTT-DMP as shown in Figure 2.2-1.

2.2.2.3 Spectral Electrochemical Techniques

Given that the optical properties of conjugated polymers are dependent on their redox state as discussed in Chapter 1, it is important to understand their spectral response as a function of their doping level. For this reason, two primary spectral electrochemical techniques are employed to understand these relationships: spectroelectrochemistry and chronoabsorptometry.

2.2.2.3.1 Spectroelectrochemistry

Spectroelectrochemistry is a technique in which an electrochemical cell (set up in a cuvette) is placed in the path of the beam in a spectrophotometer, so that spectral data can be collected as the potential of the electrochemical cell is altered. In this experiment, polymer films are either spray or blade-coated onto ITO/glass substrates, which serve as the WE in the electrochemical cell. The RE, CE, and electrolyte are the same as in the electrochemical experiments mentioned above. It is important when setting up this

experiment to ensure that no wires are blocking the beam path of the spectrophotometer through the electrochemical cell, as this will affect the overall absorbance spectrum. For all data presented in this document, spectroelectrochemical data were collected using an Agilent Techenologies Cary 5000 UV-Vis-NIR spectrophotometer under Cary WinUV control. Data were recorded at a wavelength range between 320-1800 nm. This window allows for the observation of the depleted neutral state, and the generation of the polaron and bipolaron charge carrier states in the polymer film.

Data collection for this experiment is simple. First, the polymer film is broken-in with 5 CV cycles, then a constant potential is applied. After an equilibration period (~30s), the resulting spectrum is recorded. Typically the data for this experiment are taken over the sample potential range as the CVs. Generally, spectra are recorded every 100 mV over the full potential range, but smaller increments may be used if necessary. A full spectroelectrochemical series for DOTT-BiEDOT can be seen in Figure 2.2-2. It is only necessary to break the film in once, but an equilibration period is required when each new potential is applied in order to ensure an absorbance spectrum that is representative of the polymer film at that potential. In this work, all of the spectra corresponding to a full potential range for one polymer are plotted together. Typically, potentials of interest are highlighted as they pertain to certain redox processes or redox states of the polymer. Data from these measurements can also be used to understand the potential dependent bleaching or coloration trends of polymer films. For plots of this nature, absorbance values at a specific wavelength are recorded for each polymer at each potential and plotted together. This type of plot is an easy way to directly compare the potential-dependent doping trends for a group of polymers.

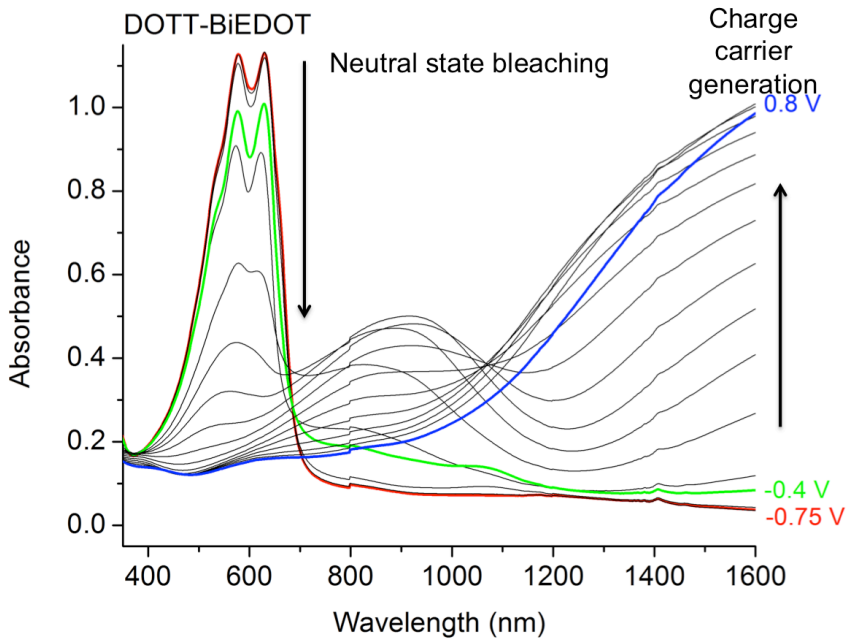

Figure 2.2-2 – Representative spectroelectrochemical data for the polymer DOTT-BiEDOT (Chapter 5) from a potential range of -0.7 to 0.8 V vs Ag/Ag^{+}.

2.2.2.3.2 Chronoabsorptometry

Chronoabsorptometry is similar to spectroelectrochemistry in that it is also a technique where an electrochemical cell is placed in a spectrophotometer, and polymer film absorption (or transmission) is monitored as a function of applied potential. An example of the data taken for this measurement is shown in Figure 2.2-3 for the polymer Pro-EH (Chapter 4). In this case, only the absorption of the polymer film at one specific wavelength (usually λ_{max}) is recorded. While spectroelectrochemistry is a static technique, chronoabsorptometry is dynamic. Throughout this measurement, the potential is altered between two extremes (typically -0.5 and 0.8 V vs Ag/Ag^{+}) at varying pulse lengths. In this work, the pulse lengths investigated are 60, 30, 10, 5, 2, 1, and 0.5 seconds. This allows us to better understand the rate of the doping reaction for polymer films. From this data, doping times can be calculated, as well as plots depicting the

relationship between pulse length and absorbance. All data presented in this work were collected using an Ocean Optics USB2000+ fiber optic spectrophotometer.

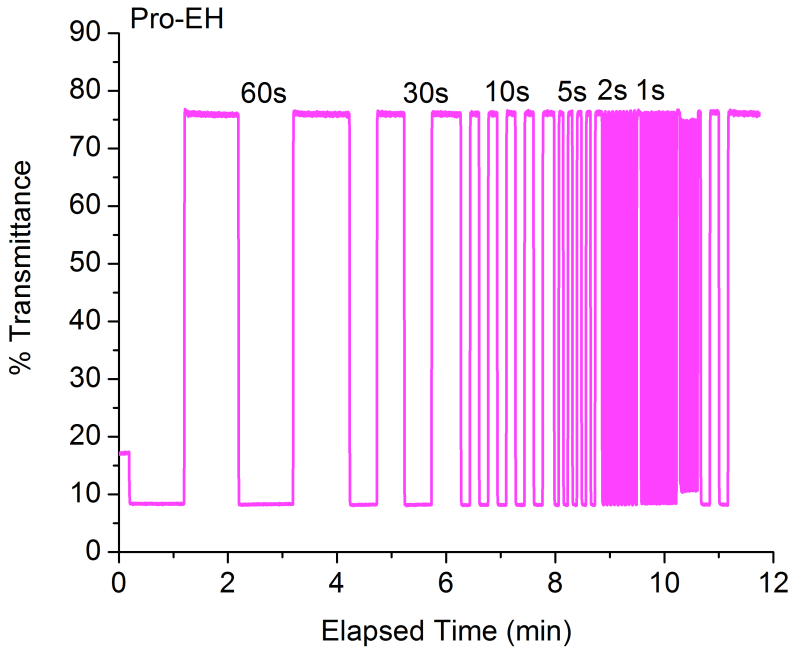

Figure 2.2-3 – Representative chronoabsorptometry data for the polymer Pro-EH (Chapter 4), between extreme potentials of -0.5 and 0.8 V vs Ag/Ag^{+}. Pulse lengths shown are 60, 30, 10, 5, 2, 1, and 0.5 seconds.

2.3 Solid-State Characterization Techniques of Dry Polymer Films

In addition to the electrochemical characterizations, a series of characterization experiments were performed on as-cast and oxidized polymer films in order to probe: 1) polymer film morphology and degree of intermolecular ordering, 2) the solid-state in-plane electrical conductivity, and 3) the atomic composition of these samples. The techniques discussed in this section include: grazing-incidence wide-angle x-ray scattering (GIWAXS), the Van der Pauw method of measuring in-plane solid-state conductivity, and x-ray photoelectron spectroscopy (XPS). Sample preparation for all of

these experiments was identical in that polymer films were blade-coated onto either Si or glass substrates (which had been cleaned according to the procedure mentioned above). In the case of the chemical oxidation experiments, which will be detailed further in this section, polymer films were dried in a vacuum oven under full vacuum at 50°C for 15 hours prior to the measurement.

2.3.1 Grazing-Incidence Wide-Angle X-ray Scattering (GIWAXS)

Grazing-incidence wide-angle x-ray scattering (GIWAXS) is a measurement technique that is used to investigate the structural properties of thin films.[86,117,118] In this experiment, an x-ray beam irradiates a sample at a fixed angle and is elastically scattered by the atoms in the sample. X-rays are well-suited for this purpose because radiation in this region of the electromagnetic spectrum has wavelengths on the order of Angstroms, which is the same length scale as the physical features that we are attempting to measure with this technique. Typically, the beam energy of the x-ray is reported rather than its wavelength. When a wavelength of light is irradiated and scattered from a sample that has features at that same length scale, interference takes place. Constructive interference patterns captured by the scattering detector can provide information about the degree of polymer order and the orientation of these ordered domains. A schematic for the set up of this experiment and the information that can be extracted from its interference pattern can be seen in Figure 2.3-1. Peaks along the Q_z direction show information about polymer chains that are stacking in a direction perpendicular to the surface of the substrate (out of plane), and peaks along the Q_{xy} direction show information about polymer chains that are stacking in a direction that is in plane with the surface of the substrate.

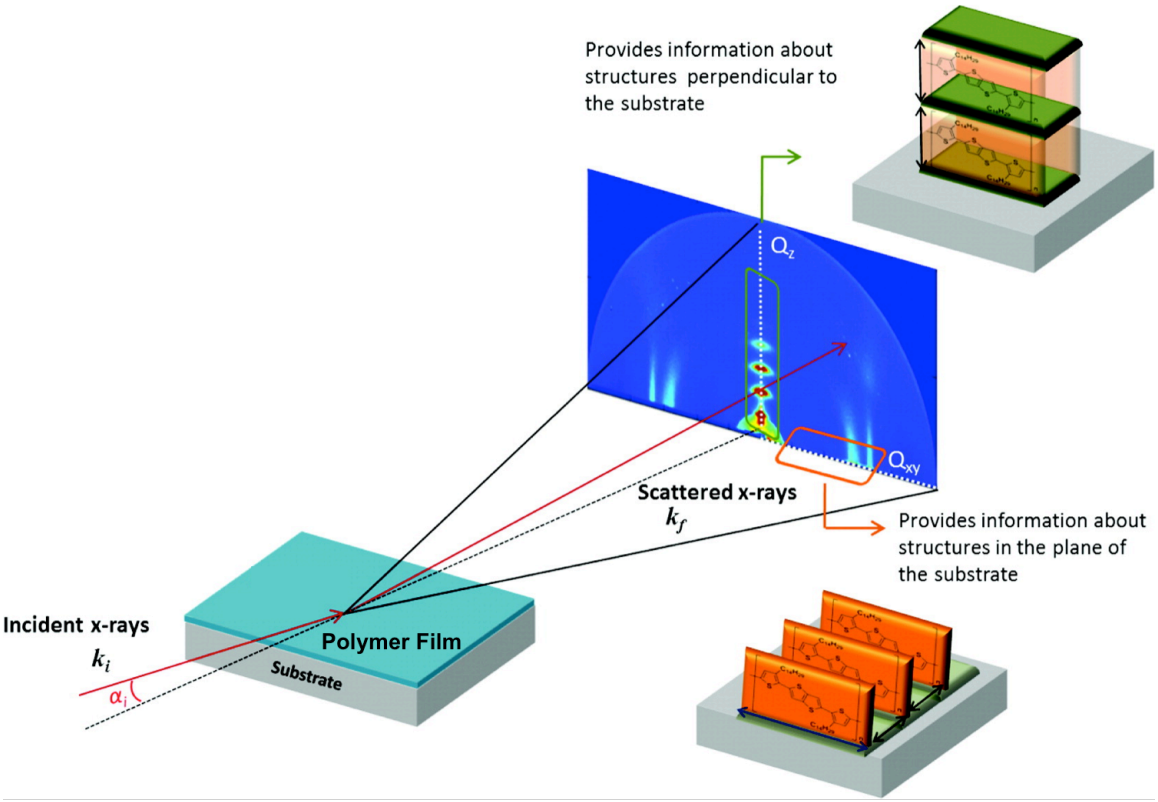

Figure 2.3-1 – Schematic of the experimental GIWAXS set up, example scattering pattern, and information in regards to the polymer chain ordering that can be extracted from GIWAXS scattering patterns. Reprinted with permission from the work by Cho *et al.*[119] © 2012 American Chemical Society.

The angle at which the x-ray beam is irradiating the sample (angle of incidence) is critical for the success of this experiment. This angle (α_i) should be above that of the critical angle of the sample, but below the critical angle of the substrate so that scattering information can be obtained for the bulk of the polymer sample. Critical angles are material dependent, and determined by the mean refractive index of the material. When analyzing scattering images it is also important to remember that the scattering intensity is proportional to the thickness of the sample. When plotting these images for comparison, the scattering intensity should be normalized for the thickness of the sample.

Some examples of different types of intermolecular ordering and how they affect the scattering patterns of GIWAXS experiments can be seen in Figure 2.3-2. In general, a more "spread-out" or "halo-like" scattering peak represents polymer films that are more amorphous.

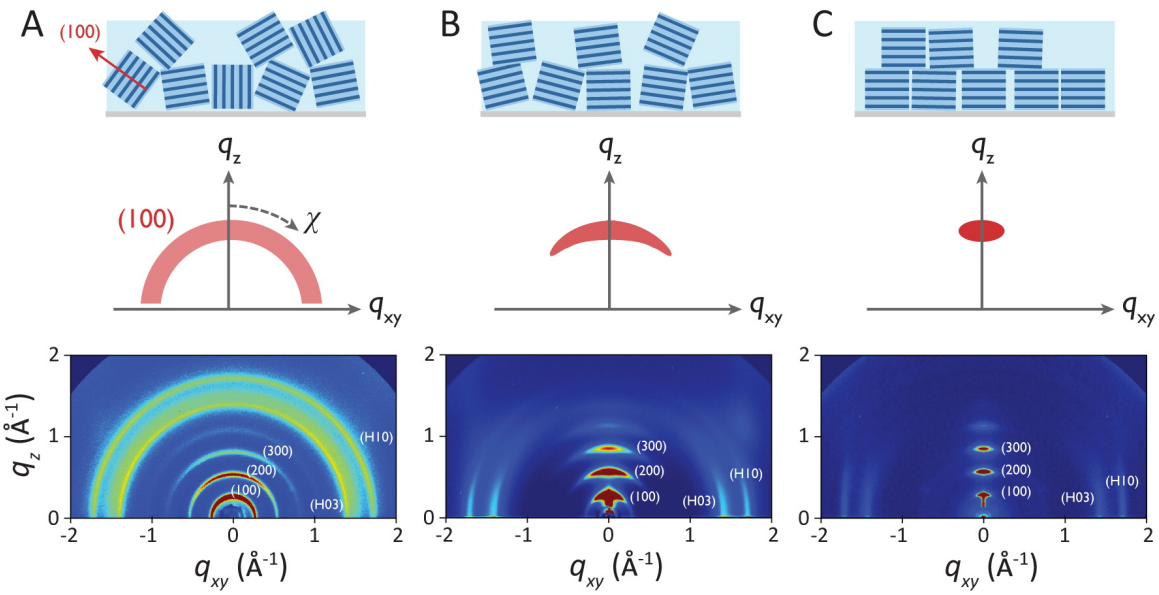

Figure 2.3-2 – Cartoons of various types of intermolecular ordering for conjugated polymer domains and the corresponding representative GIWAXS scattering patterns. Reprinted with permission from Rivnay *et al.*[86] © 2012 American Chemical Society.

Part A in Figure 2.3-2 shows an example of an amorphous sample. Here we see polymer crystallites that are highly disordered and oriented in different directions. This type of ordering results in a scattering pattern that is spread out over all angles of the image because the various crystallites are scattering the incident beam at many different angles. Moving to part B in Figure 2.3-2, we see a scattering pattern that is narrower in terms of its angular distribution. This is because the ordered polymer domains are have a more regular orientation relative to the substrate. The majority of these domains also stack in a direction that is perpendicular (out of plane) relative to the surface of the substrate, which

is why we see many peaks along the Q_z axis. Finally, part C of Figure 2.3-2 shows a highly ordered polymer film, where all of the ordered domains are stacking in the same direction and at the same angle relative to the surface of the substrate. We see very narrow and high intensity peaks along the Q_z direction and very little angular distribution. Given these general concepts, GIWAXS image analysis is quite complicated and care should be taken when attempting to interpret these scattering patterns.

Linecuts of the scattering image can be used to calculate the intermolecular stacking distances in the polymer film. As stated above, this grazing-incidence wide-angle technique can be used to calculate inter-plane distances on the order of angstroms. It is useful for conjugated polymers in that it can provide stacking distances in the lamellar (100) and π- π stacking (010) regions, and degree of crystallinity. Linecuts are taken along these axes and used to calculate inter-plane distances using Bragg's equation [$q = (2\pi)/d$], where q is the scattering vector and d is the inter-plane distance. Gaussian fits to the linecut are used to calculate the full width half maximum (FWHM) of the peaks and to calculate the crystal coherence length (L) of the crystalline domains using the Scherrer equation (Equation 2),

$$FWHM\ (2\theta) = \frac{k\lambda}{Lcos(\theta)} \tag{2}$$

where K is the Scherrer constant, λ is the wavelength of the x-rays, and θ is half of the diffraction angle. The crystal coherence length is the average size of the ordered domains from the first order (100) peak and can be used to estimate how many chains are aligned for a given direction.

GIWAXS experiments presented in this dissertation were performed at the Stanford Synchrotron Radiation Lightsource (SSRL) on beamline 11-3. In order to get access to these synchrotron sources, beam line proposals must be submitted to the relevant center. The procedures for submitting beam line proposals can be found at the SSRL website (www-ssrl.slac.stanford.edu). All samples were prepared as described above, but on Si wafers that were washed with the same cleaning procedure as when using glass substrates. On beamline 11-3, samples were irradiated with x-ray energy of 12.7 keV, and their scattering patterns were recorded using a 2-D image detector (MAR345 image plate detector). Typical exposure times were between 60-240 s. Exposure times are determined based on the intensity of the scattering pattern of the sample. For example, if a sample had a very high scattering signal, the exposure time should be decreased so that the detector is not damaged. The distance between the sample and detector was kept constant at 250 nm and the incident angle was maintained at 0.13° in order to achieve the highest scattering intensity from the sample without interference from the substrate (polymer critical angle ~0.08°). The scattering images were calibrated using a LaB_6 standard. Samples were loaded into a chamber and purged with helium in order to reduce damage to the sample and reduce the air scattering background. All data shown in this dissertation was taken with the x-ray beam normal to the blade-coating direction. The data analysis for Chapter 4 was conducted with WxDiff software developed by Dr. Stefan Mannsfeld.[120] The data analysis for Chapter 5 was conducted using the Nika software package for Wavemetrics Igor, in combination with WAXStools.[121,122] WxDiff is a software package that is more straightforward to use (and

the process of taking linecuts is simpler), however the Igor software package produces plots that are easier to customize.

The images presented in this dissertation are considered to be reproducible as multiple samples of the same polymer and doping condition were run and showed the same diffraction patterns. When planning trips to the beamline it is important to bring multiple samples because: 1) samples may be compromised during transportation, and 2) it is necessary to confirm if a scattering pattern for a given sample is reproducible. To obtain comparable data, samples should be analyzed at the same distance from the detector (as this determines the angle at which the scattered x-rays hit the detector) and purged with an inert gas such as helium to reduce any damage to the sample.

2.3.2 Chemical Doping and Solid-State Conductivity

All chemical doping experiments, and the subsequent solid-state conductivity measurements were performed in air. Samples were prepared as mentioned above on clean glass substrates, using blade-coating as the film casting technique. All dopants were dissolved in PC in an argon-filled glovebox (with the exception of F4TCNQ) at varying concentrations. Dopant solutions were drop-cast onto polymer films and left to sit for 30s unless otherwise noted. Subsequently, each film was rinsed with clean methanol and dried in the vacuum oven as mentioned previously. All solid-state sheet resistance measurements were taken using a Van der Pauw geometry with a Keithley 2400 source meter.

The advantage of this method is that it is able to accurately measure the properties of a sample of any shape, however there are a number of required properties. In order to

conduct this experiment, the sample must be: 1) of a flat shape of uniform thickness, 2) much thinner than it is wide, and 3) solid. Furthermore, the contacts must be placed along the perimeter of the sample. This is a four-point probe method that provides the average resistance of sample and is able to account for contact resistance. To make a measurement, the current is allowed to flow across two of the electrodes, and the voltage is measured across the other two. From these two values, and by using Ohm's law, the resistance of the sample can be calculated. This process is then repeated using all combinations of electrodes in order to get an average resistance for the sample, which is then normalized for the sample film thickness and used to calculate the in-plane conductivity of the sample in S cm^{-1}.

For the work presented in Chapter 4, metal contacts were deposited onto dry chemically doped polymer films through a shadow mask by thermally evaporating 10 nm of Cr followed by 90 nm of Ag. For the work presented in Chapter 5, four gold contact pads (1 mm x 1mm ~100 nm thick) were deposited onto dry chemically doped polymer films using a shadow mask and a home-built DC sputtering chamber. Contact pad and film thicknesses were measured using a Profilm 3D optical profilometer.

2.3.3 X-ray Photoelectron Spectroscopy (XPS)

X-ray photoelectron spectroscopy (XPS) is a surface sensitive quantitative spectroscopic technique performed under high vacuum, which provides information about the atomic composition of a sample. In this technique, samples are irradiated with a beam of x-rays that cause a number of electrons to be ejected from the inner shell (core electrons) of the elements in the top 1-10 nm of the sample. The detector measures the

kinetic energy of these ejected electrons. From this value, and the law of conservation of energy (Equation 3), the binding energy of each electron can be calculated,

$$E_{binding} = E_{photon} - (E_{kinetic} + \phi) \quad (3)$$

where $E_{binding}$ is binding energy, E_{photon} is the energy of the photons of the x-ray generated from the x-ray source, $E_{kinetic}$ is the measured kinetic energy of the electrons, and ø is the parameter representing the energy required for the electron to be liberated from the surface of the material. This binding energy can be related to a specific orbital of a given element.

After the high-resolution elemental XPS spectra are collected, plots of the binding energy versus counts of electrons can be made. An example plot for this type of data can be seen in Figure 2.3-3. These plots collectively represent the various species in the sample. Shifts in the binding energy can be due to different elements being bound to the element being analyzed, or in the case of conjugated polymers this could be due to parts of the sample that are in a different redox state. Typical spot sizes are on the order of hundreds of microns, so it is not possible to spatially resolve areas of the sample that may be in different oxidation states. For this reason, spectra need to be de-convoluted into a series of Gaussian peaks, and the overall sum of these peaks should reflect the shape of the experimentally collected data.

After the experimental data have been fit, the area of the overall curve can be used to calculate the atomic abundance for a given element using Equation 4,

$$AA = \frac{A_{rel}}{RSF * KE^{0.6}} \quad (4)$$

where AA is the atomic abundance, A_{rel} is the integrated area for the fits of each peak in the high-resolution elemental spectra, RSF is the relative sensitivity factor for each element, and KE is the kinetic energy of the x-ray radiation. RSF is a factor that has been calculated for each element and is proportional to the element's weight, as XPS is a technique that is more sensitive for heavier elements.

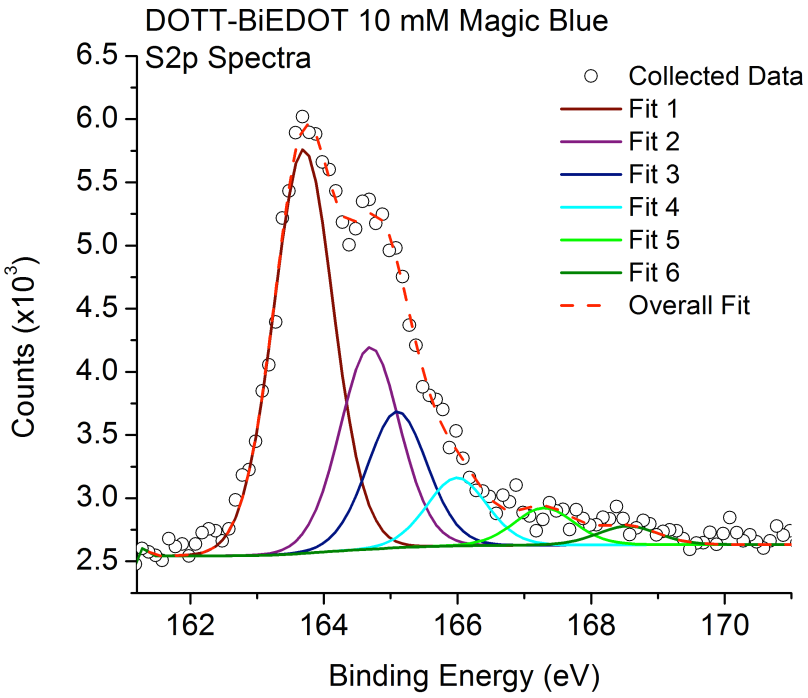

Figure 2.3-3 – Example XPS spectra and fits for the S 2p orbital of a DOTT-BiEDOT polymer film (Chapter 5) that has been chemically oxidized with a 10 mM solution of Magic Blue in propylene carbonate for 30 seconds. Open circles represent the experimentally collected data and the dashed red line represents the overall fit of the experimental data. Area of overall fit is used to calculate abundance values.

This factor is used to scale the relative peak areas so that they more accurately represent the amount of material that is in the sample. These values are standard and can be looked up in XPS manuals or textbooks.

In this work, XPS spectra were recorded using a Thermo Fisher K-Alpha Photoelectron Spectrometer, with a monochromatic Al Kα source (energy = 1487 eV) and a hemispherical 180° detector. Samples were positioned with the electron takeoff angle normal to the surface of the sample, with respect to the analyzer. In all spectra, a low energy electron "flood gun" was used to maintain sample charge neutrality during the experiment. Specific spectra recorded for each sample in this dissertation are in the appendix after the chapter in which they appear. Elemental spectra were recorded with a pass energy of 50 eV and a dwell time of 50 ms. The spot size for analysis was 400 μm. Depth profile experiments were performed using an argon ion gun, with a beam energy of 3000 eV and high current, for etch times of 50 s. The raster size used for depth profiling was 1 mm. After each etching step, survey scans and high-resolution elemental scans were performed as described above. Curve fitting and elemental ratio calculations were carried out on the high-resolution elemental spectrum of each sample, using the curve fit feature of the XPS analysis software, Casa XPS.

CHAPTER 3. CHEMICAL OXIDATION OF POLYMER ELECTRODES FOR USE IN REDOX-ACTIVE DEVICES

The work presented in this chapter could have not been made possible without the scientific input from Dr. Anna Österholm and Dr. Eric Shen. In this chapter, we will be examining the use of chemical oxidants and phosphonic acids as pre-treatment steps in the construction of electrochemical devices, and will describe what considerations need to be taken for this process and how this method can be used in the manufacture of redox-active devices. Major accomplishments in this work include: (1) the novel process and success of chemical oxidation as a pre-treatment in scalable electrochemical device construction, (2) the relationship between the properties of the polymer and effects of chemical doping, and (3) the concept that chemical doping could cause film delamination, but this effect can be rectified through the use of a surface energy modification step such as the use of phosphonic acid treatments. This chapter is adapted from the reference "Chemical Oxidation of Polymer Electrodes for Redox Active Devices: Stabilization through Interfacial Interactions", which was published in the ACS Journal of Applied Materials and Interfaces in 2017.[123]

3.1 Background and Motivation

This section will describe the number of applications for electrochemical devices involving organic conjugated polymers (CPs), which could benefit from scalable processing. To properly understand the experimental design of this work, a discussion of

the way redox-active electrochemical devices function, and routes of polymer electrode oxidation is necessary.

3.1.1 Applications of Redox Active Devices

As discussed in Chapter 1, the versatility of CPs has been realized[8,124] for a variety of electrochemical applications such as electrochromic devices (ECDs)[125-128] and pseudocapacitive CP supercapacitors,[129-131] as well as actuators[132-135] and sensors,[136,137] due to their ability to transport both electrons and ions. CPs are also of interest for biomedical applications due to their ability to immobilize bioactive ions during electrochemical synthesis.[138-141] In many of the studies focusing on redox applications, the CP is be directly deposited onto electrodes in its oxidized state through electropolymerization and is typically strongly adhered to the underlying electrode substrate, even films exceeding several microns in thickness.[142-145] Regardless of the electrodeposition method, electropolymerized films are prepared swollen with solvent molecules and ions, and have adopted a morphology that is templated by the electrolyte used during synthesis. This is a benefit in the construction of electrochemical devices in that polymer electrodes can be produced in the specific oxidation state that is needed for optimal device operation.

3.1.2 Device Architecture and Need for Scalable Device Processing

Emphasis has been placed on developing soluble, yet highly redox active, polymers that can be deposited via roll-to-roll compatible processing methods.[26] In order to construct electrochemical devices using films prepared in this manner, it is important to ensure that the active materials can be coated to a sufficient thickness without

compromising adhesion, and that they have a morphology that supports fast ion diffusion similar to electropolymerized analogs. During operation of a two-electrode electrochemical device, optimal operation relies on opposing and charge-balanced redox reactions occurring at the respective electrodes. In the case of a device incorporating two p-type materials, as the example shown in Figure 3.1-1 demonstrates, the CP^0 to CP^+ reaction occurring in one half-cell (Electroactive Polymer 1, pink) is balanced by a CP^+ to CP^0 reaction occurring in the other half-cell (Electroactive Polymer 2, blue).

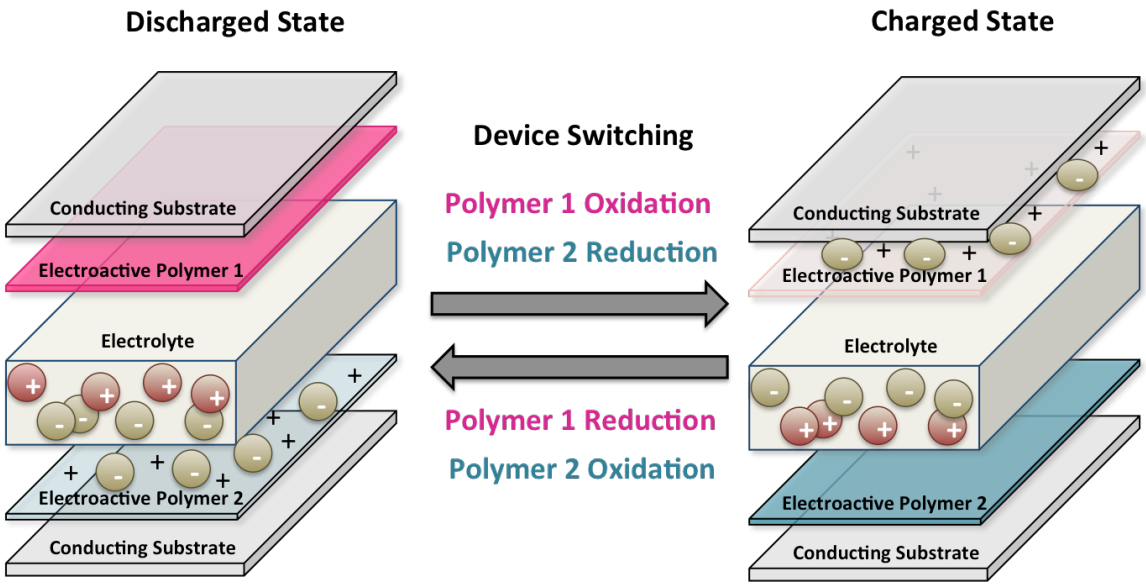

Figure 3.1-1 - Illustration of an electrochemical device incorporating p-type conjugated polymers, showing the oxidation states of each electrode in the two extreme operating voltages.

As such, in addition to the soluble polymer needing to have sufficient film thickness and substrate adhesion, one of the CP layers must be converted from its as-cast charge-neutral state into its oxidized state before device assembly. While the redox state of a thin CP film can be accurately set via application of an electrochemical potential,[99] this approach is not compatible with high-throughput roll-to-roll coating. Here, we show

that chemical oxidants can be used to controllably dope one of the polymer-coated electrodes in a more scalable fashion. Additionally, chemical doping ensures that at least one of the films is swollen with ions prior to device assembly.

3.1.3 Understanding Mechanisms of Chemical Doping

In both gas and solution phase oxidative doping of CP films, the dopant counter ion generated remains in the polymer film after doping, the nature of which greatly affects polymer properties, such as conductivity and morphology.[8,39,124,146-154] While chemical doping of polymer films for control of solid-state properties has been reported on extensively, the impact of doping polymer films for use in electrochemical devices has not been explored. Specifically, the adverse effects of using chemical doping as a post-processing method have not been evaluated with respect to its impact on the reversibility and/or stability of the polymer electrodes. Changing the polymer oxidation state, and incorporating ions into an as-cast neutral CP film using a chemical oxidant directly impacts its hydrophobicity, and potentially the morphology of the polymer film via solvent and ion swelling, which can alter the substrate-polymer interactions and lead to film delamination. During redox switching there is a constant flux of these ions and solvent molecules that force the polymer film to contract and expand,[131,155-157] which can further increase the mechanical stress and promote physical degradation and/or film delamination ultimately leading to a loss of device performance.[131,158-162]

3.1.3.1 Considerations of Chemical Oxidation on Device Operation

Here, we evaluate the effect of chemical doping as a post-processing method on the physical properties and redox behavior of two dioxythiophene-based copolymers (DOTs),

and one dioxypyrrole-based polymer (DOP), to demonstrate the applicability of using this method on polymers with a range of oxidation potentials. The DOP was included in this study as it typically reaches higher doping levels than DOTs.[163] In this work, we have evaluated a family of chemical oxidants that vary in both the oxidizing power and final form (solid metal or soluble ion) of the oxidizing agent, as well as the structure of the counterbalancing anion. We show that the oxidation potential of the polymer determines the overall extent of oxidation, and also plays a role in the degree of mechanical stress endured by the polymer film during this post-processing step. Unexpectedly, we show that the strength of the chemical dopant is not directly correlated with the extent of oxidation of the polymer. Finally, we demonstrate how to strengthen the polymer-substrate interface by using an alkylphosphonic acid treatment of a transparent metal oxide (ITO) that tunes the hydrophobicity of the substrate and improves polymer adhesion.[164,165]

3.2 Structure-Property Relationships of Polymer and Dopant Family

When studying the chemical oxidation of CPs for use in electrochemical applications, there is a need to understand not only how to control the oxidation state of the film, but also to ensure that any pre-treatment does not compromise the mechanical adhesion of the film at the electrode interface, as the film must continue to repeatedly expand and contract during device operation. To evaluate the efficacy of the Ag(I) and Fe(III) dopants to achieve the desired oxidation state, as well as to ensure that the proposed chemical oxidation step is applicable to different systems, we used three conjugated polymers that are highly disordered and have noticeably different oxidation potentials. In addition, the three polymers shown in Figure 3.2-1 were selected due their

previous use in both electrochromic devices (all three)[166,167] and supercapacitors (P(ProDOT$_2$-EDOT$_2$)).[78]

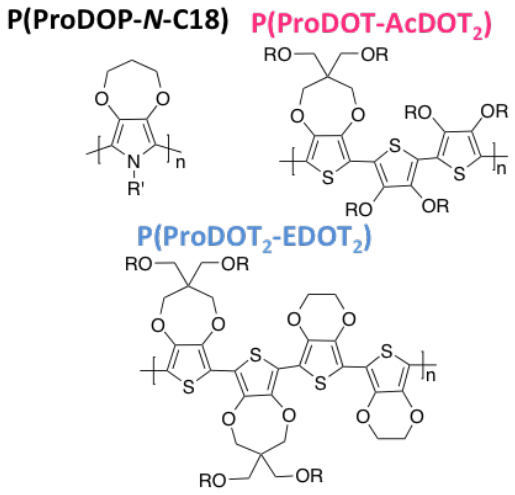

Figure 3.2-1 - Repeat unit structures of the polymers used in this study. Alkyl groups denoted with R stand for the 2-ethylhexyl branched chains, and R'=$C_{18}H_{37}$ linear chains.

The onset of oxidation of the polymers was probed by cyclic voltammetry in 0.5 M TBAPF$_6$/PC and a direct comparison is shown in Figure 3.2-2. The unfunctionalized EDOT units in P(ProDOT$_2$-EDOT$_2$) afford a sterically relaxed backbone that can easily planarize, resulting in a polymer with a low onset of oxidation (-0.6 V vs Ag/Ag$^+$). By replacing the EDOT units with alkoxy-functionalized, acyclic dioxythiophene (AcDOT) units in P(ProDOT-AcDOT$_2$), we increase the steric strain, which in turn increases the oxidation potential by 0.8 V compared to the EDOT analog (E_{onset} = 0.2 V vs Ag/Ag$^+$). The dioxypyrrole polymer P(ProDOP-*N*-C18) displays the highest degree of twist between repeat units of the three polymers, but is sufficiently electron-rich to maintain an intermediate onset of oxidation (-0.2 V vs Ag/Ag$^+$). Based on these results we expect P(ProDOT$_2$-EDOT$_2$) to be the easiest to chemically oxidize and P(ProDOT-AcDOT$_2$) to be the most difficult. P(ProDOP-*N*-C18) is interesting as it not only has an intermediate

oxidation potential, but also because pyrroles tend to require higher doping levels than DOTs to become fully oxidized.

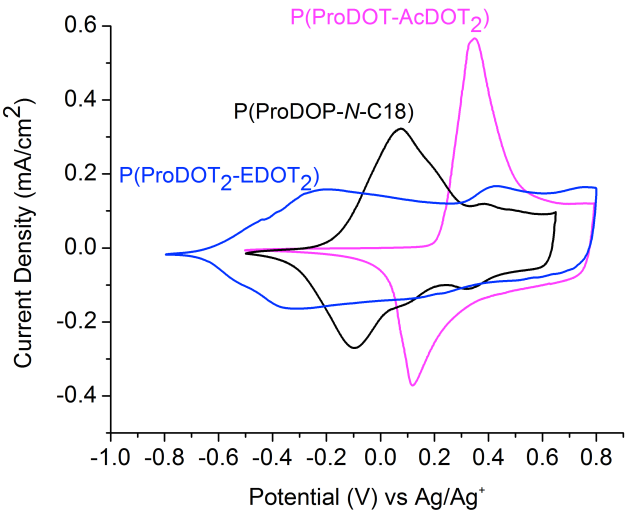

Figure 3.2-2 - Cyclic voltammograms of P($ProDOT_2$-$EDOT_2$) in blue, P(ProDOP-*N*-C18) in black, and P(ProDOT-$AcDOT_2$) in pink, performed in a three-electrode cell in 0.5 M $TBAPF_6$/PC at 50 mV/s.

As discussed in Chapter 1, the absorption profile of a CP changes as a function of its oxidation state (electrochromism), allowing us to monitor both the doping level and any changes related to film delamination simultaneously with optical absorption spectroscopy. The absorption profiles of the CPs as a function of the applied potential are shown in Figure 3.2-3 for P(ProDOP-*N*-C18) and in Supporting Figure 3-1 for P(ProDOT-$AcDOT_2$) and P($ProDOT_2$-$EDOT_2$).

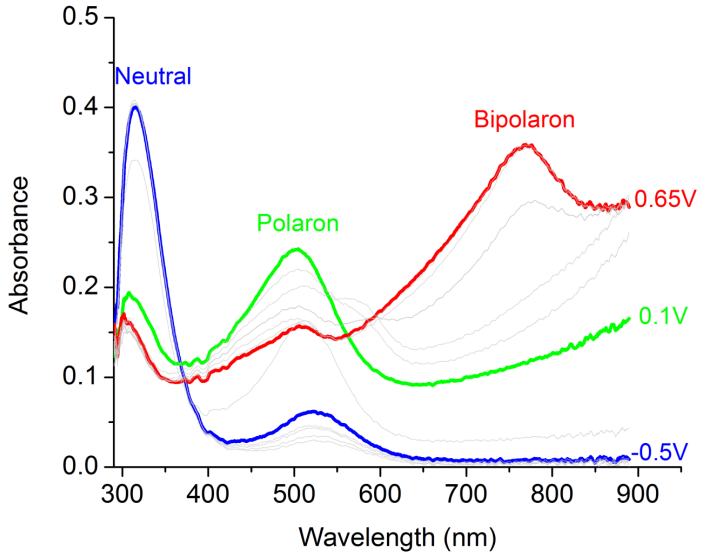

Figure 3.2-3 - UV-Vis absorption spectra as a function of potential for a spray-cast film of P(ProDOP-*N*-C18) on ITO/glass in 0.5 M $TBAPF_6$/PC.

At -0.5 V in Figure 3.2-3, P(ProDOP-*N*-C18) is in its neutral form, with an absorbance λ_{max} at 325 nm (the minor absorbance at 520 nm is due to the break-in cycling performed prior to data collection and can produce a small number of trapped polaronic charge carriers). At an intermediate potential of 0.1 V, the polymer is partially oxidized and polaronic charge carriers (cation radicals) are generated along the backbone, with a new absorption band appearing at 500 nm. At 0.65 V, the polymer film is fully oxidized as indicated by the new absorption at 750 nm, originating from bipolaronic charge carriers (dications), and the almost complete depletion of the π-π* transition and lower intensity of the polaron band. Because CPs exhibit such large changes in absorption profile as a function of oxidation state, regardless of the method of doping, monitoring film absorbance is a straightforward way to qualitatively assess the doping level.

Two common oxidizing agents of different strengths were selected to dope the three polymers: Ag(I), which is a fairly strong oxidizing agent ($E_{1/2}$ between 0.4 to 0.5 V in propylene carbonate vs Ag/Ag^+ which uses an acetonitrile medium), and Fe(III), which is a weaker oxidizing agent ($E_{1/2}$ between -0.2 to -0.1 V vs Ag/Ag^+). The $E_{1/2}$ values were determined by cyclic voltammetry (see Supporting Figure 3-2) using Ag/Ag^+ as the reference electrode, where a higher $E_{1/2}$ value corresponds to a higher oxidant strength. As illustrated in Figure 3.2-4, using the oxidation process of P(ProDOP-*N*-C18) as an example, the chemical oxidation of a conjugated polymer is accompanied by the reduction of the oxidizing agent either from Ag^+ to Ag^0 or Fe^{3+} to Fe^{2+}. In the case of the silver oxidant, reduction results in the formation of solid Ag^0, which can potentially remain inside the polymer film, whereas the reduction of iron results in a soluble ion that can be rinsed out. In addition to comparing different oxidants, we also evaluated different charge balancing counter anions (hexafluorophosphate (PF_6), trifluoromethanesulfonate (OTf), and *p*-toluenesulfonate (Tos)) as the size of the anion is expected to affect the extent of oxidation, the polymer film integrity, and the film-electrode interface.

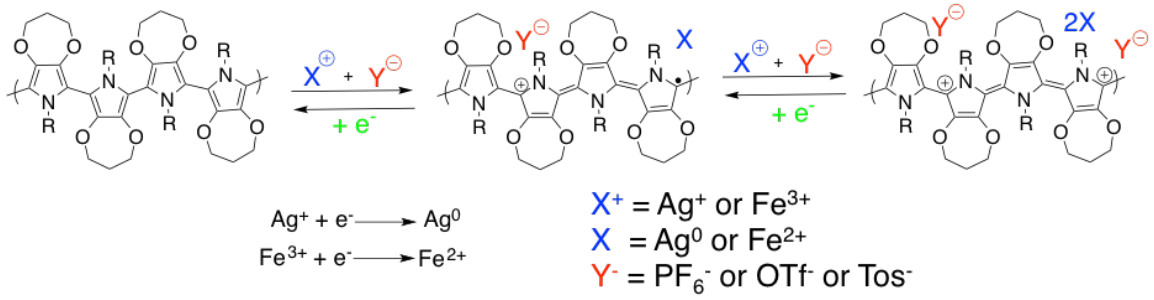

Figure 3.2-4 - An illustration of the doping mechanism with P(ProDOP-*N*-C18) as an example polymer.

3.2.1 Qualitatiave Extent of Doping using Optical Absorption

The oxidation state of a chemically doped film can be evaluated, qualitatively, by comparing its absorption spectra to a corresponding spectrum of a film under potentiostatic control, as illustrated with P(ProDOT-AcDOT_2) in Supporting Figure 3-3 where the spectrum of a chemically oxidized film is identical to the electrochemically oxidized analog, indicating the same level of oxidation is attained in each case for this polymer-dopant system. For these tests, films were immersed in dopant solutions for 20 minutes to ensure complete oxidation, though as seen in Supporting Figure 3-4, a shorter time of doping could be used. As seen in Figure 3.2-5, Fe(III)OTf oxidizes P(ProDOT-AcDOT_2) (the most difficult of the three polymers to oxidize) to a greater extent than AgOTf, as there is still a significant residual absorption at 528 nm corresponding to the π-π* transition of the neutral polymer in the latter case, while the peak is almost completely absent after doping with Fe(III)OTf. A similar, yet less extreme, effect is seen for P(ProDOP-*N*-C18) (Figure 3.2-5b) where the π-π* transition has decreased substantially with exposure to both dopants, but a residual polaron peak at 500 nm, is still observed for the film doped with AgOTf. There is no observable polaron peak for the film doped with Fe(III)OTf, and comparing this spectrum with the corresponding spectrum obtained through electrochemical oxidation (see Figure 3.2-3), confirms that the polymer is in its fully oxidized form. Turning to the last polymer in our family, exposing P(ProDOT_2-EDOT_2) to either AgOTf or Fe(III)OTf, depletes the π-π* transition, and the spectra match the corresponding spectrum for a film that has been electrochemically oxidized (Supporting Figure 3-1a).

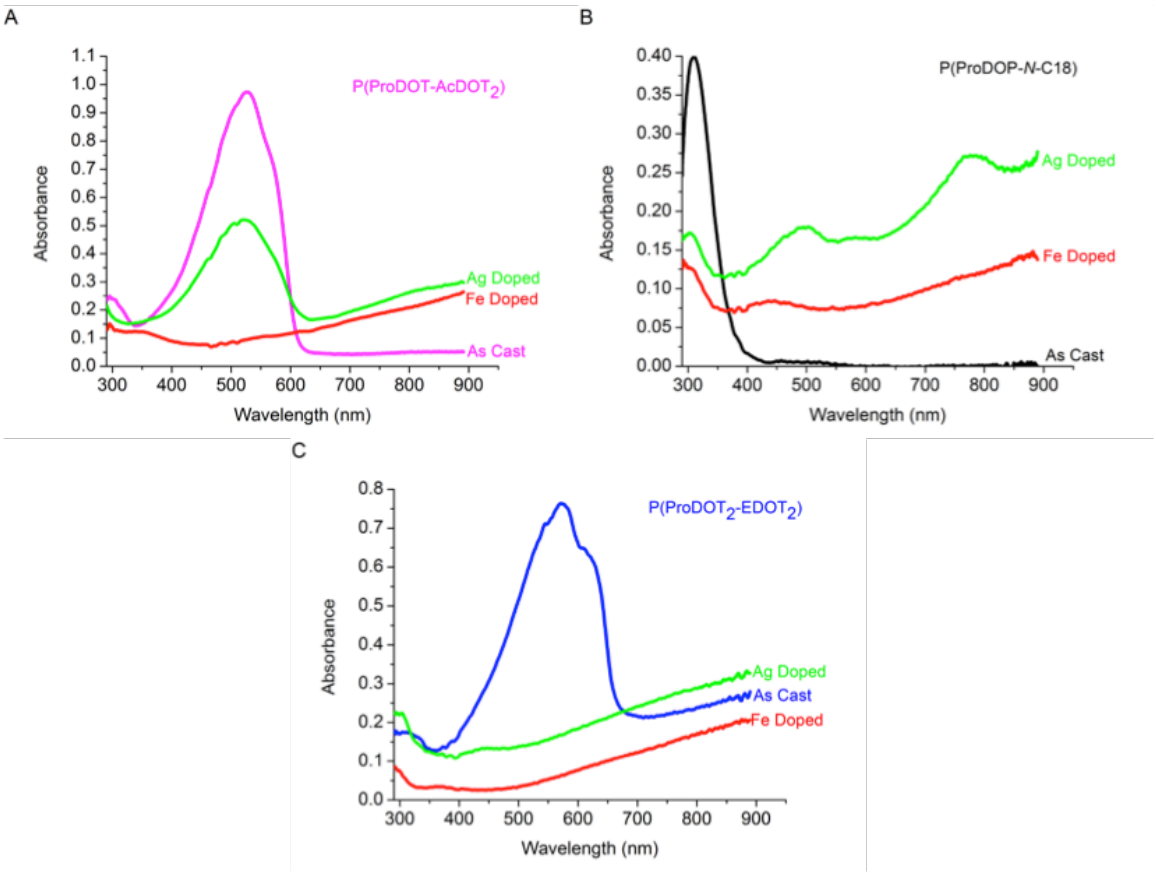

Figure 3.2-5 - UV-Vis absorption spectra for spray-cast films of P(ProDOT-AcDOT$_2$) (A), P(ProDOP-*N*-C18) (B), and P(ProDOT$_2$-EDOT$_2$) (C) on ITO/glass in the as-cast and chemically oxidized states after exposure to 10 mM solutions of either AgOTf or Fe(III)OTf$_3$ in propylene carbonate. Doping times of 20 minutes for (A) and (B), 30 seconds for (C).

The absorbance data shows that the iron and silver dopants can oxidize both the DOTs and the DOP to varying degrees, but that surprisingly, the extent of doping is not determined by the strength of the dopant. Fe(III) is a weaker dopant relative to Ag(I), but can dope all the polymers more effectively. The extent of doping was not dependent on the counterbalancing anion, as similar doping levels for P(ProDOP-N-C18) were reached for both AgOTf and $AgPF_6$, based on the similarity of the absorption spectra shown in Supporting Figure 3-5. On the other hand, the onset of oxidation of the polymer plays a larger role as to how effectively the polymer can be doped. Based on the spectra in Figure

3.2-5, P(ProDOT$_2$-EDOT$_2$), having the lowest oxidation potential, is most effectively doped by Ag(I), followed by the ProDOP derivative. P(ProDOT-AcDOT$_2$), the polymer with the highest oxidation potential, is the only one that still retains charge-neutral domains after being exposed to AgOTf.

3.2.2 Quantitative Extent of Doping using XPS

To quantify the extent of doping, oxidized P(ProDOP-*N*-C18) films were evaluated by XPS, which allowed us to calculate the ratios of sulfur:fluorine, sulfur:nitrogen, and fluorine:nitrogen as sulfur and fluorine are found exclusively in the triflate group in AgOTf and Fe(III)OTf and nitrogen is found exclusively in the pyrrole ring of P(ProDOP-*N*-C18). The doping ratios were calculated from the individual elemental atomic abundance values, as determined by integrating the fits of the high-resolution XPS spectra for each element, found in Supporting Figure 3-6. Examining Table 3-1, there is a consistent difference of a factor of three between the abundance values of sulfur and fluorine, which is expected considering the structure of the triflate group.

Table 3-1 – Elemental abundance values and doping ratios calculated from integrated XPS spectra.

Dopant Used	F 1s Atomic %	S 2p Atomic %	N 1s Atomic %	S:F	S:N	F:N
AgOTf	57	16	36	0.30	0.44	1.6
Fe(III)OTf	59	18	32	0.30	0.56	1.8

Furthermore, from the XPS spectra we were able to determine that the P(ProDOP-*N*-C18) film doped with AgOTf incorporated two charges for every five rings, whereas the film doped with Fe(III)OTf incorporated three charges for every five rings. This data is in agreement with the absorbance spectra discussed above, where it was also shown that Fe(III) oxidized P(ProDOP-*N*-C18) to a greater extent than Ag(I).

XPS was also used to verify that the dopants were able to access the bulk of the films. Figure 3.2-6 shows the XPS depth profiling results of P(ProDOP-*N*-C18) doped with AgOTf, (Figures 3.2-6a and 3.2-6b) or with Fe(III)OTf (Figures 3.2-6c and 3.2-6d).

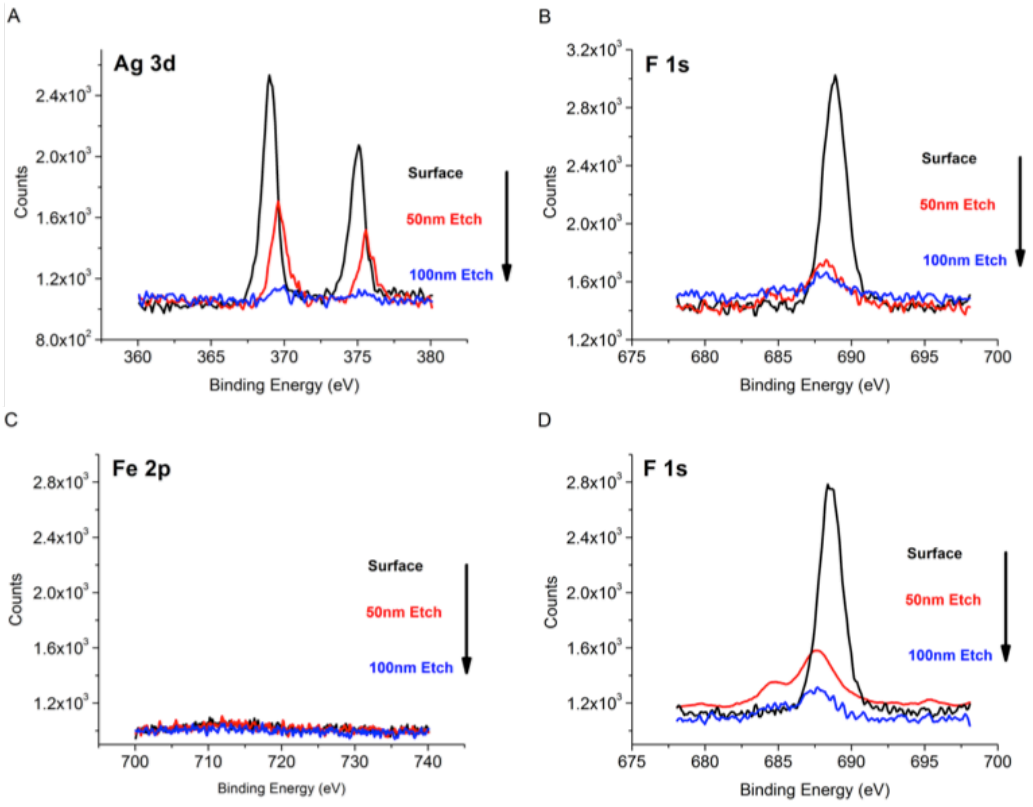

Figure 3.2-6 - X-ray photoelectron spectroscopy spectra for spray-cast P(ProDOP-*N*-C18) films on ITO/glass, doped with 10 mM solutions of either AgOTf [(A)&(B)] or Fe(III)OTf$_3$ [(C)&(D)] in propylene carbonate for 20 minutes. Part (A) includes the binding energy range for silver's 3d orbital, parts (B)&(D) include the binding energy range for fluorine's 1s orbital, and part (C) includes the binding energy range for iron's 2p orbital.

According to Figures 3.2-6a and 3.2-6b, both silver and fluorine are present throughout the bulk of the film. Because P(ProDOP-*N*-C18) is in its oxidized state, we expect a high concentration of fluorine to be present from the counterbalancing triflate ion. However, during oxidation Ag^{+} is reduced to Ag^{0} that is not soluble in PC and therefore remains in the film even after rinsing. For Fe(III)OTf (Figure 3.2-6c), on the other hand, there is no iron present in the bulk of the film, which means that the Fe^{2+} species formed during the oxidation step is rinsed out with PC. This figure highlights three important findings, (i) both the silver and the iron oxidants can access the bulk of the film (Figures 3.2-6b and 3.2-6d), (ii) the films remain in their fully oxidized state even after rinsing with PC showing that counter ions can be loaded into the film post-processing, and (iii) as long as the oxidant species that is formed is soluble, it can be effectively washed out of the film using a simple rinsing step.

3.2.3 Polymer Electrode Stability

In addition to understanding the extent of oxidation that can be achieved via chemical doping, it is important to understand how this processing step affects the long-term redox switching stability of these materials as thin electrode-supported films, as that is a critical property for any electrochemical device. Redox stability was evaluated by cyclic voltammetry between its fully neutral and fully oxidized states, where charge density for each film was monitored over 900+ cycles. Figure 3.2-7a shows a loss of charge retention for all pre-oxidized films over the course of 900 cycles. The stability trend for the polymers correlates with their onset of oxidation. P(ProDOT$_2$-EDOT$_2$) with the lowest onset of oxidation was not stable at all as the film actually delaminated as soon as it was immersed in the electrolyte solution. P(ProDOP-*N*-C18) with an intermediate

oxidation potential, was able to retain 20% of its original value after 900 cycles, whereas P(ProDOT-AcDOT$_2$) has the highest onset of oxidation, and at the end of the testing period retained ~ 90% of its charge capacity.

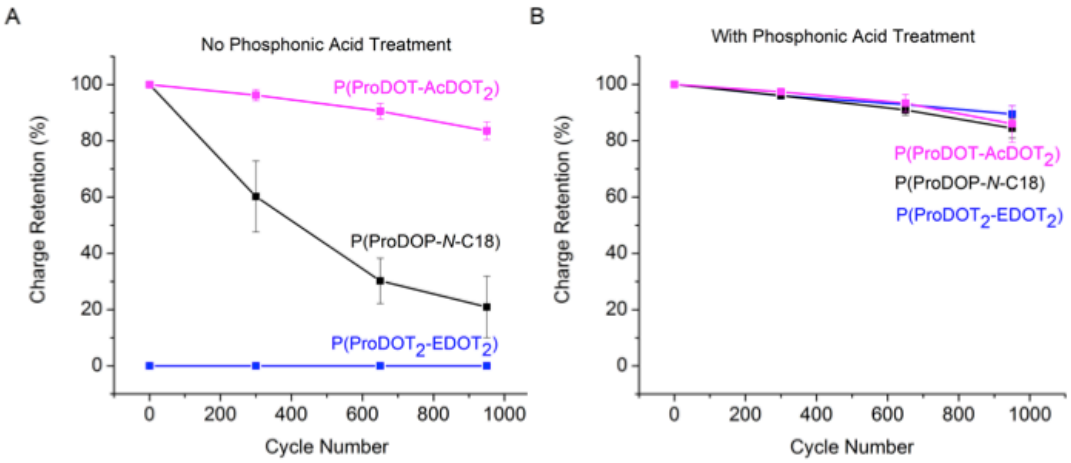

Figure 3.2-7 - Relationship between the charge retention and cycle number for spray-cast films of P(ProDOP-*N*-C18), P(ProDOT-AcDOT$_2$), and P(ProDOT$_2$-AcDOT$_2$) on ITO/glass after doping with 10 mM Fe(III)OTf$_3$/PC for 20 minutes. Prior to casting films, cleaned ITO/glass substrates were either used as-is (A) or dipped into a 2.5 mg/mL solution of phosphonic acid for 5 minutes (B).

The cyclic voltammograms used in charge density calculations for a P(ProDOT-AcDOT$_2$) film that had been doped with Fe(III)OTf$_3$ are shown in Supporting Figure 3-7. The decrease in current density indicates some loss in electroactivity, which could either be due to film delamination or a loss of redox activity, as will be discussed in more detail below. Supporting Figure 3-8, using P(ProDOP-*N*-C18) as an example, shows that the stability is primarily dependent on the oxidizing species (as the films doped with Fe(III) exhibit a larger loss of charge retention than those doped with Ag(I)) rather than the counterbalancing anion, as polymer films that were doped with the same oxidizing species had a similar charge retention over 900 cycles regardless of the nature of the counter ion.

The absorption spectra of P(ProDOT-AcDOT$_2$) in the charge neutral (colored) state taken before and after 900 cycles are the same, as shown in Supporting Figure 3-9, which means that the loss of charge retention is not due to a physical loss of polymeric material on the electrode. However, there are slight differences in in the oxidized state spectra, taken before and after doping. This coupled with the fact that there is a decrease in current density, suggests that there are small parts of the film that we cannot access electrochemically. Together, this data indicates that the polymer-electrode interface has been compromised during the pre-oxidation step with Fe(III)OTf, though the severity is polymer dependent.

3.2.3.1 Motivation and Use of Phosphonic Acids

As has been shown in the literature previously, phosphonic acid treatments can be used to enhance organic layer wetting, without inhibiting the performance of the conducting metal oxide electrode.[165] ITO is much more hydrophilic than the conjugated organic polymers, therefore it is beneficial to derivatize the substrate surface to be more hydrophobic to promote enhanced film-substrate interactions. Alkyl phosphonic acids are amphiphilic, and using them in a surface treatment helps to create a more hydrophobic surface. The difference in hydrophobicity between untreated (contact angle = 60°) and treated ITO/glass substrates (contact angle = 90°) is evidenced in Supporting Figure 3-10. As seen in Figure 3.2-7b, films of both P(ProDOT$_2$-EDOT$_2$) and P(ProDOP-*N*-C18) cast on phosphonic acid treated ITO/glass have greatly enhanced charge retention. After over 900 cycles, P(ProDOP-*N*-C18) and P(ProDOT$_2$-EDOT$_2$) are still able to retain over 90% of the original charge capacity, contrary to the untreated cases where the latter delaminates immediately upon immersion into the electrolyte solution.

The beneficial effects of phosphonic acid treatments are understandable from a chemical standpoint as well. Fe^{3+} is a strong Lewis acid in this case,[168] and is likely to interact with the oxide layer of the ITO/glass substrate, thus disrupting the substrate-polymer film interaction. When the substrate is coated with a layer of phosphonic acid, the ITO is protected and the substrate-polymer film interface is not compromised. While it is not clear why this effect is more exaggerated with polymers with lower onsets of oxidation, this phenomenon could be due to rapid incorporation of dopant molecules causing increased swelling, and higher degrees of mechanical stress as a result.

3.3 Use of Chemical Doping in Device Construction

In order to understand how chemical doping can be used as a post-processing step in the fabrication of an electrochemical device, chemically oxidized P(ProDOP-*N*-C18) films and P(ProDOT-$AcDOT_2$) films were incorporated into a colored to clear electrochromic device using the architecture shown in Figure 3.1-1. This type of electrochromic device was targeted as it can visually indicate the effects and success of chemical oxidation as a post-processing step. Incorporating these two polymers together allows for a device that is able to switch from a colored to a colorless state, where any residual color contributions originating from delamination or incomplete switching can be easily quantified spectroscopically. Photographs and switching speeds of these devices after 900 cyclic voltammograms are pictured in Figure 3.3-1; photographs of these devices after five cyclic voltammograms are pictured in Supporting Figure 3-11.

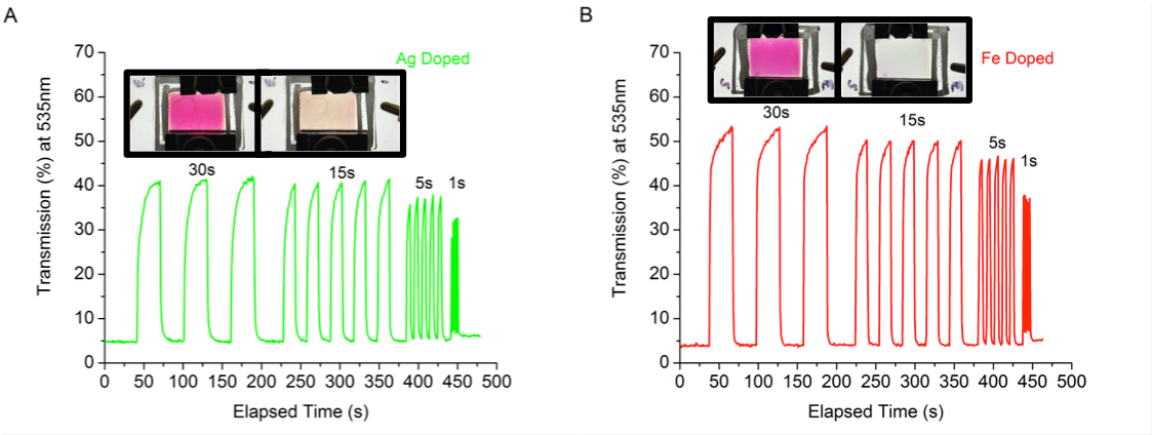

Figure 3.3-1 - Comparisons of switching speeds for magenta-to-clear ECDs, pictured colored [left] and bleached [right], where the P(ProDOP-*N*-C18) has been chemically oxidized with (A) AgOTf or (B) Fe(III)OTf$_3$ before device assembly. The devices consist of spray-cast films of P(ProDOT-AcDOT$_2$) and P(ProDOP-*N*-C18) on phosphonic acid treated ITO/glass as the electrodes and a gel electrolyte consisting of 0.5 M TBAPF$_6$/PC with 6 wt% PMMA. Prior to device construction, the P(ProDOP-*N*-C18) films were reacted with 10 mM solutions of either AgOTf (A) or Fe(III)OTf$_3$ (B) in propylene carbonate for 20 minutes.

When considering the optical properties of the devices, before and after the stability test, both the device contrast and the switching speed during bleaching and coloration, were maintained. Switching speed and contrasts were calculated by recording the differences in the % transmittance of the device at λ_{max} (540nm) at extreme potential differences of -1 V and 1 V. When comparing Supporting Figure 3-11 and Figure 3.3-1a, the device incorporating P(ProDOP-*N*-C18) oxidized with AgOTf does have some additional color contributions in the colorless state, which become more pronounced over the course of repeated switching. On the other hand, the device incorporating an electrode pre-oxidized with Fe(III)OTf$_3$ as shown in Figure 3.3-1b, does not have any color contributions in the colorless state and has a contrast that is 10% higher than the other device. The additional color contribution in the device where P(ProDOP-*N*-C18) is doped with AgOTf is most likely due to the silver particles that are deposited in the film after

doping, which can scatter and absorb incident light, demonstrating that silver (or any other dopant that can absorb and scatter light) is not a desirable chemical oxidant for the purpose of constructing electrochromic devices. Both of these devices, however, greatly outperform devices where neither of the polymer layers have been chemically or electrochemically pre-oxidized.[99]

There are also electrochemical differences in device performance, as evidenced by the cyclic voltammograms of both devices in Figure 3.3-2.

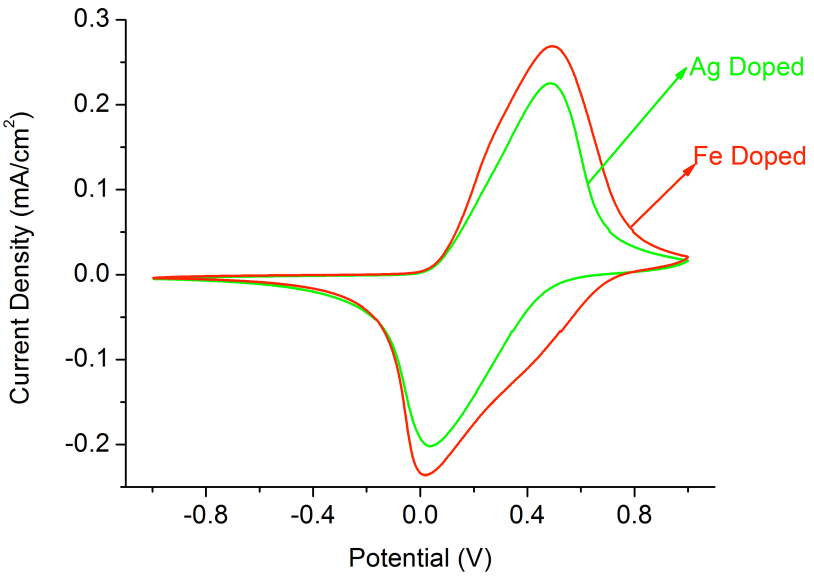

Figure 3.3-2 - Cyclic voltammograms, after 3 break-in scans, of devices consisting of spray-cast films of P(ProDOT-AcDOT$_2$) and P(ProDOP-*N*-C18) on ITO/glass as the electrodes and a gel electrolyte of 0.5 M TBAPF$_6$/PC with 6 wt% PMMA. Prior to device construction the P(ProDOP-*N*-C18) films were pre-oxidized with a 10 mM solution of either AgOTf (green curve) or Fe(III)OTf$_3$ (red curve) in propylene carbonate for 20 minutes.

The device incorporating a film doped with Fe(III)OTf$_3$ has a charge capacity of 2.5 mC/cm^2 whereas the device that has a film pre-oxidized with AgOTf has a charge capacity of 1.8 mC/cm^2. This ~30% difference is a result of the silver oxidant not being

able to oxidize the P(ProDOP-*N*-C18) as effectively as Fe(III)OTf_3 (Figure 3.2-5b). This would not only result in a device that has a lower charge density, but is also explains the lower contrast measured for this device. These results highlight the importance of using a chemical oxidant that can fully oxidize the polymer in question. While a partial oxidation does lead to a working device, and full contrast may be attained after many switches, proper pre-oxidation leads to an optimally performing device immediately after construction.

3.4 Summary of Results

We have demonstrated that chemical oxidation involves many parameters when constructing electrochemical devices. Considering the electroactive polymers and dopants in this study, the polymer with the lowest onset of oxidation was most effectively doped, and the weaker, but more Lewis acidic, dopant oxidized the polymers to a higher degree (Fe(III) compared to Ag(I)). This chemical oxidation causes a disruption in the interaction and adhesion between the electroactive polymer film and substrate, leading to delamination, however this disruption can be rectified through the use of phosphonic acid treatments on the ITO/glass substrate. Finally, chemical oxidation has proven to be a post-processing step that is effective in constructing electrochromic devices (replacing a more tedious electrochemical method), however it is essential to choose an oxidant that can oxidize polymer electrodes to the furthest extent for superior electrochemical device performance immediately after assembly. The broad impact of this method is evident when considering the many soluble conducting polymers that have been made available and can be incorporated into electrochemical devices. A standard device construction can be imagined, where the conducting polymer that will be set in its oxidized state is

processed on an alkyl phosphonic acid treated ITO substrate, then subsequently oxidized by immersing in an Fe(III) dopant solution. After washing away the soluble Fe(II) ion, the oxidized film can be paired with a neutral conjugated polymer film yielding a device that should demonstrate full charging and discharging, as well as good stability over repeated cycling.

3.5 Experimental and Supporting Information

This supporting information section includes the experimental procedures and any supporting figures used in the discussion of the work presented in Chapter 3 of this dissertation.

3.5.1 Materials and Methods

Film formation. The synthesis and purification of the electrochromic polymers used in this study, referred to as P(ProDOP-*N*-C18)[166] (M_n = 96 kDa, PDI = 1.8), P(ProDOT-AcDOT$_2$)[167] (M_n = 176 kDa, PDI = 2.2), and P(ProDOT$_2$-EDOT$_2$)[167](M_n = 6 kDA, PDI = 1.5) have been described elsewhere. The polymers were dissolved at 5 mg mL^{-1} in either toluene P(ProDOP-N-C18) and P(ProDOT-AcDOT$_2$), or chloroform P(ProDOT$_2$-EDOT$_2$). Films were spray-cast using an Iwata-Eclipse HP-BC airbrush with nitrogen as the carrier gas (10-20 psi) onto ITO-glass substrates (7 mm x 50 mm x 0.7 mm, sheet resistance 8-12 Ω sq^{-1}, Delta Technologies, Ltd) that were pre-rinsed and sonicated in sodium dodecyl sulfate-water, DI water, acetone, and isopropanol, and then allowed to air dry. Some ITO slides were dipped into a 10 mM solution of 1-dodecylphosphonic acid (95%, Alfa Aesar) in ethanol for 5 minutes and subsequently rinsed with clean ethanol. P(ProDOP-*N*-C18) films were cast were cast to an optical

density of 0.4 ± 0.1 (40 %T) at 316 nm, P(ProDOT-AcDOT$_2$) films to 1.0 ± 0.1 (10 %T) at 528 nm, and films of P(ProDOT$_2$-EDOT$_2$) to 0.75 ± 0.1 (18 %T) at 566 nm. The optical density was monitored with an Ocean Optics USB2000+ spectrophotometer detector using an Ocean Optics DH-2000-BAL fiber-optic light source.

Chemical oxidation of polymer films. After casting, polymer films were dipped into dopant solutions consisting of propylene carbonate (99.5%, Acros Organics, purified using a solvent purification system from Vac Atmospheres), with dopant concentrations of either 0.001 M or 0.01 M. The dopants chosen for this study were silver (I) hexafluorophosphate ($AgPF_6$, 98%, Alfa Aesar, $E_{1/2}$= 0.4 V), silver (I) trifluoromethanesulfonate (AgOTf, 98%, Alfa Aesar, $E_{1/2}$= 0.5 V), iron (III) trifluoromethanesulfonate (Fe(III)OTf, 90%, Alfa Aesar, $E_{1/2}$= -0.1 V), and iron (III) *p*-toluenesulfonate hexahydrate (Fe(III)Tos, technical grade, Sigma Aldrich, $E_{1/2}$= -0.2 V). $E_{1/2}$ values were determined using cyclic voltammetry. All dopant solutions, except for the case with Fe(III)Tos, were prepared in an argon-filled glovebox. For Fe(III)Tos solutions, the dopant was weighed in air and the solvent was added under a blanket of argon. The various polymer films were immersed into the oxidant solutions under a blanket of argon for 20 minutes to ensure full doping. Subsequently, each film was thoroughly rinsed with clean propylene carbonate. When preparing samples for XPS analysis, films were placed into a vacuum oven at 50 °C for 18 hours under full vacuum to ensure all of the propylene carbonate was removed from the film.

Film characterization and instrumentation. The redox response of the films was characterized using cyclic voltammetry, performed in a three-electrode cell, using a

Princeton Applied Research 273 potentiostat/galvanostat, under CorrWare control. Optical characterizations were performed using a Pine bipotentiostat (model AFCBP1) in coordination with the Ocean Optics USB2000+ spectrophotometer. The electrolyte was 0.5 M tetrabutylammonium hexafluorophosphate ($TBAPF_6$, Acros Organics, 98%, recrystallized from hot ethanol) dissolved in propylene carbonate. A platinum flag served as the counter electrode, and an Ag/Ag^+ electrode (10 mM $AgNO_3$ and 0.5 M $TBAPF_6$ in acetonitrile, 0.085 V vs Fc/Fc^+) was used as the reference electrode. Charge retention values were calculated by integrating the cyclic voltammograms over the stable potential range of the polymer. Films were cycled 50 times prior to starting the stability experiments.

XPS spectra were recorded using a Thermo Fisher K-Alpha Photoelectron Spectrometer, with a monochromatic Al-Kα source (energy = 1487 eV) and a hemispherical 180° detector. Samples were positioned with the electron take-off angle normal to the surface of the sample, with respect to the analyzer. In all spectra, a low energy electron "flood gun" was used to maintain sample charge neutrality during the measurement. Spectra were recorded for the Ag 3d, F 1s, S 2p, N1s, and Fe 2p core levels using a pass energy of 50 eV, with a spot size of 400 μm. Depth profiles were performed using an argon ion gun, with a beam energy of 3000 eV and high current, for etch times of 50 seconds. The raster size used for depth profiling was 1 mm. After each etching step, survey scans and high-resolution elemental scans were performed as described above. Curve fitting and elemental composition calculations were carried out on the high-resolution elemental spectrum of each sample, using the curve fit feature of the XPS analysis software, CasaXPS. Doping ratios were calculated from the atomic abundance

values of each element, which were calculated according to Equation 1: $Atomic\ \% = \frac{A_{rel}}{RSF * KE^{0.6}}$ where A_{rel} is the integrated area for the fits of each peak in the elemental high-resolution spectra, RSF is the relative sensitivity factor for each element (F: 4.43, N:1.8, and S:1.68), and KE is the kinetic energy.

Device construction. To construct the electrochromic devices (ECDs), ECP films were spray-cast onto ITO-glass substrates (25 mm x 75 mm x 0.7 mm, sheet resistance 8-12 Ω sq^{-1}, Delta Technologies Ltd) to the optical densities listed above. Each device consisted of one pre-oxidized polymer electrode, one neutral polymer electrode with gel electrolyte (0.5 M $TBAPF_6$ in propylene carbonate and 6 wt% PMMA 996,000 Mn) sandwiched between. VHB foam acrylic tape (series 2946, 3M) was used as the gasket material. The pre-oxidized polymer electrode was prepared by drop-casting oxidant solution (concentration 0.01 M, prepared as described above) onto the polymer film under a blanket of argon and letting it sit for 20 minutes before subsequently rinsing with clean propylene carbonate. Photography was performed in a light booth that was illuminated by a D50 (5000K) lamp, using a Nikon D90 SLR camera with a Nikon 18-105 mm VR lens and is reported without further manipulation beyond photograph cropping.

3.5.2 Supporting Figures

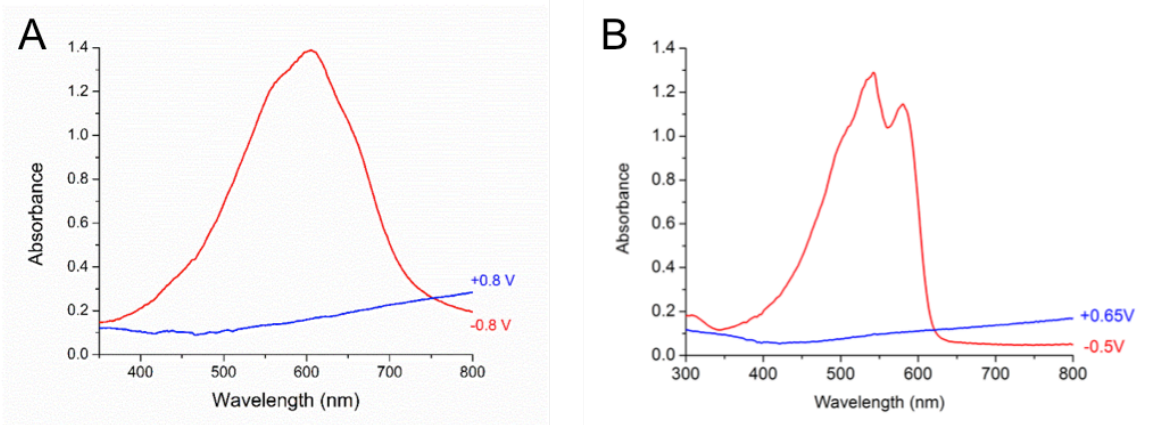

Supporting Figure 3-1 - Optical absorption spectra as a function of potential for spray-cast P(ProDOT$_2$-EDOT$_2$) (A) and P(ProDOT-AcDOT$_2$) (B) films on ITO/glass in 0.5 M TBAPF$_6$/PC

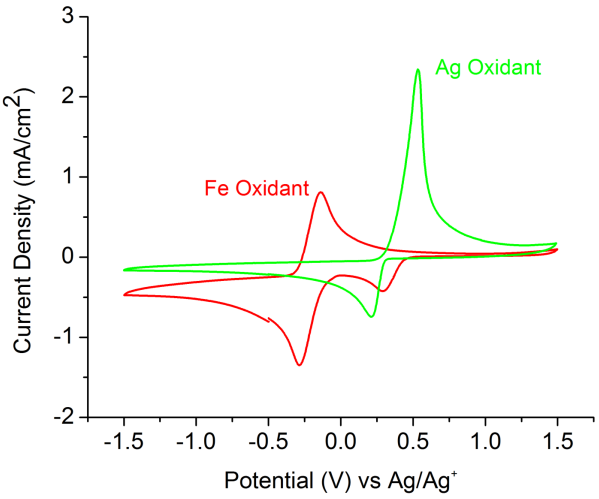

Supporting Figure 3-2 - Cyclic voltammograms for solutions of either AgPF$_6$ (green curve) or Fe(III)Tos$_3$ (red curve) in 0.5 M TBAPF$_6$/PC. A glassy carbon electrode was used as the working electrode, a platinum flag was used as the counter electrode, and an Ag/Ag$^+$ electrode was used as the reference. Experiments were performed in an inert atmosphere with scan rates of 50 mV/s.

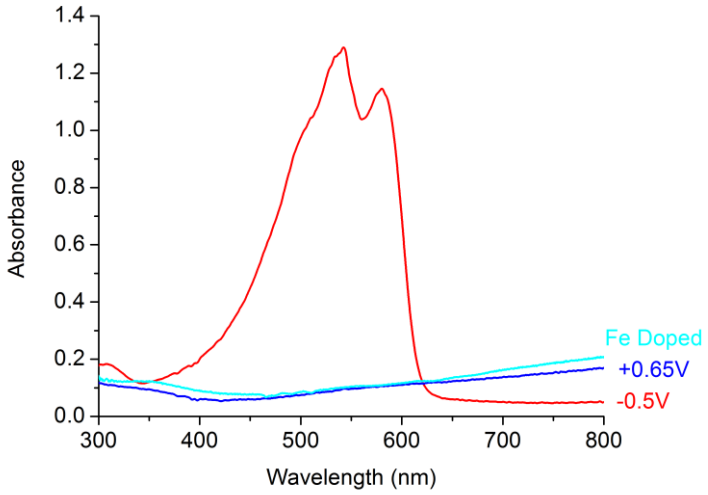

Supporting Figure 3-3 - UV-Vis absorbance spectra corresponding to a P(ProDOT-AcDOT$_2$) film doped with a solution of 10 mM Fe(III)OTf$_3$ in propylene carbonate for 20 minutes (cyan curve) and the optical absorbance spectra as a function of potential for a spray-cast P(ProDOT-AcDOT$_2$) film on ITO/glass in 0.5 M TBAPF$_6$/PC.

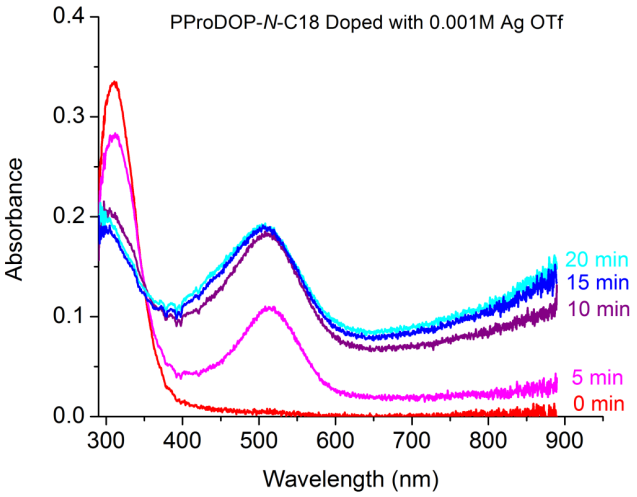

Supporting Figure 3-4 - UV-Vis absorbance spectra taken every 5 minutes for a film of P(ProDOP-*N*-C18) on ITO/glass after a reaction with a 1 mM solution of AgOTf in propylene carbonate.

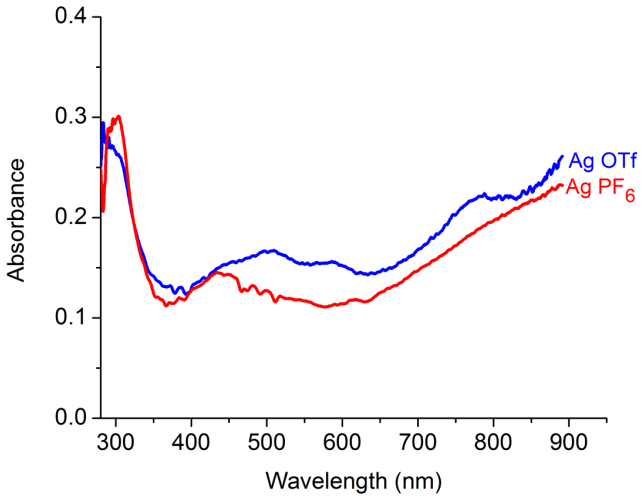

Supporting Figure 3-5 - UV-Vis absorbance spectra corresponding to P(ProDOP-*N*-C18) films doped wither with solutions of 10 mM AgOTf in propylene carbonate or 10 mM $AgPF_6$ in propylene carbonate for 20 minutes.

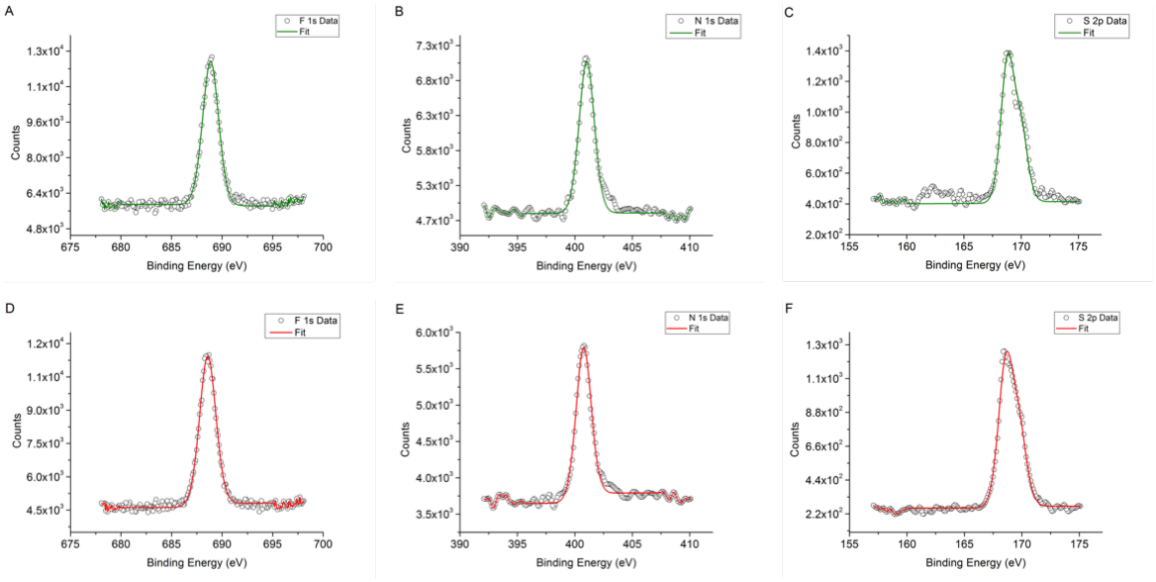

Supporting Figure 3-6 - XPS spectra in ranges for the F 1s orbital [(A)&(D)], N 1s orbital [(B)&(E)], and S 2p orbital [(C)&(F)] for P(ProDOP-*N*-C18) films that have been doped with either a 10 mM solution of AgOTf/PC [(A)-(C)], or a 10 mM solution of $Fe(III)OTf_3$/PC [(D)-(F)], for 20 minutes. After doping, polymer films were rinsed with clean propylene carbonate and dried under vacuum overnight at 50°C.

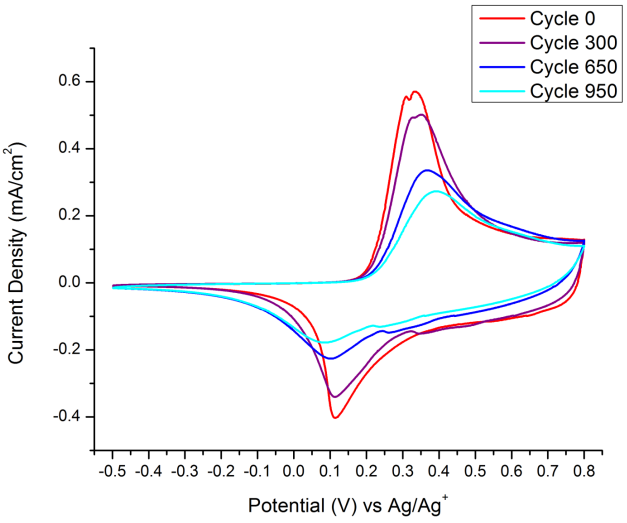

Supporting Figure 3-7 - Cyclic voltammograms for spray-cast films of P(ProDOT-AcDOT$_2$) on ITO/glass in 0.5 M TBAPF$_6$ in propylene carbonate. The polymer film/ITO/glass was used as the working electrode, a platinum flag was used as the counter electrode and an Ag/Ag$^+$ electrode was used as the reference. Experiments were performed with scan rates of 50 mV/s. Prior to electrochemical analysis the polymer films were oxidized with a 10 mM solution of Fe(III)OTf$_3$ in propylene carbonate for 20 minutes.

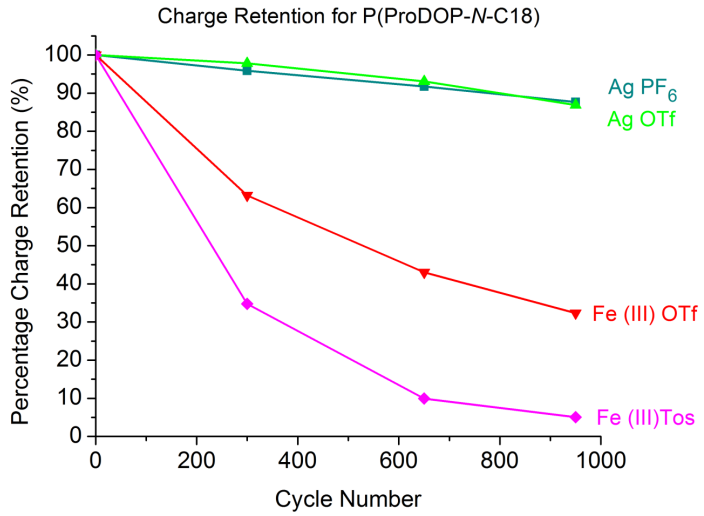

Supporting Figure 3-8 - Relationship of % of charge retention as a function of cycle number for spray-cast P(ProDOP-*N*-C18) films on ITO/glass that were doped with various solutions of dopants with a concentration of 10 mM in propylene carbonate for 20 minutes.

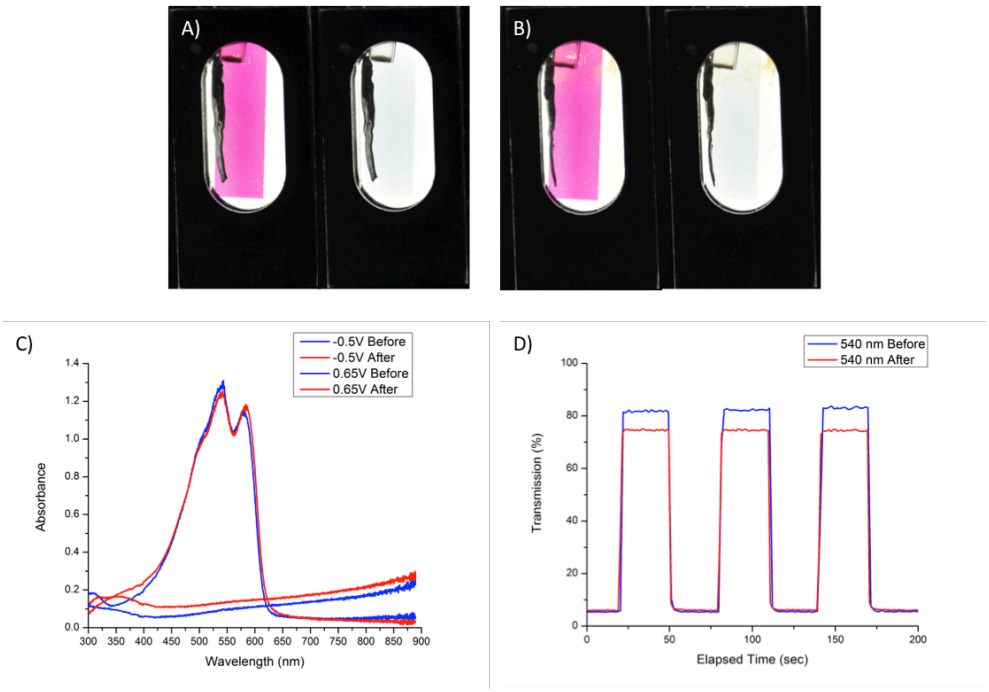

Supporting Figure 3-9 - Photographs of the reduced (left) and oxidized (right) states [(A)&(B)], UV-Vis absorption spectra (C), and % transmission as a function of time (D) for a P(ProDOT-AcDOT$_2$) spray-cast film on ITO/glass before, pictured in (A), and after, pictured in (B), 900 CV cycles. Extreme potentials of -0.5 V and 0.65 V versus Ag/Ag$^+$ were used, and in part (D), held for 30 seconds each.

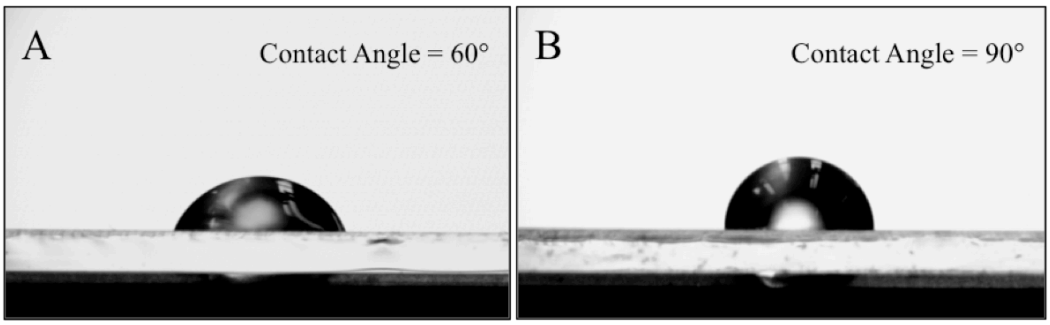

Supporting Figure 3-10 - Contact angle measurements using water droplets on ITO-glass substrates. Left, (A), shows a water droplet on an ITO-glass substrate that was cleaned, but has not been treated with phosphonic acid. Right, (B), shows a water droplet on a similarly cleaned ITO-glass substrate that has been treated with a solution of 1-dodecylphosphonic acid in ethanol with a concentration of 10 mg/mL for 5 minutes. After the solution of phosphonic acid was removed from the substrate, it was rinsed with clean ethanol and air-dried.

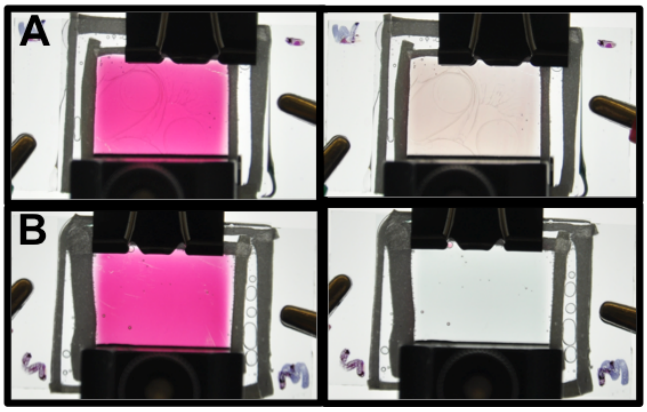

Supporting Figure 3-11 - Photographs of ECDs in the reduced (left) and oxidized (right) states, taken immediately after 5 CV break in cycles. The devices consist of spray-cast films of P(ProDOT-AcDOT$_2$) and P(ProDOP-*N*-C18) on ITO/glass as the electrodes and a solution of 0.5 M TBAPF$_6$ in propylene carbonate as the electrolyte. Prior to device construction the P(ProDOP-*N*-C18) films were reacted with a 10 mM solution of either AgOTf (A) or Fe(III)OTf$_3$ (B) in propylene carbonate for 20 minutes.

CHAPTER 4. STRUCTURAL EFFECTS OF DIOXYTHIOPHENE POLYMERS ON THE PROCESSES OF CHEMICAL AND ELECTROCHEMICAL DOPING AND CHARGE TRANSPORT

The following chapter could have not been made possible without the assistance and input from Dr. Michel de Keersmaeker, Dr. James Ponder, and Dr. Melony Ochieng. Dr. Ponder and Dr. Ochieng synthesized and confirmed the structure of the polymers used in this study. The acyclic dioxythiophene (AcDOT) polymers studied here have also been analyzed for their electrochromic properties in the dissertation of Dr. Ochieng.[31] Furthermore, Dr. de Keersmaeker provided scientific input for the discussion of the results presented in this chapter. Currently this work is being drafted into a manuscript that will be submitted for peer review.

The work presented in this chapter involves the study of a set of two 3,4-propylenedioxythiophene (ProDOT) and two acyclic dioxythiophene (AcDOT) homopolymers with each type of XDOT repeat unit having either branched or linear alkyl solubilizing side chains. We show that while altering the structure of the polymer does have an effect on the degree of intermolecular ordering within the polymer film, these as-cast morphologies to not correlate with enhanced charge transport properties. When using linear n-octyl (oct) solubilizing side chains rather than branched ethylhexyl (EH) chains, we see a multiple order of magnitude increase in the solid-state electrical conductivity for

both ProDOT and AcDOT polymers. Using Magic Blue as a chemical oxidant results in conductivities on the order of 10^{-1} S/cm. In terms of polymer redox properties, when using linear side chains we observe a decrease in the onset of oxidation by 300 mV and an increase in the electrochemical conductance.

4.1 Background and Motivation

As discussed in Chapter 1, a myriad of applications for conjugated polymers (CPs) have been explored due to their ability to transport both ions and electrons simultaneously. In general, CPs are desirable for both solid-state and redox applications because of their ability to reversibly transition between a charge-neutral (insulating) and a charged (conducting) state through either chemical[42,53,70,146,148,149,152,169] or electrochemical oxidation.[123,156,170] Neutral CPs can undergo hole and electron injection, making them useful in solid-state applications including organic field effect transistors (OFETs),[171] organic photovoltaics (OPVs),[172] and thermoelectric generators.[150,173] These applications, in addition to transparent conductive electrodes (TCEs)[100,174] (formed through chemical oxidation), take advantage of the semiconductive properties of CPs. Moreover, CPs can be redox-doped through electrochemical oxidation and used in applications such as electrochromic devices,[125-128] supercapacitors,[129-131] actuators,[132-135] OECTs and sensors.[136,137] All these redox-active applications rely on efficient transport of both ions and electrons. Furthermore, effort has also been made to make CPs compatible with high throughput printing and coating methods.[26] This typically involves incorporating long hydrocarbon or oligo(ethylene oxide) side chains onto the polymer backbone to impart solubility in common organic solvents and water.

4.1.1 Use of XDOT-based Polymers

Dioxythiophene (XDOT)-based materials have been shown to be excellent candidates for use in solution-processed electrochemical device applications.[23,125] Previous work has shown that a family of co-polymers combining 3,4-proylenedioxythiophene (ProDOT) and 3,4-ethylenedioxythiophene (EDOT) units demonstrates high solid-state conductivity values in the excess of 200 S cm^{-1} after chemical doping with $AgPF_6$.[175] Another study on oligoether functionalized ProDOT achieved solid-state conductivities of ~ 1 S cm^{-1} after doping with the chemical oxidant F4TCNQ.[176] Though these materials have been shown to have excellent performance in both electrochemical and solid-state applications, a question still remains as to how small structural changes of the backbone and side chain can affect their film morphology and their charge transport properties in both types of applications.

4.1.2 Motivation and Design for the ProDOT and AcDOT Polymer Family

In this work, we gain a comprehensive understanding of how manipulation of the structure of both the conjugated polymer backbone and the solubilizing side chain first affect the morphology of XDOT-based polymers, and how this alteration in morphology can affect the material's ionic and electronic charge transport properties. To achieve this, we evaluate a set of two 3,4-propylenedioxythiophene (ProDOT) and two acyclic dioxythiophene (AcDOT) homopolymers with each type of XDOT having either branched or linear alkyl solubilizing side chains. This family of polymers focuses on materials that have a di-substituted thiophene ring, which protects the polymer backbone from nucleophilic attack. The ProDOT and AcDOT moieties differ in their presence or

lack of a propylene bridge substituted onto the dioxythiophene ring. This bridge causes two primary structural effects: (1) increasing the distance between the solubilizing side chain and the polymer backbone and (2) positioning these side chains out of plane relative to the backbone direction. Furthermore, this bridge changes the ability of the lone pair of electrons on the oxygen atoms to interact with the conjugated π-system of the thiophene ring, adding to the electron richness of the backbone. Comparisons of branched and linear alkyl side chains in benzodithiophene-based co-polymers show evidence of changes in charge transport, aggregation and degree of ordering in thiophene-based homopolymer systems.[177] We expect that the effects of alteration of the solubilizing side chain would be more pronounced in homopolymers, in which case every thiophene ring is substituted with a solubilizing group. Here, we show that changing the side chain from a branched to a linear n-alkyl structure makes the polymer easier to oxidize through both chemical and electrochemical processes.

4.1.3 Experimental Approach

For this study, we selected, designed, and synthesized a family of four homopolymers based on ProDOTs (Pro) and AcDOTs (Ac), that contain either ethylhexyl (Pro-EH and Ac-EH) or linear n-octyl (Pro-Oct and Ac-Oct) aliphatic side chains, and substitution of these side chains at varying distances from, and orientations to, the conjugated core as depicted in Figure 4.1-1. Details on the synthesis, purity, and molecular weights of the materials can be found in Supporting Figures 4-1 to 4-6. The top two polymers, in Figure 4.1-1 Pro-EH and Ac-EH, have been previously shown to be colored-to-colorless electrochromic materials,[28,110] however the ProDOT analogue demonstrated faster doping kinetics and more effective bleaching of the neutral state

absorption peak. The bottom two, Pro-Oct and Ac-Oct, were specifically synthesized for this work in order to compare the effects of using linear versus branched solubilizing aliphatic side chains to probe how this would enhance or hinder the degree of intermolecular ordering, solid-state conductivity, and onset of oxidation of the CPs.

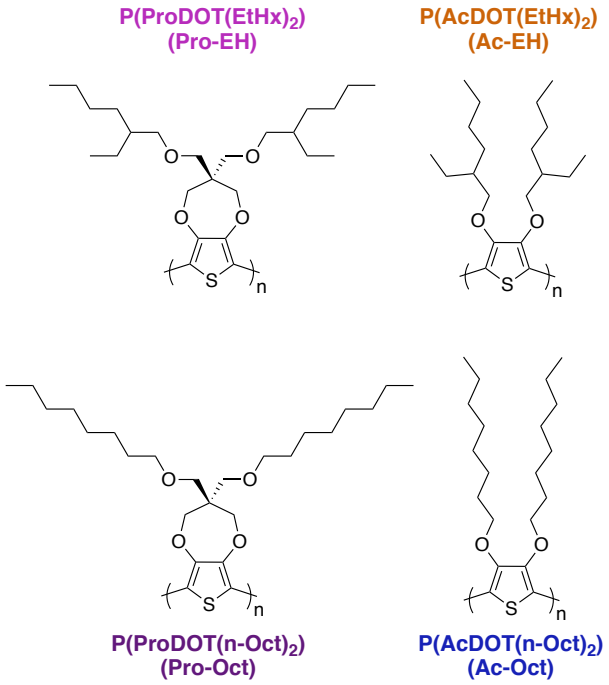

Figure 4.1-1 – Repeat unit structures for the family of dioxythiophene homopolymers used in this study.

4.2 Polymer Film Morphology

As discussed in Chapter 1, intermolecular ordering and surface topography have been shown to have a large influence on the overall charge transport properties of CPs.[111,178-181] Two methods for evaluating these properties are Grazing-Incidence Wide-Angle X-ray Scattering (GIWAXS) and Atomic Force Microscopy (AFM). GIWAXS experiments provide information about the degree of intermolecular ordering of polymer chains in the film, and AFM experiments can provide information regarding the surface

topology of polymer films and the overall degree of roughness. Both experiments provide insight as to why charge transport may be enhanced or inhibited for a given polymer by examining the as-cast morphology or changes in the morphology after doping. Earlier studies conducted on the polymer P3HT for example, show that after chemical oxidation, solid-state conductivities can be achieved up to 8 S/cm.[70] In general, these high conductivities for P3HT are attributed to enhanced intermolecular ordering and desirable morphology of the polymer films for effective doping.[66]

GIWAXS measurements were performed on the blade-coated polymer films as shown in Figure 4.2-1, where the data corresponding to the branched side chain materials is shown in Figures 4.2-1a and 4.2-1b, and the data corresponding to the linear analogues is shown in Figures 4.2-1c and 4.2-1d. The 2D images reveal that the chosen backbone repeat unit has a large impact on the preferential scattering direction. The Pro polymers (Figures 4.2-1a and 4.2-1c) are isotropic materials as evidenced by the large halos in both the (100) and the (010) planes, indicating that the polymer chains have no preferential ordering in terms of directionality relative to the substrate. In contrast, the GIWAXS images of the Ac polymers (Figures 4.2-1b and 4.2-1d) exhibit more ordered domains, as evidenced by the concentrated high intensity regions (for Ac-EH) and the preferential in plane orientation for Ac-Oct, shown by narrower lamellar scattering (100) along the Q_{xy} axis and π-π (010) scattering peaks along the Q_z axis. Further evaluation was done based on the overlay of the linecuts for all polymers along the Q_z direction in Supporting Figure 4-7a showing important information about the short-range intermolecular ordering.

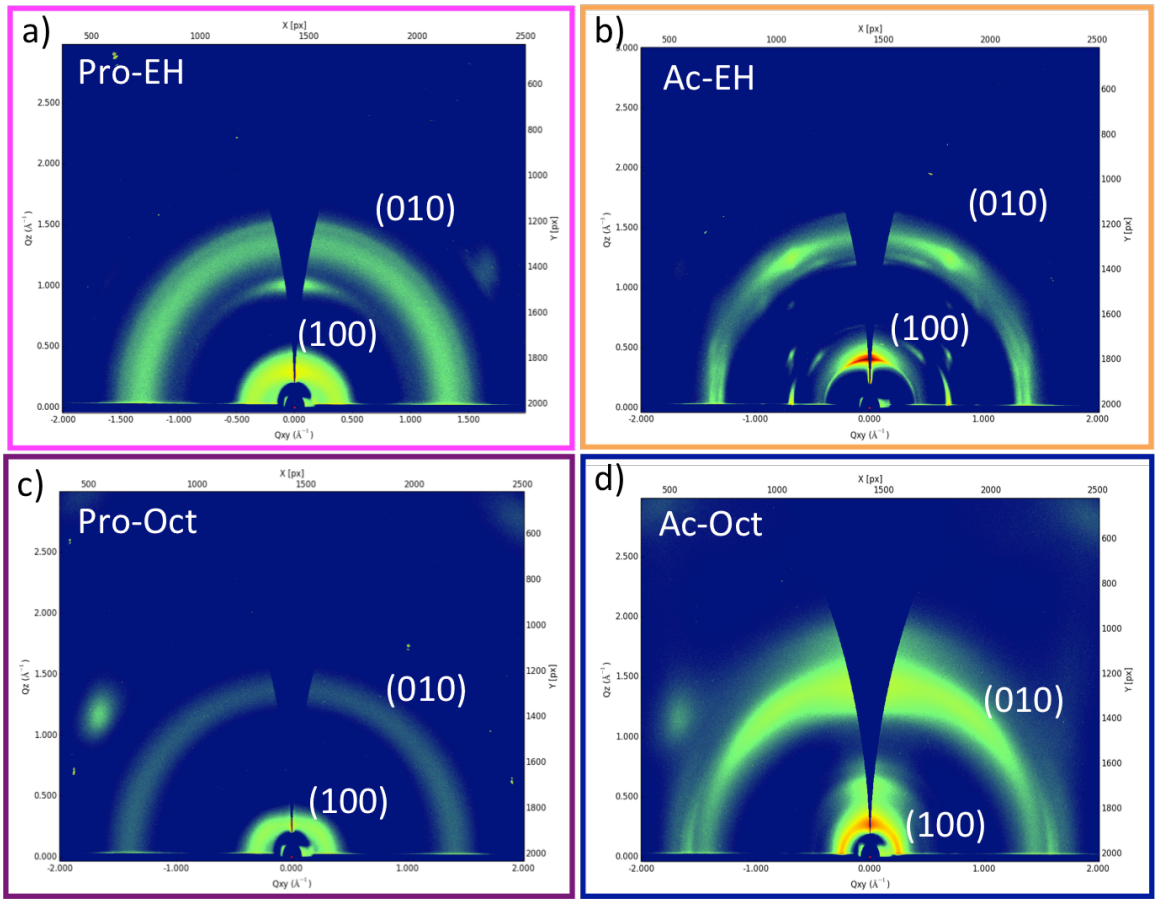

Figure 4.2-1 – GIWAXS images of blade-coated polymer films of (a) Pro-EH, (b) Ac-EH, (c) Pro-Oct, and (d) Ac-Oct.

For Pro-EH, Pro-Oct, and Ac-Oct the diffraction band is seen at $Q_z \approx 0.27$ Å^{-1} (interplanar distance d ≈ 23 Å). For the Ac-EH polymer, a shift is observed towards tighter lamellar packing (d ≈ 15.8 Å), which is explained by combination of the lack of the propylene bridge on the thiophene ring and the increased steric bulk of the branched ethylhexyl sidechains. In the case of the π-π distances, all polymers are in the same range (d ≈ 4.5 Å). For comparison, the work done by Mazaheripour et al. shows that a ProDOT polymer with oligoether side chains (9 atoms) has a lamellar spacing of 25.8 Å and π-π spacing of 3.5 Å).[176] Here, we observe tighter lamellar packing by 2 Å, which can be explained by the shorter side chains used in our work (8 atoms), and significantly larger

π-π spacing distance (1 Å), which is surprising. In the AFM height images (Supporting Figure 4-8) we see that the Ac polymers form smoother films as compared to the Pro polymers. In the phase images (Supporting Figure 4-9) we observe softer (dark) and stiffer (bright) regions of the polymer film. Both Ac polymers have distinct phases showing fibril-like structures, which correlates well with the higher degrees of ordering demonstrated by their corresponding diffraction images, though it is quite surprising considering how smooth the polymer films are. Furthermore, the AFM images corresponding to the Pro polymers show no clear distinct phases, which correlate well with the GIWAXS images showing more isotropic distributions.

4.3 Chemical and Electrochemical Doping

In general, pre-cast neutral CP films are oxidized in two ways: through chemical oxidation by reaction with an electron-accepting molecule, or through electrochemical oxidation (preferably in a three-electrode cell where the working electrode potential can be controlled). Both routes involve the incorporation of charge-balancing dopant anions and solvent molecules resulting in polymer swelling, as well as the planarization of the polymer backbone attributed to the formation of a quinoid structure which delocalizes the generated charge carriers. To understand how the Pro/Ac CP and Oct/EtHx structures affect the doping efficiency in these polymers, chemical oxidation experiments were performed by drop-casting oxidant solution onto as-cast polymer films. After doping for 30 seconds, films were rinsed and dried prior to measuring their absorption profiles and solid-state conductivity. A doping time of 30 s was chosen because all polymers were fully oxidized in this time (Supporting Figure 4-10), and longer doping times resulted in film delamination. Tris(4-bromophenyl)ammoniumyl hexachloroantimonate (commonly

referred to as Magic Blue, $E_{1/2}$ vs $Fc/Fc^+ = 0.70$ V)[65] was chosen as the chemical oxidant as it is a strong electron acceptor that can effectively oxidize all polymers in the family and provide a stable $[SbCl_6]^-$ anion as a charge compensating dopant ion. Electrochemical doping was carried out in the presence of a $TBAPF_6$ electrolyte.

4.3.1 Degree of Polymer Chain Ordering and Solid-State Conductivity After Chemical Oxidation

Upon chemical oxidation with Magic Blue, all polymers in the family are converted to their fully oxidized state as we observe full bleaching of the neutral state absorbance as shown in Supporting Figure 4-10. As we will show later, this is the same doping level that is achieved through electrochemical doping. The AFM images taken after doping with Magic Blue (Supporting Figure 4-11) show that the observed fibrillar features in the as-cast Ac polymer films disappear, but doping does not alter either the lamellar or π-π stacking distances in the bulk of the polymer films according to the GIWAXS data, as seen in Figure 4.3-1. Furthermore, these GIWAXS images show that this doping process does not alter the directionality of the ordering, as we do not see an alteration of the scattering pattern. For example, for the Ac-EH polymer we see increased intensities at the same scattering vector lengths in the diffraction image, however the distinct peaks are broader. For the other three polymers we do not see any differences in the shapes of the scattering patterns, though we observe that the overall scattering intensity is increased, which is more clearly seen in the linecuts (Supporting Figure 4-7b). This intensity increase implies that a larger number of polymer chains are intermolecularly aligned after doping, indicating that the overall degree of crystallinity in the polymer film is increased.

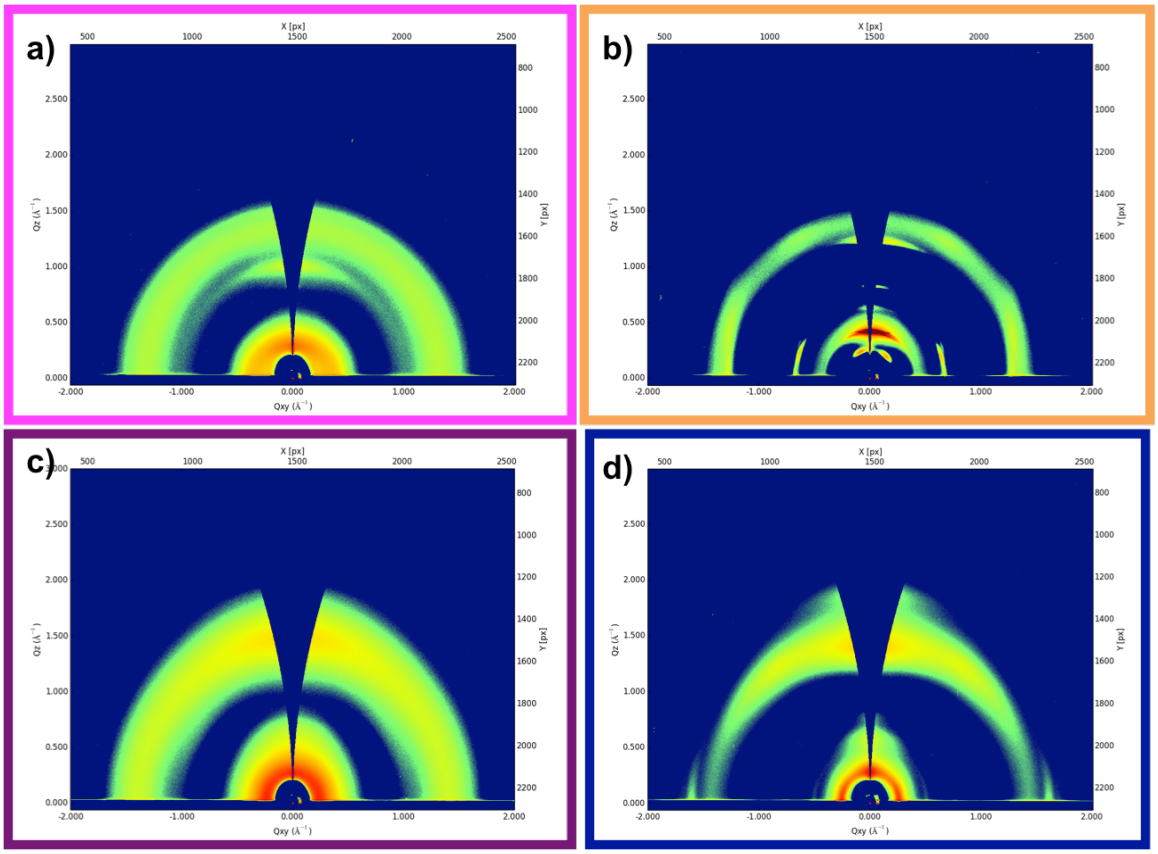

Figure 4.3-1 – GIWAXS images of blade-coated polymer films of (a) Pro-EH, (b) Ac-EH, (c) Pro-Oct, and (d) Ac-Oct after exposure of the films to a 0.01 M solution of Magic Blue in propylene carbonate for 30 seconds.

After doping with Magic Blue, all polymer films demonstrate an enhancement in their solid-state conductivity influenced by the repeat unit structure, from below 10^{-5} S cm^{-1} up to 10^{0} S cm^{-1} (Supporting Figure 4-12). When doping both the Pro and Ac polymers, a significant enhancement in solid-state conductivity is observed when using linear side chains resulting in conductivities on the order of 10^{-1} to 10^{0} S cm^{-1} as compared to the branched side chain analogues which exhibit conductivities on the order of 10^{-3} S cm^{-1}. The values for the polymers with linear side chains are comparable to those found for the previously mentioned linear oligoether functionalized ProDOT from Mazaheripour et al., doped with the molecular dopant F4TCNQ (0.8 S cm^{-1}).[176]

Interestingly, within this family, a larger change in solid-state conductivity is observed when altering the side chain rather than the backbone of the polymer repeat unit. While the GIWAXS images show higher degrees of ordering after doping and AFM images show fewer features, the structural effect on morphology due to the polymer repeat unit does not correlate with higher solid-state conductivities. This difference in solid-state conductivity likely has to do with the ability to delocalize charge both along the backbone and intermolecularly between polymer chains allowing faster transport of charge carriers in the polymer films with linear alkyl chains.

4.3.2 Electrochemical Doping

In order to develop a deeper understanding of the impact of structural alteration of sidechain and repeat unit on the oxidative doping redox processes, polymers were probed by differential pulse voltammetry (DPV) and cyclic voltammetry (CV). Figure 4.3-2a shows the DPVs taken for polymer films in the as-cast state. DPVs for polymers after electrochemical conditioning can be seen in Supporting Figure 4-13. Cyclic voltammograms for the Pro polymers can be seen in Figure 4.3-2b and for the Ac polymers in Figure 4.3-2c. When looking at the as-cast DPVs, it can be seen that Pro-EH, Pro-Oct, and Ac-Oct begin to oxidize around 0.1 V, whereas Ac-EH only starts oxidizing until after 0.3 V. After electrochemical conditioning (Supporting Figure 4-13) we can see that these relationships change with the Ac polymers being more difficult to oxidize than Pro polymers. This is due to the lack of the propylene bridge, which changes the ability of the lone pair of electrons on the oxygen atoms to interact with the conjugated π-system of the thiophene ring. Moreover, the Ac polymers demonstrate enhanced ordering and the

presence of distinct phases, which contributes to a more difficult conformational change during polymer oxidation, as will be treated more in the discussion later.

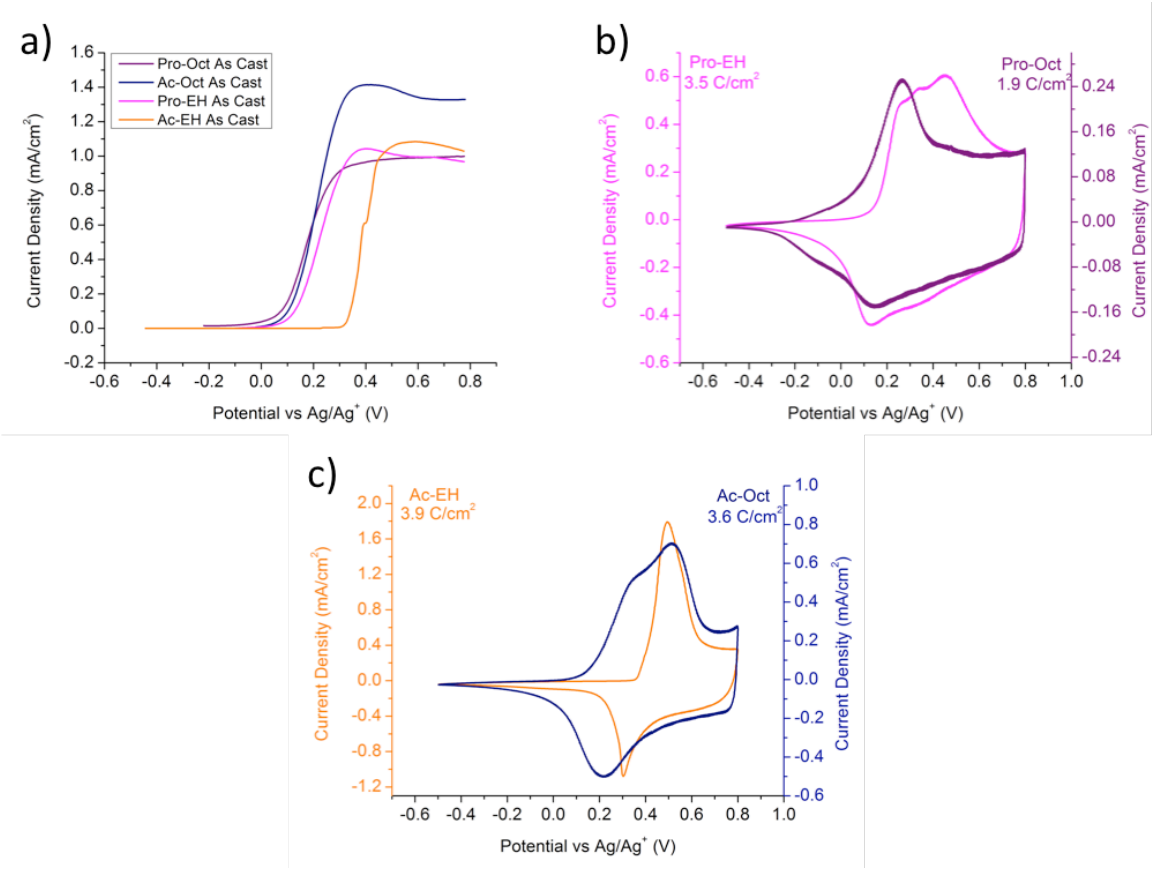

Figure 4.3-2 – Differential pulse voltammograms (a) and cyclic voltammograms (b) and (c) of Pro-EH (magenta), Ac-EH (orange), Pro-Oct (purple), and Ac-Oct (navy blue) on a glassy carbon in a 0.5 M $TBAPF_6$/PC electrolyte. Cyclic voltammograms were taken at a scan rate of 50 mV/s.

For both the Pro and Ac polymers, the onset of oxidation after electrochemical conditioning is lowered by ~300 mV when incorporating linear as opposed to branched side chains (Figures 4.3-2b, 4.3-2c and Supporting Figure 4-13). In the case of the Ac polymers, this lower onset of oxidation for Ac-Oct is due in part to a more sterically relaxed backbone that can more easily planarize due to the less bulky linear side chains. This is supported by the difference in the neutral state optical spectra (absorbance curves

highlighted in green in Figure 4.3-3 below) where the λ_{max} Ac-EH is 495 nm and Ac-Oct is 550 nm, showing a 55 nm blue-shifted neutral absorbance for Ac-EH. On the other hand, the Pro polymers show no pronounced spectral difference despite the large difference in their onsets of oxidation, likely due to the lower steric interactions of the cyclic propylene dioxybridge. It is interesting to note that the GIWAXS data shows that the polymers with linear side chains have a more isotropic scattering pattern compared to the branched side chain counterparts. The disorder appears to be beneficial in electrochemically oxidizing these materials. One reason for this may be that dopant ions can more easily penetrate and enter the conjugated polymer films.

Due to the optical changes that are induced upon electrochemical doping we are able to monitor the extent of doping of CPs as a function of their optical absorbance. Figure 4.3-3 shows the *in situ* UV-Vis absorption profiles of each polymer film as a function of applied potential of the electrochemical cell. The spectra highlighted in red correspond to the onset of oxidation for all polymers (for Ac-Oct this also corresponds to the curve at 0.2 V in cyan). For Pro-EH the first optical change is observed at 0.1 V and for Pro-Oct the first optical change is observed at -0.1 V, whereas for the Ac polymers the first optical change is observed at 0.4 V for Ac-EH and 0.2 V for Ac-Oct. It is worth noting that there is a 0.2 V drop in onset potential for each polymer family as we change from the branched to linear side chains.

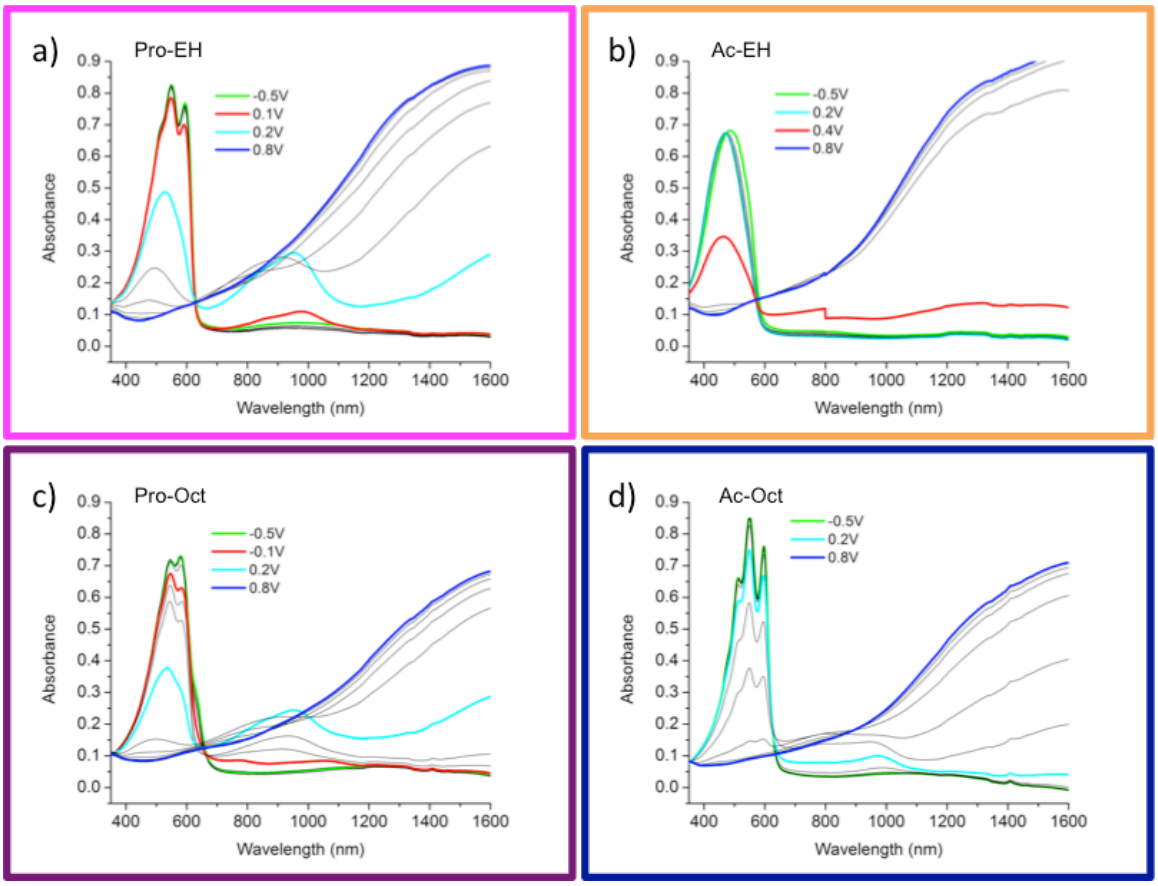

Figure 4.3-3 – *In situ* UV-vis absorption spectra as a function of electrochemical doping level (-0.5 to 0.8 V, at 0.1 V increments) for (a) Pro-EH, (b) Ac-EH, (c) Pro-Oct, and (d) Ac-Oct films on ITO/glass in a 0.5 M $TBAPF_6$ electrolyte in propylene carbonate.

This implies that the incorporation of less bulky linear side chains allows for easier doping of both types of these CPs, again indicating the influence of both side chain and backbone on the polymer redox properties.[74] Comparing all polymers at 0.2 V (cyan curve), we observe that both Pro polymers have reached a higher doping level than the Ac analogs as evidenced by a significant decrease in their π-π^* absorption peak. By 0.6 V the π-π^* peak for both Pro polymers and the Ac-Oct has been fully depleted. Increasing the potential further does not affect the doping level. For the Ac-EH polymer full bleaching does not occur until 0.7 V. For all polymers in the family, the spectra

corresponding to the fully bleached state matches that of the films that were doped with Magic Blue (Supporting Figure 4-10). Here, it is shown that both chemical and electrochemical doping routes are effective in converting the polymers from the neutral to their fully doped forms.

To better illustrate how the polymer structure affects the rate of the electrochemical doping reaction, we monitored the absorption at λ_{max} as a function of the doping level for each polymer film (Supporting Figure 4-14). The Pro-EH, Pro-Oct, and Ac-Oct polymers exhibit switching kinetics under 2 s (time to fully dope), while the Ac-EH polymer is significantly slower, as it exhibits doping kinetics on the order of more than 20 s. These results trend with the onset of oxidation of the polymer family, where Ac-EH has the slowest electrochemical doping kinetics and is the most ordered of the polymer family according to the GIWAXS results seen in Figure 4.2-1. It is interesting to note that both polymers functionalized with linear side chains demonstrated the fastest switching kinetics of the group, with doping kinetics of 1.2 s.

It is also important to understand how the structure of the polymer repeat unit can affect the electrochemical conductance of the polymer films, as this property could provide insight as to why we observe differences in the electrochemical doping kinetics. To experimentally obtain this information, polymer films were drop-cast onto interdigitated microelectrodes and the potential difference was held constant for one half of the working electrodes, and at the same time a potential sweep of +/- 5 mV was applied to the other half while the current was recorded.[115] Potential sweeps were taken as a function of the applied potential from -0.5 V to 0.8 V vs Ag/Ag^+ with 0.1 V increments as shown in Figure 4.3-4. Reverse direction curves for these experiments

(from high to low potential) can be seen in Supporting Figure 4-15, showing that hysteresis is not affected by polymer structure.

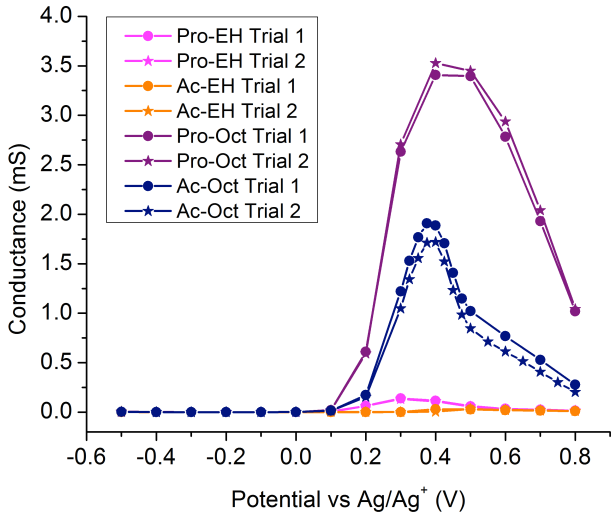

Figure 4.3-4 – *In situ* electrochemical conductance plots of Pro-EH (magenta), Ac-EH (orange), Pro-Oct (purple), and Ac-Oct (navy blue) on interdigitated electrodes from -0.5 to 0.8 V vs Ag/Ag^+ in 0.5 M $TBAPF_6$ in propylene carbonate.

A turn-on of the conductance response is seen for all polymers between 0.1 to 0.2 V, except for Ac-EH (0.4 V). There is a drastic difference in the overall magnitude of the conductance change each polymer exhibits. It should be noted that the onset potential of the conductance response is higher than the electrochemical onset of oxidation measured by DPV due to the requirement of the charge carriers to transverse fully across the insulating gap of the interdigitated electrodes. As can be seen in the spectroelectrochemical results in Figure 4.3-3, all polymers except for Ac-EH demonstrate a decrease in the π-π* absorption at an applied potential of 0.2 V. This turn-on response reflects the fact that Pro-EH, Pro-Oct, and Ac-Oct have all been sufficiently electrochemically doped in order to transport charges across the insulating gap of the

interdigitated electrode. Both Pro-EH and Pro-Oct have similar doping kinetics (Supporting Figure 4-14) and have reached the same doping level at 0.2 V as evidenced by the absorption curve showing polaron generation (Figure 4.3-3), yet Pro-Oct has a significantly higher magnitude of electrochemical conductance. Integrating the CV currents provides the amount of charge required to complete a redox switch. As seen in Figure 4.3-2, the charge corresponding to Pro-EH is 3.5 C/cm^2 and for Pro-Oct is 1.9 C/cm^2. This implies that more charges are required to dope the polymer with branched side chains to the same optical change as the linear side chain analogue. Ac-Oct only demonstrates a small change in its optical properties at 0.2 V, however this relatively low doping level is sufficient to transport charge. Turning to Ac-EH, we do not observe an electrochemical conductance response until 0.4 V, which is also where we see an optical change in the spectra in Figure 4.3-3b. For both the Pro and Ac structures, we observe higher electrochemical conductances for polymers substituted with linear side chains rather than branched. The maximum conductance values are reached at 0.4 V for both Pro-Oct and Ac-Oct. At this potential, the polaron for Pro-Oct has already begun decreasing in intensity, as shown by the absorption at 950 nm in Figure 4.3-3, whereas for Ac-Oct the polaron is at its maximum intensity. Here it is shown that the maximum conductance for Ac-Oct is achieved at a lower doping level than for Pro-Oct. For all polymers in the family a drop in the maximum conductance is observed at high potential values. One interpretation for the conductance drop at higher doping levels is that the polymers reach their maximum number of generated charge carriers causing a decrease in charge carrier mobility.

4.4 Discussion

Given the full analysis presented in this study, a "one size fits all" structure-property relationship is not immediately evident from all observed results. A combination of both electrochemical and surface analysis techniques broadens our perspective and gives us a better understanding of the mixed transport processes in the polymer film.

In this work it was shown that incorporating linear side chains onto dioxythiophene homopolymers result in an increase of the *in situ* conductance and solid-state conductivity compared their branched counterparts. Comparing Pro-Oct and Ac-Oct, we see that Pro-Oct begins oxidizing at -0.1 V and Ac-Oct only at around 0.1 V, but both have similar optical gaps in the neutral state, absorbing around 550 nm. Ac-Oct shows a lower *in situ* conductance compared to Pro-Oct, however this polymer is doped to a lesser degree at the same potential. Comparing their solid-state conductivities, Ac-Oct also has a lower value. Focusing on the polymer chain ordering using GIWAXS data shows that the Ac-Oct demonstrates a higher degree of ordering in both the neutral and oxidized state, combined with an as-cast fibril-like topology according to AFM measurements. Collectively the charge transport morphological characterizations show that the charge transport properties of Ac-Oct are ultimately affected by its inherent more ordered morphology, which results in a material that is more difficult to oxidize with lower conductivities. In other words, the material favors its neutral form and is more difficult to planarize during oxidation. While the enhanced order in the Ac-Oct polymer helps to generate more charge carriers compared to Pro-Oct, these extra charges are not able to move through the film. We see that while order is important to ensure charge

transport between chains, too much ordering and a lack of connection between ordered domains can result in materials that do not easily oxidize even if the backbone of the polymer is relatively planar. The fact that Pro-Oct shows consistently the highest electrochemical conductance, and solid-state conductivity means that isotropic and more homogenous ordering and a smooth morphology are preferred. This 'more ideal' morphology makes the polymer easier to oxidize, and shows higher conductivity values.

Turning to the branched side chain polymers studied in this polymer family, Pro-EH shows a much better performance than its Ac analogue. The Ac-EH has the lowest values for electrochemical conductance, and solid-state conductivity in combination with high degrees of anisotropic polymer ordering (with very specific scattering angles) and a fibril-like topography. These results imply that tighter packing of polymer chains in the film inhibit oxidation and redox switching. Furthermore, the torsional strain in the backbone causes conformational twisting making the film harder to oxidize than the more amorphous Pro materials. In comparison to polymers with the Oct side chains, Pro-EH demonstrates low electrochemical conductance and solid-state conductivity. This polymer is also highly amorphous, with little to no order demonstrated by both GIWAXS and AFM images. Its relaxed backbone geometry explains why Pro-EH is easy to oxidize, but its amorphous nature is what inhibits charges from effectively moving from one chain to another through the film. It is hypothesized that the bulkier EH side chains could also slow down ionic transport. The bulk of the EH side chains also explain the loss of strong intermolecular interactions like π-π stacks between the polymer chains resulting in an overall low conductivity. However, it should be noted that despite the low solid-

state conductivities of Pro-EH and Ac-EH, these polymers are still able to be effectively electrochemically doped and can be repeatedly cycled in electrochromic devices.

4.5 Conclusions

This study aims to help in understanding the delicate balance of material properties that is required to design new state-of-the-art materials for a wide range of applications. Studying this family of polymers demonstrates that a slight alteration in the polymer repeat unit structure results in large effects on the polymer's charge transport properties. Moreover, we demonstrated that incorporating linear side chains as compared to branched side chains enhances electrochemical as well as solid-state charge transport in both Pro and Ac-based polymers. Here, it is shown that intermolecular order of polymer chains plays an important role in the materials' ability to transport charges, with the understanding that some degree of order enhances charge hopping between the chains and that too much order induces separation between ordered and disordered domains, which inhibits the ease of oxidation. Similar trends were shown for both electrochemical and solid-state charge transport of the CPs, indicating that the ideas presented in this work are applicable for both types of charge transport and their corresponding applications.

4.6 Experimental and Supporting Information

4.6.1 Materials

Dr. James Ponder synthesized Pro-Oct and Dr. Melony Ochieng synthesized Ac-EH and Ac-Oct. Pro-EH was synthesized by BASF. Pro-EH[110] (M_n = 12 kg/mol, $Đ$ = 1.8, THF at 35 °C) was polymerized by direct (hetero)arylation polymerization and Ac-EH[28] (M_n = 44 kg/mol, $Đ$ = 3.1, THF at 35 °C) were prepared via an oxidative polymerization using excess $FeCl_3$ in ethyl acetate at room temperature as previously reported. Ac-Oct (M_n = 15 kg/mol, $Đ$ = 2.2, $CHCl_3$ at 40 °C) was prepared using DHAP and Pro-Oct[110] (M_n = 29 kg/mol, $Đ$ = 3.8, $CHCl_3$ at 40 °C) was prepared via an oxidative polymerization, as detailed below. Dimethoxythiophene (98%), purchased from Oxchem, and Pivalic acid (99%), purchased from Sigma, were used as received. $Pd(OAc)_2$ (98%, Strem Chemicals), K_2CO_3 (anhydrous, Oakwood Products), 18-Crown-6 (99%, Acros), and diethyldithiocarbamic acid diethylammonium salt (97%, TCI America) were all used as received. DMF (anhydrous) was purchased from EMD and used as received. DMAc (HPLC grade, Alfa Aesar) was filtered through a pad of basic alumina (Sigma Aldrich) prior to use. Methanol, acetone, toluene, ethyl acetate, and chloroform were purchased from Fisher chemicals and used without purification. Hexanes was purchased from VWR chemicals and used as received. ^{1}H-NMR and ^{13}CNMR spectra were collected on either a Varian Mercury Vx 300 MHz or a Bruker Corporation DRX 700 MHz instrument using $CDCl_3$ as a solvent.[182] 3,3-bis(octyloxymethyl)-3,4-dihydro-2H-thieno[3,4-b][1,4]dioxepine (ProDOT($nOct)_2$) was prepared using a published methods and confirmed by ^{1}H-NMR.[74] Structural characterization: ^{1}H NMR spectra for the polymers were collected using the Bruker Corporation DRX 700 MHz spectrometer. The chemical

shift was set based on residual $CHCl_3$ (in the $CDCl_3$ solvent) as an internal standard set to 7.26 ppm. Polymer molecular weights were estimated using a Tosoh EcoSEC GPC operated at 40 °C using chloroform with 0.25% triethylamine as a stabilizer. The flow rate was 1.0 mL/min and the system was calibrated against polystyrene standards.

Synthesis of Pro-Oct

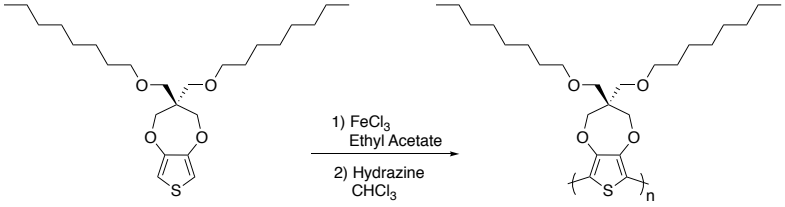

$ProDOT(nOct)_2$ (1.558 g, 3.5 mmol, 1 eq.), ethyl acetate (18 mL), and a stir bar were added to a 100 mL round bottom flask. Ferric chloride (2.87 g, 18 mmol, ~5 eq.) was added and a stopper was placed on the round bottom. The reaction was allowed to stir at room temperature overnight. The reaction mixture was then poured into methanol and filtered using a nylon pad (with a pore size of 0.45 μm) and washed with a large volume of methanol. The solid was then suspended in $CHCl_3$ and ~5 mL of hydrazine monohydrate was added. The resulting solution was precipitated into methanol and filtered into a soxhlet thimble and washed (via soxhlet) with methanol, acetone, hexanes, and finally dissolved into chloroform. The chloroform solution was concentrated and precipitated into methanol. The polymer was then dried under high vacuum overnight. The polymer was obtained as a purple/black solid (0.383 g, 25 % yield). ^1H NMR (700 MHz, $C_2D_2Cl_4$, 50°C) δ 4.19 (br, 4H), 3.63 (s, 4H), 3.48 (s, 4H), 1.56 (s, 4H), 1.40-1.24 (br, 22H), 0.90 (s, 6H). Anal. calcd. for $C_{25}H_{42}O_4S$ C 68.45, H 9.65, S 7.31, Found C 68.45, H 9.63, S 7.23. M_n: 29.1 kg/mol, M_w/M_n: 3.8, vs. PS in $CHCl_3$ at 40°C.

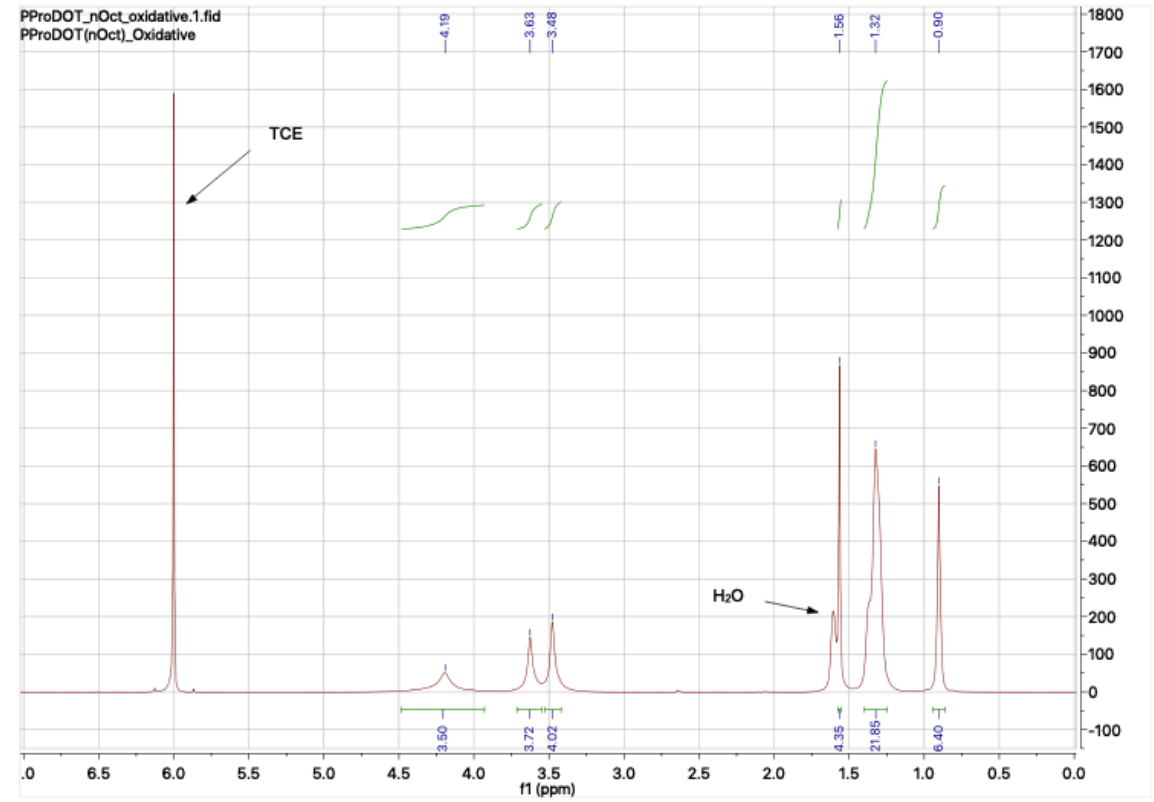

Supporting Figure 4-1 – ^{1}H-NMR (700 MHz) spectrum of Pro-Oct in TCE-D2.

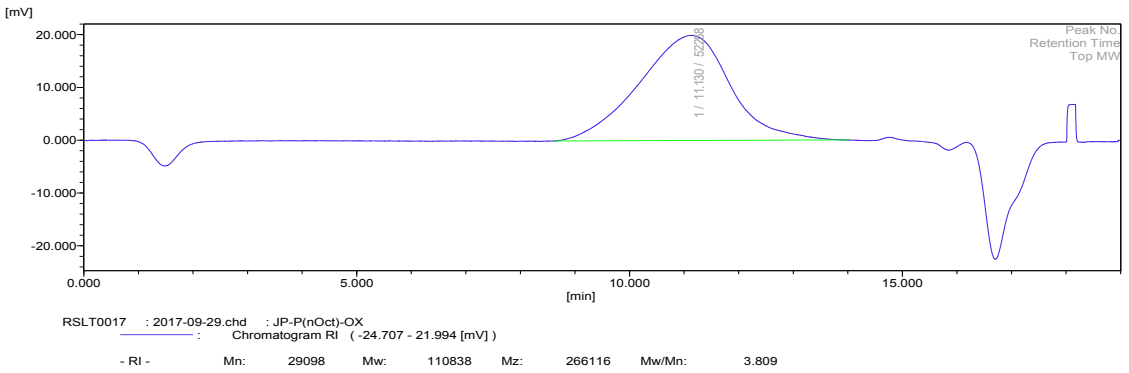

Supporting Figure 4-2 – Gel permeation chromatogram for Pro-Oct in $CHCl_3$ at 40^oC calibrated vs polystyrene standards.

Materials for Synthesis of Ac Polymers

The Ac-based polymers are the same as those reported in the dissertation of Dr. Melony Ochieng.[31] The synthetic details and structural confirmation data have been reproduced here.

Dimethoxythiophene (98%), purchased from Oxchem, and Pivalic acid (99%), purchased from Sigma, were used as received. $Pd(OAc)_2$ (98%, Strem Chemicals), K_2CO_3 (anhydrous, Oakwood Products), 18-Crown-6 (99%, Acros), and diethyldithiocarbamic acid diethylammonium salt (97%, TCI America) were all used as received. DMF (anhydrous) was purchased from EMD and used as received. DMAc (HPLC grade, Alfa Aesar) was filtered through a pad of basic alumina (Sigma Aldrich) prior to use. Methanol, acetone, toluene, and chloroform were purchased from Fisher chemicals and used without purification. Hexanes were purchased from VWR chemicals and used as received. ^{1}H-NMR and ^{13}CNMR spectra were collected on either a Varian Mercury Vx 300 MHz or 700 MHz instruments using $CDCl_3$ as a solvent. 3,4-

bis(octyloxy)thiophene was prepared by BASF. P(AcDOT)-EH[28] was prepared using a published methods and confirmed by ^{1}H-NMR.

Synthesis of 3,4-bis(octyloxy)thiophene

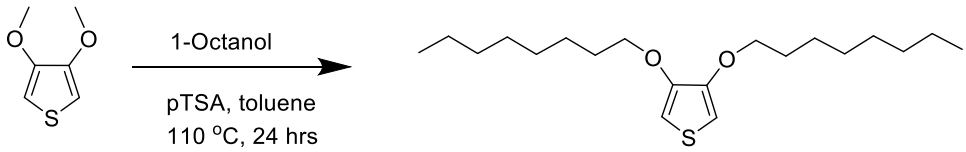

In a dry 500 mL round bottom flask with a magnetic stir bar, dimethoxythiophene (10.0 g, 0.069 mol) and 1-octanol (24.0 g, 0.185 mol) was added under argon followed by anhydrous toluene (300 mL). *p*-toluenesulfonic acid (1.3g, 0.006 mol) was added while the solution was stirring. The reaction was refluxed overnight at 110 °C. After completion, the flask was cooled to ambient temperature and quenched with 100 mL of a saturated $NaHCO_3$ solution. The organic layer was extracted 3 times with DCM and dried using $MgSO_4$. The solvent was concentrated and the crude was purified by silica gel chromatography using pure hexanes to obtain 17.800 g of a clear white solids (75%). ^{1}H NMR (300 MHz, $CDCl_3$) δ (ppm) 6.15 (s, 2H), 3.97 (t, J = 6.8 Hz, 4H), 1.81 (p, 4H), 1.49 – 1.37 (m, 4H), 1.31 (b, J = 12.7, 9.5 Hz, 16H), 0.96 – 0.81 (m, 6H).^{13}C NMR (75 MHz, $CDCl_3$) δ(ppm) 147.67, 96.93, 70.72, 31.96, 29.51, 29.41, 29.14, 26.12, 22.82, 14.26.

Synthesis of 2,5-dibromo-3,4-bis(octyloxy)thiophene.

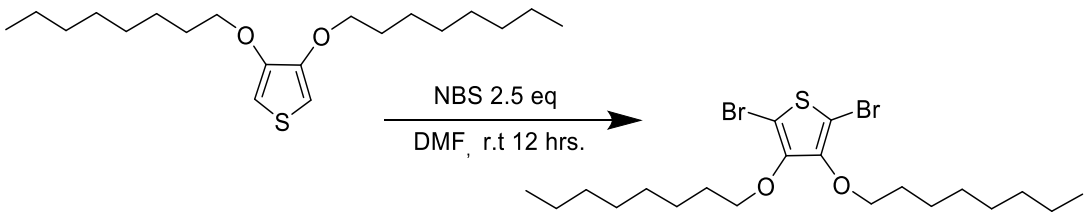

In a dry 250 mL round bottom flask with a magnetic stir bar, 3,4-bis(octyloxy)thiophene (1.000 g, 0.0029 mol) was added. The flask was then degassed before 100 mL of anhydrous DMF was added via syringe. The solution was stirred for ten minutes at 0 °C under argon. While stirring at 0 °C, a solution of 1.340 g of N-bromosuccinimide (NBS) (0.0075 mol, 2.5 eq) in anhydrous DMF was added dropwise. The vessel was brought to room temperature and then allowed to stir for 12 hrs while covered with aluminum foil. After completion, the product was washed with brine and extracted with 200 mL of 1:1 ethyl ether/ethyl acetate. The organic layer was then washed three times with deionized water and then dried over magnesium sulfate. The solvent was removed under reduced pressure. The resulting crude oil was purified by column chromatography using hexanes on neutral silica resulting in a clear, colorless oil 1.160 g (80.3%). ^{1}H NMR (300 MHz, $CDCl_3$) δ (ppm) 4.05 (t, J = 6.6 Hz, 4H), 1.72 (p, 4H), 1.53 – 1.39 (m, 4H), 1.39 – 1.21 (m, 16H), 0.94 – 0.82 (m, 6H).^{13}C NMR (75 MHz, $CDCl_3$) δ (ppm) 147.75, 95.40, 74.10, 31.98, 30.08, 29.49, 29.42, 26.01, 22.81, 14.26.

Synthesis of Ac-Oct

To a 50 mL Schlenk tube equipped with stir bar 2,5-dibromo-3,4-bis(octyloxy)thiophene (1.000 g, 1.0 eq.), 3,3-dimethyl-3,4-dihydro-2H-thieno[3,4-b][1,4]dioxepine (0.371g, 1.0 eq.) palladium(II) acetate (0.009 g, 2 mol%), pivalic acid (0.103 g, 0.5 eq.), and

potassium carbonate (0.691 g, 2.5 eq.) were added. 20 mL of DMAc was added to dissolve the contents and the tube was sealed under a blanket of argon. The reaction mixture was premixed for 5 minutes before it was lowered into a 140 °C oil bath. The solution was left to stir vigorously overnight (~12 hours). After the flask was removed from the oil bath and allowed to cool to room temperature, the polymer was precipitated into methanol and stirred for one hour. The precipitate was filtered into a Soxhlet extraction thimble and washed with methanol, acetone, hexanes, toluene, and chloroform. The washings were conducted until the color was no longer observed during extraction. ~20 mg of a palladium scavenger (diethylammonium diethyldithiocarbamate) and ~20 mg of 18- crown-6, was added to the chloroform fraction and then stirred for 2 hours at 50 °C. The chloroform was removed under reduced pressure and polymer was precipitated into ~300 mL of methanol. The precipitate was vacuum filtered using a nylon pad (with a pore size of 20 μm) and washed with a large volume of methanol before letting it air dry. The dried material was collected into a vial and dried under vacuum for two days.

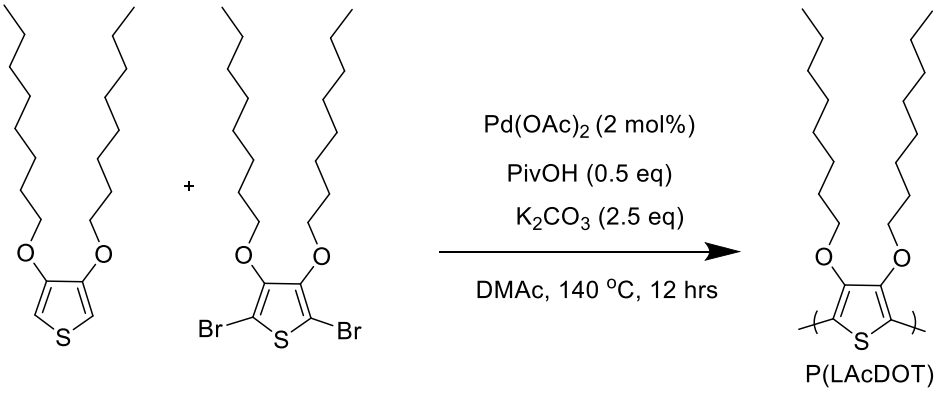

The polymer was obtained as a metallic looking purple solid in 50% yield (0.4938 g). ^{1}H NMR (700 MHz, $CDCl_3$) δ 4.16 (Br, 4H), 1.91 (s, 4H), 1.31 (dd, J = 13.6, 6.3 Hz, 18H),

0.89 (t, J = 6.9 Hz, 6H). Anal. calcd. for $C_{20}H_{34}O_2S$ C 70.96, H 10.12, S 9.47, Found C 70.69, H 10.03, S 9.48. M_n: 29 kg/mol, M_w/M_n: 3.6, *vs.* PS in $CHCl_3$ at 40 °C.

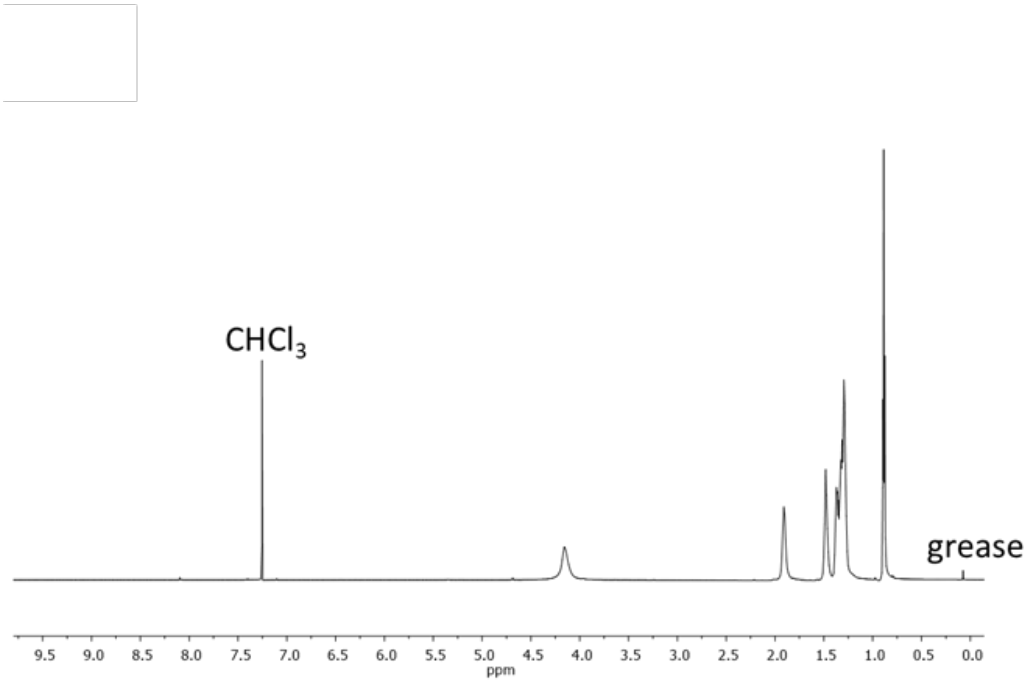

Supporting Figure 4-3 – ^{1}H-NMR spectrum (700 MHz) of Ac-Oct in $CDCl_3$.

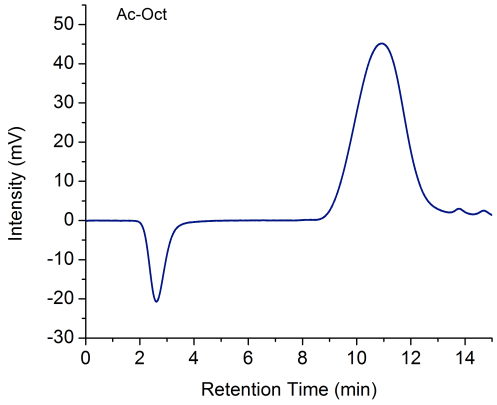

Supporting Figure 4-4 – Gel permeation chromatogram for Ac-Oct in $CHCl_3$ at 40^{o}C calibrated vs polystyrene standards.

Synthesis of Ac-EH[28]

In a round-bottomed flask equipped with a stir bar, iron (III) chloride (4.290 g, 3.0 eq.) was dissolved in 20 ml of ethyl acetate for ten minutes in an ice bath. 3,4-Di(2-ethylhexyloxy)thiophene (3.000 g, 1.0 eq) was dissolved in ethyl acetate (40 mL) and added to the stirring solution of iron (III) chloride. The reaction mixture immediately turned dark green and was stirred for an additional 10 minutes in the ice bath. The solution was then removed from the ice bath and allowed to stir overnight at room temperature. Once the reaction was complete, the solution was precipitated into a beaker containing 250 mL of methanol and the mixture was stirred for 5 min. The doped polymer was collected by suction filtration using a Nylon pad (with a pore size of 20 μm) and washed with methanol (2 x 80 mL). The doped polymer was suspended in chloroform (50 mL) and hydrazine monohydrate (2 mL) was added dropwise, effecting a change in color of the mixture to light-orange/brown. The mixture was concentrated to ~10 mL and precipitated into a stirring solution of methanol (100 mL). The mixture was concentrated again to ~10 mL and precipitated into a stirring solution of methanol (100 mL). The precipitate was vacuum filtered, using a Nylon pad (with a pore size of 20 μm) as the filter. The dried polymer was collected into a vial and left to dry under high vacuum for two to three days.

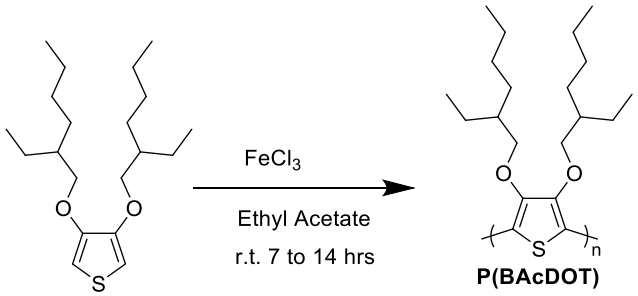

P(BAcDOT)

The orange polymer was collected by suction filtration and dried *in vacuo*. Polymer yield was 1.300 g (43%). ^{1}H NMR (700 MHz, $CDCl_3$) δ (ppm) 3.92 (d, J = 4.5 Hz, 4H), 1.81 – 1.70 (m, 2H), 1.59 – 1.49 (m, 2H), 1.45 – 1.36 (m, 4H), 1.35 – 1.21 (m, 11H), 0.91 – 0.80 (m, 12H). Anal. calcd. for $C_{20}H_{34}O_2S$ C 70.96, H 10.12, S 9.47, Found C 70.85, H 10.05, S 9.48. M_n: 44 kDa, M_w/M_n: 3.0, *vs.* PS in THF at 35 °C.

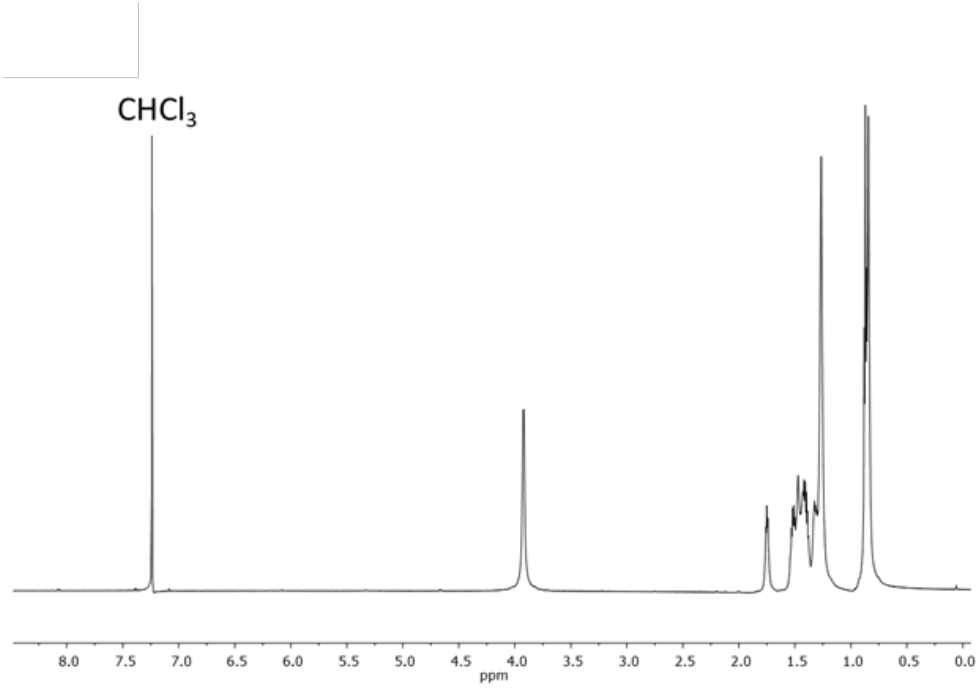

Supporting Figure 4-5 – ^{1}H-NMR spectrum (700 MHz) for Ac-EH in $CDCl_3$ at 50^{o}C.

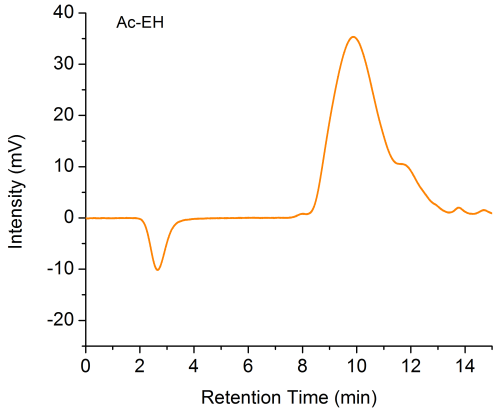

Supporting Figure 4-6 – Gel permeation chromatogram for Ac-EH in $CHCl_3$ at 40°C calibrated vs polystyrene standards.

4.6.2 Film Formation

Before film formation, 30-40 mg mL^{-1} polymer samples were prepared in toluene in the case of Pro-EH and Ac-EH, or chloroform in the case of Pro-Oct and Ac-Oct. Films for AFM were blade-coated onto glass slides and for GIWAXS studies they were blade-coated onto silicon. For spectroelectrochemical studies, polymer films were coated onto ITO-glass substrates (25 mm x 75 mm x 0.7 mm, sheet resistance 8-12 Ω sq^{-1}, Delta Technologies, Ltd). All substrates were pre-rinsed and sonicated in solutions of sodium dodecyl sulfate-water, water, acetone, and finally isopropanol, and allowed to air dry. Once dry, polymer films were blade-coated with a custom blade-coater built in-house[183] using a gap height of 100 μm and various coating speeds depending on the solution viscosity. Films of each polymer were cast to a pre-determined optical density of 0.75 ± 0.1 (10% T) at λ_{max} (547 nm for Pro-EH, 495 nm for Ac-EH, 545 nm for Pro-Oct, and 550 nm for Ac-Oct). The spectroscopic properties of all films cast in this study were

monitored with an Ocean Optics USB2000+ spectrophotometer detector using an Ocean Optics DH-2000-BAL fiber-optic light source.

For electrochemical characterizations including differential pulse voltammetry (DPV), and cyclic voltammetry (CV), films are deposited by sequentially dropping four 1 μL drops of the polymer solutions with concentrations of 1 mg mL^{-1} onto polished glassy carbon electrodes after which the films are allowed to air dry. For the *in-situ* conductance measurements, three 0.5 μL drops of the polymer solutions with concentrations of 1 mg mL^{-1} were sequentially dropped onto Pt interdigitated microelectrodes (Abtech Scientific Inc. IME 1050.5 series) equipped with 50 pairs of 10 μm electrodes separated by a 10 μm insulating channel and allowed to air dry.

4.6.3 Morphological Characterization

AFM measurements were performed using a Bruker atomic force microscope (Dimension icon) with a Bruker Tap 150 cantilever (Model: RTESP-150) in standard tapping mode. Samples were prepared as described above.

GIWAXS measurements were conducted at the Stanford Synchrotron Radiation Lightsource on beamline 11-3. Samples were prepared as described above on Si wafers that were washed using the same procedure as the glass substrates. Samples were irradiated with X-ray energy of 12.7 keV and their GIWAXS patterns were recorded with a 2-D image detector (MAR345 image plate detector). Typical exposure times were 240 s. The distance between the sample and the detector was kept at 250 mm and the incident angle was maintained at 0.13° in order to achieve the highest scattering intensity from the sample without interference from the substrate (polymer critical angle ~0.08°).[184] The

scattering images were calibrated using a LaB_6 standard. Samples were loaded into a chamber and purged with helium to reduce damage to the sample and reduce the air scattering background. Samples were loaded into the chamber with the blade-coating direction normal to the direction of the incident x-ray beam. The data analysis was conducted with WxDiff software developed by Dr. Stefan Mannsfeld.[120]

4.6.4 Chemical Oxidation of Polymer Films

After casting, polymer films were exposed to dopant solutions made from propylene carbonate (99.5%, Acros Organics, purified using a solvent purification system from Vacuum Atmospheres), with a dopant ion concentration of 0.01 M. The dopant used for this study, tris(4-bromophenyl)ammoniumyl hexachloroantimonate (Sigma Aldrich, technical grade), is here referred to as "Magic Blue". Dopant solutions were prepared in an argon-filled glovebox. To perform chemical oxidation, a dopant solution with a concentration of 0.01 M in propylene carbonate was drop-cast onto polymer films under a blanket of argon for 30 seconds. Subsequently, each film was rinsed with clean methanol. When preparing samples for atomic force microscopy (AFM), grazing-incidence wide-angle X-ray scattering (GIWAXS), and solid-state conductivity measurements, polymer films were dried under full vacuum at 50°C for 15 hours in a vacuum oven to ensure complete solvent removal.

4.6.5 Solid-State Conductivity

Metal contacts were vapor deposited on dry chemically oxidized films through a shadow mask by thermally evaporating 10 nm of Cr followed by 90 nm of Au. The solid-

state sheet resistance was measured using a Keithley 2400 source meter and four-point probe using a van der Pauw geometry.

4.6.6 Electrochemical Conductivity

For all electrochemical characterizations the electrolyte solution was 0.5 M tetrabutylammonium hexafluorophosphate ($TBAPF_6$, Acros Organics, 98% and recrystallized using 200 mL of ethanol for every 100 g of salt) dissolved in propylene carbonate. A Pt flag served as the counter electrode and an Ag/Ag^+ electrode (10 mM $AgNO_3$ and 0.5 M $TBAPF_6$ in acetonitrile, +85 mV vs Fc/Fc^+) was used as the reference electrode. The redox response of the films was characterized using DPV (step size 2 mV and step time 0.1 s) and CV (with a scan rate of 50 mV/s) performed in a three-electrode cell, using a Princeton Applied Research 273 potentiostat/galvanostat under CorrWare control.

Spectroelectrochemistry measurements were performed in coordination with an Agilent Technologies Cary 5000 UV-Vis-NIR Spectrophotometer under Cary WinUV control. Chronoabsorptometry where the transmittance was monitored at λ_{max} was used to evaluate the electrochromic switching times of all CP films by switching them repeatedly between -0.5 V and 0.8 V using various pulse lengths (60, 30, 10, 5, 2, 1, and 0.5 s).

In-situ conductance measurements were performed in a four-electrode cell using a Pine bipotentiostat (model AFCBP1) under control of the Aftermath software. One of the working electrodes of the interdigitated electrode was held at a given potential E (range from -0.5 to 0.8 V vs Ag/Ag^+) while cycling the second working electrode E ± 0.005 V at

0.5 mVs^{-1}.[101,116] The slope of the resulting i/E curve was used to determine the film's conductance.

4.6.7 Additional Supporting Figures

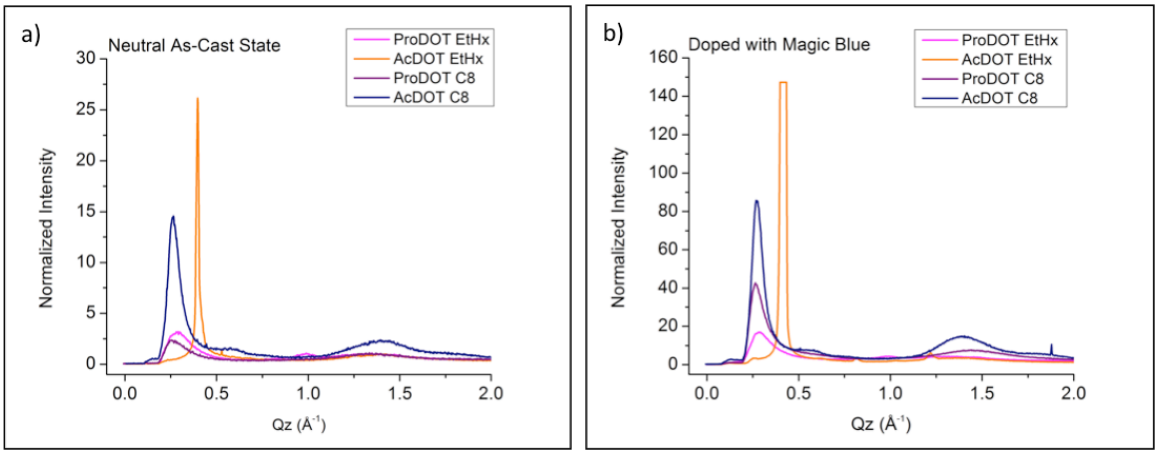

Supporting Figure 4-7 – Linecuts along the Q_z direction from GIWAXS images of neutral polymer films (a), or after exposure of the films to a 10 mM solution of Magic Blue in propylene carbonate for 30 seconds (b). Ac-EH curve plateaus due to high scattering intensity maxing out detector.

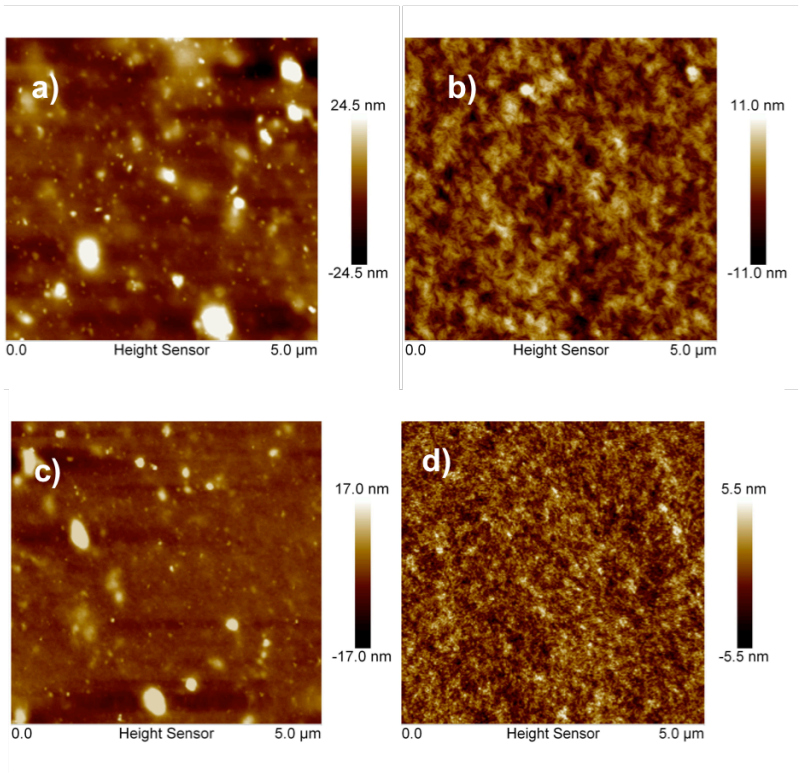

Supporting Figure 4-8 – AFM height images of blade-coated films of Pro-EH (a), Ac-EH (b), Pro-Oct (c), and Ac-Oct (d) on glass substrates.

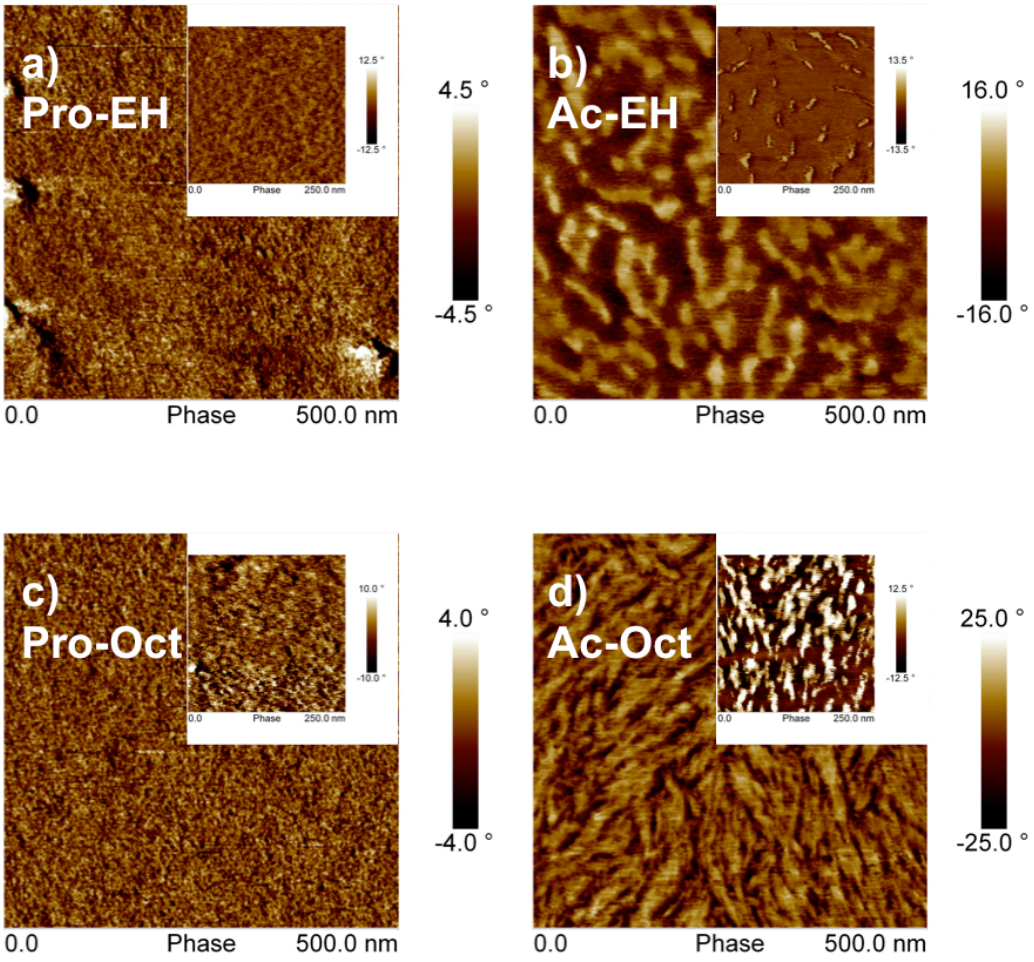

Supporting Figure 4-9 – AFM phase images of as-cast blade-coated films of Pro-EH (a), Ac-EH (b), Pro-Oct (c), and Ac-Oct (d) on glass substrates.

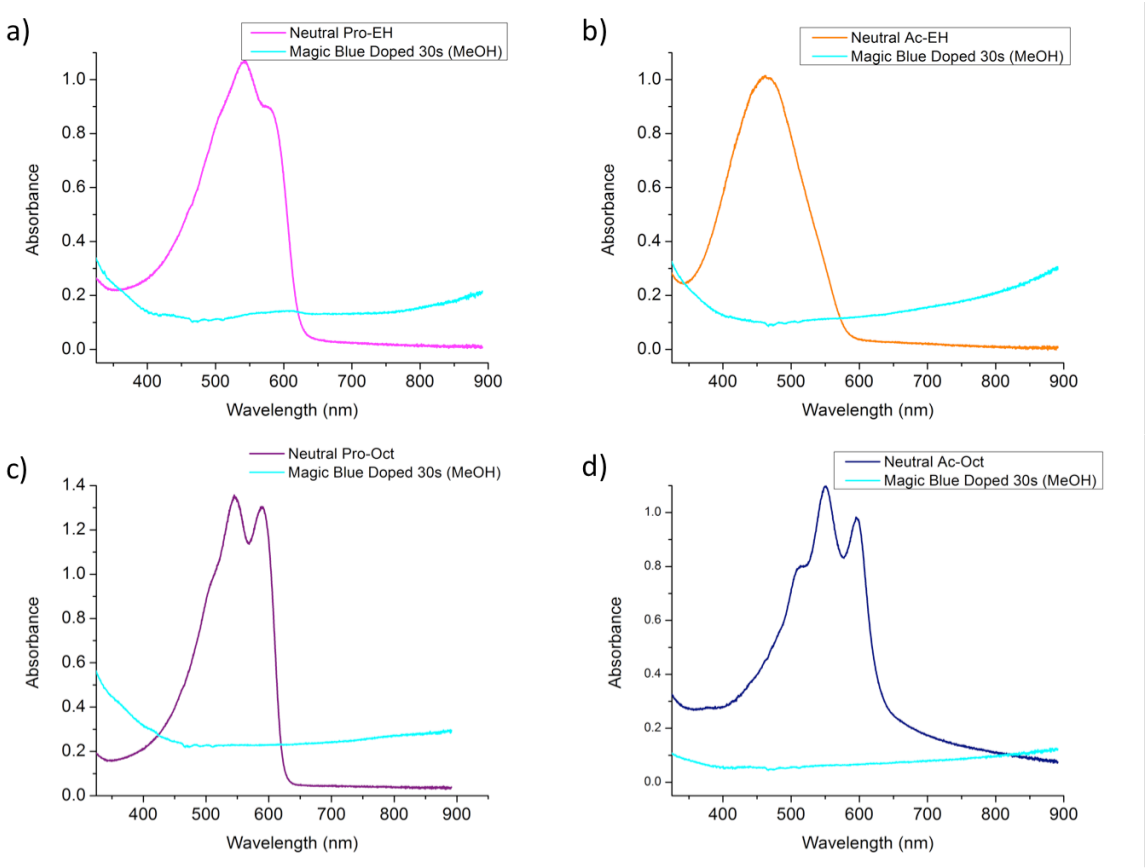

Supporting Figure 4-10 – UV-vis absorption spectra of blade-coated polymer films of (a) Pro-EH, (b) Ac-EH, (c) Pro-Oct, and (d) Ac-Oct on glass substrates before and after exposure to a 10 mM solution of Magic Blue in propylene carbonate for 30 seconds and a subsequent methanol rinse.

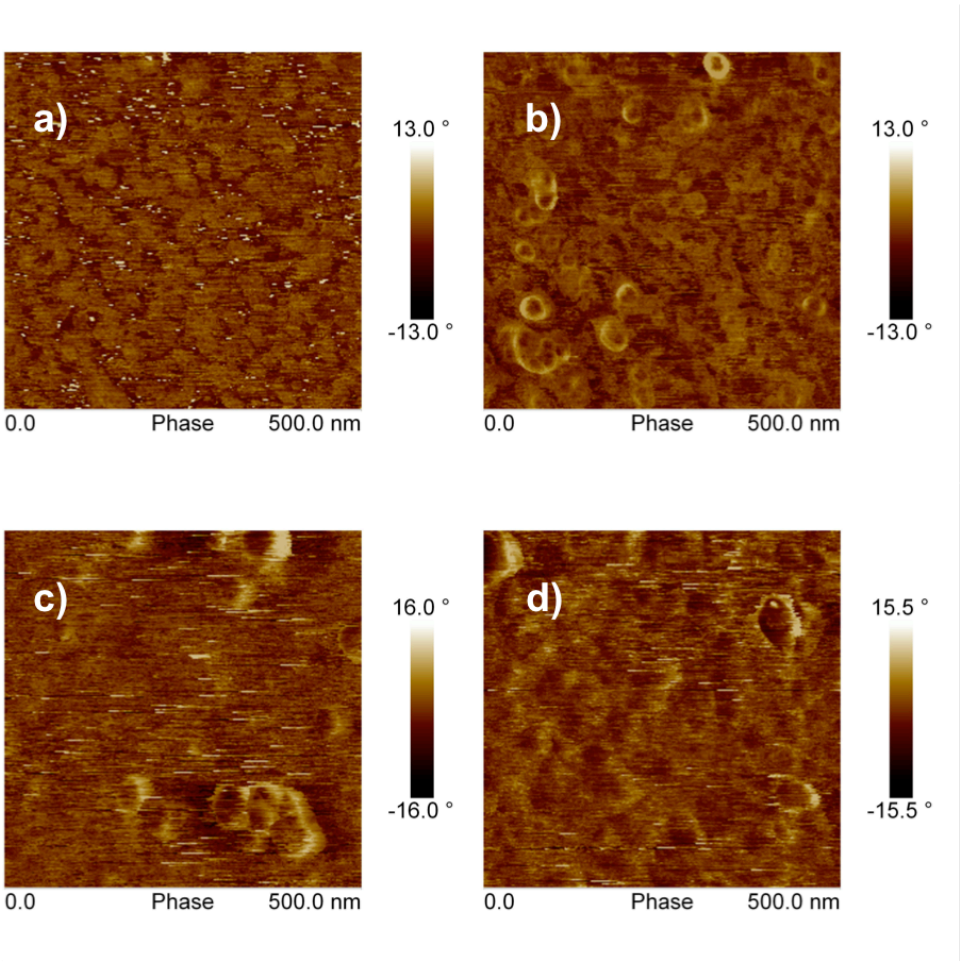

Supporting Figure 4-11 – AFM phase images of blade-coated films of Pro-EH (a), Ac-EH (b), Pro-Oct (c), and Ac-Oct (d) on glass after exposure to a 10 mM Magic Blue solution in propylene carbonate for 30 seconds and a subsequent methanol rinse.

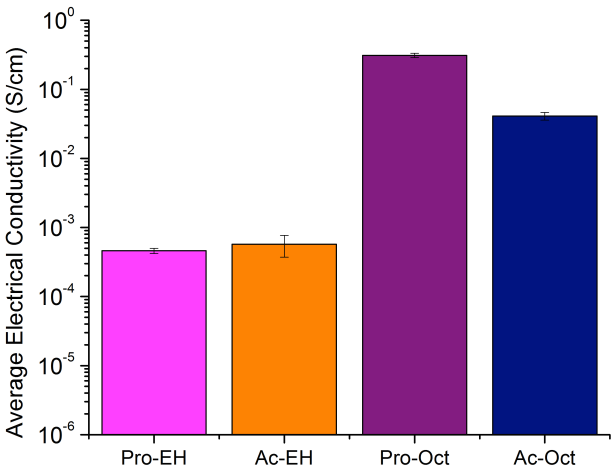

Supporting Figure 4-12 – The average electronic conductivity values of blade-coated polymer films on glass substrates after exposure to a 10 mM Magic Blue solution in propylene carbonate for 30 seconds and a subsequent methanol rinse.

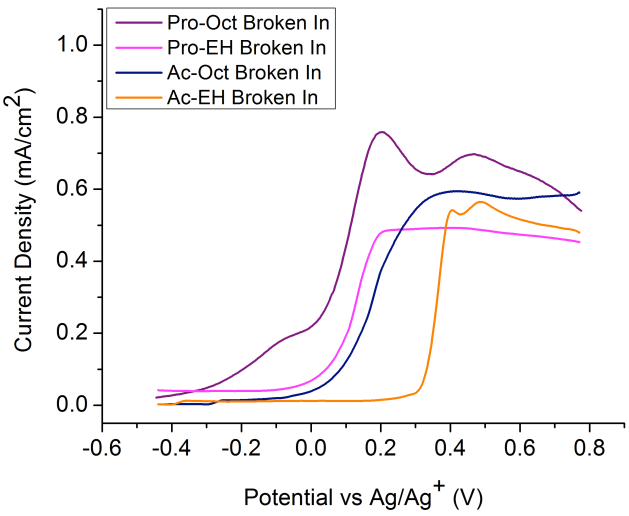

Supporting Figure 4-13 – Differential pulse voltammograms for drop-cast films after 5 conditioning CV cycles of Pro-EH (magenta), Ac-EH (orange), Pro-Oct (purple), and Ac-Oct (navy blue) on a glassy carbon electrode in a 0.5 M electrolyte of $TBAPF_6$ in propylene carbonate.

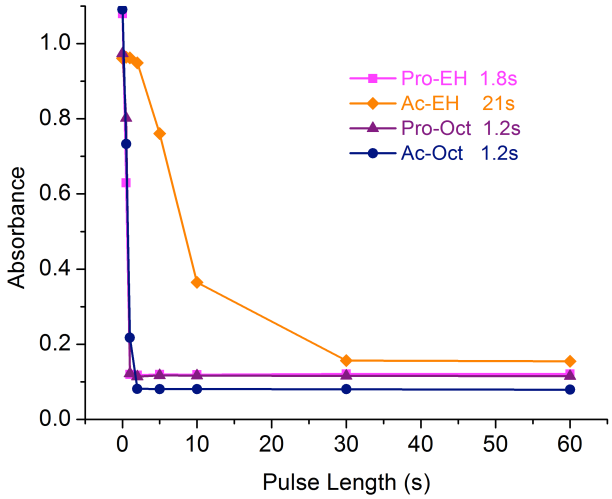

Supporting Figure 4-14 – The change in absorbance monitored at λ_{max} for blade-coated films of (a) Pro-EH (547 nm), (b) Ac-EH (495 nm), (c) Pro-Oct (545 nm), and (d) Ac-Oct (550 nm) coated on ITO/glass as the potential is stepped between -0.5 and 0.8 V vs Ag/Ag^+ for various time intervals (60, 30, 10, 5, 2, 1, 0.5, and 0 s) in 0.5 M $TBAPF_6$/PC.

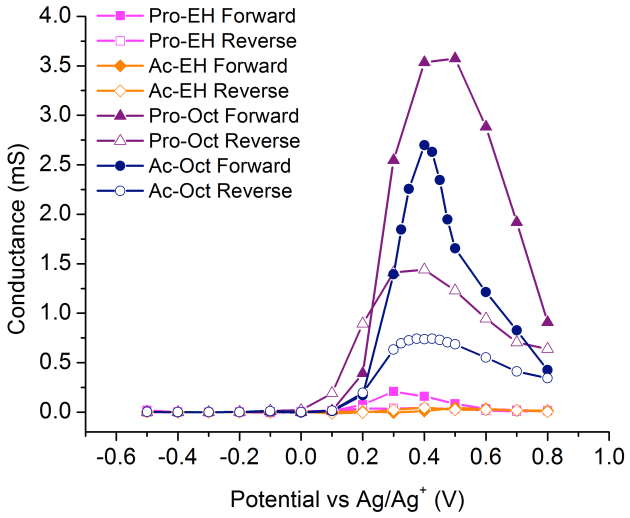

Supporting Figure 4-15 – *In situ* electrochemical conductance plots in the forward direction (-0.5 to 0.8 V, solid symbols) and reverse direction (0.8 to -0.5 V, open symbols) of Pro-EH (magenta), Ac-EH (orange), Pro-Oct (purple), and Ac-Oct (navy blue) on interdigitated electrodes in the potential range of -0.5 to 0.8 V vs Ag/Ag^+ in a 0.5 M $TBAPF_6$ electrolyte in propylene carbonate.

CHAPTER 5. DIOXYTHIENOTHIOPHENE (DOTT) POLYMERS: A FUSED THIOPHENE APPROACH TO UNDERSTANDING THE STRUCTURE-PROPERTY RELATIONSHIPS OF HIGHLY CONDUCTIVE POLYMERS

The work presented in this chapter would have not been made possible without the efforts of Dr. James Ponder and Mr. Shawn Gregory. Dr. Ponder synthesized and confirmed the structure of all of the polymers used in this study. He is currently writing a manuscript detailing their synthesis and electrochromic properties. Mr. Gregory sputtered the metal contacts and performed all of the data collection for the solid-state conductivity measurements presented in this work. Currently the work presented here is being drafted into a manuscript that will be submitted for peer review.

In the work presented in this chapter, we evaluate a series of dioxythienothiophene (DOTT)-based polymers for their structure-property relationships as they relate to charge transport for both solid-state and electrochemical applications. The family includes: the homopolymer, two 3,4-ethylenedioxythiophene (EDOT) co-polymers, a dimethyl ProDOT (DMP) co-polymer, and a bulky neopentyl dioxythiophene (NeoDOT) co-polymer. We show that all of the soluble DOTT polymers can be completely either chemically or electrochemically oxidized, through the full depletion of their neutral π-π^* absorbance. The DOTT homo polymer and DOTT-NeoDOT co-polymer show high degrees of intermolecular ordering according to GIWAXS

measurements, however this order inhibits both chemical and electrochemical oxidation. DOTT-NeoDOT has a high degree of intermolecular ordering and the highest onset of electrochemical oxidation at 0.30 V vs Ag/Ag^+. In comparison, DOTT-BiEDOT has lower degrees of intermolecular ordering and the lowest onset of oxidation at -0.47 V vs Ag/Ag^+. Furthermore, this polymer has the highest solid-state conductivity of the family, which approaches 20 S/cm after chemical oxidation with the molecular dopant F4TCNQ. This study is the first to report the effects of chemical doping and charge transport on a family of soluble dioxythienothiophene-based materials.

5.1 Background and Motivation

The motivation for this work builds from the motivation and knowledge gained for the systems studied in Chapter 4. As discussed throughout this document, conjugated polymers (CPs) have been investigated as active materials in both solid-state and redox-active applications due to their ability to transition from a charge-neutral (insulating) state, to a charged (conducting) state through the processes of either chemical or electrochemical oxidation (doping). Solid-state applications, which capitalize on the electronic charge transport of CPs include radio frequency shielding (RFS) devices,[102,103] thermoelectric generators,[185,186] and transparent conductive electrodes (TCEs).[8,100,124] Redox-active applications require the transport of both electronic and ionic charge and some polymer applications include: electrochromic devices (ECDs),[4,187] supercapacitors,[78,188] and organic electrochemical transistors (OECTs).[27,189] Though there is diversity in the applications of CPs, all benefit from materials that can be easily oxidized and efficiently transport charge.

5.1.1 Structure Property Relationships of Charge Transport

Significant effort has been put into establishing the groundwork for understanding the fundamental structure-property relationships of CPs as they relate to the transport of electronic and ionic charge. In terms of solid-state applications, it has been shown that higher degrees of intermolecular ordering can lead to enhanced electrical conductivity[42,91,190] and charge transport in general,[191] however there is still a question about how this degree of order can relate to ionic transport and electrochemical switching. Some work has suggested that high degrees of intermolecular ordering can lead to inhibited transport of ionic charge.[27,72] Furthermore, it has been shown that doping efficiency of CPs can be improved and electrical conductivities can be increased through the proper selection of a chemical oxidant (dopant).[45,192] The work presented by Scholes *et al.* demonstrated that the ability of the polymer microstructure to incorporate the molecular dopant can also govern the mobility of the generated carriers.[193] In terms of redox-active applications, work in the literature has shown that manipulation of the repeat unit of the polymer can affect properties such as the onset of oxidation,[19] redox capacity,[78,109] and doping kinetics.[74] Alteration of the structure of the side chain of the polymer has also been shown to affect the degree of swelling during electrochemical doping and therefore ionic transport through the polymer film.[27,71,194] In the field of bioelectronics in particular, there has been significant effort towards understanding the structure-property relationships of the mixed transport of ions and electrons, and how the morphology of solution-processed CP films can affect these charge transport properties.[137,195,196]

5.1.2 Use of Dioxythiophene (XDOT) Systems

Dioxythiophene (XDOT)-based materials have been shown to be desirable active materials for use in both solid-state and redox-active applications. For example, a family of soluble dioxythiophene polymers was shown to have high solid-state conductivities after doping (over 200 S/cm).[80] Polymers with repeat units based on 3,4-propylenedioxythiophene (ProDOT) have also been shown to be effective active materials in electrochromic[23] and OECT applications.[81] As discussed in Chapter 4, dioxythiophene-based polymers can perform well in both solid-state and electrochemical applications.

5.1.3 Use of Fused Thiophene Systems

Since 1986, thienothiophene (TT)-based materials have been investigated for their electrochemical properties.[197] Additionally, these fused materials have been shown to be highly conducting due to their planar structure and increased degree of intermolecular ordering after chemical oxidation.[94,95,198-200] These materials have also demonstrated high degrees of crystallinity before chemical oxidation and high mobilities.[201,202] A TT-based polymer with oligoether sidechains has been shown to have electrical conductivities on the order of 100 S/cm[203] and its hydrocarbon sidechain counterpart (PBTTT) has demonstrated high degrees of intermolecular ordering.[67] These materials have also been shown to be effective electrochromic materials[204,205] and charge storage materials in supercapacitors.[206] Given the investigations that have been made concerning TT-based polymers, there is still a lack of holistic understanding of how alteration of the steric twisting of their backbone would affect the transport of both electronic and ionic charge.

5.1.3.1 Development of Dioxythienothiophene (DOTT) Polymers

Dioxythienothiophene-based (DOTT) polymers are a group of materials that combine the electron-rich dioxythiophene and planar thienothiophene moieties. The work from Turbiez *et al.* in 2005 showed that an electrochemically polymerized DOTT homo polymer has electrochromic properties that are similar to those of poly(ethlenedioxythiophene) (PEDOT).[207] This work also demonstrated the highly planar backbone structure of DOTT chains, with the DOTT units in an *anti* conformation and dihedral angles of less than 7°. The authors highlighted how these nearly planar structures were achieved due to non-bonding S-O interactions, with S-O distances (2.80 and 2.83 Å) below the sum of the van der Waals radii of sulfur and oxygen (3.35 Å). It should be noted that these types of interactions have also been observed for EDOT-based conjugated systems, however bis-EDOT distances were shown to be (~2.90 Å).[208]

Since then, DOTTs have been shown to be effective redox-active materials in applications such as electrochromic[204,205] and charge storage devices,[206] however investigations of how alteration of the polymer backbone structure can affect properties such as the degree of intermolecular ordering and charge transport have yet to be explored. It is predicted that their planar structure should promote higher degrees of intermolecular ordering as compared to a ProDOT homo polymer for example (Chapter 4), and their more electron rich backbone should lower their onset of electrochemical oxidation, as compared to PBTTT for example.

5.1.4 Approach

In this work, we gain a comprehensive understanding of how a DOTT moiety can affect the morphology and charge transport of a soluble CP family for use in both solid-state and redox-active applications. To achieve this, we evaluated a series of DOTT-based polymers which includes the homopolymer, two 3,4-ethylenedioxythiophene (EDOT) co-polymers, a dimethyl ProDOT (DMP) co-polymer, and finally a bulky neopentyl dioxythiophene (NeoDOT) co-polymer. In order to further understand the processes of chemical oxidation, we doped this family of polymers with either a bulky organic salt, Tris(4-bromophenyl)ammoniumyl hexachloroantimonate (commonly referred to as "Magic Blue") or planar electron-accepting organic molecule, 2,3,5,6-Tetrafluoro-7,7,8,8-tetracyanoquinodimethane (commonly referred to as F4TCNQ). To our knowledge, this is the first time studies have been conducted on the chemical oxidation of DOTT CPs. We show that DOTT moieties in soluble CPs leads to increased degrees of intermolecular order, but that too much of this order inhibits both electronic charge transport and the ease of electrochemical oxidation. The DOTT homo polymer and DOTT-NeoDOT co-polymer show the highest degrees of intermolecular order in the family, but solid-state conductivities that are four orders of magnitude lower than the other polymers. Furthermore, the electrical conductivity of DOTT-BiEDOT is enhanced by two orders of magnitude, and approaches 20 S/cm after oxidation with the weaker, but more planar chemical oxidant F4TCNQ as compared to Magic Blue. Finally, it is shown that chemically oxidized DOTT polymers have enhanced air stability and retain up to 70% of their original conductivity after storage in ambient conditions for two weeks, as compared to state-of-the-art materials such as PBTTT.

For this study, we designed a family of polymers that incorporate a DOTT moiety as depicted in Figure 5.1-1. Details on the synthesis, purity, and molecular weights of these materials can be found in the Supporting Information section of this chapter. The DOTT moiety was targeted due to its fused and planar structure, with evidence from work in the literature that this would enhance inter-chain ordering and solid-state conductivity in the doped and oxidized state.

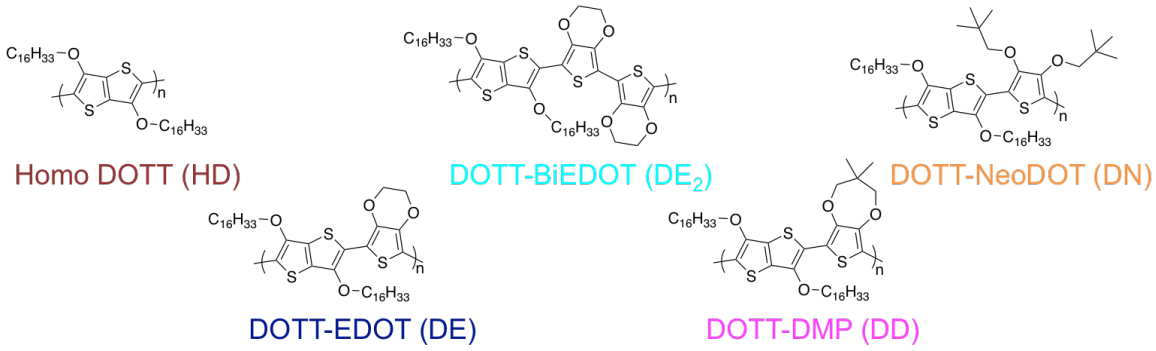

Figure 5.1-1 – Repeat unit structures of the polymers used in this study.

In order to gain a holistic understanding of the structure-property relationships of the DOTT family, the homo polymer (HD), as well as four co-polymers were synthesized. Previous work showed that the incorporation of EDOT structures into the repeat unit of a soluble dioxythiophene polymer can lead to increased solid-state conductivities after chemical oxidation and relax the steric strain of the polymer backbone.[80] The DMP unit was included following the work conducted by Savagian et al., which showed that dioxythiophene polymers that incorporate the DMP moiety are redox-active in both organic and aqueous electrolytes.[81] The DMP unit was also targeted as it would induce less steric bulk than a ProDOT unit substituted with long solubilizing side chains, but still possess substituted groups that are out of plane relative to the polymer backbone due to

the sp^3 hybridized carbon in the propylene bridge. Furthermore, it has not yet been explored how both the EDOT and DMP moieties can affect properties such as the degree of intermolecular ordering and the interactions between molecular dopants and conjugated polymer chains in dioxythienothiophene polymer systems. Finally, the polymer DOTT-NeoDOT (DN) was included in this study in order to understand how the DOTT material properties would be affected by a more sterically strained backbone. The neopentyl side chains substituted onto the dioxythiophene provide larger amount of steric bulk as compared to either the EDOT or DMP units, resulting in a polymer that should have a more twisted backbone relative to the other polymers in the family. Building from the previous work in Chapter 4 involving acyclic dioxythiophenes, this is expected to result in a polymer that is more difficult to oxidize than the rest of the family, and result in highly ordered polymer films.

5.2 Characterization of Intermolecular Ordering

The degree of intermolecular ordering has been shown to have a large influence on the charge transport properties of CPs. One method for evaluating this property is grazing-incidence wide-angle x-ray scattering (GIWAXS). GIWAXS measurements can show the degree and directionality of the polymer chain ordering relative to the sample substrate, and can also be used to extract interchain spacing distances. For this work, it is not only important to understand how the polymer repeat unit can affect the film morphology, but also how this morphology can be altered after doping with a molecular chemical oxidant and how this relates to the polymer film's electrical conductivity.

GIWAXS measurements were performed on blade-coated polymer films as shown in Figure 5.2-1. The scattering images reveal that the polymer backbone structure does have an effect on the degree of ordering and directionality of the polymer films. We see that Homo DOTT (Figure 5.2-1a), DOTT-BiEDOT (Figure 5.2-1c), and DOTT-DMP (Figure 5.2-1d) have preferential lamellar ordering (100) in along the Q_{xy} direction and preferential π-π stacking (010) along the Q_z direction, showing that the polymer chains are most ordered in plane relative to the substrate. These trends are evidenced by the more narrow (100) peaks along the Q_{xy} direction as compared to the more diffuse (100) peaks along the Q_z direction.

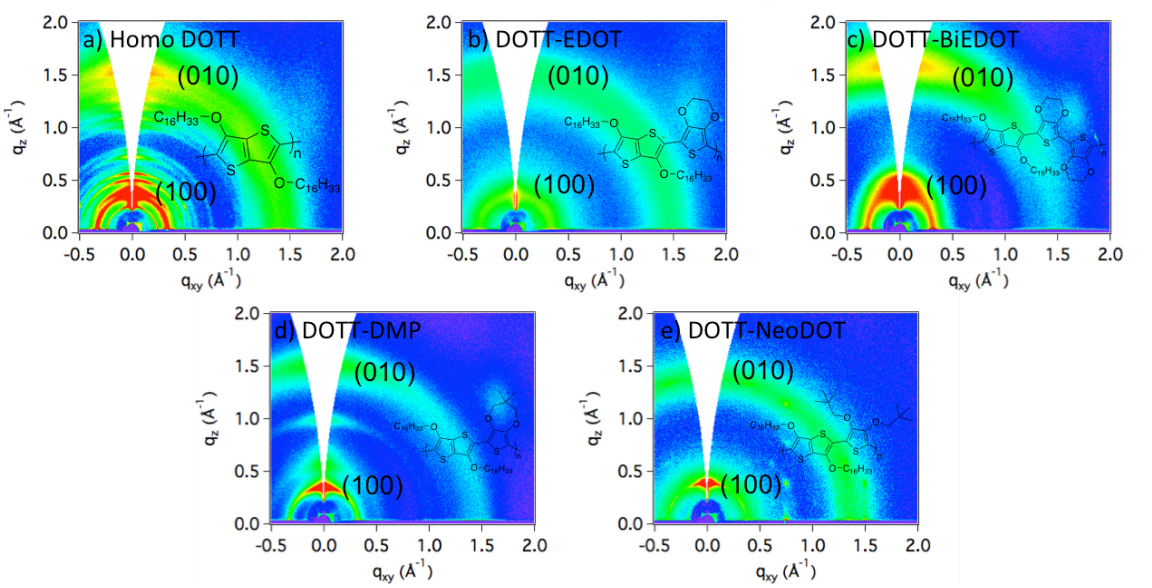

Figure 5.2-1 – GIWAXS images of as-cast blade-coated films of Homo DOTT (a), DOTT-EDOT (b), DOTT-BiEDOT (c), DOTT-DMP (d), and DOTT-NeoDOT (e) on silicon wafers.

Q_z linecuts of all polymers can be seen in Supporting Figure 5-1. Homo DOTT is shown to be the most highly ordered of the group (Figure 5.2-1a) as shown by the multiple signals along the Q_z and Q_{xy} axes relating to high degrees of lamellar ordering. It

is hypothesized that the large number of scattering signals could be due to the presence of multiple polymorphs in the film, as many peaks are observed very close together. If no polymorphs were observed, we would expect for each of these peaks to occur at distances that are integer multiples of each other. DOTT-EDOT (Figure 5.2-1b) in contrast, is shown to be the least ordered of the group as evidenced by the halos in the (100) and (010) planes.

Homo DOTT, DOTT-EDOT, and DOTT-DMP, show the lamellar (100) diffraction band at $Q_z = 0.34$ Å^{-1} (interplanar distance d = 18 Å). The scattering images for DOTT-BiEDOT (Figure 5.2-1c) and DOTT NeoDOT (Figure 5.2-1e), show a slight shift towards tighter lamellar spacings (smaller q), of 17 Å and 16 Å respectively. Given the length of the side chains of these materials (10 carbon atoms), all of these spacing distances indicate lamellar interdigitation. In the case of the π-π stacking distances (010 plane), all of the polymers show diffraction bands at $Q_z = 1.5$ Å^{-1} (interplanar distance d = 4.2 Å), with the exception of DOTT-NeoDOT (Figure 5.2-1e), which shows a diffraction band at $Q_z = 1.3$ Å^{-1} (interplanar distance d = 4.8 Å). The spacing distances for the majority of the DOTT polymers are tighter than those found for branched and linear chain dioxythiophene homopolymers, which had interplanar distances of 4.5 Å (Chapter 4). DOTT-NeoDOT on the other hand has a larger π-π stacking distance by 0.3 Å than the dioxythiophene polymers. All of these dioxy-based thiophene and thienothiophene polymers have larger π-π stacking distances by about 1 Å as compared to P3HT for example, which is in the range of 3.7-3.8 Å.[41,66,91,209] It is interesting to note that DOTT-NeoDOT has the smallest lamellar spacing distance and the largest π-π stacking distance. This trend is likely due to the steric bulk of the neopentyl groups on the dioxythiophene.

While this bulk does not increase the distance between the lamellae, it prevents the backbones of the polymer chains from coming close together. Despite the differences in the scattering patterns of these polymers, all materials, except Homo DOTT, show smooth and continuous films as evidenced by the atomic force microscopy (AFM) images, as seen in Supporting Figure 5-2, and photographs, as seen in Supporting Figure 5-3. The Homo DOTT polymer shows films that are rougher (Figure 5-2a) than the other polymers in the family, as the AFM height image shows a height range that is 2.5 times larger than for the other images. Films of Homo DOTT are still continuous as evidenced by the photograph in Supporting Figure 5-3a. It is interesting to note that Homo DOTT has a high degree of intermolecular ordering and a more rough film topography as compared to the other polymers in the family. It could be hypothesized that the more highly ordered system is creating a topography consisting of peaks and valleys in the polymer film, causing it to be rougher.

5.3 Chemical Oxidation and Solid-State Conductivity

It is not only important to understand how the polymer structure can affect overall morphology, but it is also important to understand how these properties relate to the processes of doping and overall electrical conductivity. In this study, all polymer films were chemically oxidized after film formation using solutions of chemical oxidants in propylene carbonate. Sequential doping was chosen as the doping method as it has been shown to disrupt the polymer microstructure to a lesser degree than co-processing the polymer and dopant.[41,53,70] Propylene carbonate was selected as the solvent for the chemical oxidant solutions as it can dissolve the chemical oxidants, but not the polymer films and is the same solvent used for the electrochemical characterizations that will be

discussed in the next section. After exposure for 30 s, polymer films were rinsed with clean methanol in order to remove any excess dopant before further experimentation. For this work, two dopants were selected in order to probe the structure-property relationships of the DOTT polymers and chemical oxidants. These two dopants were Magic Blue and F4TCNQ. These dopants were selected as they are both considered to be strong electron acceptors,[65] with $E_{1/2}$ values above 0.2 V vs Ag/Ag^+ as shown in Supporting Figure 5-4, but have different structures after accepting an electron as shown in Supporting Figure 5-5. Doping times of 30 seconds were selected because upon further exposure to solutions of Magic Blue, polymer films showed delamination from the substrate. Here, Magic Blue has two components, both the electron-accepting triphenyl amine and the counterbalancing $SbCl_6$ anion, whereas the single F4TCNQ molecule acts as both the electron acceptor and counterbalancing anion to the charged polymer film.

As the optical properties of the polymers in the DOTT family depend on their redox state, we are able to track their extent of oxidation using UV-vis spectroscopy. In their neutral state, all of the polymers absorb in the visible region of the spectrum. Upon exposure to either 10 mM Magic Blue or F4TCNQ, all polymers are oxidized from their neutral form, and absorb in the infrared. Figure 5.3-1 shows example spectra corresponding to DOTT-EDOT (Figure 5.3-1a) and DOTT-NeoDOT (Figure 5.3-1b), and the spectra corresponding to the remaining polymers can be seen in Supporting Figure 5-6. The $SbCl_6$ anion in Magic Blue does not absorb light in the shown region of the spectrum, so there are not any additional contributions besides the oxidized polymer absorption when using this chemical oxidant. In contrast, F4TCNQ in its neutral and radical anion state (as shown in red) both absorb in the visible region of the spectrum.[210]

The peak occurring around 400 nm corresponds to the neutral F4TCNQ molecule, and the peaks seen between 600-900 nm correspond to a mix of the polaronic charge carriers from the oxidized polymers as well as the F4TCNQ anion.

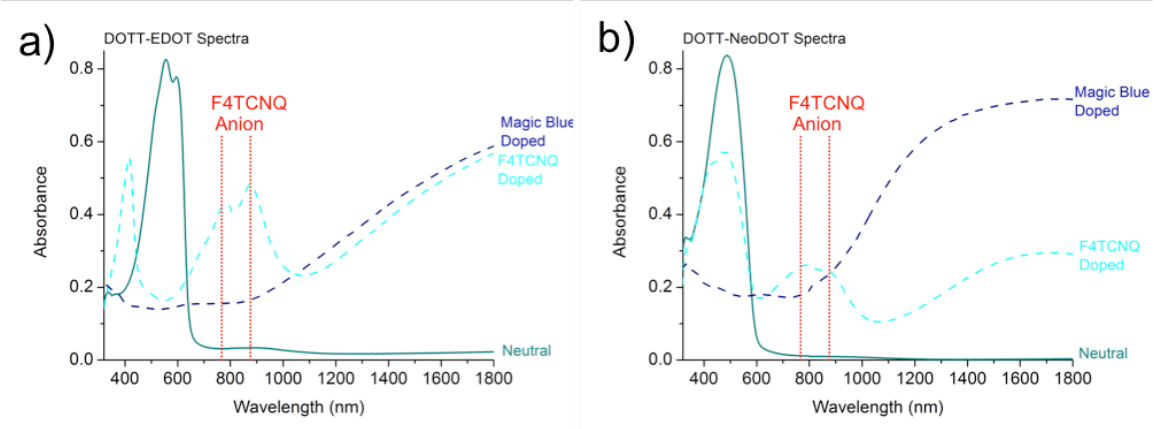

Figure 5.3-1 – UV-vis absorption spectra of blade-coated polymer films of (a) DOTT-EDOT and (b) DOTT-NeoDOT on glass before and after 30 s of exposure to a 10 mM solution of either Magic Blue (dark blue curve) or F4TCNQ (cyan curve) in propylene carbonate and a subsequent methanol rinse. Absorbance at 400 nm corresponds to the neutral F4TCNQ molecule.

When doping with both Magic Blue and F4TCNQ, it can be seen that the neutral π-π^* absorbance of DOTT-EDOT is fully depleted, while this absorbance is still observed when doping DOTT-NeoDOT with F4TCNQ. In fact, it is quite surprising that DOTT-NeoDOT is even partially oxidized when using F4TCNQ, as the $E_{1/2}$ value of the dopant is almost identical to the onset of oxidation of the polymer. It should be noted that these electrochemical measurements are used as estimates for the energy levels of these materials, but the observation of charge transfer is still unexpected and interesting. The neutral absorbance for Homo DOTT is also not fully depleted when doping with F4TCNQ (Supporting Figure 5-6a). It can be seen that both dopants result in the generation of polaronic charge carriers for Homo DOTT and DOTT-NeoDOT, as

evidenced by their absorbance in the near infrared. The electrochemical properties of the polymer family will be discussed further on, but this difference in the extent of oxidation likely has to do with the differences in morphology of the polymer films. From the GIWAXS measurements of Homo DOTT and DOTT-NeoDOT (Figure 5.2-1a and 5.2-1e) we see that Homo DOTT is highly ordered and DOTT-NeoDOT has tighter lamellar spacing distances as compared to the other polymers. Work from Thomas *et al.* in 2018, showed that for a thiophene polymer with branched side chains, the steric bulk from the polymer sidechain can prevent effective charge transfer and complete doping when using F4TCNQ in vapor phase doping.[45] In this work, the authors concluded that due to the bulk of the (2-ethyl)hexyl side chain caused the molecular dopant to reside between the π-faces of the polymer crystallites, resulting in only partial charge transfer. Here, it is hypothesized that because Homo DOTT is highly ordered and DOTT-NeoDOT possesses more steric bulk in its repeat unit, these polymers are in a more locked conformation and have film morphologies preventing effective charge transfer with F4TCNQ. In contrast, it is likely that the higher strength of the Magic Blue dopant allows it to fully dope these more highly ordered polymers.

Turning to the more disordered polymer systems, the spectra corresponding to DOTT-BiEDOT (Supporting Figure 5-6b), and DOTT-DMP (Supporting Figure 5-6c), show that when doping with either Magic Blue or F4TCNQ a complete depletion of the neutral π-π^* transition and growth of absorbance between 900-1800 nm can also be observed. DOTT-BiEDOT is a unique polymer in the family in that it is sufficiently easy to oxidize that it is oxidized in air. The absorbance centered at 850 nm in the neutral curve of Supporting Figure 5-6b corresponds to polaronic charge carriers. As can be seen

in Figure 5.3-1 and Supporting Figure 5-6, this is not present for any of the other polymers in the family.

In addition to understanding how the structure and morphology of the polymers can affect the extent of oxidation after exposure to chemical oxidants, it is also important to understand how this parameter can affect the overall electrical conductivity. Electrical conductivity (σ) can be represented as the product of charge carrier concentration (n), charge mobility (μ), and charge carried (e), ($\sigma = n \cdot \mu \cdot e$).[40] This representation is an oversimplification as the mobile carrier concentration and its mobility fluctuates significantly as a function of energetic and spatial coordinate in semicrystalline polymers.[191,211] Despite this oversimplification, electrical conductivity measurements as a function of dopant species and concentration can provide guidance and reasoning for future electrical conductivity optimizations when used in conjunction with structural and spectral characterizations.

Figure 5.3-2 shows the electrical conductivity as a function of polymer repeat unit (Homo DOTT [HD], DOTT-EDOT [DE], DOTT-BiEDOT [DE_2], DOTT-DMP [DD], and DOTT-NeoDOT [DN]) and dopant species. In the pristine state (not doped), these polymers have electrical conductivities less than 10^{-5} S/cm. Upon doping with 10 mM Magic Blue or F4TCNQ, all polymers in this study show at least a two order of magnitude increase in the electrical conductivity after chemical oxidation.

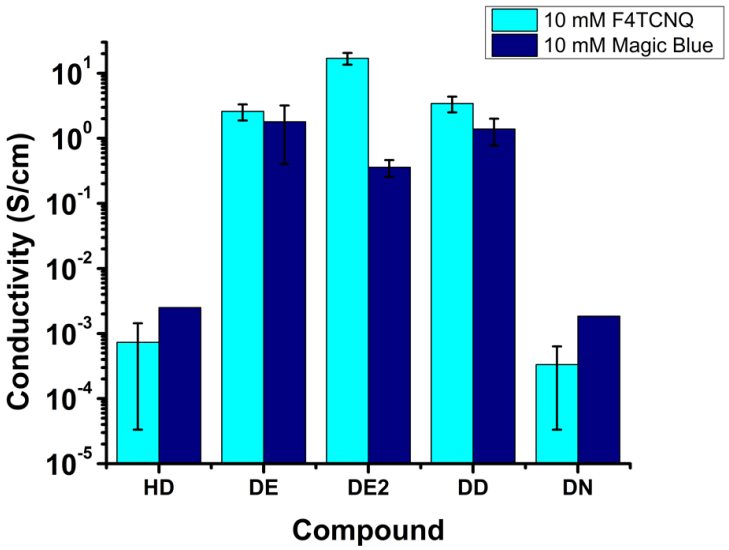

Figure 5.3-2 – The electronic conductivity values of blade-coated polymer films on glass after exposure to either a 10 mM Magic Blue or 10 mM F4TCNQ solution in propylene carbonate for 30 seconds and a subsequent methanol rinse.

The conductivity of DOTT-BiEDOT (DE_2) increases by 6 orders of magnitude and approaches 20 S/cm, which exceeds many values reported in the literature by up to two orders of magnitude for the commonly studied P3HT:F4TCNQ system using various chemical doping procedures including solution co-processing,[64,66,70,178,199,212] and sequential doping.[41,70,91,200] We observe that in general, DOTT-EDOT (DE), DOTT-BiEDOT (DE_2), and DOTT-DMP (DD) show the highest electrical conductivities by 3 orders of magnitude as compared to Homo DOTT (HD) and DOTT-NeoDOT (DN) when doping with either Magic Blue or F4TCNQ. Furthermore, we observe that as the dopant chemical species changes from Magic Blue to F4TCNQ, electrical conductivity generally increases (Figure 5.3-2). This observation is initially counterintuitive as Magic Blue has a higher oxidation potential than F4TCNQ and should generate more charge carriers (Supporting Figure 5-3). We observe at a 10 mM concentration that Magic Blue does

indeed generate more charge carriers than F4TCNQ (Supporting Table 5-1 and Supporting Table 5-2), but we also observe that the microstructure is more heavily disrupted by Magic Blue than F4TCNQ given the larger lamellar and π-π spacing distances after chemical oxidation with Magic Blue as seen in Supporting Table 5-3. For example, we see that for Homo DOTT the lamellar spacing is 2.1 Å larger when doping with Magic Blue as compared to F4TCNQ. Turning to the π-π spacing distance of this polymer, the spacing is 1 Å larger when doping with Magic Blue. Turning to the DOTT-BiEDOT polymer, we see a 3.7 Å increase in the lamellar spacing when doping with Magic Blue as compared to F4TCNQ and a 0.6 Å increase in the π-π spacing distance. We hypothesize that doping with Magic Blue disrupts the microstructure to a greater extent than F4TCNQ because Magic Blue doping involves an octahedral $SbCl_6$ counterion while F4TCNQ doping yields a planar anion.[210] Recent studies have suggested that bulkier counterions likely disrupt the microstructure and decrease electrical conductivity more than their planar counterparts,[213] and we believe that the $SbCl_6$ versus F4TCNQ comparison herein supports this observation.

Because of its higher electrical conductivity values, F4TCNQ doping was further explored by varying its dopant concentration. Figure 5.3-3 shows the electrical conductivity as a function of F4TCNQ doping concentration (1 to 50 mM) and polymer repeat unit. We note the electrical conductivity generally increases with increasing doping concentration, and this is commonly observed. Interestingly however, we observe that the electrical conductivity for DE, DE_2, and DD plateaus when excessively doped with chemical oxidants; oftentimes, the electrical conductivity decreases when excessively chemically doped.[75,213,214]

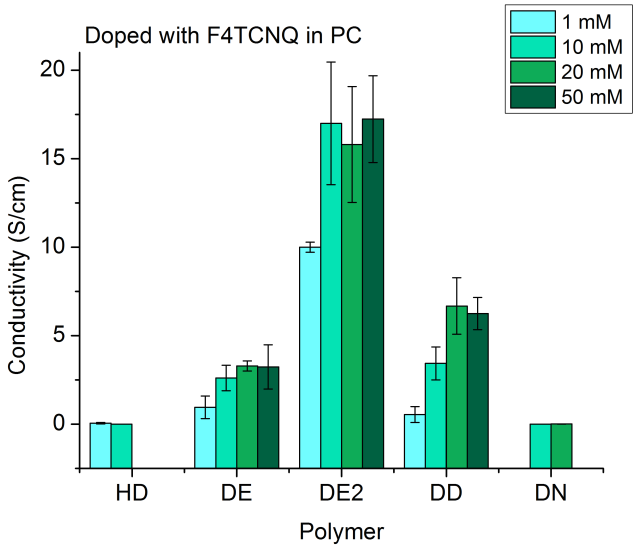

Figure 5.3-3 – The electronic conductivity values of blade-coated polymer films on glass after exposure to F4TCNQ dopant solutions of varying concentrations in propylene carbonate for 30 seconds and a subsequent methanol rinse.

The electrical conductivity of DE, DE_2, and DD remain effectively invariant as doping increases from 20 to 50 mM (the measured values are within error bars). Based on XPS characterizations (Supporting Table 5-2), we see that increased F4TCNQ dopant concentration leads to increased charge carrier concentration. This implies that increased numbers of charge carriers for DE, DE_2, and DD do not inhibit their mobility. It is hypothesized that this is due to the ease at which these polymers are able to delocalize charge carriers along their backbones.

Additionally, we observe that electrical conductivity increases from DE to DD to DE_2 at 50 mM F4TCNQ. We can relate this trend to the increased degree of structural order and tighter π-π spacing distances demonstrated by DE_2 as compared to the other polymers after doping with F4TCNQ as seen in Supporting Figure 5-7. In addition to conductivity values approaching 20 S/cm, polymers in the DOTT family also demonstrate enhanced air stability in the doped state. Supporting Figure 5-8 shows the

polymers' normalized retained conductivity as a function of the number of days oxidized films have been stored in ambient lab conditions. Measurements were taken for DE, DE_2, and DD films that were oxidized with solutions of F4TCNQ with concentrations ranging from 1-50 mM in propylene carbonate. As seen in Supporting Figure 5-8, the concentration of dopant has little effect on the overall retention of original conductivity, rather the degree of retention depends on the polymer structure. DE and DD have similar trends in that they lose up to 50% of their original conductivity, however DE_2 retains over 70 % of its original conductivity after stored in ambient conditions for 2 weeks. This is a significant increase in the doped air stability of polymers such as PBTTT, which in our experimentation was shown to lose all of its conductivity within 3 hours of doping.

5.4 Electrochemical Characterization

Considering the variety of applications for CPs, it is also important to understand how the structure of the DOTT family can affect their redox properties. In order to understand the electrochemical doping process of the DOTT polymers, films were drop-cast onto glassy carbon electrodes and studied using conventional voltammetry techniques. The onset of oxidation is probed by differential pulse voltammetry (DPV). Cyclic voltammetry (CV) is used to measure the ease at which an electron can be removed from the polymer film and the polymer film's current response as a function of applied potential. The DPV results can be seen in Supporting Figure 5-9, and the CVs of each polymer are shown in Figure 5.4-1.

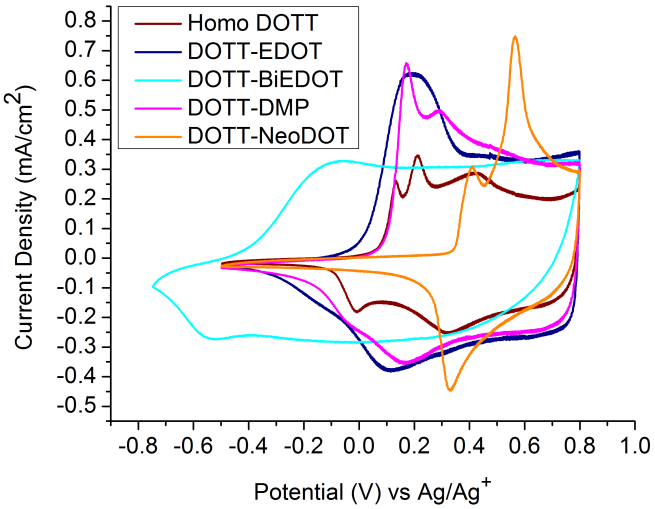

Figure 5.4-1 – Cyclic voltammograms for drop-cast films of Homo DOTT in red, DOTT-EDOT in navy blue, DOTT-BiEDOT in cyan, DOTT-DMP in magenta, and DOTT-NeoDOT in orange on a glassy carbon electrode as the working electrode in a three-electrode cell in a 0.5 M $TBAPF_6$ electrolyte in propylene carbonate at a scan rate of 50 mV/s.

As with the morphology of the polymer films, we see that the polymer repeat unit structure has an effect on the onset of oxidation of the material. These onsets measured through DPV cover a range of almost 0.9 V, with DOTT-BiEDOT being the easiest to oxidize at -0.62 V and DOTT-NeoDOT being the hardest to oxidize at 0.30 V. We see that with the addition of one EDOT moiety, the onset of oxidation is lowered by 0.14 V from 0.05 V for Homo DOTT, to -0.09 V for DOTT-EDOT. This onset is further lowered by 0.53 V the addition of a second EDOT unit for DOTT-BiEDOT. The onset of oxidation for DOTT-DMP occurs at -0.04 V. We see that the onsets of oxidation are within 0.1 V for Homo DOTT and DOTT-DMP and we would expect that when doping these two polymers they would generate a similar number of charges. We can see from the CV curve areas in Figure 5.4-1 that the relative area for DOTT-DMP is larger than for Homo DOTT. Furthermore, from the XPS experiments (Supporting Table 5-2) we see

that for a given concentration of F4TCNQ, fewer charge carriers are being generated for Homo DOTT as compared to the other polymers in the family. We hypothesize that the higher degrees of ordering observed for Homo DOTT is one reason why this polymer cannot generate as many charge carriers as DOTT-DMP. The microstructure of Homo DOTT is significantly more perturbed (Supporting Table 5-3), with lamellar stacking distances increasing up to 5 Å after doping. This implies that it is more difficult for dopant and electrolyte ions to penetrate the polymer matrix in order to generate or stabilize any introduced charges.

These results also correspond nicely with the results found for the Pro/Ac system studied in Chapter 4. In both cases we see that polymers with sterically strained backbones (Ac-EH and DOTT-NeoDOT) have the highest onsets of oxidation in their respective families. Furthermore, we see that their onsets of electrochemical oxidation are very similar, as they both occur around 0.3 V. Both of these polymers exhibit high degrees of intermolecular ordering according to GIWAXS measurements. It is hypothesized that for both dioxythiophene and dioxythienothiophene-based polymers, a high degree of steric strain causes polymers to be in a more "locked" conformation, which inhibits their ease of oxidation and causes the polymer chains to pack in a more regular fashion.

As was discussed in the previous section, because the optical properties of these polymers are dependent on their redox state, we are able to monitor the polymer's doping level as a function of applied potential. Figure 5.4-2 shows the results for example spectroelectrochemical experiments for DOTT-EDOT (Figure 5.4-2a) and DOTT-NeoDOT (Figure 5.4-2b).

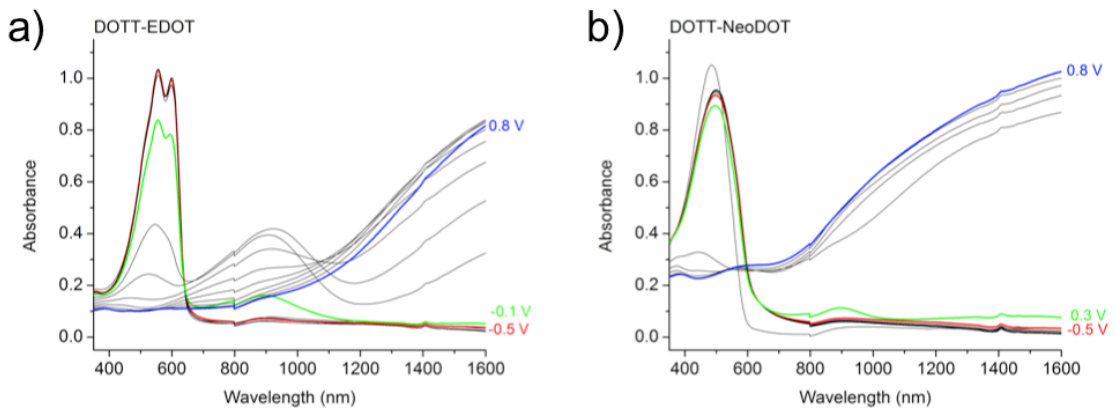

Figure 5.4-2 – UV-vis absorption spectra as a function of applied potential of spray-coated polymer films of (a) DOTT-EDOT, and (b) DOTT-NeoDOT on ITO/glass in a 0.5 M $TBAPF_6$ electrolyte in propylene carbonate.

The full spectroelectrochemical series for all polymers in the family collectively can be seen in Supporting Figure 5-10. When increasing the potential from -0.5 to 0.8 V vs Ag/Ag^+ it can be seen that all polymers are fully oxidized, as evidenced through the complete depletion of their neutral π-π^* absorbance. Furthermore, upon the depletion of the neutral absorbance, we see a growth of absorbance beyond 700 nm for all materials. Here, the repeat unit of the polymer causes a difference in the number of intermediate states between the fully neutral polymer film (highlighted in red, at -0.5 V) and the fully oxidized polymer film (highlighted in blue, at 0.8 V). Homo DOTT (Supporting Figure 5-10a), DOTT-EDOT (Figure 5.4-2a), DOTT-BiEDOT (Supporting Figure 5-10c), and DOTT-DMP (Supporting Figure 5-10d) all have multiple intermediate states before the full depletion of their neutral absorbance, whereas DOTT-NeoDOT (Figure 5.4-2b), shows an almost immediate transition from the neutral to the fully oxidized state.

In order to directly compare the trends for all the polymers, the results of these spectroelectrochemical experiments are shown collectively in Figure 5.4-3, where the

absorbance at λ_{max} for each polymer is plotted as a function of the applied potential. The extent of electrochemical doping follows the same trend as was seen with the extent of oxidation.

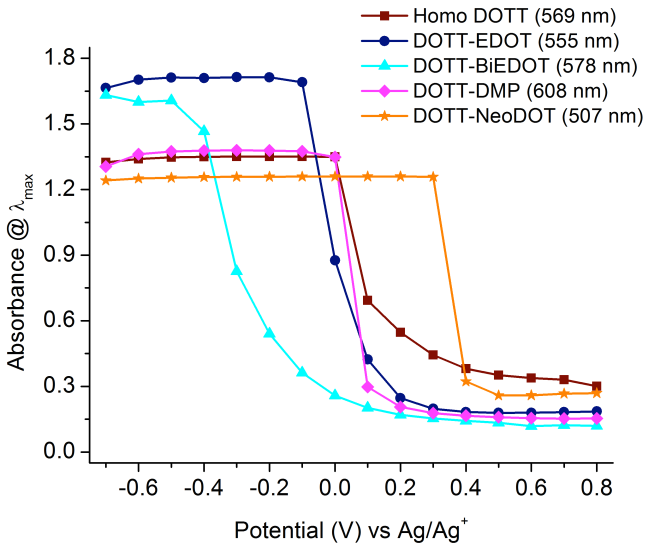

Figure 5.4-3 – Absorbance values at each polymers λ_{max} taken from UV-vis absorption spectra as a function of applied potential from -0.7 to 0.8 V versus Ag/Ag^+ for blade-coated Homo DOTT (red), DOTT-EDOT (navy blue), DOTT-BiEDOT (cyan), DOTT-DMP (magenta), and DOTT-NeoDOT (orange) films on ITO/glass in a 0.5 M $TBAPF_6$ electrolyte in propylene carbonate.

The neutral π-π^* absorption for DOTT-BiEDOT begins to deplete at -0.6 V and the material is fully oxidized by 0.4 V. In contrast, the π-π^* absorption of DOTT-NeoDOT does not begin to deplete until 0.4 V, and no further evidence of optical changes are observed at higher potentials. Turning to DOTT-DMP and Homo DOTT once again, it is interesting to note that it takes higher potentials to achieve the same degree of doping for Homo DOTT as compared to DOTT-DMP. We see that more of the neutral π-π^* absorption peak is depleted at 0.1 V for DOTT-DMP as compared to that of Homo DOTT. Again, we observe evidence that it is harder for Homo DOTT to be doped

as compared to DOTT-DMP, though they have the same onset of oxidation according to DPV. This is further support of the idea that the increased degree of intermolecular chain ordering inhibits both the electrochemical and chemical doping of the Homo DOTT polymer.

To further probe the effects of polymer structure on the redox processes of the DOTT polymer family, electrochemical conductance experiments were performed. Polymer films were drop-cast onto interdigitated microelectrodes, which were incorporated into an electrochemical cell.[115] The potential difference was held constant on one half of the microelectrodes, while the other half was cycled +/- 5 mV around the applied potential and the resulting current response was recorded. The potential window used for these experiments was -0.5 to 0.8 V vs an Ag/Ag^+ reference electrode and results were recorded at 0.1 V increments as shown in Figure 5.4-4. The conductance curve for each polymer was calculated from the average of three separate films. To confirm the reversibility of the polymer conductance, reverse direction curves (from high to low potential) can be seen in Supporting Figure 5-11, and a smaller conductance axis for polymers demonstrating low conductance values can be seen in Supporting Figure 5-12. The turn-on conductance response is observed to vary with the polymer onset of oxidation. DOTT-BiEDOT shows a turn-on at the lowest potential of -0.3 V, followed by DOTT-EDOT at 0.0 V, and DOTT-DMP at 0.1 V. All three of these polymers achieve high conductance values of around 6 mS at high potentials. As with the electrical conductivity data collected after chemical doping, the conductance of these materials does not drop back to 0 at the highest potential of 0.8 V. Similar to the trends observed for the electrical conductivity data, we again see that Homo DOTT and DOTT-NeoDOT

have the lowest conductance values overall. Homo DOTT does not demonstrate a conductance response until 0.2 V, and DOTT-NeoDOT turns on at 0.4 V (Supporting Figure 5-12).

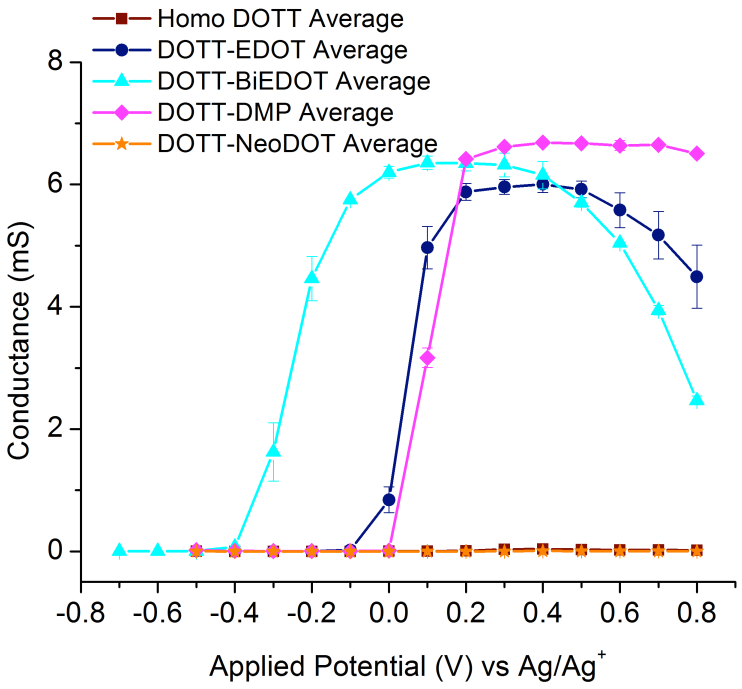

Figure 5.4-4 – *In situ* electrochemical conductance of Homo DOTT (red), DOTT-EDOT (navy blue), DOTT-BiEDOT (cyan), DOTT-DMP (magenta), and DOTT-NeoDOT (orange) from -0.5 to 0.8 V vs Ag/Ag^+ in a 0.5 M $TBAPF_6$ electrolyte in propylene carbonate. Averages taken from values collected from three films of each polymer.

In comparison with the other polymers in the family, these materials have significantly lower overall conductance values. This experiment again highlights how polymer film morphology can affect charge transport. Considering their similar onsets of oxidation, it would be expected that Homo DOTT and DOTT DMP would have similar turn-on values, however Homo DOTT requires a higher potential to give a conductance response. Similar to the electrical conductivity data, we also see that Homo DOTT is significantly

less conductive than DOTT-DMP. Again, this is likely due to the fact that the highly ordered microstructure of Homo DOTT is perturbed during doping, which leads to the inhibition of any charge transport processes.

5.5 Conclusions and Perspective

The work presented in this study built on the knowledge of structure-property relationships of DOTT-based conjugated polymers as it relates to their charge transport properties. Soluble DOTT polymers were shown to have conductivities that approach 20 S/cm after chemical doping with F4TCNQ and have electrochemical onsets of oxidation below 0 V vs Ag/Ag^{+}. It was shown that materials with intermediate degrees of ordering had superior properties in that they had: higher electrical conductivities, lower onsets of oxidation, and higher electrochemical conductance values as compared to the materials that had higher degrees of ordering. GIWAXS measurements showed that the polymers that demonstrated higher degrees of ordering were more perturbed during the doping process, which resulted in poorer performance. Comparing results for the polymers Homo DOTT and DOTT-DMP show that while polymers may have the same electrochemical ease of oxidation, they can have a three order of magnitude difference in their solid-state conductivity after chemical oxidation. The GIWAXS results for DOTT-DMP showed that this polymer had an intermediate degree of order as compared to Homo DOTT. After doping with F4TCNQ, the microstructure of this polymer film was not disrupted, which implied that the molecular dopant was able to interact with the polymer matrix such that charge transfer could occur and the newly generated charges could be effectively delocalized without being trapped. We find that highly ordered polymer films are more difficult to oxidize and transport charge as compared to less

ordered polymer systems. It was hypothesized that highly ordered polymer systems have a more "locked conformation" which prevents the ease of oxidation and delocalization of charge along the backbone.

Furthermore, when selecting dopants for high electrical conductivity applications, the strength of the dopant is not the sole determinant in the overall electrical conductivity value. Results showed that it is important to understand the geometric interactions between the polymer film and chemical oxidant, which is a concept that has been shown in other work reported in the literature.[45] Even though Magic Blue had a sufficient oxidizing strength, its bulky structure caused the microstructure of the polymer films to be more perturbed than when doping with F4TCNQ. A combination of GIWAXS, XPS, UV-Vis absorption, and in-plane solid-state conductivity measurements showed that the two chemical oxidants could generate charge carriers in polymers that were highly ordered, but a combination of the disruptions of the microstructure of the polymer films and bulkiness of the substituents on the polymer backbone prevented high conductivities from being attained. This unique family of polymers has demonstrated the multiple factors that can inhibit both chemical and electrochemical oxidation and transport of charge.

5.6 Experimental and Supporting Information

Dr. James Ponder synthesized and performed all of the structural confirmation experimentation for the polymers studied in this work. These details are reported in a forthcoming manuscript that he is currently writing and have been reproduced here.

5.6.1 Materials Synthesis and Characterization

$Pd(OAc)_2$ (98 %, Strem Chemicals), pivalic acid (99 %, Sigma), K_2CO_3 (anhydrous, Oakwood Products), 18-crown-6 (99 %, Acros), diethyldithiocarbamic acid diethylammonium salt (97 %, TCI America), 2-hexyldecyl alcohol (97%, Sigma), sodium methoxide (95%, sigma), potassium iodide (>99%, Sigma), copper(I) iodide (98%, Sigma), *para*-toluenesulfonic acid monohydrate (*p*TSA, >98.5%, Sigma), and 3,4,7,8-Tetramethyl-1,10-phenanthroline (98%, Fluorochem) were used as received. DMAc (HPLC grade, Alfa Aesar) was filtered through a pad of alumina (basic, Sigma Aldrich) and degassed by argon bubbling before use. Tetrabutylammonium hexafluorophosphate ($TBAPF_6$, 98%, Alfa Aesar) was purified by recrystallized from hot ethanol. Propylene carbonate was used as the electrolyte solvent (PC, Acros Organics, 99.5 %) and was purified and dried using a solvent purification system from Vacuum Atmospheres. EDOT (97%) was obtained from Alfa Aesar and vacuum distilled prior to use. 2-2'-BiEDOT was prepared via a previously reported method.[215] 3,6-Dimethoxy-thieno[3,2-*b*]thiophene was prepared following a previously reported route.[216]

3,6-Di(2-hexyldecyloxy)-thieno[3,2-*b*]thiophenes (DOTT-HxDc)

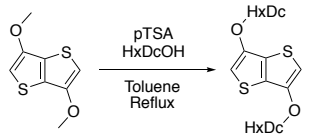

2-5-Dibromo-3,6-di(2-hexyldecyloxy)-thieno[3,2-*b*]thiophenes (DOTT-HxDc-Br)

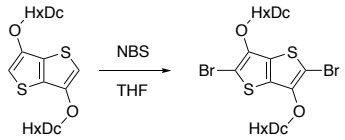

3,4-Dineopentyloxy-thiophene (NeoDOT)

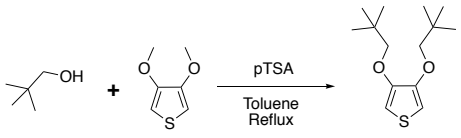

Into a 250 mL round bottom flask with a stir bar was added freshly distilled 3,4-dimethoxythiophene (1.50 g, 10.4 mmol), neopentyl alcohol (2.75 g, 31.2 mmol), PTSA (0.179 g, 1.04 mmol), and toluene (100 mL). A soxhlet condenser with a cellulose thimble filled with 3 Å molecular sieves was attached to the head of the flask. Solution was refluxed for 24 hours then cooled to room temperature. Et_2O (50mL) was added to the mixture and was washed with H_2O (3 x 100 mL). The organic solvent was removed in vacuo and the product was purified via column chromatography (1:9 EtOAc:Hexanes) to afford a white crystalline solid in 74% yield (1.97 g). Melt point: 58-59 °C. ^{1}H NMR ($CDCl_3$, ppm): δ 6.14 (s, 2H), 3.60 (s, 4H),1.03 (s, 18H); ^{13}C NMR ($CDCl_3$, ppm): δ 148.14, 97.76, 79.98, 32.01, 26.54. HRMS, $C_{14}H_{24}O_2SNa$ Calculated m/z: 279.1389, Measured m/z: 279.1390.

ProDOT-NeoDOT

To a 25 mL schlenk tube equipped with a stir bar, ProDOT(2-EtHxOCH$_2$)$_2$-Br$_2$ (0.500 g, 0.835 mmol), NeoDOT (0.500g, 0.835 mmol), 2 mol% palladium acetate (3.7

mg, 0.017 mmol), pivalic acid (0.0.85 g, 0.835 mmol), and potassium carbonate (0.346 g, 2.51 mmol) were added. The mixture was then vacuum purged for 45 minutes followed by three purge and argon back-fill cycles. DMAc (8.4 mL) was degassed by bubbling with argon for 45 minutes and then injected into the flask to dissolve the contents. The reaction mixture was stirred at 140 ˚C for 24 hours and then removed from the heat and allowed to cool to r.t. The polymer dispersion was dissolved with $CHCl_3$ and precipitated into methanol and stirred for 45 minutes. The precipitate was filtered into a soxhlet extraction thimble and washed with methanol, acetone, hexanes, and chloroform respectively. The washings were conducted until color was no longer observed during extraction. After dissolution from the soxhlet thimble, the solvent was removed via rotovap and then 20 mL of chloroform was added followed by 100 mg of the palladium scavenger diethylammonium diethyldithiocarbamate, 150 mg of 18-crown-6 and then stirred for 6 hours at 50 °C. The polymer was then precipitated into 300 mL of methanol. The precipitate was filtered over a 0.45 μm Nylon pad and washed with 300 mL of pure methanol and allowed to dry. The dried material was collected into a tared vial and vacuum dried to give an orange-red solid in 81% yield (469 mg). ^{1}H-NMR (300 MHz, $CHCl_3$) δ 4.12 (br s, 4H), 3.77 (br s, 4H), 3.55 (br s, 4H), 3.28 (br, s, 4H), 1.49-0.85 (br m, 54H). Anal. calcd. for $C_{39}H_{64}O_6S_2$ C 67.59, H 9.31, S 9.25; Found C 67.73, H 9.48, S 9.30. GPC: Mn: 21.2 kDa, *Đ*: 1.8, in $CHCl_3$ vs PS.

General Polymerization Conditions of DOTT copolymers.

Homo DOTT (GPC: Mn: 7.6 kDa, *Đ*: 1.7, in $CHCl_3$ vs PS)

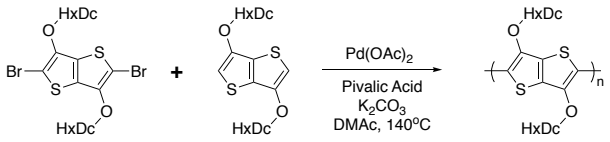

DOTT-NeoDOT (GPC: Mn: 12 kDa, *Đ*: 1.8, in $CHCl_3$ vs PS)

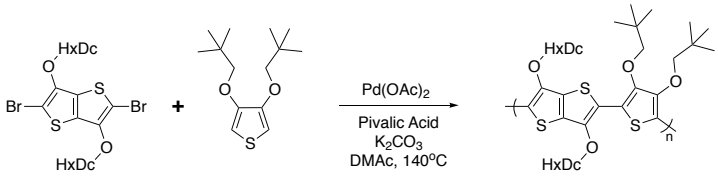

DOTT-DMP (GPC: Mn: 44 kDa, *Đ*: 2.8, in $CHCl_3$ vs PS)

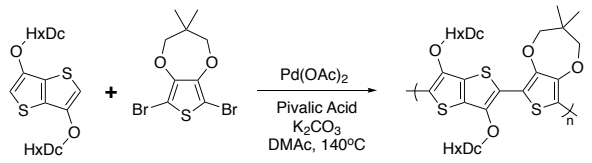

DOTT-EDOT (GPC: Mn: 30 kDa, *Đ*: 1.8, in $CHCl_3$ vs PS)

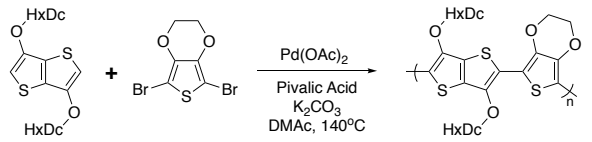

DOTT-BiEDOT (GPC: peak could not be observed due to refractive index matching of polymer in solution with pristine solution)

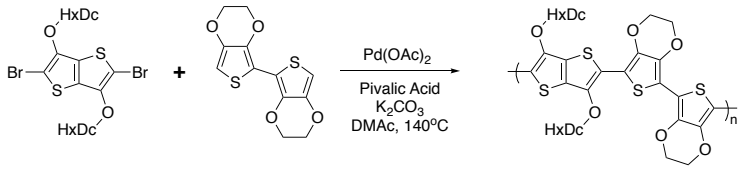

5.6.2 Film Formation

The Poly[2,5-bis(3-hexadecylthiophen-2-yl)thieno[3,2-b]thiophene] (PBTTT-C16) sample used for comparison for air stability measurements was purchased from Luminescence Technology Corporation (LT-S9060 PBTTT-C16, MW = > 40,000) and was used without further purification. Before film formation, 30-40 mg mL^{-1} polymer samples were prepared in chloroform. Films were blade-coated onto either glass substrates or ITO-glass substrates (25 mm x 75 mm x 0.7 mm, sheet resistance 8-12 Ω sq^{-1}, Delta Technologies, Ltd) that were pre-rinsed and sonicated in solutions of sodium dodecyl sulfate-water, water, acetone, and finally isopropanol, and allowed to air dry. Once dry, polymer films were blade-coated with a custom blade-coater built in-house with a gap height of 100 μm and various coating speeds depending on solution viscosity. Films of each polymer were cast to a pre-determined optical density of 0.95 ± 0.1 at λ_{max} (552 nm for Homo DOTT, 555 nm for DOTT-EDOT, 566 nm for DOTT-BiEDOT, 588 nm for DOTT-DMP, and 492 nm for DOTT-NeoDOT). The spectroscopic properties of all films cast in this study were monitored with an Ocean Optics USB2000+ spectrophotometer detector using an Ocean Optics DH-2000-BAL fiber-optic light source.

5.6.3 Characterization of Intermolecular Ordering

AFM measurements were performed using a Bruker atomic force microscope (Dimension icon) with a Bruker Tap 150 cantilever (Model: RTESP-150) in standard tapping mode. Samples were prepared as described above on glass.

GIWAXS measurements were conducted at the Stanford Synchrotron Radiation Lightsource on beamline 11-3. Samples were prepared as described above on Si wafers that were washed using the same procedure as the glass substrates. Samples were irradiated with X-ray energy of 12.7 keV and their GIWAXS patterns were recorded with a 2-D image detector (MAR345 image plate detector). Typical exposure times were 180 s. The distance between the sample and the detector was kept at 250 mm and the incident angle was maintained at 0.13° in order to achieve the highest scattering intensity from the sample without interference from the substrate (polymer critical angle ~0.08°). The scattering images were calibrated using a LaB_6 standard. Samples were loaded into a chamber and purged with helium to reduce damage to the sample and reduce the air scattering background. Samples were loaded into the chamber with the blade-coating direction normal to the direction of the incident x-ray beam. The data analysis was conducted using the Nika software package for Wavemetrics Igor, in combination with WAXStools.[121,122] The images presented in this work are considered to be reproducible as multiple samples of the same polymer and doping condition were run and showed the same diffraction patterns.

5.6.4 Electrochemical Characterization

For all electrochemical characterizations the electrolyte solution was 0.5 M tetrabutylammonium hexafluorophosphate ($TBAPF_6$, Acros Organics, 98% and recrystallized using 200 mL of ethanol for every 100 g of salt) dissolved in propylene carbonate. A platinum flag served as the counter electrode and an Ag/Ag^+ electrode (10 mM $AgNO_3$ and 0.5 M $TBAPF_6$ in acetonitrile, +0.085 V vs Fc/Fc^+) was used as the reference electrode. The redox response of the films was characterized using DPV (step size 2 mV and step time 0.1 s) and CV (scan rate 50 mV/s) performed in a three-electrode cell, using a Princeton Applied Research 273 potentiostat/galvanostat under CorrWare control and *in situ* conductance measurements were performed in a four-electrode cell using a Pine bipotentiostat (model AFCBP1) under control of Aftermath.

For electrochemical characterizations including differential pulse voltammetry (DPV), cyclic voltammetry (CV), four 1μL drops of polymer solutions with concentrations of 1 mg mL^{-1} were sequentially dropped onto polished glassy carbon electrodes and allowed to air dry. For the *in situ* conductance measurements, three 0.5 μL drops of polymer solutions with concentrations of 1 mg mL^{-1} were sequentially dropped onto Pt interdigitated microelectrodes (Abtech Scientific Inc. IME 1050.5 series) with 50 digits, 10 μm in width, and 10 μm separation and allowed to air dry.

For *in situ* conductance measurements on the interdigitated electrodes, one of the working electrodes was held at a given potential E (range from -0.5 to 0.8 V vs Ag/Ag^+) while cycling the second working electrode E ± 0.005 V at 0.5 mVs^{-1}. The slope of the resulting current density versus potential curve was used to determine the film

conductance. Films were formed by drop-casting three 0.5 μL drops from 1mg/mL solutions.

Spectroelectrochemistry (and UV-Vis) measurements were performed in coordination with an Agilent Technologies Cary 5000 UV-Vis-NIR Spectrophotometer under Cary WinUV control. Corresponding photographs of the electrochemical cells used in these experiments were taken in a lightbooth that was illuminated by a D50 (5000K) lamp, using a Nikon D90 SLR camera with a Nikon 18-105 mm VR lens and are reported without further manipulation beyond photograph cropping.

5.6.5 Chemical Oxidation of Polymer Films

After casting, polymer films were exposed to dopant solutions made from propylene carbonate (99.5%, Acros Organics, purified using a solvent purification system from Vacuum Atmospheres) and varying concentrations of the dopant. The dopants used for this study, tris(4-bromophenyl)ammoniumyl hexachloroantimonate (Sigma Aldrich, technical grade), is here referred to as "Magic Blue", and Tetrafluorotetracyanoquinodimethane (TCI America, purified by sublimation), is here referred to as "F4TCNQ". Dopant solutions were prepared in an argon-filled glovebox in the case of Magic Blue and in air in the case of F4TCNQ. To perform chemical oxidation, dopant solutions with varying concentrations were drop-cast onto polymer films for 30 seconds. Subsequently, each film was rinsed with clean methanol. When preparing samples for atomic force microscopy (AFM), grazing-incidence wide-angle x-ray scattering (GIWAXS), and solid-state conductivity measurements, polymer films

were dried under full vacuum at 50°C for 15 hours in a vacuum oven to ensure full removal of solvent.

5.6.6 XPS of Oxidized Polymer Films

XPS spectra were recorded using a Thermo Fisher K-Alpha Photoelectron Spectrophotometer, with a monochromatic Al K-α source (energy 1487 eV) and a hemispherical 180° detector. Samples were positioned with the electron takeoff angle normal to the surface of the sample, with respect to the analyzer. In all spectra, a low energy electron "flood gun" was used to maintain sample charge neutrality during the measurement. Spectra were recorded for the S 2p, C 1s, F 1s, and Cl 2p core levels using a pass energy of 50 eV, with a spot size of 400 μm. Curve fitting and elemental composition calculations were carried out on the high-resolution elemental spectrum of each sample, using the curve-fit feature of the XPS analysis software CasaXPS. Doping ratios were calculated from the atomic abundance values of each element which were calculated according to the equation: $atomic\ abundance = \frac{A_{rel}}{RSF * KE^{0.6}}$ where A_{rel} is the integrated area for the fits of each peak in the elemental high-resolution spectra, RSF is the relative sensitivity factor for each element, and KE is the kinetic energy. Example plots of fitted XPS data can be seen in Supporting Figure 5-13.

5.6.7 Solid-State Conductivity Measurements

Four gold contact pads (1 mm × 1 mm, ~ 100 nm thick) were deposited on doped films using a shadow mask and a home-built DC sputtering chamber. Contact pad and film thicknesses were measured using a Profilm 3D optical profilometer. Initial electrical conductivity and Seebeck measurements were made on a custom setup[217,218] on the same

day as contact pad deposition. Micromanipulators with tungsten tips were used to make electrical contact to the gold contact pads and in-plane electrical conductivity was acquired using the four-probe Van der Pauw technique. All measurements were made in ambient atmosphere and lighting.

5.6.8 Supporting Figures and Tables

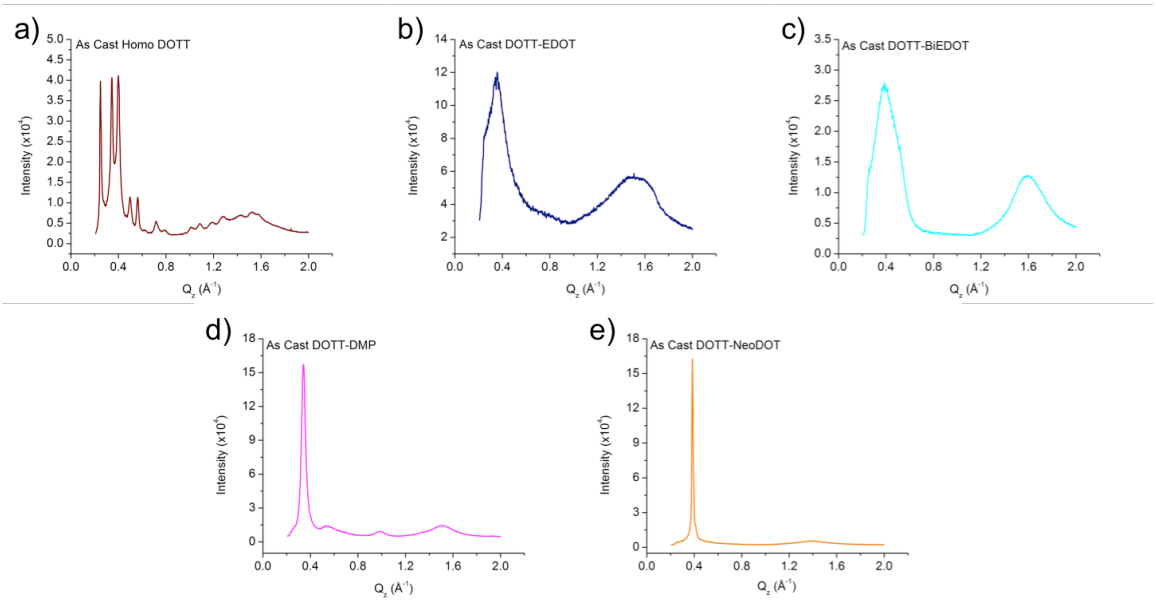

Supporting Figure 5-1 – Linecuts along the Q_z direction for GIWAXS images of as-cast blade-coated films coated from chloroform of Homo DOTT (a), DOTT-EDOT (b), DOTT-BiEDOT (c), DOTT-DMP (d), and DOTT-NeoDOT (e) on glass. Films coated with a custom-built in-house blade-coater.

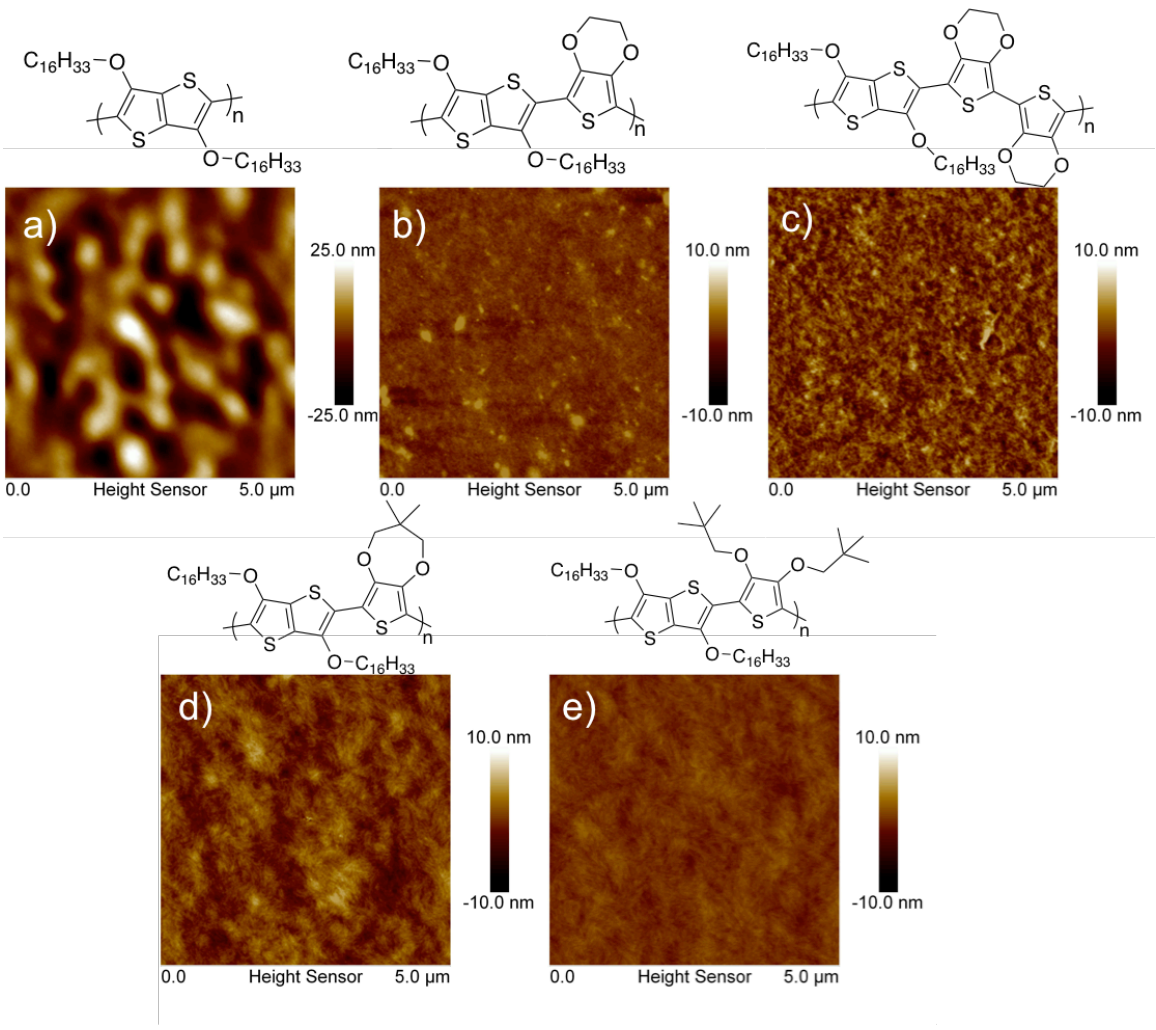

Supporting Figure 5-2 – AFM height images of as-cast blade-coated films coated from chloroform of Homo DOTT (a), DOTT-EDOT (b), DOTT-BiEDOT (c), DOTT-DMP (d), and DOTT-NeoDOT (e) on glass substrates. Films coated with a custom-built in-house blade-coater.

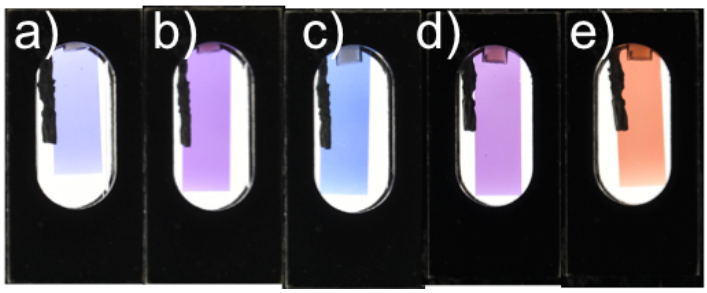

Supporting Figure 5-3 – Photographs of polymer films Homo DOTT (a), DOTT-EDOT (b), DOTT-BiEDOT (c), DOTT-DMP (d), and DOTT-NeoDOT (e) on ITO/glass in a 0.5 M $TBAPF_6$ electrolyte in propylene carbonate at -0.5 V versus Ag/Ag^+.

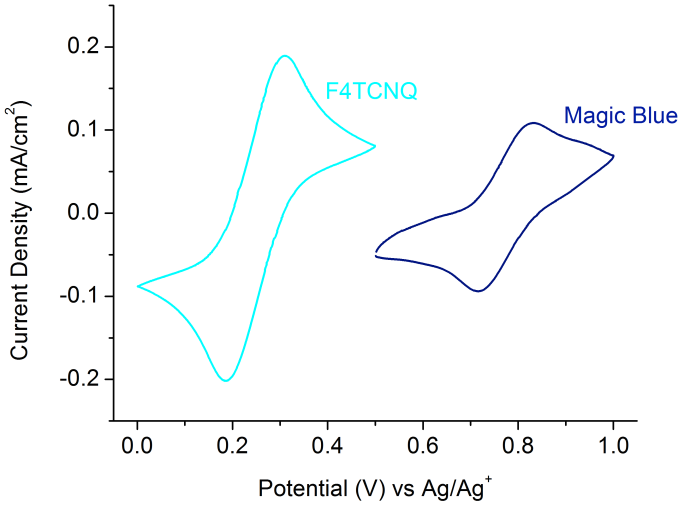

Supporting Figure 5-4 – Cyclic voltammograms of 10 mM Magic Blue and F4TCNQ in a 0.5 M $TBAPF_6$ electrolyte in propylene carbonate. CVs were performed with a glassy carbon rod as the working electrode, platinum flag as the counter electrode, and an Ag/Ag^+ reference electrode with $E_{1/2}$ = 55 mV for the Fc/Fc^+ redox couple and a scan rate of 5 mV/s.

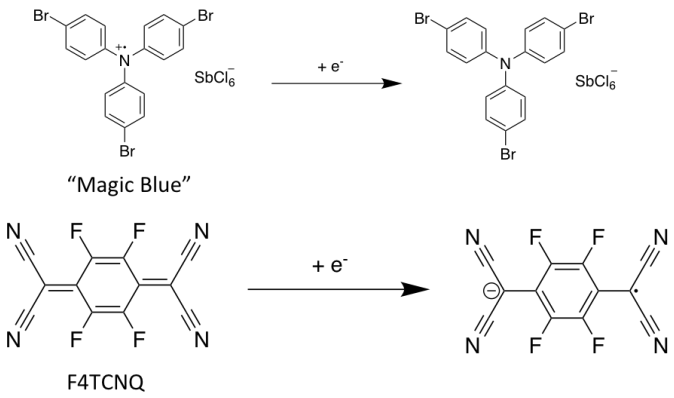

Supporting Figure 5-5 – Electron accepting reactions for the Magic Blue and F4TCNQ dopants.

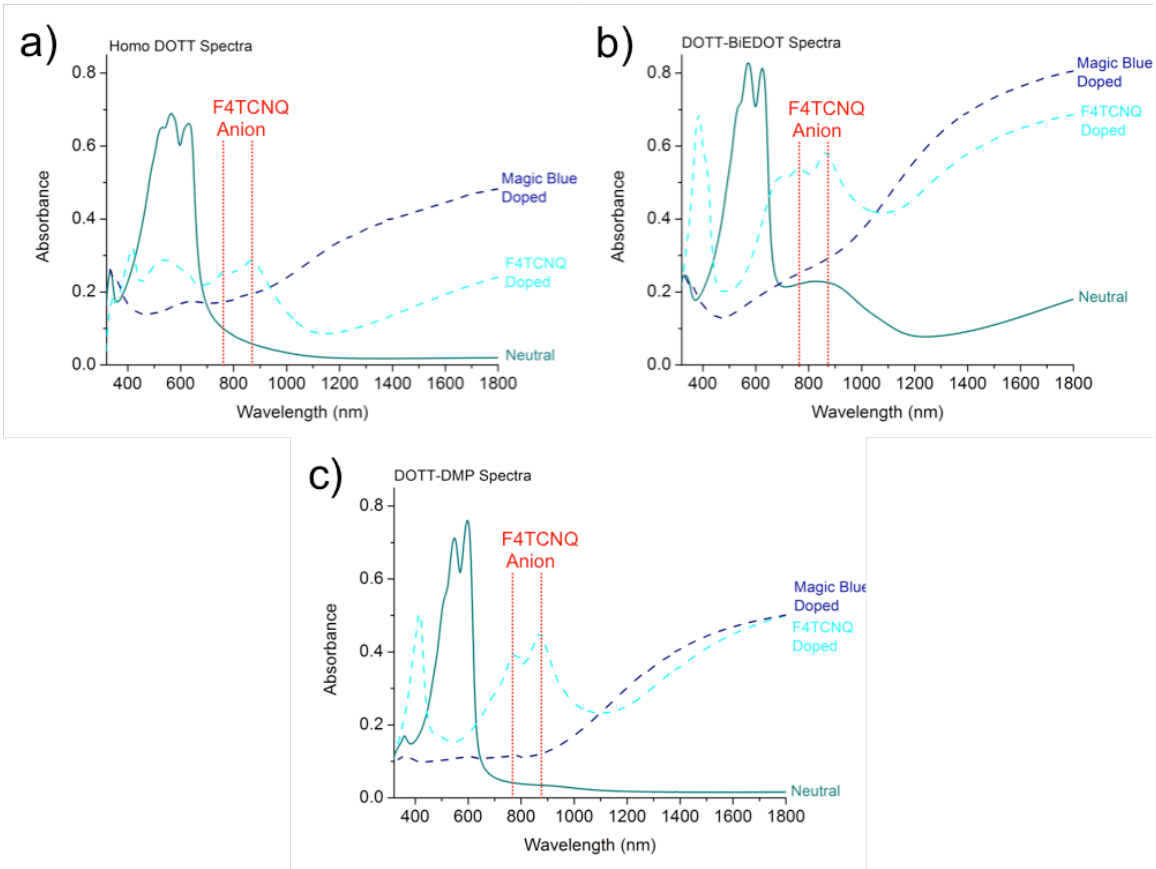

Supporting Figure 5-6 – UV-vis absorption spectra of a blade-coated polymer film of (a) Homo DOTT , (b) DOTT-BiEDOT, and (c) DOTT-DMP on glass before and after 30 seconds of exposure to a 10 mM solution of either Magic Blue (dark blue curve) or F4TCNQ (cyan curve) in propylene carbonate and a subsequent methanol rinse. Absorbance at 400 nm corresponds to the neutral F4TCNQ molecule.

Supporting Table 5-1 – Average doping ratios calculated from XPS atomic abundance values for polymer films doped with a 10 mM Magic Blue solution in propylene carbonate.

Polymer	Cl 2p Abundance	S 2p Abundance	S:Cl	Number of Rings Per Dopant
Homo DOTT	59.3	37.1	5.8	6
DOTT-EDOT	105.1	74.7	4.7	5
DOTT-BiEDOT	155.7	62.8	2.4	2
DOTT-DMP	100.3	81.1	5.0	5
DOTT-NeoDOT	145.2	54.2	2.2	2

Supporting Table 5-2 – Average doping ratios (rings/dopant) calculated from XPS atomic abundance values (F 1s and S 2p) for polymer films doped with various concentrations of F4TCNQ in propylene carbonate.

Polymer	1 mM F4TCNQ	10 mM F4TCNQ	50 mM F4TCNQ
Homo DOTT	46	19	9
DOTT-EDOT	32	8	8
DOTT-BiEDOT	8	5	6
DOTT-DMP	10	7	7
DOTT-NeoDOT	94	5	6

Supporting Table 5-3 – Calculated spacing values from GIWAXS images of as-cast and chemically oxidized polymer films with solutions of either 10 mM F4TCNQ or Magic Blue in propylene carbonate.

Polymer	Lamellar As-Cast (Å)	Lamellar F4TCNQ Doped (Å)	Lamellar Magic Blue Doped (Å)	Pi-Pi As-Cast (Å)	Pi-Pi F4TCNQ Doped (Å)	Pi-Pi Magic Blue Doped (Å)
Homo DOTT	18.4	20.9	23.0	4.2	3.8	4.8
DOTT-EDOT	18.4	18.5	19.5	4.3	4.0	4.7
DOTT-BiEDOT	17.0	20.0	23.7	4.0	3.7	4.3
DOTT-DMP	18.6	18.5	17.7	4.3	3.9	4.5
DOTT-NeoDOT	16.4	18.2	19.1	4.7	4.8	4.8

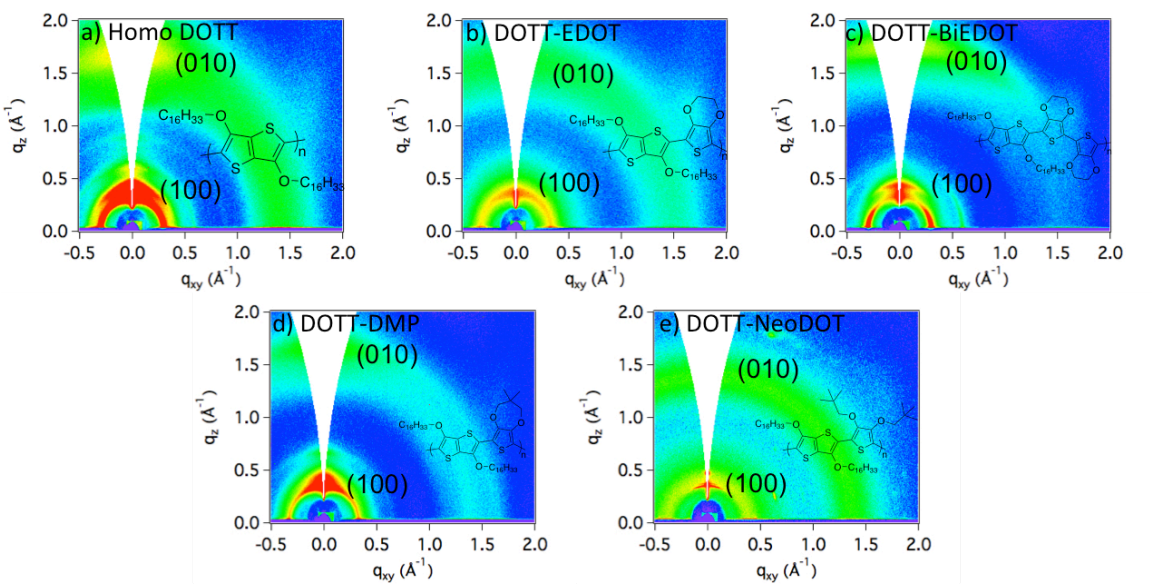

Supporting Figure 5-7 – GIWAXS images of blade-coated films of Homo DOTT (a), DOTT-EDOT (b), DOTT-BiEDOT (c), DOTT-DMP (d), and DOTT-NeoDOT (e) on silicon wafers after a 30 second exposure to a 10 mM F4TCNQ solution in propylene carbonate and subsequent rinse in clean methanol.

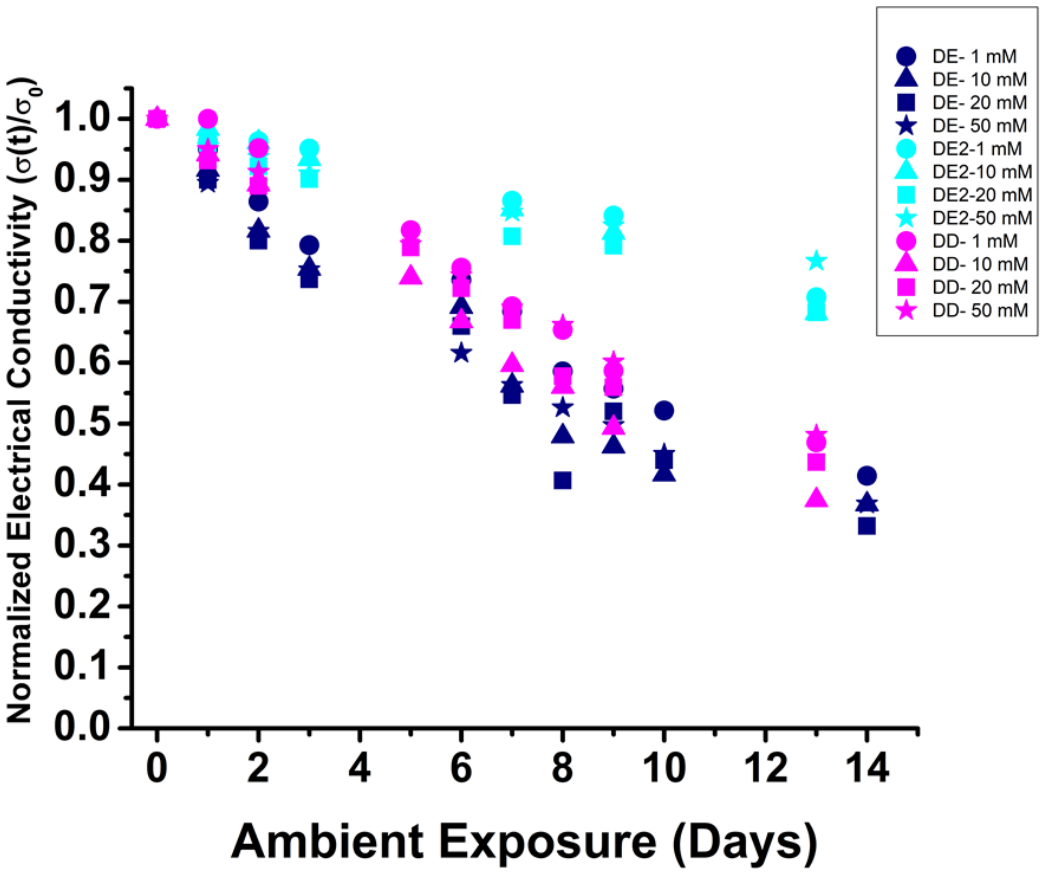

Supporting Figure 5-8 – Normalized electrical conductivity values of blade-coated polymer films on glass substrates after exposure to a F4TCNQ dopant solution in propylene carbonate for 30 seconds and a subsequent methanol rinse. Concentrations range from 1-50 mM.

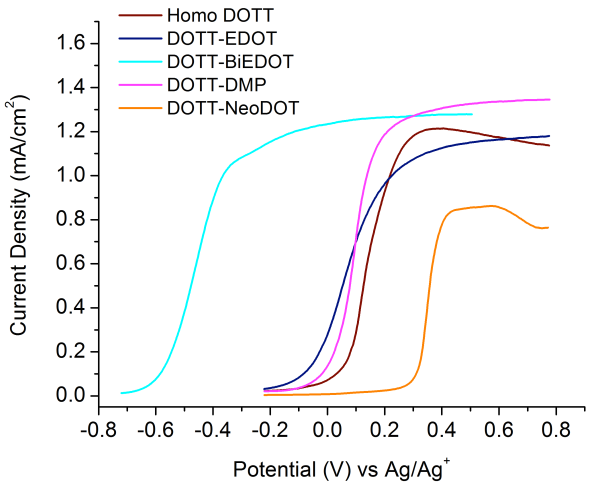

Supporting Figure 5-9 – Differential pulse voltammograms for drop-cast films of Homo DOTT in red, DOTT-EDOT in navy blue, DOTT-BiEDOT in cyan, DOTT-DMP in magenta, and DOTT-NeoDOT in orange on a glassy carbon electrode as the working electrode in a three-electrode cell in a 0.5 M $TBAPF_6$ electrolyte in propylene carbonate after 5 CV conditioning cycles.

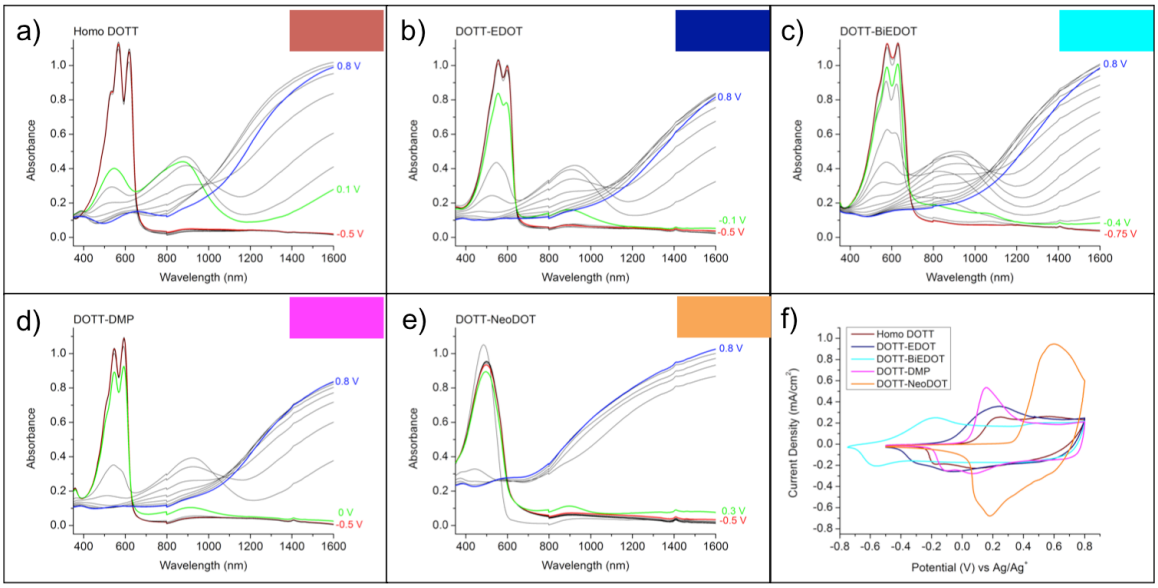

Supporting Figure 5-10 – UV-vis absorption spectra as a function of applied potential of spray-coated polymer films of Homo DOTT (a), DOTT-EDOT (b), DOTT-BiEDOT (c), DOTT-DMP (d), and DOTT-NeoDOT (e) on ITO/glass in a 0.5 M $TBAPF_6$ electrolyte in propylene carbonate. Part (f) shows the conditioning CV cycles with a scan rate of 50 mV/s.

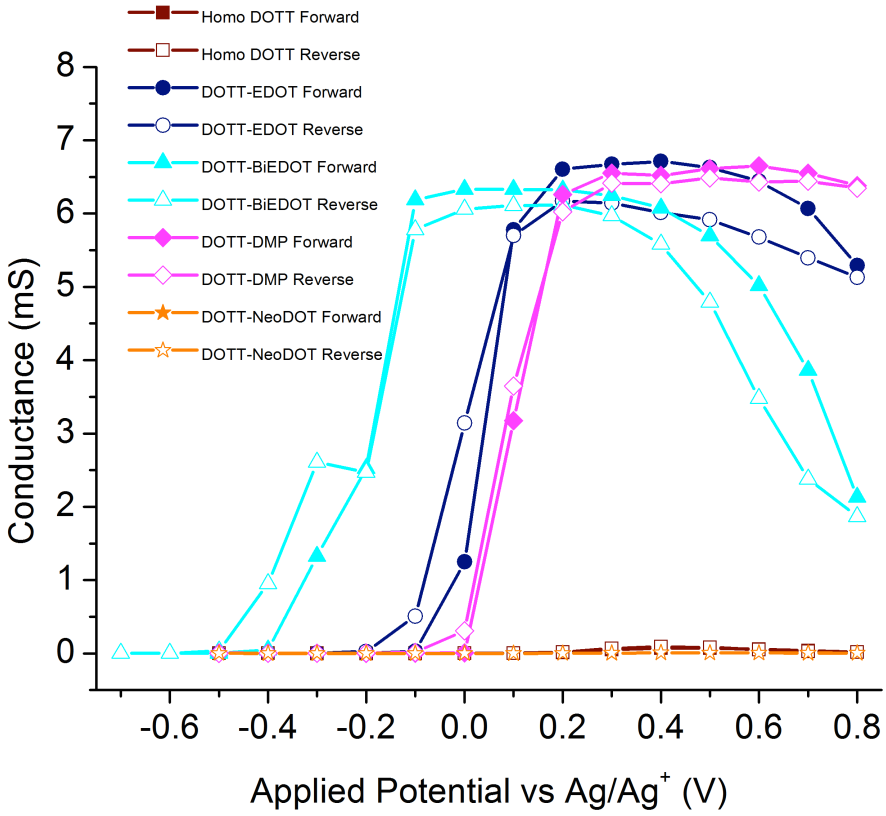

Supporting Figure 5-11 – *In situ* electrochemical conductance plots of Homo DOTT (red), DOTT-EDOT (navy blue), DOTT-BiEDOT (cyan), DOTT-DMP (magenta), and DOTT-NeoDOT (orange) from -0.5 to 0.8 V versus Ag/Ag^+ in a 0.5 M $TBAPF_6$ electrolyte in propylene carbonate. Data taken in the forward direction corresponds to -0.5 to 0.8 V (solid symbols) and data taken in the reverse direction corresponds to 0.8 to -0.5 V (open symbols).

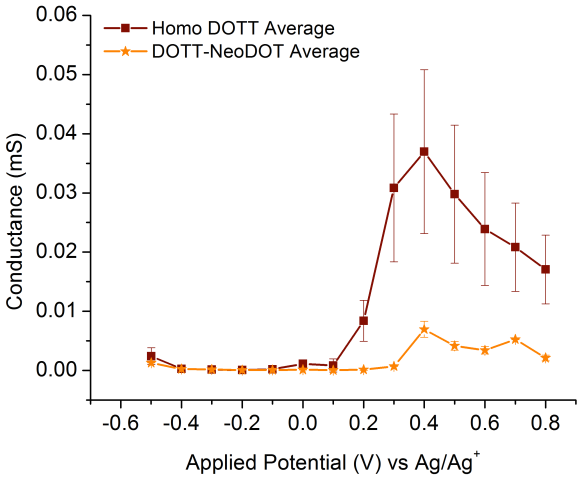

Supporting Figure 5-12 – *In situ* electrochemical conductance plots of Homo DOTT (red) and DOTT-NeoDOT (orange) from -0.5 to 0.8 V versus Ag/Ag^+ in a 0.5 M $TBAPF_6$ electrolyte in propylene carbonate. Averages taken from values collected from three films of each polymer.

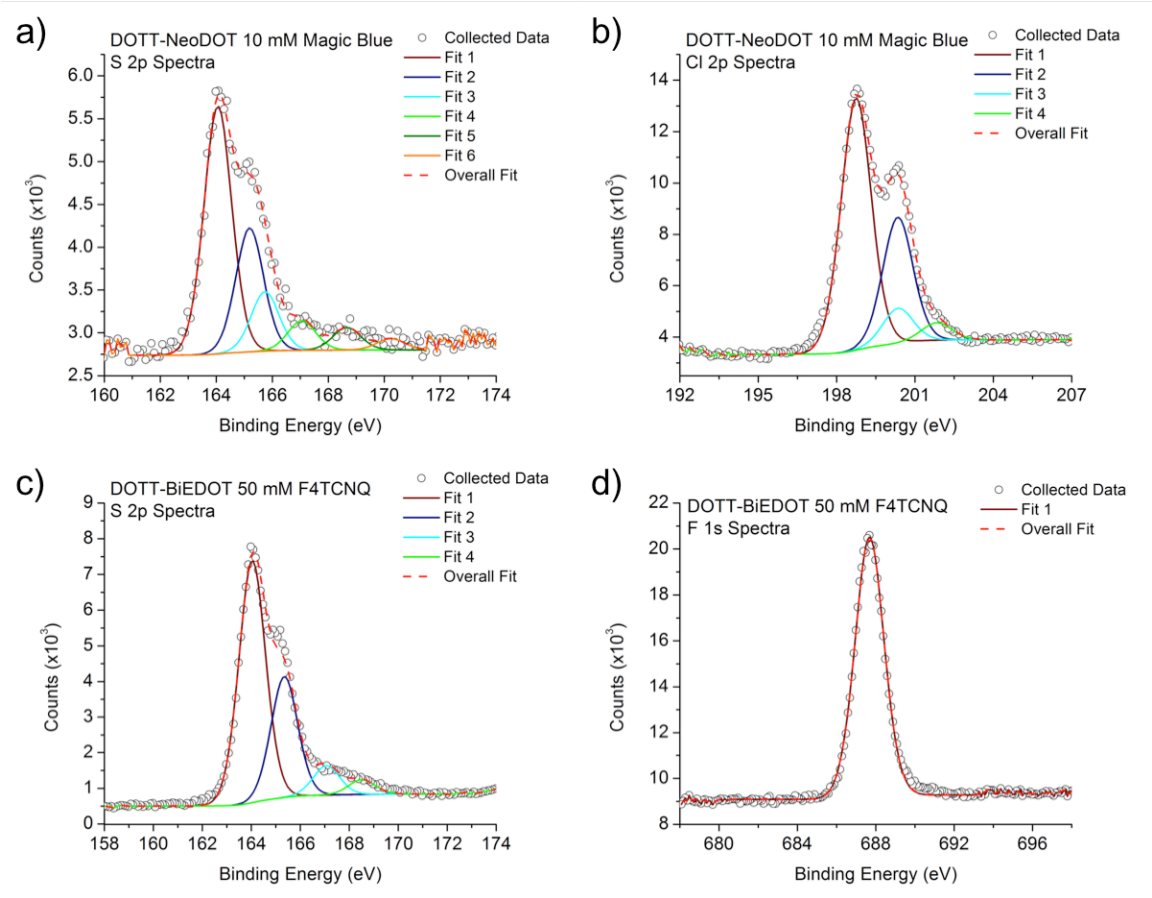

Supporting Figure 5-13 – Example plots of fitted XPS spectra corresponding to a polymer film of DOTT-NeoDOT [(a)&(b)] doped with a 10 mM solution of Magic Blue in propylene carbonate and a polymer film of DOTT-BiEDOT [(c)&(d)] doped with a 50 mM solution of F4TCNQ in propylene carbonate. Spectra were recorded after polymer films were rinsed with clean methanol and dried under vacuum at 50°C. Areas of the fitted spectra were used to calculate relative abundance values and doping ratios for chemically oxidized polymer films.

CHAPTER 6. SUMMARY AND OUTLOOK FOR FUTURE RESEARCH

The work shown and discussed in this thesis is presented in an effort to expand upon the knowledge of the structure-property relationships of conjugated dioxythiophenes, probe the effects of chemical and electrochemical oxidation, and highlight how they could be useful in practical applications. The entirety of the work can be summarized in two main aims: 1) to understand structure-property relationships as they relate to electrochemical charge transport and device applications and 2) to understand structure-property relationships as they relate to solid-state charge transport and devices.

The work discussed in Chapter 3 showed how chemical oxidation can be used as a novel pre-treatment step in the construction of electrochemical devices and that the extent of oxidation is not determined solely by the strength of the oxidant. Chapters 4 and 5 expanded on this idea, where systematic studies of families of dioxythiophene polymers were probed for their structure-property relationships as they related to understanding charge transport properties after both chemical and electrochemical oxidation. Ultimately, it was shown through the work in these two chapters that too much intermolecular ordering can lead to polymers that are difficult to oxidize through both methods of oxidation. Chapter 5 especially highlighted the idea of comparing different molecular dopants for the chemical oxidative doping of dioxythienothiophene-based

polymers. Again, it was shown that the doping strength of the chemical oxidant was not the sole determining factor in enhanced charge transport properties. Doping with the stronger dopant, Magic Blue, resulted in solid-state conductivities that were lower by an order of magnitude for the polymer DOTT-BiEDOT. Furthermore, it was shown that this stronger, but bulkier dopant perturbed the microstructure of Homo DOTT and DOTT-BiEDOT to a larger degree.

In essence, the work presented in this dissertation has added to the collective knowledge of dioyxthiophene polymers. For a given family of dioyxthiophene-based polymers that had small structural changes, it was shown: 1) how the electrochemical redox properties and solid-state charge transport properties are interrelated, and 2) the structure-property relationships of this class of polymer and the processes of chemical doping. The following sections will describe how this work can be expanded upon for further research and understanding in the field.

6.1 Electrochemical Applications

As has been mentioned many times, conjugated polymers are desirable materials for electrochemical devices and applications due to their ability to transport ions and electrons simultaneously. These types of devices can be useful for a number of redox-active applications such as: electrochromic displays, charge storage devices, and bioelectronic sensors and transistors.

The results shown in Chapter 3 confirmed that polymer electrodes pre-oxidized with a chemical process are comparable to those that were electrochemically pre-oxidized and that this chemical oxidation pre-treatment can be used in the construction of

electrochemical devices. This work was motivated through fundamental questions, as well as practical considerations. In order for these devices to be made in a truly scalable and industrially applicable way, it is suggested that other dopants be considered and studied for this purpose. One of the practical drawbacks of the work was that the chemical oxidant solutions of Ag^{+} and Fe^{3+} salts had to be made under an inert atmosphere due to the oxygen and water sensitivity of the dopants. One could suggest the dopant that that was introduced in the work in Chapter 5, F4TCNQ. This dopant can be handled and dissolved in air and is still sufficiently strong to extract an electron from the dioxythiophene polymers. One drawback of F4TCNQ however, is that its reduced form absorbs in the visible region of the spectrum, causing the film to take on a slight blue color. This dopant would work for applications such as charge storage devices, which do not have color requirements, however it would affect the contrast of devices for electrochromic displays.

Further work could be done in order to use dopants that can be handled in air, but do not contribute any color to the polymer electrode for these types of applications. One solution to this problem could be through the use of Lewis acid dopants. As was discussed in the introduction, Lewis acids such as triflimidic acid (HTFSI) have been shown to effectively dope P3HT.[45] Unfortunately, this acid is hydroscopic and reacts with water. Triflic acid (the acid form of the anion trifluoromethanesulfonate, used in Chapter 3) could be another contender, but it is also hydroscopic. P-toluenesulfonic acid (tosylic acid) however, can be dissolved in water. This anion was also investigated in Chapter 3 in the form of Fe(III) Tosylate hexahydrate. A systematic study could be proposed where these three acids, as shown in Figure 6.1-1, are investigated in order to understand how

acidic doping can affect the functionality of conjugated polymer electrodes for the construction of electrochemical devices. Currently, it is unknown if acid doping will have the same delamination effects as was shown for redox doping in Chapter 3. Furthermore, if tosylic acid was shown to be an effective dopant, it could be the solution for the practical processing problem of constructing electrochemical devices in air.

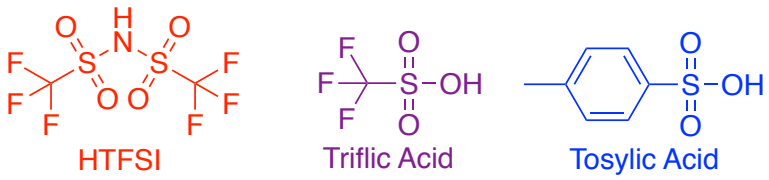

Figure 6.1-1 – Proposed acids for use in future chemical doping studies of polymer electrodes for use in redox-active electrochemical devices.

Dioxythiophenes have been well studied as electrochromic materials, but the understanding of their use as active materials in bioelectronic devices is still developing. Considering the work presented in Chapters 4 and 5, DOTT polymer backbone structures could be combined with oligo ether side chains to create a family of polymers that would have a broad redox window in water. Further studies could be conducted to understand a number of properties. First, it could be shown as to how manipulation of the side chain structure can affect the morphology and charge transport properties of these new materials. These studies would be initially done comparing the original DOTT family (with hexyldecyl alkoxy chains) to polymers substituted with oligoether chains of the same length. Given the results of that study, further studies could be done on polymers substituted with oligoether chains of varying lengths in order to see if the amount of insulating material (being the side chain) has any effect on the charge transport properties of the material. Additionally, studies could be conducted to understand how these

morphology differences could affect properties of polymer film swelling and ion migration through out the film. These studies would be performed in both organic and water-based electrolytes.

6.2 Solid-State Properties and Applications

The results of the work shown in Chapters 4 and 5 heavily focused on the effects of structure of dioxythiophene polymers on their film morphology and in-plane solid-state conductivity after doping. For devices and applications concerning solid-state conductivity, the question always is: how can the conductivity magnitude be raised? While not the most fundamental scientific question, this question is still frequently asked in the field of conjugated polymers and could be the focus of future work.

Turning to the work presented in Chapter 5, conductivities were attained on the order of 10^1 S/cm. Experimental parameters were selected in order to design a fundamental study, however a number of these could be investigated in order to probe the highest conductivity possible. Work presented by Ponder *et al*.[80] demonstrated that conductivities of 250 S/cm could be attained for a co-polymer consisting of one ProDOT and two EDOT units (PE_2, shown in Figure 1.5-1). It is likely that the DOTT-BiEDOT polymer could attain or surpass these values. It is suggested that other dopants be investigated, as well as varying dopant times and concentrations. These investigations should include all of the doping routes discussed in the introduction, such as sequential versus co-processing solution doping for example. Again, when considering the work presented by Thomas *et al.*,[45] it would be interesting to see if acid doping had any effect on the overall conductivity of DOTT-BiEDOT. Conductivity as well as morphology

studies could be conducted in order to see if acid doping results in altered polymer film morphologies, different doping mechanisms (formation of a CTC), and higher solid-state conductivity values.

The overall conductivity values of the DOTT polymer family could also be increased through the use of a different doping technique. To date, the DOTT family has not been doped using a vapor phase process. As discussed in the introduction, during solution-based chemical oxidation, polymer films must swell in order to allow penetration both the dopant and solvent molecules. It is currently unknown whether this swelling (and de-swelling after drying) disrupts the microstructure of the polymer film. In addition, while the XPS work in Chapter 3 demonstrated that dopant ions penetrate throughout the full depth of the film, it is unknown whether a different doping process (such as vapor phase doping) would result in a higher concentration of dopant ions and charge carriers in the polymer film.

Furthermore, it could be interesting to understand what other properties the DOTT polymer family possesses. For example, the thermal properties of these materials were not investigated in the work presented here. It could be quite interesting to probe whether thermal annealing could affect film morphology and therefore conductivity. Studies where the casting solvent is altered could also be conducted for the same purpose. As was shown in the work by Müller *et al*.[97], the degree of aggregation due to the selected casting solvent can caused reduced conductivity values. Only chloroform was used in the work presented here, so it would be interesting to see if a different solvent or solvent combination could affect the polymer film morphology and conductivity.

Again, combining the results from Chapters 4 and 5, it would be interesting to probe the effects of altering the side chains of the DOTT polymer family on the properties of morphology and conductivity. From the ProDOT and AcDOT work in Chapter 4 it was shown that the use of linear side chains increased the solid-state conductivity by 3 orders of magnitude, this potentially could be the same trend for the DOTT polymer family, but it has not been investigated to date. It is hypothesized that the reduced bulk of the linear side chains will cause a relaxation in the polymer backbone, which would lead to increased conductivity values and reduced electrochemical onsets of oxidation.

The work shown collectively in Chapters 4 and 5 demonstrated that there should be balance in terms of the molecular ordering demonstrated by polymer films and their ease of oxidation through both chemical and electrochemical mechanisms. It is suggested that when designing future polymers for these purposes, that this idea of balance be taken into consideration. It is evident that too much ordering can inhibit the oxidation processes of conjugated polymers, while a significant lack of ordering prevents effective charge transport through the polymer film. It was demonstrated by Pro-EH in Chapter 4 that this may not be a problem when designing polymers for redox-active devices, but the magnitude of solid-state conductivity is decreased.

One route that has not yet been investigated is that of blending dioxythiophene-based polymers in order to alter the properties of film morphology and conductivity. One way we could strike a balance in terms of the degree of ordering is to blend polymers that present extreme properties. For example, one way that we could achieve this is by blending Homo DOTT and DOTT-EDOT. In terms of the degree of ordering, these two

had the highest and lowest, respectively, in the family. It would be interesting to see if the conductivity of the blend was an average of the two polymers, or if it was enhanced beyond the value attained by DOTT-EDOT alone.

REFERENCES

(1) Facchetti, A. π-Conjugated Polymers for Organic Electronics and Photovoltaic Cell Applications. *Chem. Mater.* **2011**, *23*, 733-758.

(2) Amb, C. M.; Dyer, A. L.; Reynolds, J. R. Navigating the Color Palette of Solution-Processable Electrochromic Polymers. *Chem. Mater.* **2011**, *23*, 397-415.

(3) Andersson Ersman, P.; Kawahara, J.; Berggren, M. Printed passive matrix addressed electrochromic displays. *Org. Electron.* **2013**, *14*, 3371-3378.

(4) Mortimer, R. J.; Dyer, A. L.; Reynolds, J. R. Electrochromic organic and polymeric materials for display applications. *Displays* **2006**, *27*, 2-18.

(5) Bredas, J. L.; Street, G. B. Polarons, bipolarons, and solitons in conducting polymers. *Acc. Chem. Res.* **1985**, *18*, 309-315.

(6) Brédas, J.-L.; Beljonne, D.; Coropceanu, V.; Cornil, J. Charge-Transfer and Energy-Transfer Processes in π-Conjugated Oligomers and Polymers: A Molecular Picture. *Chem. Rev.* **2004**, *104*, 4971-5004.

(7) Coropceanu, V.; Cornil, J.; da Silva Filho, D. A.; Olivier, Y.; Silbey, R.; Brédas, J.-L. Charge Transport in Organic Semiconductors. *Chem. Rev.* **2007**, *107*, 926-952.

(8) Shirakawa, H.; Louis, E. J.; MacDiarmid, A. G.; Chiang, C. K.; Heeger, A. J. Synthesis of electrically conducting organic polymers: halogen derivatives of polyacetylene, (CH). *Chem. Commun.* **1977**, 578-580.

(9) Su, W. P.; Schrieffer, J. R.; Heeger, A. J. Solitons in Polyacetylene. *Phys. Rev. Lett.* **1979**, *42*, 1698-1701.

(10) Salzner, U.; Lagowski, J. B.; Pickup, P. G.; Poirier, R. A. Comparison of geometries and electronic structures of polyacetylene, polyborole, polycyclopentadiene, polypyrrole, polyfuran, polysilole, polyphosphole, polythiophene, polyselenophene and polytellurophene. *Synth. Met.* **1998**, *96*, 177-189.

(11) Little, W. A. Possibility of Synthesizing an Organic Superconductor. *Phys. Rev.* **1964**, *134*, A1416-A1424.

(12) Jahn, H. A.; Teller, E.; Donnan, F. G. Stability of polyatomic molecules in degenerate electronic states - Orbital degeneracy. *Proc. Royal Soc. A - Mat. Phys. Sci.* **1937**, *161*, 220-235.

(13) Heywang, G.; Jonas, F. Poly(alkylenedioxythiophene)s—new, very stable conducting polymers. *Adv. Mater.* **1992**, *4*, 116-118.

(14) Beaujuge, P. M.; Reynolds, J. R. Color Control in π-Conjugated Organic Polymers for Use in Electrochromic Devices. *Chem. Rev.* **2010**, *110*, 268-320.

(15) Elschner, A. K., Stephan; Lovenich, Wilfried; Merker, Udo; Reuter, Knud *PEDOT: Principles and Applications of an Intrinsically Conductive Polymer*; 1st ed.; CRC Press: Boca Raton, 2010.

(16) Müller, H. K.; Hocker, J.; Menke, K.; Ehinger, K.; Roth, S. Long-term conductivity decrease in polyacetylene samples. *Synth. Met.* **1985**, *10*, 273-280.

(17) Rosseinsky, D. R.; Mortimer, R. J. Electrochromic Systems and the Prospects for Devices. *Adv. Mater.* **2001**, *13*, 783-793.

(18) Roncali, J. Conjugated poly(thiophenes): synthesis, functionalization, and applications. *Chem. Rev.* **1992**, *92*, 711-738.

(19) Dietrich, M.; Heinze, J.; Heywang, G.; Jonas, F. Electrochemical and spectroscopic characterization of polyalkylenedioxythiophenes. *J. Electroanal. Chem.* **1994**, *369*, 87-92.

(20) Kumar, A.; Reynolds, J. R. Soluble Alkyl-Substituted Poly(ethylenedioxythiophenes) as Electrochromic Materials. *Macromolecules* **1996**, *29*, 7629-7630.

(21) Kumar, A.; Welsh, D. M.; Morvant, M. C.; Piroux, F.; Abboud, K. A.; Reynolds, J. R. Conducting Poly(3,4-alkylenedioxythiophene) Derivatives as Fast Electrochromics with High-Contrast Ratios. *Chem. Mater.* **1998**, *10*, 896-902.

(22) Sankaran, B.; Reynolds, J. R. High-Contrast Electrochromic Polymers from Alkyl-Derivatized Poly(3,4-ethylenedioxythiophenes). *Macromolecules* **1997**, *30*, 2582-2588.

(23) Cirpan, A.; Argun, A. A.; Grenier, C. R. G.; Reeves, B. D.; Reynolds, J. R. Electrochromic devices based on soluble and processable dioxythiophene polymers. *J. Mater. Chem.* **2003**, *13*, 2422-2428.

(24) Reeves, B. D.; Grenier, C. R. G.; Argun, A. A.; Cirpan, A.; McCarley, T. D.; Reynolds, J. R. Spray Coatable Electrochromic Dioxythiophene Polymers with High Coloration Efficiencies. *Macromolecules* **2004**, *37*, 7559-7569.

(25) Gaupp, C. L.; Welsh, D. M.; Reynolds, J. R. Poly(ProDOT-Et2): A High-Contrast, High-Coloration Efficiency Electrochromic Polymer. *Macromol. Rapid Commun.* **2002**, *23*, 885-889.

(26) Mei, J.; Bao, Z. Side Chain Engineering in Solution-Processable Conjugated Polymers. *Chem. Mater.* **2014**, *26*, 604-615.

(27) Flagg, L. Q.; Bischak, C. G.; Onorato, J. W.; Rashid, R. B.; Luscombe, C. K.; Ginger, D. S. Polymer Crystallinity Controls Water Uptake in Glycol Side-Chain Polymer Organic Electrochemical Transistors. *J. Am. Chem. Soc.* **2019**, *141*, 4345-4354.

(28) Dyer, A. L.; Craig, M. R.; Babiarz, J. E.; Kiyak, K.; Reynolds, J. R. Orange and Red to Transmissive Electrochromic Polymers Based on Electron-Rich Dioxythiophenes. *Macromolecules* **2010**, *43*, 4460-4467.

(29) Kerszulis, J. A., Reading the Rainbow: Tailoring the Properties of Electrochromic Polymers. Georgia Institute of Technology, **2014**.

(30) Bulloch, R. H., Redox-Active Conjugated Polymers for Electrochromic and Supercapacitive Applications. Georgia Institute of Technology, **2015**.

(31) Ochieng, M. A., Systematic Studies of Side Chains on Optoelectronic Properties of 3,4-dioxythiophene-based Polymers. Georgia Institute of Technology, **2019**.

(32) Vukusic, P.; Sambles, J. R.; Lawrence, C. R. Colour mixing in wing scales of a butterfly. *Nature* **2000**, *404*, 457-457.

(33) Beaujuge, P. M.; Vasilyeva, S. V.; Liu, D. Y.; Ellinger, S.; McCarley, T. D.; Reynolds, J. R. Structure-Performance Correlations in Spray-Processable Green Dioxythiophene-Benzothiadiazole Donor–Acceptor Polymer Electrochromes. *Chem. Mater.* **2012**, *24*, 255-268.

(34) Beaujuge, P. M.; Ellinger, S.; Reynolds, J. R. Spray Processable Green to Highly Transmissive Electrochromics via Chemically Polymerizable Donor–Acceptor Heterocyclic Pentamers. *Adv. Mater.* **2008**, *20*, 2772-2776.

(35) Amb, C. M.; Beaujuge, P. M.; Reynolds, J. R. Spray-Processable Blue-to-Highly Transmissive Switching Polymer Electrochromes via the Donor–Acceptor Approach. *Adv. Mater.* **2010**, *22*, 724-728.

(36) Schanda, J. *Colorimetry: Understanding the CIE System*; John Wiley & Sons, Inc.: United States of America, 2007.

(37) Palumbiny, C. M.; Heller, C.; Schaffer, C. J.; Körstgens, V.; Santoro, G.; Roth, S. V.; Müller-Buschbaum, P. Molecular Reorientation and Structural Changes in Cosolvent-Treated Highly Conductive PEDOT:PSS Electrodes for Flexible Indium Tin Oxide-Free Organic Electronics. *J. Phys. Chem. C* **2014**, *118*, 13598-13606.

(38) Stafström, S.; Brédas, J. L.; Epstein, A. J.; Woo, H. S.; Tanner, D. B.; Huang, W. S.; MacDiarmid, A. G. Polaron lattice in highly conducting polyaniline: Theoretical and optical studies. *Phys. Rev. Lett.* **1987**, *59*, 1464-1467.

(39) Yamamoto, J.; Furukawa, Y. Electronic and vibrational spectra of positive polarons and bipolarons in regioregular poly(3-hexylthiophene) doped with ferric chloride. *J. Phys. Chem. B* **2015**, *119*, 4788-4794.

(40) Bubnova, O.; Crispin, X. Towards polymer-based organic thermoelectric generators. *Energy Environ. Sci.* **2012**, *5*, 9345-9362.

(41) Scholes, D. T.; Hawks, S. A.; Yee, P. Y.; Wu, H.; Lindemuth, J. R.; Tolbert, S. H.; Schwartz, B. J. Overcoming Film Quality Issues for Conjugated Polymers Doped with F4TCNQ by Solution Sequential Processing: Hall Effect, Structural, and Optical Measurements. *J. Phys. Chem. Lett.* **2015**, *6*, 4786-4793.

(42) Scholes, D. T.; Yee, P. Y.; Lindemuth, J. R.; Kang, H.; Onorato, J.; Ghosh, R.; Luscombe, C. K.; Spano, F. C.; Tolbert, S. H.; Schwartz, B. J. The Effects of Crystallinity on Charge Transport and the Structure of Sequentially Processed F4TCNQ-Doped Conjugated Polymer Films. *Adv. Funct. Mater.* **2017**, *27*, 1702654.

(43) Thomas, E. M.; Brady, M. A.; Nakayama, H.; Popere, B. C.; Segalman, R. A.; Chabinyc, M. L. X-Ray Scattering Reveals Ion-Induced Microstructural Changes During Electrochemical Gating of Poly(3-Hexylthiophene). *Adv. Funct. Mater.* **2018**, *28*, 1803687.

(44) Guardado, J. O.; Salleo, A. Structural Effects of Gating Poly(3-hexylthiophene) through an Ionic Liquid. *Adv. Funct. Mater.* **2017**, *27*, 1701791.

(45) Thomas, E. M.; Davidson, E. C.; Katsumata, R.; Segalman, R. A.; Chabinyc, M. L. Branched Side Chains Govern Counterion Position and Doping Mechanism in Conjugated Polythiophenes. *ACS Macro Lett.* **2018**, *7*, 1492-1497.

(46) Karl, N. Charge carrier transport in organic semiconductors. *Synth. Met.* **2003**, *133-134*, 649-657.

(47) Zaumseil, J.; Sirringhaus, H. Electron and Ambipolar Transport in Organic Field-Effect Transistors. *Chem. Rev.* **2007**, *107*, 1296-1323.

(48) Stafström, S. Electron localization and the transition from adiabatic to nonadiabatic charge transport in organic conductors. *Chem. Soc. Rev.* **2010**, *39*, 2484-2499.

(49) Cornil, J.; Lemaur, V.; Calbert, J.-P.; Brédas, J.-L. Charge Transport in Discotic Liquid Crystals: A Molecular Scale Description. *Adv. Mater.* **2002**, *14*, 726-729.

(50) Baranovskii, S. D. Theoretical description of charge transport in disordered organic semiconductors. *Phys. Status Solidi B* **2014**, *251*, 487-525.

(51) Bässler, H. Injection, transport and recombination of charge carriers in organic light-emitting diodes. *Polym. Adv. Technol.* **1998**, *9*, 402-418.

(52) Wu, M. W.; Conwell, E. M. Transport in α-sexithiophene films. *Chem. Phys. Lett.* **1997**, *266*, 363-367.

(53) Jacobs, I. E.; Moulé, A. J. Controlling Molecular Doping in Organic Semiconductors. *Adv. Mater.* **2017**, *29*, 1703063.

(54) Kulszewicz-Bajer, I.; Proń, A.; Abramowicz, J.; Jeandey, C.; Oddou, J.-L.; Sobczak, J. W. Lewis Acid Doped Polyaniline: Preparation and Spectroscopic Characterization. *Chem. Mater.* **1999**, *11*, 552-556.

(55) Endo, J.; Matsumoto, T.; Kido, J. Organic Electroluminescent Devices with a Vacuum-Deposited Lewis-Acid-Doped Hole-Injecting Layer. *J.J.A.P.* **2002**, *41*, L358-L360.

(56) Zalar, P.; Kuik, M.; Henson, Z. B.; Woellner, C.; Zhang, Y.; Sharenko, A.; Bazan, G. C.; Nguyen, T.-Q. Increased Mobility Induced by Addition of a Lewis Acid to a Lewis Basic Conjugated Polymer. *Adv. Mater.* **2014**, *26*, 724-727.

(57) Poverenov, E.; Zamoshchik, N.; Patra, A.; Ridelman, Y.; Bendikov, M. Unusual Doping of Donor–Acceptor-Type Conjugated Polymers Using Lewis Acids. *J. Am. Chem. Soc.* **2014**, *136*, 5138-5149.

(58) Han, Y.; Barnes, G.; Lin, Y.-H.; Martin, J.; Al-Hashimi, M.; AlQaradawi, S. Y.; Anthopoulos, T. D.; Heeney, M. Doping of Large Ionization Potential Indenopyrazine Polymers via Lewis Acid Complexation with Tris(pentafluorophenyl)borane: A Simple Method for Improving the Performance of Organic Thin-Film Transistors. *Chem. Mater.* **2016**, *28*, 8016-8024.

(59) Pingel, P.; Arvind, M.; Kölln, L.; Steyrleuthner, R.; Kraffert, F.; Behrends, J.; Janietz, S.; Neher, D. p-Type Doping of Poly(3-hexylthiophene) with the Strong Lewis Acid Tris(pentafluorophenyl)borane. *Adv. Electron. Mater.* **2016**, *2*, 1600204.

(60) Lüssem, B.; Keum, C.-M.; Kasemann, D.; Naab, B.; Bao, Z.; Leo, K. Doped Organic Transistors. *Chem. Rev.* **2016**, *116*, 13714-13751.

(61) Teran, N. B., Customized Conjugation: Tailored Pi-Systems for Organic Electronic Applications. Georgia Institute of Technology, **2015.**

(62) Akamatu, H.; Inokuchi, H.; Matsunaga, Y. Electrical Conductivity of the Perylene–Bromine Complex. *Nature* **1954**, *173*, 168-169.

(63) Méndez, H.; Heimel, G.; Opitz, A.; Sauer, K.; Barkowski, P.; Oehzelt, M.; Soeda, J.; Okamoto, T.; Takeya, J.; Arlin, J.-B.; Balandier, J.-Y.; Geerts, Y.; Koch, N.; Salzmann, I. Doping of Organic Semiconductors: Impact of Dopant Strength and Electronic Coupling. *Angew. Chem. Int. Ed.* **2013**, *52*, 7751-7755.

(64) Aziz, E. F.; Vollmer, A.; Eisebitt, S.; Eberhardt, W.; Pingel, P.; Neher, D.; Koch, N. Localized Charge Transfer in a Molecularly Doped Conducting Polymer. *Adv. Mater.* **2007**, *19*, 3257-3260.

(65) Connelly, N. G.; Geiger, W. E. Chemical Redox Agents for Organometallic Chemistry. *Chem. Rev.* **1996**, *96*, 877-910.

(66) Duong, D. T.; Wang, C.; Antono, E.; Toney, M. F.; Salleo, A. The chemical and structural origin of efficient p-type doping in P3HT. *Org. Electron.* **2013**, *14*, 1330-1336.

(67) Cochran, J. E.; Junk, M. J. N.; Glaudell, A. M.; Miller, P. L.; Cowart, J. S.; Toney, M. F.; Hawker, C. J.; Chmelka, B. F.; Chabinyc, M. L. Molecular Interactions and Ordering in Electrically Doped Polymers: Blends of PBTTT and F4TCNQ. *Macromolecules* **2014**, *47*, 6836-6846.

(68) Zhang, Y.; de Boer, B.; Blom, P. W. M. Controllable Molecular Doping and Charge Transport in Solution-Processed Polymer Semiconducting Layers. *Adv. Funct. Mater.* **2009**, *19*, 1901-1905.

(69) Duong, D. T.; Phan, H.; Hanifi, D.; Jo, P. S.; Nguyen, T.-Q.; Salleo, A. Direct Observation of Doping Sites in Temperature-Controlled, p-Doped P3HT Thin Films by Conducting Atomic Force Microscopy. *Adv. Mater.* **2014**, *26*, 6069-6073.

(70) Jacobs, I. E.; Aasen, E. W.; Oliveira, J. L.; Fonseca, T. N.; Roehling, J. D.; Li, J.; Zhang, G.; Augustine, M. P.; Mascal, M.; Moulé, A. J. Comparison of solution-mixed and sequentially processed P3HT:F4TCNQ films: effect of doping-induced aggregation on film morphology. *J. Mater. Chem. C* **2016**, *4*, 3454-3466.

(71) Giovannitti, A.; Sbircea, D.-T.; Inal, S.; Nielsen, C. B.; Bandiello, E.; Hanifi, D. A.; Sessolo, M.; Malliaras, G. G.; McCulloch, I.; Rivnay, J. Controlling the mode of operation of organic transistors through side-chain engineering. *Proc. Natl. Aacad. Sci.* **2016**, *113*, 12017-12022.

(72) Dong, B. X.; Nowak, C.; Onorato, J. W.; Strzalka, J.; Escobedo, F. A.; Luscombe, C. K.; Nealey, P. F.; Patel, S. N. Influence of Side-Chain Chemistry on Structure and Ionic Conduction Characteristics of Polythiophene Derivatives: A Computational and Experimental Study. *Chem. Mater.* **2019**, *31*, 1418-1429.

(73) Cao, K.; Shen, D. E.; Österholm, A. M.; Kerszulis, J. A.; Reynolds, J. R. Tuning Color, Contrast, and Redox Stability in High Gap Cathodically Coloring Electrochromic Polymers. *Macromolecules* **2016**, *49*, 8498-8507.

(74) Österholm, A. M.; Ponder, J. F.; De Keersmaecker, M.; Shen, D. E.; Reynolds, J. R. Disentangling Redox Properties and Capacitance in Solution-Processed Conjugated Polymers. *Chem. Mater.* **2019**.

(75) Gregory, S. A.; Menon, A. K.; Ye, S.; Seferos, D. S.; Reynolds, J. R.; Yee, S. K. Effect of Heteroatom and Doping on the Thermoelectric Properties of Poly(3-alkylchalcogenophenes). *Adv. Energy Mater.* **2018**, *8*, 1802419.

(76) Kerszulis, J. A.; Amb, C. M.; Dyer, A. L.; Reynolds, J. R. Follow the Yellow Brick Road: Structural Optimization of Vibrant Yellow-to-Transmissive Electrochromic Conjugated Polymers. *Macromolecules* **2014**, *47*, 5462-5469.

(77) Kerszulis, J. A.; Johnson, K. E.; Kuepfert, M.; Khoshabo, D.; Dyer, A. L.; Reynolds, J. R. Tuning the painter's palette: subtle steric effects on spectra and colour in conjugated electrochromic polymers. *J. Mater. Chem. C* **2015**, *3*, 3211-3218.

(78) Österholm, A. M.; Ponder, J. F.; Kerszulis, J. A.; Reynolds, J. R. Solution Processed PEDOT Analogues in Electrochemical Supercapacitors. *ACS Appl. Mater. Interfaces* **2016**, *8*, 13492-13498.

(79) Ponder, J. F.; Österholm, A. M.; Reynolds, J. R. Designing a Soluble PEDOT Analogue without Surfactants or Dispersants. *Macromolecules* **2016**, *49*, 2106-2111.

(80) Ponder Jr., J. F.; Menon, A. K.; Dasari, R. R.; Pittelli, S. L.; Thorley, K. J.; Yee, S. K.; Marder, S. R.; Reynolds, J. R. Conductive, Solution-Processed Dioxythiophene Copolymers for Thermoelectric and Transparent Electrode Applications. *Adv. Energy Mater.* **2019**, *9*, 1900395.

(81) Savagian, L. R.; Österholm, A. M.; Ponder Jr., J. F.; Barth, K. J.; Rivnay, J.; Reynolds, J. R. Balancing Charge Storage and Mobility in an Oligo(Ether) Functionalized Dioxythiophene Copolymer for Organic- and Aqueous- Based Electrochemical Devices and Transistors. *Adv. Mater.* **2018**, *30*, 1804647.

(82) Terje A. Skotheim, R. L. E., John R. Reynolds *Handbook of Conducting Polymers*; 2nd ed.; Marcel Dekker: New York, New York, 1998.

(83) Beaujuge, P. M.; Fréchet, J. M. J. Molecular Design and Ordering Effects in π-Functional Materials for Transistor and Solar Cell Applications. *J. Am. Chem. Soc.* **2011**, *133*, 20009-20029.

(84) Keg, P.; Lohani, A.; Fichou, D.; Lam, Y. M.; Wu, Y.; Ong, B. S.; Mhaisalkar, S. G. Direct Observation of Alkyl Chain Interdigitation in Conjugated Polyquarterthiophene Self-Organized on Graphite Surfaces. *Macromol. Rapid Commun.* **2008**, *29*, 1197-1202.

(85) McCulloch, I.; Heeney, M.; Bailey, C.; Genevicius, K.; MacDonald, I.; Shkunov, M.; Sparrowe, D.; Tierney, S.; Wagner, R.; Zhang, W.; Chabinyc, M. L.; Kline, R. J.; McGehee, M. D.; Toney, M. F. Liquid-crystalline semiconducting polymers with high charge-carrier mobility. *Nat. Mater.* **2006**, *5*, 328-333.

(86) Rivnay, J.; Mannsfeld, S. C. B.; Miller, C. E.; Salleo, A.; Toney, M. F. Quantitative Determination of Organic Semiconductor Microstructure from the Molecular to Device Scale. *Chem. Rev.* **2012**, *112*, 5488-5519.

(87) Kim, S.-M.; Kim, C.-H.; Kim, Y.; Kim, N.; Lee, W.-J.; Lee, E.-H.; Kim, D.; Park, S.; Lee, K.; Rivnay, J.; Yoon, M.-H. Influence of PEDOT:PSS crystallinity and composition on electrochemical transistor performance and long-term stability. *Nat. Commun.* **2018**, *9*, 3858.

(88) Gueye, M. N.; Carella, A.; Massonnet, N.; Yvenou, E.; Brenet, S.; Faure-Vincent, J.; Pouget, S.; Rieutord, F.; Okuno, H.; Benayad, A.; Demadrille, R.; Simonato, J.-P. Structure and Dopant Engineering in PEDOT Thin Films: Practical Tools for a Dramatic Conductivity Enhancement. *Chem. Mater.* **2016**, *28*, 3462-3468.

(89) Shi, W.; Zhao, T.; Xi, J.; Wang, D.; Shuai, Z. Unravelling Doping Effects on PEDOT at the Molecular Level: From Geometry to Thermoelectric Transport Properties. *J. Am. Chem. Soc.* **2015**, *137*, 12929-12938.

(90) Wei, Q.; Mukaida, M.; Naitoh, Y.; Ishida, T. Morphological Change and Mobility Enhancement in PEDOT:PSS by Adding Co-solvents. *Adv. Mater.* **2013**, *25*, 2831-2836.

(91) Hynynen, J.; Kiefer, D.; Yu, L.; Kroon, R.; Munir, R.; Amassian, A.; Kemerink, M.; Müller, C. Enhanced Electrical Conductivity of Molecularly p-Doped Poly(3-hexylthiophene) through Understanding the Correlation with Solid-State Order. *Macromolecules* **2017**, *50*, 8140-8148.

(92) Verploegen, E.; Miller, C. E.; Schmidt, K.; Bao, Z.; Toney, M. F. Manipulating the Morphology of P3HT–PCBM Bulk Heterojunction Blends with Solvent Vapor Annealing. *Chem. Mater.* **2012**, *24*, 3923-3931.

(93) Zhang, Q.; Sun, Y.; Xu, W.; Zhu, D. Thermoelectric energy from flexible P3HT films doped with a ferric salt of triflimide anions. *Energy Environ. Sci.* **2012**, *5*, 9639-9644.

(94) Patel, S. N.; Glaudell, A. M.; Peterson, K. A.; Thomas, E. M.; O'Hara, K. A.; Lim, E.; Chabinyc, M. L. Morphology controls the thermoelectric power factor of a doped semiconducting polymer. *Sci. Adv.* **2017**, *3*.

(95) Vijayakumar, V.; Zhong, Y.; Untilova, V.; Bahri, M.; Herrmann, L.; Biniek, L.; Leclerc, N.; Brinkmann, M. Bringing Conducting Polymers to High Order: Toward Conductivities beyond 105 S cm−1 and Thermoelectric Power Factors of 2 mW m−1 K−2. *Adv. Energy Mater.* **2019**, *9*, 1900266.

(96) Alberga, D.; Perrier, A.; Ciofini, I.; Mangiatordi, G. F.; Lattanzi, G.; Adamo, C. Morphological and charge transport properties of amorphous and crystalline P3HT and PBTTT: insights from theory. *Phys. Chem. Chem. Phys.* **2015**, *17*, 18742-18750.

(97) Müller, L.; Nanova, D.; Glaser, T.; Beck, S.; Pucci, A.; Kast, A. K.; Schröder, R. R.; Mankel, E.; Pingel, P.; Neher, D.; Kowalsky, W.; Lovrincic, R. Charge-

Transfer–Solvent Interaction Predefines Doping Efficiency in p-Doped P3HT Films. *Chem. Mater.* **2016**, *28*, 4432-4439.

(98) Kang, K.; Watanabe, S.; Broch, K.; Sepe, A.; Brown, A.; Nasrallah, I.; Nikolka, M.; Fei, Z.; Heeney, M.; Matsumoto, D.; Marumoto, K.; Tanaka, H.; Kuroda, S.-i.; Sirringhaus, H. 2D coherent charge transport in highly ordered conducting polymers doped by solid state diffusion. *Nat. Mater.* **2016**, *15*, 896.

(99) Eric Shen, D.; Österholm, A. M.; Reynolds, J. R. Out of sight but not out of mind: the role of counter electrodes in polymer-based solid-state electrochromic devices. *J. Mater. Chem. C* **2015**, *3*, 9715-9725.

(100) Kim, Y. H.; Sachse, C.; Machala, M. L.; May, C.; Müller-Meskamp, L.; Leo, K. Highly Conductive PEDOT:PSS Electrode with Optimized Solvent and Thermal Post-Treatment for ITO-Free Organic Solar Cells. *Adv. Funct. Mater.* **2011**, *21*, 1076-1081.

(101) Singh, R.; Tharion, J.; Murugan, S.; Kumar, A. ITO-Free Solution-Processed Flexible Electrochromic Devices Based on PEDOT:PSS as Transparent Conducting Electrode. *ACS Appl. Mater. Interfaces* **2017**, *9*, 19427-19435.

(102) Dhawan, S. K.; Singh, N.; Venkatachalam, S. Shielding behaviour of conducting polymer-coated fabrics in X-band, W-band and radio frequency range. *Synth. Met.* **2002**, *129*, 261-267.

(103) Chung, D. D. L. Materials for Electromagnetic Interference Shielding. *J. Mater. Eng. Perform.* **2000**, *9*, 350-354.

(104) Alberico, D.; Scott, M. E.; Lautens, M. Aryl−Aryl Bond Formation by Transition-Metal-Catalyzed Direct Arylation. *Chem. Rev.* **2007**, *107*, 174-238.

(105) Schipper, D. J.; Fagnou, K. Direct Arylation as a Synthetic Tool for the Synthesis of Thiophene-Based Organic Electronic Materials. *Chem. Mater.* **2011**, *23*, 1594-1600.

(106) Estrada, L. A.; Deininger, J. J.; Kamenov, G. D.; Reynolds, J. R. Direct (Hetero)arylation Polymerization: An Effective Route to 3,4-Propylenedioxythiophene-Based Polymers with Low Residual Metal Content. *ACS Macro Lett.* **2013**, *2*, 869-873.

(107) Ponder, J. F., A PEDOT by Any Other Name: Tuning the Electroactivity of Dioxy-heterocycles for Redox and Solid State Applications. Georgia Institute of Technology, **2017.**

(108) Heinze, J.; Springer Berlin Heidelberg: Berlin, Heidelberg, 1990, p 1-47.

(109) Heinze, J.; Frontana-Uribe, B. A.; Ludwigs, S. Electrochemistry of Conducting Polymers—Persistent Models and New Concepts. *Chem. Rev.* **2010**, *110*, 4724-4771.

(110) Padilla, J.; Österholm, A. M.; Dyer, A. L.; Reynolds, J. R. Process controlled performance for soluble electrochromic polymers. *Sol. Energy Mater. Sol. Cells* **2015**, *140*, 54-60.

(111) Richter, L. J.; DeLongchamp, D. M.; Amassian, A. Morphology Development in Solution-Processed Functional Organic Blend Films: An In Situ Viewpoint. *Chem. Rev.* **2017**, *117*, 6332-6366.

(112) Hernandez, J. L., A Mechanistic Understanding of Solvent Additives' Influence on Polymer:Fullerene Phase Separation for Organic Photovoltaics. Georgia Institute of Technology, **2017.**

(113) Bard, A. J. a. F., Larry R. *Electrochemical Methods Fundamentals and Applications*; 2nd ed.; Wiley, 2000.

(114) Odin, C.; Nechtschein, M. Slow relaxation in conducting polymers: the case of poly(3-methylthiophene). *Synth. Met.* **1991**, *44*, 177-188.

(115) Imae, I.; Mashima, T.; Sagawa, H.; Komaguchi, K.; Ooyama, Y.; Harima, Y. In situ conductivity measurements of polythiophene partially containing 3,4-ethylenedioxythiophene and 3-hexylthiophene. *J. Solid State Electrochem.* **2015**, *19*, 71-76.

(116) Morvant, M. C.; Reynolds, J. R. In situ conductivity studies of poly(3,4-ethylenedioxythiophene). *Synth. Met.* **1998**, *92*, 57-61.

(117) Müller-Buschbaum, P. The Active Layer Morphology of Organic Solar Cells Probed with Grazing Incidence Scattering Techniques. *Adv. Mater.* **2014**, *26*, 7692-7709.

(118) Portale, G.; Hermida-Merino, D.; Bras, W. Polymer research and synchrotron radiation perspectives. *Eur. Polym. J.* **2016**, *81*, 415-432.

(119) Cho, E.; Risko, C.; Kim, D.; Gysel, R.; Cates Miller, N.; Breiby, D. W.; McGehee, M. D.; Toney, M. F.; Kline, R. J.; Bredas, J.-L. Three-Dimensional Packing Structure and Electronic Properties of Biaxially Oriented Poly(2,5-bis(3-alkylthiophene-2-yl)thieno[3,2-b]thiophene) Films. *J. Am. Chem. Soc.* **2012**, *134*, 6177-6190.

(120) Mannsfeld, S. wxdiff: Diffraction Image Processing and Data Analysis Software. **2011**.

(121) Ilavsky, J. Nika: software for two-dimensional data reduction. *J. Appl. Crystallogr.* **2012**, *45*, 324-328.

(122) Oosterhout, S. D.; Savikhin, V.; Zhang, J.; Zhang, Y.; Burgers, M. A.; Marder, S. R.; Bazan, G. C.; Toney, M. F. Mixing Behavior in Small Molecule:Fullerene Organic Photovoltaics. *Chem. Mater.* **2017**, *29*, 3062-3069.

(123) Pittelli, S. L.; Shen, D. E.; Österholm, A. M.; Reynolds, J. R. Chemical Oxidation of Polymer Electrodes for Redox Active Devices: Stabilization through Interfacial Interactions. *ACS Appl. Mater. Interfaces* **2018**, *10*, 970-978.

(124) Chiang, C. K.; Fincher, C. R.; Park, Y. W.; Heeger, A. J.; Shirakawa, H.; Louis, E. J.; Gau, S. C.; MacDiarmid, A. G. Electrical Conductivity in Doped Polyacetylene. *Phys. Rev. Lett.* **1977**, *39*, 1098-1101.

(125) Argun, A. A.; Cirpan, A.; Reynolds, J. R. The First Truly All-Polymer Electrochromic Devices. *Adv. Mater.* **2003**, *15*, 1338-1341.

(126) Otley, M. T.; Alamer, F. A.; Zhu, Y.; Singhaviranon, A.; Zhang, X.; Li, M.; Kumar, A.; Sotzing, G. A. Acrylated Poly(3,4-propylenedioxythiophene) for Enhancement of Lifetime and Optical Properties for Single-Layer Electrochromic Devices. *ACS Appl. Mater. Interfaces* **2014**, *6*, 1734-1739.

(127) Jensen, J.; Hösel, M.; Kim, I.; Yu, J.-S.; Jo, J.; Krebs, F. C. Fast Switching ITO Free Electrochromic Devices. *Adv. Funct. Mater.* **2014**, *24*, 1228-1233.

(128) Cai, G.; Wang, J.; Lee, P. S. Next-Generation Multifunctional Electrochromic Devices. *Acc. Chem. Res.* **2016**, *49*, 1469-1476.

(129) Dubal, D. P.; Ayyad, O.; Ruiz, V.; Gomez-Romero, P. Hybrid energy storage: the merging of battery and supercapacitor chemistries. *Chem. Soc. Rev.* **2015**, *44*, 1777-1790.

(130) Bryan, A. M.; Santino, L. M.; Lu, Y.; Acharya, S.; D'Arcy, J. M. Conducting Polymers for Pseudocapacitive Energy Storage. *Chem. Mater.* **2016**, *28*, 5989-5998.

(131) Snook, G. A.; Kao, P.; Best, A. S. Conducting-polymer-based supercapacitor devices and electrodes. *J. Power Sources* **2011**, *196*, 1-12.

(132) Pabst, O.; Perelaer, J.; Beckert, E.; Schubert, U. S.; Eberhardt, R.; Tünnermann, A. All inkjet-printed piezoelectric polymer actuators: Characterization and applications for micropumps in lab-on-a-chip systems. *Org. Electron.* **2013**, *14*, 3423-3429.

(133) Okuzaki, H.; Kuwabara, T.; Funasaka, K.; Saido, T. Humidity-Sensitive Polypyrrole Films for Electro-Active Polymer Actuators. *Adv. Funct. Mater.* **2013**, *23*, 4400-4407.

(134) Otero, T. F.; Martinez, J. G.; Arias-Pardilla, J. Biomimetic electrochemistry from conducting polymers. A review: Artificial muscles, smart membranes, smart drug delivery and computer/neuron interfaces. *Electrochim. Acta* **2012**, *84*, 112-128.

(135) Smela, E. Conjugated Polymer Actuators for Biomedical Applications. *Adv. Mater.* **2003**, *15*, 481-494.

(136) Simon, D. T.; Gabrielsson, E. O.; Tybrandt, K.; Berggren, M. Organic Bioelectronics: Bridging the Signaling Gap between Biology and Technology. *Chem. Rev.* **2016**, *116*, 13009-13041.

(137) Rivnay, J.; Owens, R. M.; Malliaras, G. G. The Rise of Organic Bioelectronics. *Chem. Mater.* **2014**, *26*, 679-685.

(138) Green, R. A.; Lovell, N. H.; Wallace, G. G.; Poole-Warren, L. A. Conducting polymers for neural interfaces: Challenges in developing an effective long-term implant. *Biomaterials* **2008**, *29*, 3393-3399.

(139) Green, R. A.; Lovell, N. H.; Poole-Warren, L. A. Impact of co-incorporating laminin peptide dopants and neurotrophic growth factors on conducting polymer properties. *Acta Biomater.* **2010**, *6*, 63-71.

(140) Green, R. A.; Lovell, N. H.; Poole-Warren, L. A. Cell attachment functionality of bioactive conducting polymers for neural interfaces. *Biomaterials* **2009**, *30*, 3637-3644.

(141) Zinger, B.; Miller, L. L. Timed release of chemicals from polypyrrole films. *J. Am. Chem. Soc.* **1984**, *106*, 6861-6863.

(142) Svirskis, D.; Travas-Sejdic, J.; Rodgers, A.; Garg, S. Electrochemically controlled drug delivery based on intrinsically conducting polymers. *J. Control. Release* **2010**, *146*, 6-15.

(143) Martin, D. C. Molecular design, synthesis, and characterization of conjugated polymers for interfacing electronic biomedical devices with living tissue. *MRS Commun.* **2015**, *5*, 131-153.

(144) Kim, B. C.; Hong, J.-Y.; Wallace, G. G.; Park, H. S. Flexible Electronics: Recent Progress in Flexible Electrochemical Capacitors: Electrode Materials, Device Configuration, and Functions (Adv. Energy Mater. 22/2015). *Adv. Energy Mater.* **2015**, *5*, n/a-n/a.

(145) Mortimer, R. J. Electrochromic Materials. *Annu. Rev. Mater. Res.* **2011**, *41*, 241-268.

(146) Chiang, C. K.; Gau, S. C.; Fincher, C. R.; Park, Y. W.; MacDiarmid, A. G.; Heeger, A. J. Polyacetylene, (CH)x: n-type and p-type doping and compensation. *Appl. Phys. Lett.* **1978**, *33*, 18-20.

(147) Clarke, T. C.; Krounbi, M. T.; Lee, V. Y.; Street, G. B. Photoinitiated doping of polyacetylene. *Chem. Comm.* **1981**, 384-385.

(148) Schottland, P.; Zong, K.; Gaupp, C. L.; Thompson, B. C.; Thomas, C. A.; Giurgiu, I.; Hickman, R.; Abboud, K. A.; Reynolds, J. R. Poly(3,4-alkylenedioxypyrrole)s: Highly Stable Electronically Conducting and Electrochromic Polymers. *Macromolecules* **2000**, *33*, 7051-7061.

(149) Sonmez, G.; Schottland, P.; Zong, K.; Reynolds, J. R. Highly transmissive and conductive poly[(3,4-alkylenedioxy)pyrrole-2,5-diyl] (PXDOP) films prepared by air or transition metal catalyzed chemical oxidation. *J. Mater. Chem.* **2001**, *11*, 289-294.

(150) Bubnova, O.; Khan, Z. U.; Malti, A.; Braun, S.; Fahlman, M.; Berggren, M.; Crispin, X. Optimization of the thermoelectric figure of merit in the conducting polymer poly(3,4-ethylenedioxythiophene). *Nat. Mater.* **2011**, *10*, 429-433.

(151) Yan, H.; Sada, N.; Toshima, N. Thermal transporting properties of electrically conductive polyaniline films as organic thermoelectric materials. *J. Therm. Anal. Calorim.* **2002**, *69*, 881-887.

(152) Higgins, A.; Mohapatra, S. K.; Barlow, S.; Marder, S. R.; Kahn, A. Dopant controlled trap-filling and conductivity enhancement in an electron-transport polymer. *Appl. Phy. Lett.* **2015**, *106*, 163301.

(153) Guo, S.; Kim, S. B.; Mohapatra, S. K.; Qi, Y.; Sajoto, T.; Kahn, A.; Marder, S. R.; Barlow, S. n-Doping of Organic Electronic Materials using Air-Stable Organometallics. *Adv. Mater.* **2012**, *24*, 699-703.

(154) Kolesov, V. A.; Fuentes-Hernandez, C.; Chou, W.-F.; Aizawa, N.; Larrain, F. A.; Wang, M.; Perrotta, A.; Choi, S.; Graham, S.; Bazan, G. C.; Nguyen, T.-Q.; Marder, S. R.; Kippelen, B. Solution-based electrical doping of semiconducting polymer films over a limited depth. *Nat. Mater.* **2017**, *16,* 474-480.

(155) Irvin, D. J.; Goods, S. H.; Whinnery, L. L. Direct Measurement of Extension and Force in Conductive Polymer Gel Actuators. *Chem. Mater.* **2001**, *13*, 1143-1145.

(156) Schroeder, A. H.; Kaufman, F. B. The influence of polymer morphology on polymer film electrochemistry. *J. Electroanal. Chem.* **1980**, *113*, 209-224.

(157) Chen, X.; Inganäs, O. Doping-induced volume changes in poly(3-octylthiophene) solids and gels. *Synth. Met.* **1995**, *74*, 159-164.

(158) Abidian, M. R.; Corey, J. M.; Kipke, D. R.; Martin, D. C. Conducting-Polymer Nanotubes Improve Electrical Properties, Mechanical Adhesion, Neural Attachment, and Neurite Outgrowth of Neural Electrodes. *Small* **2010**, *6*, 421-429.

(159) Talbi, H.; Just, P.-E.; Dao, L. H. Electropolymerization of aniline on carbonized polyacrylonitrile aerogel electrodes: applications for supercapacitors. *J. Appl. Electrochem.* **2003**, *33*, 465-473.

(160) Park, J. H.; Park, O. O. Hybrid electrochemical capacitors based on polyaniline and activated carbon electrodes. *J. Power Sources* **2002**, *111*, 185-190.

(161) Trivedi, D. C. Influence of the anion on polyaniline. *J. Solid State Electrochem.* **1998**, *2*, 85-87.

(162) Murray, P.; Spinks, G. M.; Wallace, G. G.; Burford, R. P. Electrochemical induced ductile—brittle transition in tosylate-doped (pTS) polypyrrole. *Synth. Met.* **1998**, *97*, 117-121.

(163) Wynne, K. J. S., G. Bryan Poly(pyrrol-2-ylium tosylate): Electrochemical Synthesis and Physical and Mechanical Properties. *Macromolecules* **1985**, *18*, 2361-2368.

(164) Li, X.; Ibrahim Dar, M.; Yi, C.; Luo, J.; Tschumi, M.; Zakeeruddin, S. M.; Nazeeruddin, M. K.; Han, H.; Grätzel, M. Improved performance and stability of perovskite solar cells by crystal crosslinking with alkylphosphonic acid ω-ammonium chlorides. *Nat. Chem.* **2015**, *7*, 703-711.

(165) Paniagua, S. A.; Li, E. L.; Marder, S. R. Adsorption studies of a phosphonic acid on ITO: film coverage, purity, and induced electronic structure changes. *Phys. Chem. Chem. Phys.* **2014**, *16*, 2874-2881.

(166) Knott, E. P.; Craig, M. R.; Liu, D. Y.; Babiarz, J. E.; Dyer, A. L.; Reynolds, J. R. A minimally coloured dioxypyrrole polymer as a counter electrode material in polymeric electrochromic window devices. *J. Mater. Chem.* **2012**, *22*, 4953.

(167) Kerszulis, J. A.; Johnson, K. E.; Kuepfert, M.; Khoshabo, D.; Dyer, A. L.; Reynolds, J. R. Tuning the painter's palette: subtle steric effects on spectra and colour in conjugated electrochromic polymers. *J. Mater. Chem. C* **2015**, *3*, 3211-3218.

(168) Ahrland, S.; Chatt, J.; Davies, N. R. The relative affinities of ligand atoms for acceptor molecules and ions. *Chem. Soc. Rev.* **1958**, *12*, 265-276.

(169) Bubnova, O.; Khan, Z. U.; Malti, A.; Braun, S.; Fahlman, M.; Berggren, M.; Crispin, X. Optimization of the thermoelectric figure of merit in the conducting polymer poly(3,4-ethylenedioxythiophene). *Nat. Mater.* **2011**, *10*, 429-433.

(170) Groenendaal, L.; Zotti, G.; Aubert, P.-H.; Waybright, S. M.; Reynolds, J. R. Electrochemistry of Poly(3,4-alkylenedioxythiophene) Derivatives. *Adv. Mater.* **2003**, *15*, 855-879.

(171) Holliday, S.; Donaghey, J. E.; McCulloch, I. Advances in Charge Carrier Mobilities of Semiconducting Polymers Used in Organic Transistors. *Chem. Mater.* **2014**, *26*, 647-663.

(172) Holliday, S.; Li, Y.; Luscombe, C. K. Recent advances in high performance donor-acceptor polymers for organic photovoltaics. *Prog. Polym. Sci.* **2017**, *70*, 34-51.

(173) Endrődi, B.; Mellár, J.; Gingl, Z.; Visy, C.; Janáky, C. Molecular and Supramolecular Parameters Dictating the Thermoelectric Performance of Conducting Polymers: A Case Study Using Poly(3-alkylthiophene)s. *J. Phys. Chem. C* **2015**, *119*, 8472-8479.

(174) Kim, N.; Kee, S.; Lee, S. H.; Lee, B. H.; Kahng, Y. H.; Jo, Y.-R.; Kim, B.-J.; Lee, K. Highly Conductive PEDOT:PSS Nanofibrils Induced by Solution-Processed Crystallization. *Adv. Mater.* **2014**, *26*, 2268-2272.

(175) Ponder Jr., J. F.; Menon, A. K.; Dasari, R. R.; Pittelli, S. L.; Thorley, K. J.; Yee, S. K.; Marder, S. R.; Reynolds, J. R. Conductive, Solution-Processed Dioxythiophene Copolymers for Thermoelectric and Transparent Electrode Applications. *Adv. Energy Mater.*, *0*, 1900395.

(176) Mazaheripour, A.; Thomas, E. M.; Segalman, R. A.; Chabinyc, M. L. Nonaggregating Doped Polymers Based on Poly(3,4-Propylenedioxythiophene). *Macromolecules* **2019**, *52*, 2203-2213.

(177) McDearmon, B.; Page, Z. A.; Chabinyc, M. L.; Hawker, C. J. Organic electronics by design: the power of minor atomic and structural changes. *J. Mater. Chem. C* **2018**, *6*, 3564-3572.

(178) Yim, K.-H.; Whiting, G. L.; Murphy, C. E.; Halls, J. J. M.; Burroughes, J. H.; Friend, R. H.; Kim, J.-S. Controlling Electrical Properties of Conjugated Polymers via a Solution-Based p-Type Doping. *Adv. Mater.* **2008**, *20*, 3319-3324.

(179) Kuei, B.; Gomez, E. D. Chain conformations and phase behavior of conjugated polymers. *Soft Matter* **2017**, *13*, 49-67.

(180) Hildner, R.; Köhler, A.; Müller-Buschbaum, P.; Panzer, F.; Thelakkat, M. π-Conjugated Donor Polymers: Structure Formation and Morphology in Solution, Bulk and Photovoltaic Blends. *Adv. Energy Mater.* **2017**, *7*, 1700314.

(181) Yang, X.; Loos, J. Toward High-Performance Polymer Solar Cells: The Importance of Morphology Control. *Macromolecules* **2007**, *40*, 1353-1362.

(182) Welsh, D. M.; Kumar, A.; Meijer, E. W.; Reynolds, J. R. Enhanced Contrast Ratios and Rapid Switching in Electrochromics Based on Poly(3,4-propylenedioxythiophene) Derivatives. *Adv. Mater.* **1999**, *11*, 1379-1382.

(183) Stafford, C. M.; Roskov, K. E.; III, T. H. E.; Fasolka, M. J. Generating thickness gradients of thin polymer films via flow coating. *Rev. Sci. Instrum.* **2006**, *77*, 023908.

(184) Grand, C.; Zajaczkowski, W.; Deb, N.; Lo, C. K.; Hernandez, J. L.; Bucknall, D. G.; Müllen, K.; Pisula, W.; Reynolds, J. R. Morphology Control in Films of Isoindigo Polymers by Side-Chain and Molecular Weight Effects. *ACS Appl. Mater. Interfaces* **2017**, *9*, 13357-13368.

(185) Kroon, R.; Mengistie, D. A.; Kiefer, D.; Hynynen, J.; Ryan, J. D.; Yu, L.; Müller, C. Thermoelectric plastics: from design to synthesis, processing and structure–property relationships. *Chem. Soc. Rev.* **2016**, *45*, 6147-6164.

(186) Russ, B.; Glaudell, A.; Urban, J. J.; Chabinyc, M. L.; Segalman, R. A. Organic thermoelectric materials for energy harvesting and temperature control. *Nat. Rev. Mater.* **2016**, *1*, 16050.

(187) Jensen, J.; Hösel, M.; Dyer, A. L.; Krebs, F. C. Development and Manufacture of Polymer-Based Electrochromic Devices. *Adv. Funct. Mater.* **2015**, *25*, 2073-2090.

(188) Liu, D. Y.; Reynolds, J. R. Dioxythiophene-Based Polymer Electrodes for Supercapacitor Modules. *ACS Appl. Mater. Interfaces* **2010**, *2*, 3586-3593.

(189) Inal, S.; Rivnay, J.; Hofmann, A. I.; Uguz, I.; Mumtaz, M.; Katsigiannopoulos, D.; Brochon, C.; Cloutet, E.; Hadziioannou, G.; Malliaras, G. G. Organic electrochemical transistors based on PEDOT with different anionic polyelectrolyte dopants. *J. Polym. Sci. Pol. Phys.* **2016**, *54*, 147-151.

(190) Yee, P. Y.; Scholes, D. T.; Schwartz, B. J.; Tolbert, S. H. Dopant-Induced Ordering of Amorphous Regions in Regiorandom P3HT. *J. Phys. Chem. Lett.* **2019**, 4929-4934.

(191) Noriega, R.; Rivnay, J.; Vandewal, K.; Koch, F. P. V.; Stingelin, N.; Smith, P.; Toney, M. F.; Salleo, A. A general relationship between disorder, aggregation and charge transport in conjugated polymers. *Nat. Mater.* **2013**, *12*, 1038.

(192) Liang, Z.; Zhang, Y.; Souri, M.; Luo, X.; Boehm, Alex M.; Li, R.; Zhang, Y.; Wang, T.; Kim, D.-Y.; Mei, J.; Marder, S. R.; Graham, K. R. Influence of dopant size and electron affinity on the electrical conductivity and thermoelectric properties of a series of conjugated polymers. *J. Mater. Chem. A* **2018**, *6*, 16495-16505.

(193) Scholes, D. T.; Yee, P. Y.; McKeown, G. R.; Li, S.; Kang, H.; Lindemuth, J. R.; Xia, X.; King, S. C.; Seferos, D. S.; Tolbert, S. H.; Schwartz, B. J. Designing Conjugated Polymers for Molecular Doping: The Roles of Crystallinity, Swelling, and Conductivity in Sequentially-Doped Selenophene-Based Copolymers. *Chem. Mater.* **2019**, *31*, 73-82.

(194) Inal, S.; Rivnay, J.; Leleux, P.; Ferro, M.; Ramuz, M.; Brendel, J. C.; Schmidt, M. M.; Thelakkat, M.; Malliaras, G. G. A High Transconductance Accumulation Mode Electrochemical Transistor. *Adv. Mater.* **2014**, *26*, 7450-7455.

(195) Rivnay, J.; Inal, S.; Salleo, A.; Owens, R. M.; Berggren, M.; Malliaras, G. G. Organic electrochemical transistors. *Nat. Rev. Mater.* **2018**, *3*, 17086.

(196) Nielsen, C. B.; Giovannitti, A.; Sbircea, D.-T.; Bandiello, E.; Niazi, M. R.; Hanifi, D. A.; Sessolo, M.; Amassian, A.; Malliaras, G. G.; Rivnay, J.; McCulloch, I. Molecular Design of Semiconducting Polymers for High-Performance Organic Electrochemical Transistors. *J. Am. Chem. Soc.* **2016**, *138*, 10252-10259.

(197) Jow, T. R.; Jen, K. Y.; Elsenbaumer, R. L.; Shacklette, L. W.; Angelopoulos, M.; Cava, M. P. Electrochemical studies of fused-thiophene systems. *Synth. Met.* **1986**, *14*, 53-60.

(198) Karpov, Y.; Erdmann, T.; Raguzin, I.; Al-Hussein, M.; Binner, M.; Lappan, U.; Stamm, M.; Gerasimov, K. L.; Beryozkina, T.; Bakulev, V.; Anokhin, D. V.; Ivanov, D. A.; Günther, F.; Gemming, S.; Seifert, G.; Voit, B.; Di Pietro, R.; Kiriy, A. High Conductivity in Molecularly p-Doped Diketopyrrolopyrrole-Based Polymer: The Impact of a High Dopant Strength and Good Structural Order. *Adv. Mater.* **2016**, *28*, 6003-6010.

(199) Glaudell, A. M.; Cochran, J. E.; Patel, S. N.; Chabinyc, M. L. Impact of the Doping Method on Conductivity and Thermopower in Semiconducting Polythiophenes. *Adv. Energy Mater.* **2015**, *5*, 1401072.

(200) Hamidi-Sakr, A.; Biniek, L.; Bantignies, J.-L.; Maurin, D.; Herrmann, L.; Leclerc, N.; Lévêque, P.; Vijayakumar, V.; Zimmermann, N.; Brinkmann, M. A Versatile Method to Fabricate Highly In-Plane Aligned Conducting Polymer Films with Anisotropic Charge Transport and Thermoelectric Properties: The Key Role of Alkyl Side Chain Layers on the Doping Mechanism. *Adv. Funct. Mater.* **2017**, *27*, 1700173.

(201) Weller, T.; Rundel, K.; Krauss, G.; McNeill, C. R.; Thelakkat, M. Highly Efficient and Balanced Charge Transport in Thieno[3,4-c]pyrrole-4,6-dione Copolymers: Dramatic Influence of Thieno[3,2-b]thiophene Comonomer on Alignment and Charge Transport. *J. Phys. Chem. C* **2018**, *122*, 7565-7574.

(202) Vijayakumar, V.; Zaborova, E.; Biniek, L.; Zeng, H.; Herrmann, L.; Carvalho, A.; Boyron, O.; Leclerc, N.; Brinkmann, M. Effect of Alkyl Side Chain Length on Doping Kinetics, Thermopower, and Charge Transport Properties in Highly Oriented F4TCNQ-Doped PBTTT Films. *ACS Appl. Mater. Interfaces* **2019**, *11*, 4942-4953.

(203) Kiefer, D., Molecular Doping of Polar Conjugated Polymers. Chalmers University of Technology, **2019.**

(204) Li, W.; Guo, Y.; Shi, J.; Yu, H.; Meng, H. Solution-Processable Neutral Green Electrochromic Polymer Containing Thieno[3,2-b]thiophene Derivative as Unconventional Donor Units. *Macromolecules* **2016**, *49*, 7211-7219.

(205) Yin, Y.; Li, W.; Zeng, X.; Xu, P.; Murtaza, I.; Guo, Y.; Liu, Y.; Li, T.; Cao, J.; He, Y.; Meng, H. Design Strategy for Efficient Solution-Processable Red

Electrochromic Polymers Based on Unconventional 3,6-Bis(dodecyloxy)thieno[3,2-b]thiophene Building Blocks. *Macromolecules* **2018**, *51*, 7853-7862.

(206) Guo, Y.; Li, W.; Yu, H.; Perepichka, D. F.; Meng, H. Flexible Asymmetric Supercapacitors via Spray Coating of a New Electrochromic Donor–Acceptor Polymer. *Adv. Energy Mater.* **2017**, *7*, 1601623.

(207) Turbiez, M.; Frère, P.; Leriche, P.; Mercier, N.; Roncali, J. Poly(3,6-dimethoxy-thieno[3,2-b]thiophene): a possible alternative to poly(3,4-ethylenedioxythiophene) (PEDOT). *Chem. Commun.* **2005**, 1161-1163.

(208) Raimundo, J.-M.; Blanchard, P.; Frère, P.; Mercier, N.; Ledoux-Rak, I.; Hierle, R.; Roncali, J. Push–pull chromophores based on 2,2′-bi(3,4-ethylenedioxythiophene) (BEDOT) π-conjugating spacer. *Tetrahedron Lett.* **2001**, *42*, 1507-1510.

(209) Méndez, H.; Heimel, G.; Winkler, S.; Frisch, J.; Opitz, A.; Sauer, K.; Wegner, B.; Oehzelt, M.; Röthel, C.; Duhm, S.; Többens, D.; Koch, N.; Salzmann, I. Charge-transfer crystallites as molecular electrical dopants. *Nat. Commun.* **2015**, *6*, 8560.

(210) Kiefer, D.; Kroon, R.; Hofmann, A. I.; Sun, H.; Liu, X.; Giovannitti, A.; Stegerer, D.; Cano, A.; Hynynen, J.; Yu, L.; Zhang, Y.; Nai, D.; Harrelson, T. F.; Sommer, M.; Moulé, A. J.; Kemerink, M.; Marder, S. R.; McCulloch, I.; Fahlman, M.; Fabiano, S.; Müller, C. Double doping of conjugated polymers with monomer molecular dopants. *Nat. Mater.* **2019**, *18*, 149-155.

(211) Kang, S. D.; Snyder, G. J. Charge-transport model for conducting polymers. *Nat. Mater.* **2016**, *16*, 252.

(212) Kiefer, D.; Yu, L.; Fransson, E.; Gómez, A.; Primetzhofer, D.; Amassian, A.; Campoy-Quiles, M.; Müller, C. A Solution-Doped Polymer Semiconductor:Insulator Blend for Thermoelectrics. *Adv. Sci.* **2017**, *4*, 1600203.

(213) Un, H.-I.; Gregory, S. A.; Mohapatra, S. K.; Xiong, M.; Longhi, E.; Lu, Y.; Rigin, S.; Jhulki, S.; Yang, C.-Y.; Timofeeva, T. V.; Wang, J.-Y.; Yee, S. K.; Barlow, S.; Marder, S. R.; Pei, J. Understanding the Effects of Molecular Dopant on n-Type Organic Thermoelectric Properties. *Adv. Energy Mater.* **2019**, *9*, 1900817.

(214) Yamamoto, J.; Furukawa, Y. Electronic and Vibrational Spectra of Positive Polarons and Bipolarons in Regioregular Poly(3-hexylthiophene) Doped with Ferric Chloride. *J. Phys. Chem. B* **2015**, *119*, 4788-4794.

(215) Sotzing, G. A.; Reynolds, J. R.; Steel, P. J. Poly(3,4-ethylenedioxythiophene) (PEDOT) prepared via electrochemical polymerization of EDOT, 2,2′-Bis(3,4-ethylenedioxythiophene) (BiEDOT), and their TMS derivatives. *Adv. Mater.* **1997**, *9*, 795-798.

(216) S. Fuller, L.; Iddon, B.; A. Smith, K. Thienothiophenes. Part 2.1 Synthesis, metallation and bromine→lithium exchange reactions of thieno[3,2-b]thiophene and its polybromo derivatives. *J. Chem. Soc., Perkin Transactions 1* **1997**, 3465-3470.

(217) Menon, A. K.; Uzunlar, E.; Wolfe, R. M. W.; Reynolds, J. R.; Marder, S. R.; Yee, S. K. Metallo-organic n-type thermoelectrics: Emphasizing advances in nickel-ethenetetrathiolates. *J. Appl. Polym. Sci.* **2017**, *134*.

(218) Yee, S. K.; Coates, N. E.; Majumdar, A.; Urban, J. J.; Segalman, R. A. Thermoelectric power factor optimization in PEDOT:PSS tellurium nanowire hybrid composites. *Phys. Chem. Chem. Phys.* **2013**, *15*, 4024-4032.

VITA

SANDRA L. PITTELLI

Sandra L. Pittelli was born in Annapolis, Maryland. After many years of enjoying life on the Chesapeake Bay, she earned her bachelor's degree in Chemistry from Rensselaer Polytechnic Institute (RPI). While at RPI, she began doing research on kinetically stable proteins found in legumes under the guidance of Dr. Wilfredo Colón. She also had the opportunity to participate as an NSF undergraduate research fellow for the University of Maryland Center for Environmental Science under the guidance of Dr. Michael Gonsior. After obtaining her bachelor's degree in 2014, she traveled south to Atlanta and enrolled as a graduate student at the Georgia Institute of Technology. She joined the research group of Dr. John Reynolds at the end of that year, and began her journey in learning about conjugated polymers and their applications. Her thesis work has focused on understanding the processes of chemical and electrochemical doping and the structure-property relationships of dioxythiophene polymers. She expects to graduate with her doctoral degree in December 2019 and will continue her career as a scientific consultant at Exponent in Philadelphia, PA. Beyond her work in the lab she enjoys concerts, outdoor activities, and any movie directed by Quentin Tarantino.